Size-Control Regulation during Regeneration

How to Stop Growth?

Rita Drumond Mateus

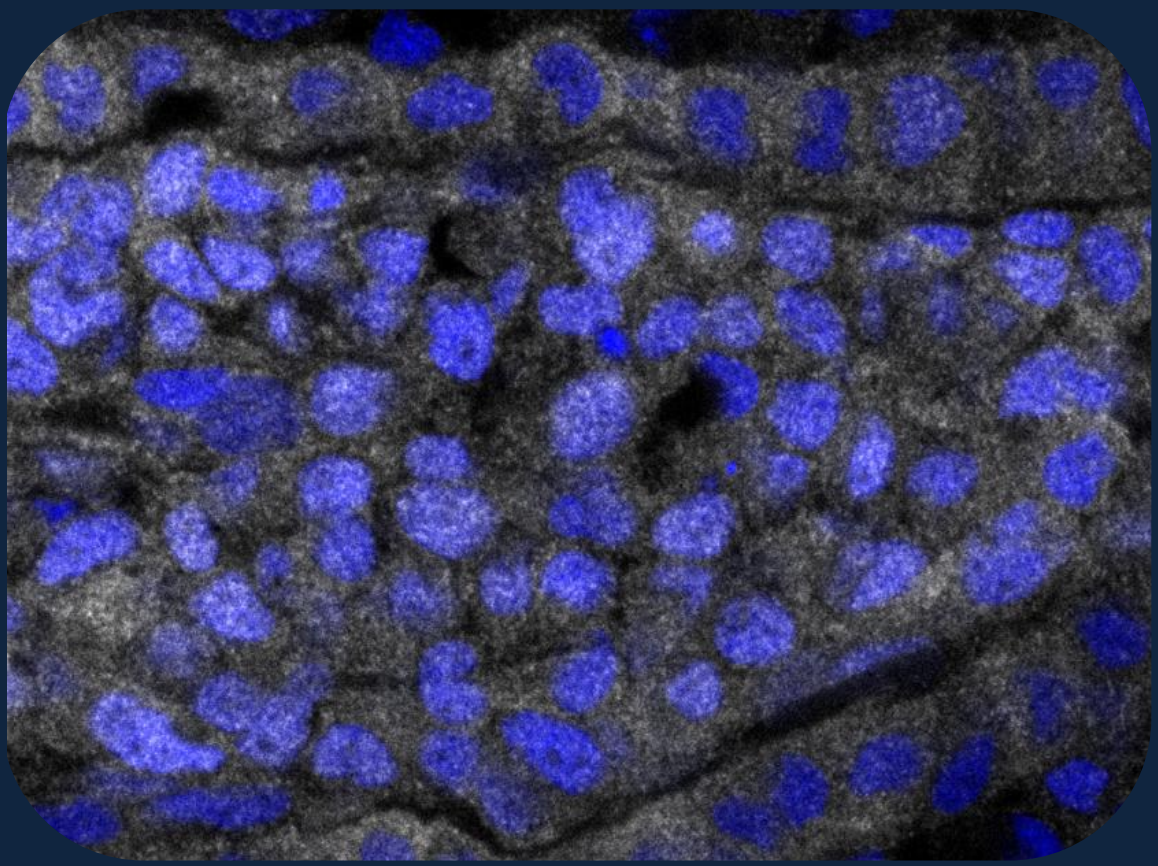

Dissertation presented to obtain the Ph.D degree in Biology

Instituto de Tecnologia Química e Biológica | Universidade Nova de Lisboa

Oeiras,
September, 2014

INSTITUTO
DE TECNOLOGIA
QUÍMICA E BIOLÓGICA
/UNL

Knowledge Creation

ITQB-UNL | Av. da República, 2780-157 Oeiras, Portugal
Tel (+351) 214 469 100 | Fax (+351) 214 411 277

www.itqb.unl.pt

Size-Control Regulation during Regeneration

How to Stop Growth?

Rita Drumond Mateus

Dissertation presented to obtain the Ph.D degree in Biology

Instituto de Tecnologia Química e Biológica | Universidade Nova de Lisboa

Oeiras, September, 2014

INSTITUTO
DE TECNOLOGIA
QUÍMICA E BIOLÓGICA
/UNL

Knowledge Creation

The research described in the present thesis was performed at Instituto de Medicina Molecular, Faculdade de Medicina, Universidade de Lisboa and at Chronic Diseases Research Center, Faculdade de Ciências Médicas, Universidade Nova de Lisboa, Lisboa, Portugal. This work was accomplished under the supervision of Dr. António Jacinto and Dr. Fernando Casares. Rita Drumond Mateus is a student belonging to the PhD Programme at Instituto de Tecnologia Química e Biológica, Universidade Nova de Lisboa, Portugal.

Financial Support from **Fundação para a Ciência e Tecnologia** (**FCT**)

Ph.D. Fellowship: SFRH/BD/62126/2009

SUPERVISOR:

António Alfredo Coelho Jacinto, PhD

Group leader at Centro de Estudos de Doenças Crónicas (CEDOC), Faculdade de Ciências Médicas, Universidade Nova de Lisboa, Lisboa, Portugal

CO-SUPERVISOR:

Fernando Casares, PhD

Group leader at Centro Andaluz de Biología del Desarrollo (CABD), Universidade Pablo de Olavide/CSIC, Sevilla, Spain

EXAMINING COMMITTEE:

Elly Tanaka, PhD *(Principal Examiner)*

Group leader at Center for Regenerative Therapies (CRTD), Dresden, Germany

José Bessa, PhD *(Principal Examiner)*

Group leader at Instituto de Biologia Molecular e Celular (IBMC), Porto, Portugal

Leonor Saúde, PhD

Group leader at Instituto de Medicina Molecular (IMM), Faculdade de Medicina da Universidade de Lisboa; Prof. Auxiliar da Faculdade de Medicina da Universidade de Lisboa, Lisboa, Portugal

Sólveig Thorsteinsdóttir, PhD

Group leader at Centro de Biologia Ambiental (CBA), Faculdade de Ciências da Universidade de Lisboa; Prof. Agregada da Faculdade de Ciências da Universidade de Lisboa, Lisboa, Portugal

“In regard to regeneration it has been evident for some time, that the specification or the differentiation (with its concomitant products), cannot be unreservedly utilized as a basis for an explanation of formative processes that take place. (…) There must be something else behind what we see that is responsible for the change that takes place. (…) Several years ago a consideration of a number of results in regeneration led me to state that this relation might be expressed as a ***sort of tension***.”

In *THE DYNAMIC FACTOR IN REGENERATION*

T.H. Morgan, 1909

Acknowledgements

First of all I would like to thank António Jacinto, my supervisor, for having me in the laboratory. As a mentor and friend, for always allowing me to do whatever I wanted in the lab and for all the useful advice on any topic. This really made me grow as a person and a scientist. For always being late – I'm finally patient! (a little, at least).

I would also like to acknowledge my thesis committee members, Leonor Saúde, Florence Janody and specially my tutor Lara Carvalho, who always kept me on track and gave me excellent scientific advice.

Of course, a big **THANK YOU!** to everyone in the Tissue Repair and Morphogenesis (and UMO) lab. You guys were amazing in creating a friendly environment to work in – all the jokes, cakes, "euromilhões", parties, amazing movies and songs, retreats and meetings. Also, our sister labs at IMM, UBD and UDEV, it was great to be able to work with you, especially after 8pm ☺ A special thank you with hugs to the people I worked closer: Sara Sousa, Lara Carvalho, Maria Gagliardi, Mariana Simões, Raquel Lourenço, Telmo Pereira, Inês Tenente, Gonçalo Brito, the other Lara Carvalho, Fábio Valério e Ana Farinho.

I would like to thank all the amazing effort of Maria Gagliardi, Lara Carvalho, Raquel Lourenço and Sara Sousa in reading and commenting my thesis. Without you I could not have done this so fast! Also Neuza Teixeira and Cláudia Queiroga for all your help with the ITQB requirements, it really helped!

A todos os meus amigos, mesmo os que estão longe, vocês sabem quem são ;) podemos finalmente ir celebrar!
Um Obrigada com abraços fortes à minha família inteira, por estes 5 anos do "não posso, tenho que ir trabalhar"!

E a **todos** os que acreditam em mim, me fazem crescer e me fazem todos os dias querer continuar a fazer ciência!

THESIS PUBLICATIONS

- Mateus R., Pereira T., Sousa S., de Lima JE., Pascoal S., Saúde, L. and Jacinto, A. (2012) **In Vivo Cell and Tissue Dynamics Underlying Zebrafish Fin Fold Regeneration.** PLoS ONE 7(12): e51766. (doi:10.1371/journal.pone.0051766)

- Mateus, R., Brito, G., Farinho, A., Valério, F. and Jacinto, A. **Yap control of tissue growth is dependent on cell density and F-actin cytoskeleton during zebrafish caudal fin regeneration.** *(In preparation)*

ABSTRACT

Functional regeneration of organs upon injury is a key process for animals survival. Contrary to humans, some vertebrates are remarkably competent in regenerating after acute organ or appendage lesions. This advantageous skill allows overcoming limitations in repair even in adult stages, when tissues are fully developed, via a process of epimorphic regeneration. One such organism is the zebrafish, which can regenerate several organs, namely its heart, retina, spinal cord and fins.

In this work, the zebrafish caudal fin and fin fold were used as model systems due to their capacity to recover their original size and shape upon numerous amputations. The achievement of the correct size during regeneration, which entails a precise growth control program and existence of positional memory mechanisms, has remained little understood. This robust process involves the formation of a highly proliferative cell mass, the blastema, which directs the regenerative process to achieve proportionate growth and pattern. By seeking new regulators of growth during regeneration, through a combination of candidate gene approaches and medium-throughput screens, we have investigated the underlying mechanisms of size-control during epimorphic regeneration.

By establishing the regenerating fin fold as a suitable model for live imaging studies, we characterized its regenerative process with *in vivo* detail. Importantly, we observed dynamically and quantitatively the tissue movements, cell behaviors and cell shape changes that occur during fin fold development and regeneration. Additionally in this system, we developed and performed a chemical screen assay searching for new regulators of fin fold size upon amputation. By screening 1200 small molecules belonging to the Prestwick library, we identified 14 novel compounds that inhibit regenerative growth, from which 8 were referenced as neuroactive substances having effects in several classes of neurotransmitters.

The combined knowledge from the live imaging and chemical screen approaches uncovered significant mechanistic differences between the fin fold and adult caudal fin regeneration models. In particular, the fin fold does not have a spatially restricted distal area of proliferation; nevertheless this process has a confined time of occurrence. Moreover, the fin fold growth rate necessary to recover final size does not appear to depend exclusively on the increase of cell numbers, since the tissue continues to expand in size, even when cell division is low. Furthermore, we confirmed that this effect is not a result of differences in cell division orientation that could contribute for the final size and form of the regenerating fin fold.

This work also explored the differences in proximal-distal (PD) compartments of the adult caudal fin blastema and how these could contribute for fin regenerative growth. Once formed the blastema has a proximal mesenchymal region that exhibits high proliferation and differentiation rates that become less prominent towards the distal tip. Interestingly, we observed that the blastema showed different cell densities and associated cell morphologies along those PD regions. The observation that the mesenchymal blastema has different levels of cell density (i.e. confluency) suggested a natural occurring process of contact inhibition of proliferation. Importantly, we found that these modifications were tightly associated with the dynamic intracellular location of Yap, the Hippo pathway effector. Recently, it was shown that this highly conserved signal-transducing pathway is able to regulate final organ size via control of cell proliferation, apoptosis and cell differentiation. Of relevance, the Hippo pathway was shown to transduce physical information provided by the extracellular environment, namely differences in cell contacts or matrix rigidity. This prompted us to characterize the role of the Hippo pathway *in vivo.* In particular, we studied Yap activation during epimorphic regeneration of the caudal fin.

We started by addressing the activation state of Yap in the blastema. For this, we quantified the intracellular localization of Yap as a proxy for its

activation. In the distal domain, with high cell density, Yap is mainly cytoplasmic (inactive), while in the proximal, lower cell density domain, Yap is largely nuclear (active). The functional relevance of Yap localization was confirmed by conditional genetic manipulation during blastema formation: overexpression of a Yap constitutively active transgenic (Hsp70:RFP-CAyap) led to an increase in blastema proliferation, while overexpression of a Yap dominant negative transgenic (Hsp70:RFP-DNyap) resulted in the opposing phenotype. This characterization showed that uncontrolled growth can occur in the blastema, when this pathway is misregulated. This resulted in functional consequences, since it halted the fin regenerative program, indicating that Yap is on top of a complex network of tissue growth regulation during regeneration.

To find possible adhesion and cytoskeleton associated proteins acting as cell density sensors in the blastema, through which Yap function could be mediated, we performed an immunohistochemistry screen searching for differences in expression along the PD axis of the blastema. Interestingly, Alpha-Catenin and F-actin were found to be present in the mesenchymal cells in a proximal-distal gradient. Moreover, Yap inactivation correlated with high cell density areas where Alpha-Catenin and F-actin were localized. In addition, by interfering with F-actin polymerization *in vivo*, we showed that Yap activation is dependent on F-actin intracellular distribution, this being an upstream regulator of Yap during the regenerative process.

This study identified a mechanism for the regulation of Yap activity within the regenerating blastema based in cell density differences of the mesenchymal tissue. These findings provided evidence for the existence of a mechanotransduction process involving changes in cell morphology, junction assembly and cytoskeleton remodeling. Altogether, we propose that alterations in mechanical tension through these factors, lead to a graded control of Yap, contributing to tissue growth recovery in epimorphic regeneration.

Overall, the work presented in this thesis provides evidence for multiple growth control mechanisms at work during zebrafish fin regeneration. We propose that signaling molecules together with mechanical forces are able to direct proliferation and contribute for the restoration final fin size.

RESUMO

A regeneração de órgãos após lesões é um processo chave para a sobrevivência dos animais. Ao contrário dos Humanos, alguns vertebrados são notavelmente competentes a reformar membros ou órgãos internos após danos severos. Esta habilidade é extremamente vantajosa para superar limitações em processos de reparação pois ocorre mesmo em estádios adultos, após desenvolvimento total dos tecidos, através de um processo de regeneração epimórfica. Um organismo capaz de utilizar este tipo de regeneração é o peixe-zebra. Este animal é capaz de regenerar vários órgãos, nomeadamente o coração, a retina, a espinal medula e as barbatanas, entre outros.

Neste trabalho, a barbatana caudal adulta do peixe zebra e o seu primórdio, foram utilizados como modelos de regeneração, devido à capacidade de recuperação do seu tamanho e forma originais após várias amputações. A obtenção do tamanho correcto durante a regeneração, que implica um programa de controlo de crescimento preciso e também mecanismos de memória posicional, tem permanecido pouco compreendida. Este processo robusto envolve a formação de uma massa de células altamente proliferativa, o blastema, que guia o processo regenerativo de forma a se obter crescimento e formas proporcionais. Ao procurar novos reguladores do crescimento durante a regeneração através de uma combinação de métodos, genes candidatos e screens de médio impacto, nós investigámos os mecanismos fundamentais de controlo de crescimento durante a regeneração epimórfica.

Ao estabelecer o primórdio da barbatana caudal de peixe zebra como um modelo adequado para aquisição de imagens em tempo real, nós caracterizámos o seu processo regenerativo com detalhe *in vivo*. Observou-se e quantificou-se de forma dinâmica os movimentos dos tecidos, comportamentos e mudanças de forma das células, que ocorrem durante o

desenvolvimento e regeneração desta estrutura. Adicionalmente neste sistema, nós desenvolvemos e desempenhámos um ensaio de procura de compostos químicos, de forma a encontrar novo reguladores do crescimento após amputação do primórdio da barbatana caudal do peixe zebra. Ao screenar 1200 moléculas pertencentes à biblioteca química Prestwick, nós identificámos 14 novos compostos que inibem o crescimento regenerativo, dos quais 8 estão registados como substâncias neuroactivas, tendo efeitos em várias classes de neurotransmissores.

O conhecimento combinado das abordagens de aquisição de imagens em tempo real e pesquisa de químicos, revelou differenças mecanísticas significativas entre o processo regenerativo da barbatana caudal adulta e seu primórdio. Em particular, o primórdio da barbatana não tem uma área de proliferação restrita à sua zona distal; todavia, este processo ocorre durante um tempo confinado. Além disso, a taxa de crescimento do primórdio da barbatana para recuperação do seu tamanho original não parece depender exclusivamente no aumento do número de células, pois o tecido continua a expandir, mesmo quando a divisão celular é baixa. Em reforço, nós confirmámos que este efeito não é um resultado de diferenças na orientação da divisão celular que possam contribuir para a regeneração do tamanho e formas finais do primórdio da barbatana caudal.

Este trabalho também explorou as diferenças entre compartimentos proximais-distais do blastema da barbatana caudal adulta e como este podem contribuir para o seu crescimento regenerativo. Após formado, o blastema tem uma região mesenquimatosa proximal que exibe elevada proliferação e diferenciação celulares; estes tornam-se menos evidentes em direcção à ponta distal do blastema. Nós observámos que o blastema tem diferentes densidades celulares, associadas com diferentes morfologias ao longo destas regiões proximo-distais (PD). A observação que o blastema mesenquimatoso tem diferentes níveis de densidade celular (i.e. confluência) sugeriram a ocorrência de um processo natural de inibição da proliferação por contacto. Associado a estas modificações, encontrou-se a

localização intracelular dinâmica de Yap, o efector da via de sinalização Hippo. Recentemente, esta via tem emergido como uma via de transdução de sinal altamente conservada, que é capaz de regular o tamanho final do órgão por meio de controlo da proliferação celular, apoptose celular e diferenciação. De relevância, foi mostrado que a via Hippo é capaz de traduzir informação física proporcionado pelo ambiente extracelular, nomeadamente diferenças em pontos de contacto das células ou rigidez da matriz extracelular. Isto levou-nos caracterizar o papel da via Hippo *in vivo*. Em particular, estudámos a activação de Yap durante a regeneração epimórfica da barbatana caudal.

Começámos por abordar estado de activação de Yap no blastema. Para isso, foi quantificada a localização intracelular de Yap como um proxy para a sua activação. No domínio distal, com elevada densidade celular, Yap é principalmente citoplasmático (inactivo), enquanto que no domínio proximal onde existe densidade celular inferior, Yap é em grande parte nuclear (activo). A importância funcional da localização de Yap foi confirmada por manipulação genética condicional, durante a formação do blastema: a sobre-expressão de um transgénico com Yap constitutivamente activo (Hsp70: RFP-CAyap) conduziu a um aumento na proliferação blastema, enquanto que a sobre-expressão de um transgénico com Yap dominante negativo (Hsp70: RFP-DNyap) resultou no fenótipo oposto. Esta caracterização mostrou que o crescimento descontrolado pode ocorrer no blastema, quando esta via é desregulada. Isto resultou em consequências funcionais, uma vez que o programa regenerativo da barbatana foi interrompido, indicando que Yap está no topo de uma rede complexa de regulação do crescimento de tecidos durante a regeneração.

Para encontrar possíveis proteínas associadas a adesão e citoesqueleto que possam actuar como sensores de densidade celular no blastema, através do qual a função Yap poderia ser mediada, foi realizada uma procura recorrendo imunohistoquímica de forma a encontrar diferenças na expressão de genes ao longo do eixo proximal-distal do blastema.

Curiosamente, Alfa-Catenina e F-actina foram encontradas ao ter uma localização nas células mesenquimais sob a forma de um gradiente de proximal para distal. Além disso, Alpha-catenina e F-actina foram localizados nas zonas de inativação de Yap onde existe alta densidade celular. Além disso, ao interferir com a polimerização de F-actina *in vivo*, mostrou-se que a activação de Yap é dependente da distribuição intracelular de F-actina, sendo este um regulador a montante de Yap durante o processo regenerativo.

Este estudo identificou um mecanismo para a regulação da actividade de Yap dentro do blastema durante a regeneração, com base em diferenças de densidade de células do tecido mesenquimal. Estes resultados forneceram evidências para a existência de um processo de mecanotransdução envolvendo alterações na morfologia celular, formação de contactos celulares e remodelação do citoesqueleto. Ao todo, propomos que as alterações na tensão mecânica através destes factores, conduzem a um controlo graduado da activação de Yap, contribuindo para a recuperação do tecido durante a regeneração epimórfica.

No geral, o trabalho apresentado nesta tese fornece provas para vários mecanismos de controlo de crescimento a actuar durante a regeneração da barbatana caudal do peixe-zebra. Propomos que moléculas de sinalização, juntamente com forças mecânicas são capazes de dirigir a proliferação celular e contribuir para a restauração do tamanho final deste membro.

ABBREVIATIONS

Abbreviation	*Full form*
ΔCt	Cycling threshold
µM	microMolar
µl	microliter
AEC	Apical ectodermal cap
AP	Anterior-Posterior
bp	Base pairs
°C	degree Celsius
cDNA	Complementary DNA
Dpa	Days post amputation
Dpf	Days post fertilization
DV	Dorsal-Ventral
E3	Embryo medium
ECM	Extracellular Matrix
EDU	5-ethynyl-2'-deoxyuridine
F-actin	Filamentous actin
FDA	Food and Drug Administration
Fgf	Fibroblast growth factor
G	Gram
GFP	Green fluorescent protein
h	hour
Hpa	Hours post amputation

Abbreviation	*Full form*
Hpf	Hours post fertilization
Kpa	Kilo Pascal
mg	milligram(s)
min	minute(s)
ml	millilitre(s)
mM	milliMolar
mRNA	messenger RNA
nl	nanoliter(s)
PCR	Polymerase chain reaction
PD	Proximal-Distal
PDZ binding motif	Post synaptic density protein; Disc large tumor suppressor; Zonula occludens-1
qPCR	Quantitative real-time polymerase chain reaction
RNA	Ribonucleic Acid
Shh	Sonic hedgehog
Taz	Transcriptional co-Activator with PDZ binding motif
TGFβ	Transforming Growth Factor beta
Yap	Yes Associated Protein
Wnt	Wingless
wt	Wild-type

TABLE OF CONTENTS

Chapter I - Introduction

Chapter II - Dynamics of Fin Fold Regeneration

Chapter III - Chemical Modulation of Zebrafish Fin Fold Regeneration

Chapter IV - Mechanisms of Tissue Growth Control during Adult Zebrafish Caudal Fin Regeneration

Chapter V - Discussion

CHAPTER I

INTRODUCTION

“Beauty depends on size as well as symmetry.”

Aristotle

CONTENTS

Rita Mateus wrote this chapter based on the referred bibliography.

1. Epimorphic Regeneration

In the animal kingdom, some vertebrates are known for their proficiency in regenerate tissues upon injury, reconstructing flawless and fully functional replicas. This extraordinary process was initially described by Lazzaro Spallanzani, who showed that after major amputation, salamanders and toads formed faithful *reproductions* from the existing tissues (Spallanzani, 1769). The concept of *epimorphosis* (from the Greek: *epi*, upon; *morphosis*, form) was later introduced by Thomas H. Morgan in the 1900's to describe the regenerative process in which there is a complete regrowth of damaged appendages, tissues or organs through the formation of a specialized structure called blastema (Morgan, 1901)(Morgan, 1906).

The blastema is characterized as being a cell mass composed of progenitors of all cell types needed to reconstitute the injured tissue parts (Morgan, 1901). Typically, the canonical blastema is structurally organized in layers of epidermis surrounding a group of mesenchymal cells. These mesenchymal cells have a central role during regeneration since they will constitute the so-called progenitor cell mass. This structure is a niche that creates the necessary conditions for the blastema cells to proliferate and differentiate, particularly in terms of signaling molecules and growth factors, allowing the re-formation of the missing organ. Closely associated with the mesenchymal blastema cells is the surrounding wound epidermis, classically called the apical ectodermal cap (AEC) by Thornton (Thornton, 1968). The AEC is formed upon sealing of the wound and thickening of the epidermis. Aside of its structural roles, it provides multiple signaling factors that instruct the behavior of the underlying mesenchyme (Murawala et al., 2012)(Campbell et al., 2011). Importantly, AEC removal or its substitution with other epithelia impairs the regenerative process (Mescher, 1976)(Tassava and Garling, 1979)(Christensen and Tassava, 2000).

The origin of the blastema cells that give rise to the new structure has been a subject of intense investigation in the regeneration field. In particular, the process of epimorphic regeneration (or epimorphosis) takes place in animals that have undergone normal development with complete body axis formation and terminal cellular differentiation (Morgan, 1901)(Nacu and Tanaka, 2010). This presents a challenge for the cells that will compose the blastema, since they must acquire the properties that allow them to provide the necessary cell types the injured tissue is composed of. These properties reflect an exceptional transition to a developmental programme within an adult tissue. Recently, several studies have shown that the origin of the blastema cells can result from a step-wise dedifferentiation process: fully differentiated cells from the vicinities of the wound sense the injury, migrate towards the stump, and dedifferentiate in a lineage restricted fashion constituting a heterogeneous progenitor pool, the blastema (Echeverri et al., 2001)(Kragl et al., 2009)(Jopling et al., 2010)(Knopf et al., 2011)(Sousa et al., 2011)(Stewart and Stankunas, 2012). In this dedifferentiated state, the blastema cells acquire features closer to an embrionary state, namely through the expression of early genes specific of their lineage (Knopf et al., 2011). These cells also change their morphology and proliferate at high rates until differentiation cues are established. Differentiation occurs gradually and always unidirectionally along the proximal-distal axis, with mature cells initially being positioned closer to the amputation plane and patterning proceeding to the distal direction (Knopf et al., 2011)(Sousa et al., 2011)(Roensch et al., 2013).

The plasticity potential of the blastema cells has also been a relevant question in the field. The blastema cells were shown to dedifferentiate and become lineage restricted progenitors, therefore contributing only to specific cell types within the regenerating tissue. In addition, it was reported that transdifferentiation, the process of a dedifferentiated cell acquiring a different fate from its origin (Jopling et al., 2011), does not naturally occur during the epimorphic regenerative process – neither between major

developmental tissue classes (neuroectoderm, mesoderm and ectoderm) nor amongst specific lineage classes within the damaged tissue (Tu and Johnson, 2011)(Gargioli and Slack, 2004). However, exceptions have been described: when specific genetic and X-ray manipulations are performed, dedifferentiated blastema cells give rise to cell types other than their own (Dunis and Namenwirth, 1977)(Kragl et al., 2009)(Singh et al., 2012). This reveals that the blastema cells have the potential to become pluripotent when challenged. It still remains to be established whether this phenomenon can occur in all lineages within the blastema or whether there is a specific lineage capable of converting into a pluripotent stem cell like state.

An additional essential feature of epimorphic regeneration is its nerve dependency. In the absence of innervation, proliferation is halted and consequently regeneration is impaired (Singer, 1952)(Geraudie and Singer, 1985). Moreover, it has been shown that the function of the nerves is linked to the beginning of this process, since the presence of nerves can alone induce a blastema but is not required for its maintenance, outgrowth and differentiation (Endo et al., 2004)(Satoh et al., 2007). This indicates that the nerves provide important early signals to the blastema cells. To date, the protein newt Anterior Gradient (nAG) is the only molecule described to be secreted by the intrarray nerve fibers into the mesenchymal blastema (and later by glands in the wound epidermis), contributing for the newt regenerative response (Kumar et al., 2007). Conserved factors, transversal to several animal model systems, are yet to be identified.

Importantly, epimorphic regeneration shows remarkable robustness, occurring in animals in an unlimited manner, leaving no scar and being able to take place independently of the age of the animal (Azevedo et al., 2011)(Shao et al., 2011)(Itou et al., 2012). Connected to these features are the striking properties of maintenance of original size and shape upon damage. These reveal a level of cellular coordination and complexity that likely incorporates signaling factors and accurate control mechanisms, which will be introduced in sections 2 and 3.

1.1 Zebrafish Caudal Fin Regeneration

The ability of the fish fin to regenerate was initially observed by Broussolet (1786) and later largely established by Thomas H. Morgan (Morgan, 1900)(Morgan, 1902). The zebrafish caudal fin is able to regenerate through a process of epimorphic regeneration. This bilobed structure is comprised of segmented bony rays (*lepidotrichia*) that have a cartilage-like structure in their distal tip (*actinotrichia*). Upon amputation, each ray forms an independent blastema that contains cells of different lineages and developmental origins. These include neuroectoderm derived lineages, composed by the pigment cells (melanocytes, iridophores and xanthophores), and the nerves (lateral line, intrarray motor and sensory nerves with associated glia); the mesodermal lineages that contain the vascular endothelium (arteries and veins), the scleroblasts (the fish osteoblasts) and the dermal fibroblasts (both medial mesenchymal cells and perivascular cells); blood cells (plasma cells, macrophages and neutrophils); and the ectoderm derived epidermis (Tu and Johnson, 2011)(Lund et al., 2014) (Figure 1).

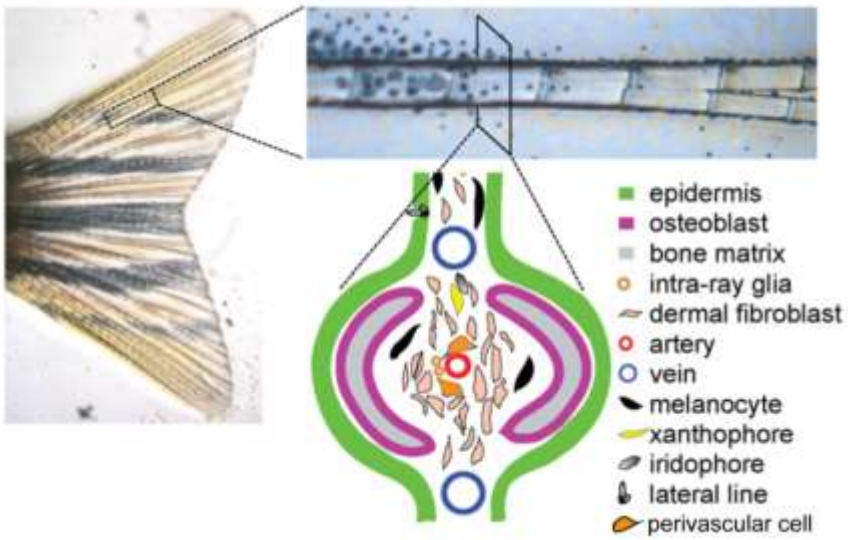

Figure 1. Cell types present in the adult zebrafish caudal fin. The caudal fin is composed

of 16-18 bony rays, each an independent unit. A transversal section from a bony ray reveals the cell types present in this structure. Adapted from Tu and Johnson, 2011.

Upon amputation, these cell types will integrate the newly regenerated fin, respecting their original developmental lineages. The fin regenerative process is unidirectional and takes approximately 10-15 days. Also, the total duration of this process is temperature-sensitive, since higher temperatures will result in faster regeneration rates (Ferretti and Health, 2006)(Boominathan and Ferreira, 2012). Even so, fin regeneration proceeds in the following phases (Figure 2):

1) Wound healing phase – As soon as the injury is inflicted, a layer of epithelial cells quickly migrates to the open wound, resulting in wound closure (initial 3 hours post amputation, hpa). It is thought that this process relies on acto-myosin contractility and collective cell migration (Poleo et al., 2001)(Santos-Ruiz et al., 2005). This new epithelial layer then develops into a structured multilayered wound epidermis formed by three distinct epithelial layers: an outer sheet composed of flat, condensed cells; a medial region composed of looser cells, in which mucous cells differentiate; and a basal layer consisting of well-organized cuboidal cells that exhibit protrusions and lie on an extracellular basement membrane (Santamaria et al., 1991)(Santos-Ruiz et al., 2002). Notably the wound healing phase occurs independently of blood supply and of cell proliferation (Santos-Ruiz et al., 2002)(Nechiporuk and Keating, 2002). After 12-18 hpa, the wound epidermis is fully established becoming the apical ectodermal cap (AEC). The AEC, in particular its basal epidermal layer, will constitute an important signaling center for the underlying intrarray mesenchyme (Lee et al., 2009).

2) Blastema formation – This self-organizing structure forms as early as 12 hpa when intrarray differentiated mesenchymal cells migrate towards the distal tip of each damaged bony ray. Morphologically the blastema cells appear homogeneous since they change to a rounder morphology as part of the dedifferentiation process (Sousa et al., 2011). Currently, it is still

unknown which signals emanate from the injury site and whether these can constitute also dedifferentiation factors.

Taking into account that only a limited group of cells from the first segment – adjacent to the amputation plane – sense the injury and migrate, an important feature of the blastema is its proliferative nature. To overcome the need in numbers to replace the missing organ, the blastema contributing cells start to divide even before reaching the stump; once they arrive there, they start to proliferate at higher rates, forming the progenitor cell mass that will reconstitute the lost parts. The blastema is completed within the first 48 hpa and when fully formed is divided in two zones: a distal zone where there is little proliferation and a proximal zone with highly proliferative cells (Nechiporuk and Keating, 2002). The distal zone is typically associated with less differentiated cells ("stem-cell like") due to the limited amount of proliferation and the high concentration of signaling factors that maintain this state, such as MsxB, Notch, Wnt and Retinoic Acid (Nechiporuk and Keating, 2002)(Münch et al., 2013)(Grotek et al., 2013)(Wehner et al., 2014)(Blum and Begemann, 2011). It is thought that the maintenance of this specialized distal region occurs via signaling interactions from the basal epidermal layer and the underlying mesenchyme (Lee et al., 2009).

3) Regenerative outgrowth – At this stage, the blastema is more structured along the proximal-distal axis, presenting: a distal-most region where proliferation is scarce; a distal region which contains rapidly proliferating cells; and a proximal region with moderately proliferating cells, in which the major differentiation and patterning events occur. Asin the previous phase, the lateral basal epidermal layer expresses a number of signaling molecules important for tissue patterning, namely Shh and Lef1 (Lee et al., 2009). During outgrowth, the cell cycle accelerates significantly, going from a 6 hour long G2 phase (during blastema formation) to just one hour. The total duration of regenerative outgrowth phase as well as mechanisms that regulate its termination, remain uncharacterized.

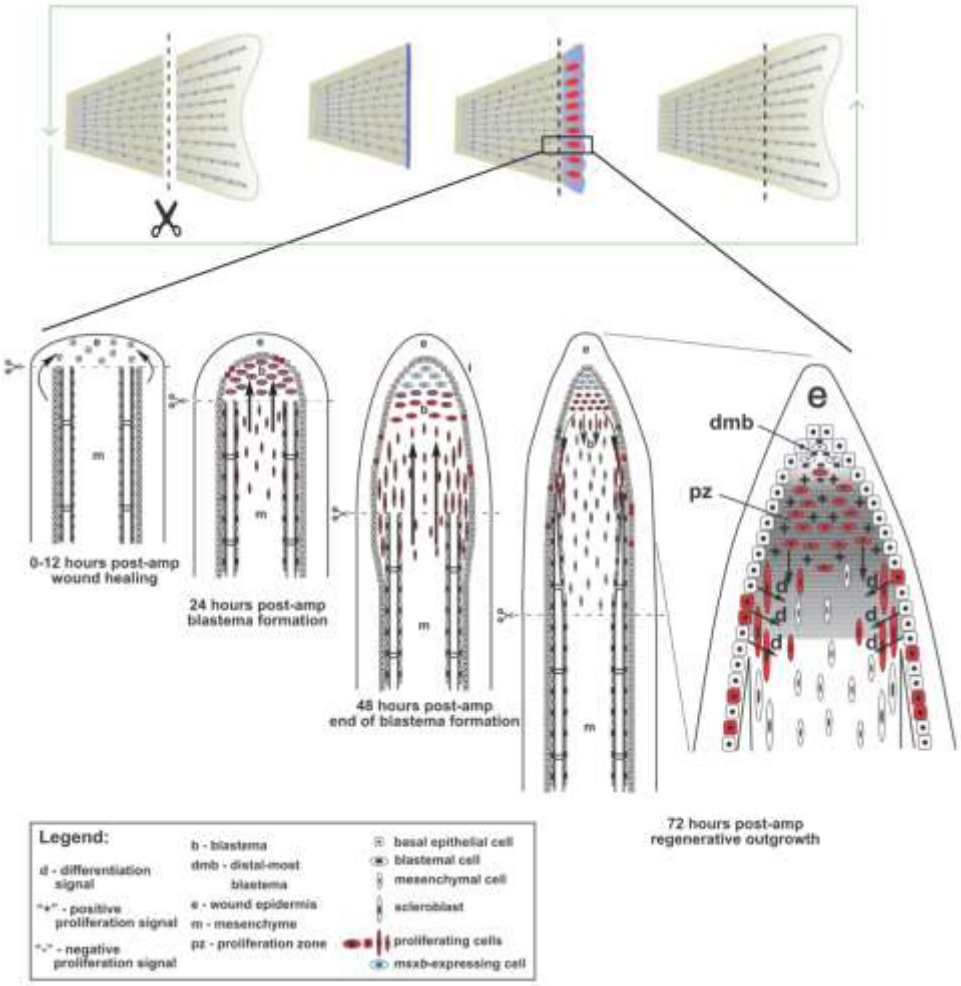

Figure 2. Zebrafish caudal fin regeneration. Upon amputation, regeneration takes place in several stages: wound healing, blastema formation and outgrowth. Blastema formation is essential and requires migration and proliferation of intrarray mesenchymal cells. Once fully formed, the blastema is divided in distal-most, distal and proximal regions, which have different functions. This process can occur repeatedly without consequences for the animal. Adapted from Kawakami, 2010; Nechiporuk and Keating, 2002.

1.2 Zebrafish Fin Fold Regeneration

During larval stages, the zebrafish exhibits an analogous structure to the adult caudal fin, the fin primordium or fin fold. Therefore, the fin fold has been established as a simpler but comparable regenerating system to the adult caudal fin model (Kawakami et al., 2004). At 2 days post fertilization (dpf), this avascular and boneless appendage is composed of several cell types, namely: two folded layers of epidermis which present different potential and have underlying basement membranes (Dane and Tucker, 1985)(Guellec et al., 2004)(Slanchev et al., 2009); a medial layer of dermal fibroblasts (Wood and Thorogood, 1984)(Feitosa et al., 2012); nerve fibers (peripheral axons of somatosensory Rohon-Beard neurons)(Rieger and Sagasti, 2011); resident blood cells (neutrophils and macrophages); and actinotrichia (Durán et al., 2011)(Zhang et al., 2010).

The fin fold's regenerative process occurs in three days, although faster than the adult system, it too has three phases (Figure 3): wound healing, blastema formation and regenerative outgrowth. During the wound healing, there is the sealing of the open wound (occurring in approximately one hour), performed by the surrounding epidermis, culminating in the formation of the specialized wound epithelium. Early signals emanated by the epidermis contribute to a successful regenerative process and promote the recruitment of immune cells towards the vicinity of the stump. These propagate in gradients and comprise calcium, hydrogen peroxide and changes in osmotic pressure (Niethammer et al., 2009)(Yoo et al., 2012)(Enyedi et al., 2013). During blastema formation, mesenchymal cells accumulate distally and proliferate. Lastly, during regenerative outgrowth, the structure is re-patterned (Kawakami et al., 2004). While the wound healing phase occurs in the first 3 hours, the duration of the blastema and outgrowth phases overlap, with no clear boundaries between each other.

In spite of the 2 dpf larval fin fold is still undergoing development and is not composed of fully differentiated cells, several studies have supported the idea that epimorphic regeneration occurs in this system. Of relevance, there is conservation of upregulated signaling molecules upon fin fold amputation also required in adult caudal fin and heart regeneration (Yoshinari et al., 2009)(Mathew et al., 2009)(Ishida et al., 2010). Also, the fact that regeneration in the fin fold system is unidirectional and the achievement of correct size and shape after amputation recapitulate the current developmental stage, favor the hypothesis that the fin fold regenerates via an epimorphic regeneration mechanism.

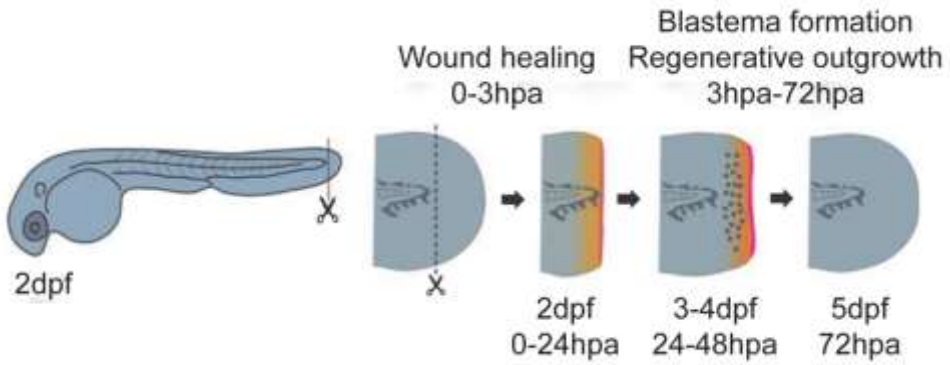

Figure 3. Zebrafish fin fold regeneration. Upon amputation, regeneration of the zebrafish fin fold takes place in similar steps as the adult: wound healing, blastema formation and regenerative outgrowth. This process occurs as fin development is taking place from 2dpf to 5dpf. Adapted from Kawakami, 2010.

2. Positional Information

Epimorphic regeneration, as observed in zebrafish caudal fins, has highly beneficial properties; the injured organs recover their original size and pattern and can regenerate countless times. Underlying this mechanism is the existence of positional information that instructs cells on how to pattern

the recovering organ. This concept was presented by Lewis Wolpert to describe the process by which a group of cells have their spatial location specified, leading to defined patterns of cell differentiation (Wolpert, 1969). Ultimately, this will stipulate the final form of tissues and organs during embryonic development.

The positional information mechanism accounts for situations where cells in a coordinate system respond to a specific region, source or *field*, from which positional values are defined and interpreted (Huxley and Beer, 1934)(Wolpert, 2011). This array of values is graded, varying along an axis or several axes in which spatial information flows, being a multidimensional process. Three basic features are needed for positional information to occur: 1) a mechanism establishing *polarity* (i.e. the orientation along the axis in which positional information is measured by the cells); 2) a mechanism enabling the cells to interpret the signaling differences within the given information, such as concentration thresholds; and 3) the existence of at least one self-limiting reaction, such as degradation of the morphogen (Wolpert, 1969)(Wartlick et al., 2009).

Classically the signals that are presented to the cells for determination of their position within a forming tissue are of biochemical nature. Alan Turing originally proposed the term *morphogen* to describe chemical substances that would "*produce form*" through diffusion (Turing, 1952). These propagate extracellularly through graded concentrations, conferring information in the target tissues via activated cell surface receptors, leading to specific spatial patterns of gene expression (Turing, 1952)(Wolpert, 1969)(Wartlick et al., 2011). Additionally, external forces can also lead to changes in final shape and pattern along time (Gustafson and Wolpert, 1967), therefore they may convey additional signals for positional information. This has been recently observed during *Drosophila* and zebrafish gastrulation, where mesoderm specification is achieved by specific tissue deformations that affect localized gene expression (Desprat et al., 2008)(Brunet et al., 2013).

2.1 Positional Memory in Regeneration

Within the field of positional information, there is positional memory, an unique instance of positional information that occurs during appendage epimorphic regeneration (Wolpert, 1969). Upon injury, cells that give rise to the blastema preserve their original comprehensive patterning information, using it to then re-populate the new organ. Initially observed by Lazzaro Spallanzani, and subsequently widely studied amongst the regeneration field (Spallanzani, 1769)(Morgan, 1906)(Nabrit, 1929)(Iten and Bryant, 1976)(Maden, 1976), the molecular details of how positional memory is achieved and regulated are still not fully understood.

Whereas during development extracellular secreted factors are major regulators of positional information during development, in regeneration positional memory appears to be controlled by a combination of cell autonomous and non-autonomous graded factors along the proximo-distal (PD) axis. Evidence supporting this is based in graft experiments in which limb cells from a distal region were transplanted to a proximal region. Remarkably, upon amputation the contribution of these cells along the PD axis was maintained, indicating an invariant PD positional identity, independent of their current surroundings, resembling a cell autonomous regulation. On the other hand, due to the unidirectionality of the regenerative process, in such transplants, proximal regions give rise to complete patterned distal structures (Kragl et al., 2008)(Tamura et al., 2010). This reflects the *rule of distal transformation*, in which regenerating cells with proximal identities are able to produce distal identity cells. Complementing this view, during zebrafish fin regeneration, the blastema cells become spatially restricted: once the blastema is fully formed, cells from different lineages acquire similar positions to the differentiated cells before injury, in determinate regions along the medial-lateral axis (Tu and Johnson, 2011).

Closely associated with positional memory of cells during regeneration, is the attainment of correct final size. Importantly, the regenerative growth rate will increase proportionally with the amount of injured tissue. This allows completion of the regenerative process always within the same time period, regardless of differences in amputation planes along the proximal-distal axis. Additionally, it indicates that according to the PD position value the cells possess, there are precise instructing guidelines for the recovery of the injured tissue (Morgan, 1906)(Wolpert, 1969). A signaling molecule associated with regulation of this process is Fgf (Lee et al., 2005). During zebrafish caudal fin regeneration, it was shown that this growth factor modulates the PD growth rate, by controlling cell proliferation levels. This indicates that this molecule can act in a PD gradient along the caudal fin; however Fgf was also shown to not be the positional memory granting molecule, as PD identity and size were maintained upon conditional depletion of this signaling pathway.

Despite much attention in the regulation of positional information along the proximal-distal axis, other axes also convey positional memory during regeneration. One well demonstrated case is the anterior-posterior (AP) axis of zebrafish pectoral fin, which shows particular transcription factor signatures according to the rays' position (Nachtrab et al., 2013). In particular, it was shown that while the most anterior rays express specifically *alx4a,* the most posterior rays have unambiguous expression of *hand2*. These two factors were shown to be crucial in the maintenance of the AP axis during regeneration, since their conditional manipulation led to misregulation of regenerative patterning, resulting in fins with rays presenting the morphology of only one of the AP axis signatures. Interestingly the cells that appear to respond to these signals are the same in both anterior and posterior rays: the intrarray osteoblasts and fibroblasts. The establishment of the AP axis transcription factor signatures occurs during fin embryonic development, before these cell types have been differentiated and patterned (Yelon et al., 2000), indicating a robust

mechanism for positional information and memory. A relevant question is whether similar PD axis establishment occurs during fin development, since both these cell types contribute to the blastema and its position-dependent growth rate.

3. Organ Size and Growth Control

Organ size and its growth control are fundamental aspects of animal development and regeneration. Classically, Stephen J. Gould introduced two types of correlations between animal (or organ) size and shape: isometric or allometric. The first represents the maintenance of geometrical similarity with size increase, resulting in constant growth proportions with respect to body size. The latter represents growth in different proportions with respect to body size. Allometry can be positive, when there is a greater increase of the organ growth rate when compared to the growth rate of total body size; or allometry can be negative, when the organ growth rate decreases as the total body size growth rate increases (Gould, 1966). The adult dimension of organs, and ultimately animals, results from a combination of tissue specific isometric and allometric growth.

During zebrafish development, the body and fins grow isometrically in relation to each other, maintaining proportionality and scaling in a constant manner (Goldsmith et al., 2006). There are examples of zebrafish mutants that fail to retain isometric fin growth during development, leading to animals with longer or shorter fins when compared to body size and siblings fin size (Goldsmith et al., 2003)(Iovine and Johnson, 2000)(Goldsmith et al., 2003).

Faithful recovery of original fin size during normal caudal fin regeneration means that cells within the blastema precisely control their growth rate, by increasing it in a small timeframe, leading to a transitory positive allometric growth type, until pre-injury fin size is attained and isometric growth rates

are re-implemented. At one level, final organ form and mass depend on the number of cells within the organ and, on another level, on the size of the cells (Conlon and Raff, 1999). Thus these processes must be controlled by basic cellular mechanisms that instruct cells to divide, to die, to grow or to stop in a timely and restrained manner.

3.1 Mechanisms of cell behavior

To reach final organ size during both development and regeneration, cell proliferation, cell death and cell size must be precisely coordinated.

Cell proliferation as the process in which one cell divides, to give rise to two daughter cells, can be stimulated or inhibited by a number of factors, hence is an extremely regulated process. The factors that promote cell division, commonly designated as mitogens, activate intracellular signaling pathways that prompt the production and/or activation of cell cycle components, allowing the progression of the cell cycle. Conversely, proliferation inhibitors, block the cell cycle, usually interfering at its checkpoints. The concentration of these factors, with mitogen concentrations often being limiting, can influence the rate of the undergoing cell cycle, allowing for proper control of cell numbers.

Cell death occurs by several mechanisms, but apoptosis (or programmed cell death) is the most common cell death route during development and regeneration (Kuan et al., 2000)(Chera et al., 2009). This process entails an activation of an intracellular program leading to the cell self-destruction. Apoptosis is many times triggered by low concentrations of extracellular survival factors (which inhibit the activation of apoptosis) or increased levels of extracellular apoptosis inducing factors (Raff, 1992). Hence, apoptosis is many times the resorted mechanism for controlling cell numbers within an organ.

Cell growth occurs when cells increase their mass. This process is closely interconnected to cell proliferation, since when cells divide they duplicate their contents before cytokinesis occurs (Gao et al., 1997)(Conlon and Raff, 1999). Although cell proliferation depends on cell growth, the reverse is not true, as growth does not depend on progression of the cell cycle (Neufeld et al., 1998). The mechanisms by which cells control their size remain largely unknown, but it is thought that certain molecules act as growth factors that activate intracellular signaling pathways, stimulating protein synthesis and other biosynthetic processes. This would in turn lead to an increase in the macromolecule producing rate within the cell, which would surpass the macromolecule degrading rate, resulting in cell enlargement (Conlon and Raff, 1999).

3.2 Mechanisms of growth transduction

Common to the previously described processes is the promiscuity in factor function. Often, survival factors also function as mitogens and as growth factors. Importantly, mechanisms that stop cell proliferation, cell survival or cell growth are determinant in attaining final organ size, in particular during a regenerative process. These regulatory mechanisms are yet poorly understood, but it is generally accepted that differences in cell number make a larger contribution towards organ size specification than differences in cell size (Raff, 1996)(Conlon and Raff, 1999).

Considering extracellular mechanisms that regulate cell numbers and consequently cease proliferation, two processes have emerged as central in detecting information from the cells' surrounding environment to regulate final organ size: cell contact inhibition and the extracellular matrix (ECM) stiffness. These two cases reflect mechanotransduction phenomena, where

mechanical stimuli are transformed into biochemical responses (Vogel and Sheetz, 2006).

The concept of contact inhibition of proliferation was initially introduced in the 1960s and greatly characterized by Harry Eagle and Elliot M. Levine, to describe the phenomenon by which cells in a monolayer slow their proliferative rates, with a cell cycle arrest in G1, as they reach confluence (Eagle and Levine, 1967). This led to the concept that the greater contact between cell surfaces, the greater inhibition of cell proliferation. The association between cell density and cell-cell contacts proposed the following requirements: the existence of cell receptors at the membrane level that sense and partake in physical interaction between different cell surfaces; intracellular signaling pathways that are influenced by the surface receptors in a contact dependent fashion; and the establishment of a functional connection between the receptors and the signaling pathways by molecular mechanisms (Mcclatchey and Yap, 2012). Importantly, junctional adhesion complexes, namely cadherins and catenins, have been shown to act as cell surface receptors in this context, not only by establishing cell contacts with the neighboring cells according to cell density, but also by mediating downstream cell signaling and proliferation (Stepniak et al., 2009). In fact cadherins and catenins are considered mechanosensory molecules, as they can detect differences in microenvironment forces and change their conformation accordingly, leading to the stabilization of the adhesion sites between cells (Liu et al., 2010)(Gomez et al., 2011) (Figure 4 Adherens junction box).

Coupled to the early cell contact inhibition observations, it was shown that an increase in cell confluence led to a decrease in the growth factor cell response, even in unlimited growth factor medium conditions, slowing proliferation (Vogel et al., 1980). This regulation remains unclear, but some models have been proposed: 1) junctional complexes may work as physical barriers that separate the growth factor receptors from their ligands; 2) interaction between growth factor receptors and cadherins can lead to

intracellular signaling inhibition; or 3) comprehensive changes in cell architecture after cell-cell junction formation stimulated by density could limit the growth factor signaling response (Mcclatchey and Yap, 2012).

The ECM is the primary extracellular component of all tissues and organs, consisting of a 3D surrounding scaffold that provides physical support to cells. This meshwork is a combination of secreted proteins that include collagens, elastins, proteoglycans, laminins and fibronectin. This composition is highly dynamic as it varies according to the tissue and it is continuously remodeled. The ECM has numerous and complex biological functions, namely in cell migration (as an adhesion substrate for cells to migrate) and in regulating multiple intercellular biochemical signals, hence contributing to many cell processes, including proliferation and apoptosis.

Depending on the tissue, the ECM can present various levels of rigidity (i.e. stiffness), which corresponds to the measured displacement per unit of applied force of the matrix substrate (Vogel and Sheetz, 2006). A certain rigidity is conditional to the ECM components existing at a given time, their organization and degree of molecular crosslinking (DuFort et al., 2011). This can trigger individual cell responses, since higher matrix rigidities lead to increased ECM attachment by the cells. The mechanical cues dependent on ECM stiffness have been shown to play key roles in the control of cell proliferation and differentiation, contributing to the achievement of final organ form and size. Regarding cell proliferation, stiffer ECMs (approximately 40KPa) elicit an increase in cell numbers while softer ECMs (approximately 0.7KPa) lead to the arrest of the cell cycle (Engler et al., 2006).

As in contact inhibition of proliferation, mechanotransduction via the ECM also requires the presence of cell surface receptors, intracellular signaling pathways that transduce the information and a functional link between the two. The interactions between the cells and the ECM can occur through specialized cell surface receptors, the integrins – which establish the link between the extracellular environment and cytoskeleton adaptors in focal

adhesion complexes, acting as mechanosensors (DuFort et al., 2011) (Figure 4 Focal adhesion box).

Both cell contact inhibition and ECM stiffness lead to changes in cell geometry: high cell densities and/or soft matrices result in rounder cells that proliferate less (Figure 4A); conversely larger intercellular spaces and/or high ECM rigidities, allow the cells to become flattened and spread out, promoting proliferation (Figure 4B) (Vogel and Sheetz, 2006)(DuFort et al., 2011). This also reflects a combined action with the cell cytoskeleton and contractility, since the junctional complexes or integrins are linked to filamentous (F)-actin microfilaments. F-actin microfilaments can act by themselves as mechanosensors, being remodeled and distributed according to the upstream input and signaling for downstream cell behaviors.

The cellular processes of contact inhibition of proliferation and ECM stiffness entail the cells' capacity to integrate multiple upstream cues at the mechanosensory level, allowing modes of regulation of final cell numbers during developmental and regenerating processes, independently of diffusion of extracellular chemical signals. Few studies have addressed the role of the ECM in regeneration (Calve and Simon, 2012)(Mercer et al., 2013) and characterization of regenerative systems where contact inhibition may occur are unexplored. These processes should function in regeneration like in other systems: as sensors of the integrity of the tissue, in such a way that discontinuities or disruptions within the damaged tissues are reflected in cell-cell contacts or ECM stiffness allowing cells to grow faster and restore proper cell numbers (Peyton et al., 2007).

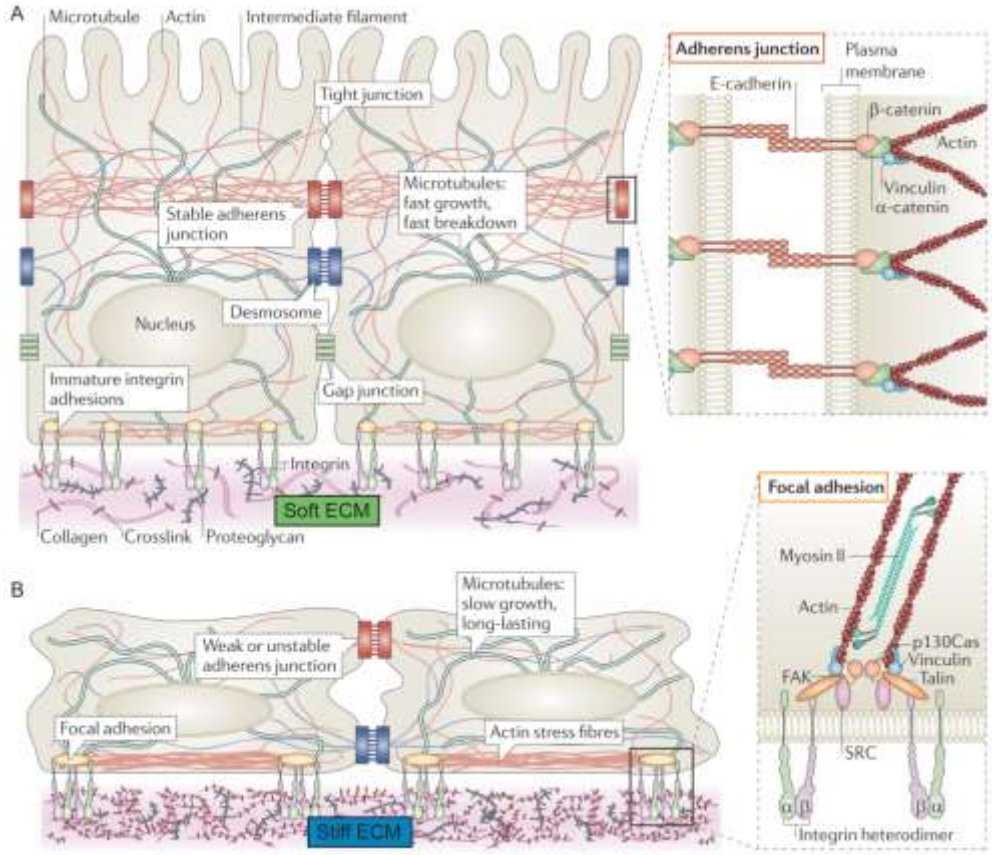

Figure 4. The cell mechanosensory network. A Cells in soft ECMs have immature cell-matrix adhesions but are able to establish stable cell-cell contacts, such as adherens junctions. The cell cytoskeleton in these conditions is concentrated at the cortical level, apically, linking intracellularly the cell junctions. Adherens junctions are cell-cell communication complexes that use transmembrane proteins (such as E-cadherin) that connect to several intracellular adaptor proteins and the cell cytoskeleton. **B** Cells in stiff ECMs have reduced cell-cell junctions, but mature focal adhesions. The cell cytoskeleton in these conditions is concentrated basally, linking intracellularly the focal adhesions. Focal adhesions are composed of transmembrane heterodimers of integrins which connect to intracellular adaptor proteins (such as Talin), also establishing the link to the cell cytoskeleton. Adapted from DuFort et al., 2011.

4. Hippo/Yap Pathway

The Hippo pathway has emerged as a highly conserved signal-transducing pathway that is able to regulate final organ size via control of cell proliferation, apoptosis and cell differentiation. The initial identification of this kinase cascade was found in *Drosophila* genetic screens, which identified tumor suppressor genes that when mutated lead to overgrowth phenotypes. Remarkably, there is a conservation of the core Hippo pathway both in structure and in function throughout the eukaryotic kingdom. In mammals, many of the core components of the pathway have suffered gene duplications, but most of them have homologs and a similar role to their *Drosophila* counterparts. The *Drosophila* studies led to the recognition of a core module of proteins composed of two kinases, Hippo and Warts (Mst1, Mst2 and Lats1, Lats2 respective mammalian homologs), together with their respective adaptor proteins, Salvador and Mats (Mob in mammals)(Pan, 2010)(Udan et al., 2003)(Justice et al., 1995)(Xu et al., 1995)(Tapon et al., 2002)(Kango-Singh et al., 2002)(Lai et al., 2005). When activated, these factors promote sequential phosphorylation of each other, culminating in the phosphorylation of the pathway effector Yorkie (Yki, Yap and Taz mammalian homologs), which results in its cytoplasmic retention (Huang et al., 2005)(Lei et al., 2008) (Figure 5A,B). When the core kinase cassette is inhibited, Yorkie is free to enter the nucleus, where it acts as a transcriptional co-activator by associating with its DNA binding partner, Scalloped (Goulev et al., 2008). When active, Yorkie (via Scalloped) promotes the transcription of specific target genes that stimulate proliferation and inhibit apoptosis, such as *cyclinE* or *diap1*. In addition to Scalloped, Yorkie can have other DNA binding partners in a tissue dependent manner (Goulev et al., 2008).

A multitude of upstream regulators of the *Drosophila* pathway have been found that comprise different groups of proteins leading to activation of the

core components. For example, Merlin together with Expanded and Kibra form an apical protein complex that is able to activate Hippo, leading to the subsequent activation of the pathway (Yu et al., 2010). This complex responds to the transmembrane polarity protein Crumbs. Alternatively, the core cassette can be activated by the action of the atypical cadherins Fat and Dachsous, which is modulated by Four-jointed activity (Cho et al., 2006). Upon activation, Fat and Dachsous act via the unconventional myosin Dachs and the actin adaptor Zyxin, which phosphorylates Warts (Rauskolb et al., 2011).

Other cell contact proteins, associated with adherens junctions, such as E-Cadherin, Alpha-Catenin, Ajuba and Echinoid lead to activation of the core components of the pathway (Robinson and Moberg, 2011)(Yue et al., 2012). Associated with septate junctions are Scribbled, Lgl and Discs-large that also elicit activation of the kinase cassette (Genevet and Tapon, 2011). More recently, GPCRs have also been implicated in the activation of the pathway via F-actin, by a still unclear mechanism (Regué et al., 2013) (Figure 5A).

On the other hand, the conservation of upstream inputs of the mammalian Hippo pathway activation is still not very explored. Although upstream regulation by Nf2 (Merlin homolog) and Kibra is observed, regulation by the Fat-Dachsous module, Echinoid and even Expanded appear to have evolved specifically within the Diptera order. Instead, mammals have Angiomotin, which associates to Crumbs polarity complex at the tight junctions level, performs similar functions to Expanded. Of note, Yap and Taz are structurally more diverse when compared to the fly Yorkie, as they contain a serine-rich phospho motif in their C-terminal that targets them to ubiquitylation and proteasome-mediated degradation (Bossuyt et al., 2013).

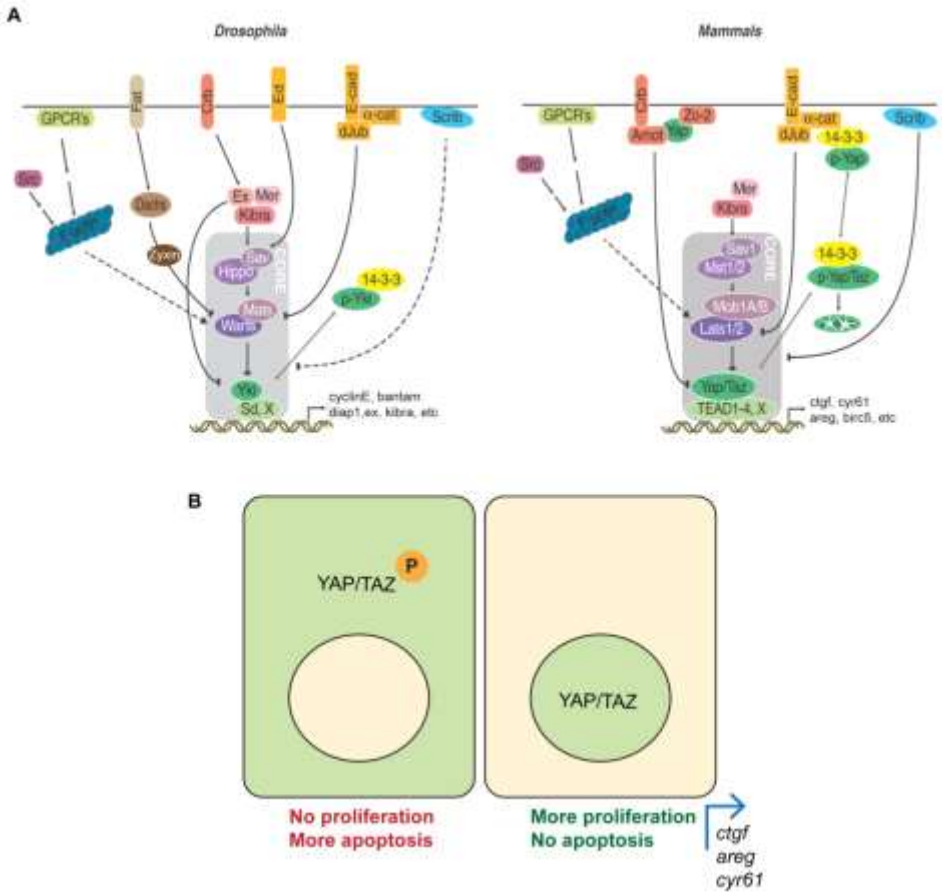

Figure 5. A The *Drosophila* and mammalian Hippo pathways. Upstream regulatory components typically have a member which is connected to the cell membrane and several cytoplasmic proteins. Hippo pathway core components are all cytoplasmic and are activated in a kinase cascade fashion, until reaching Yorkie(Yki)/Yap/Taz. This protein, when activated, can stimulate the transcription of target genes by connecting with DNA binding partners (Scalloped, Sd or TEAD1-4). Adapted from Bossuyt et al., 2013. **B** Intracellular Yap/Taz (Yorkie) activation dynamics. When the Hippo pathway is active, Yap/Taz are retained in the cytoplasm, inactive through phosphorylation. Conversely, when the Hippo pathway is inactive, Yap/Taz are free to enter the nucleus, being active and able to form a complex with their DNA binding partners.

Structurally and functionally, Yap and Taz are mostly redundant, differing principally in their WW domains: while Yap has two tandem WW domains, Taz only has one. These domains detect a PPxY motif (Proline, Proline, any

aminoacid, Tyrosine) important for Yap/Taz localization. Also, Yap has a PxxΦP motif (where Φ is a hydrophobic residue) that is not conserved in Taz, possibly accounting for differences in TEA-Domain binding (TEAD, Scalloped homolog)(Zhao et al., 2008) and causing differences in target transcriptional activation (Varelas, 2014). Interestingly, Yap/Taz transcriptional targets, such as *connective tissue growth factor* (*ctgf*), *cysteine-rich 61* (*cyr61*) and *amphiregulin* (*areg)*, also promote proliferation and prevent apoptosis, but are not homologs of *Drosophila* bona-fide targets (Zhao et al., 2008)(Zhang et al., 2009).

Considering Yap/Taz motifs, they share a PDZ-binding motif at their C-termini, which allows interactions with numerous transmembrane and cytoskeleton proteins and a transcriptional activation domain (TAD). In addition, an N-terminal TEAD binding region, contains the specific and conserved phosphorylation site targeted by 14-3-3 upon Lats1/2 induction (Ser127 in human Yap, Ser89 in human Taz). Substitution of these TEAD binding sites with alanines jeopardizes Lats 1/2 ability to inactivate Yap/Taz, leading to Yap/Taz overactivation and consequently overgrowth phenotypes (Varelas, 2014) (Figure 6).

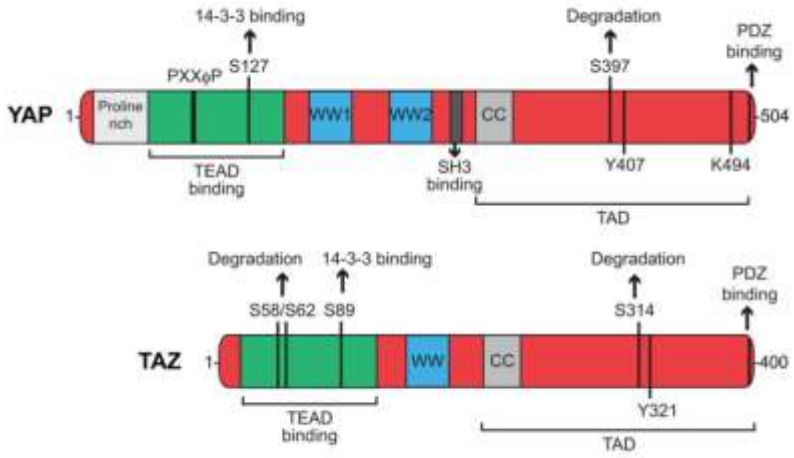

Figure 6. Mammalian Yap and Taz functional structures. Adapted from Varelas, 2014.

4.1 Mechanotransduction pathway – link with the cytoskeleton and cell geometry

Recently the Hippo pathway has been identified as an intracellular signaling pathway that can transduce physical information provided by the extracellular environment through cell surface receptors, shedding new light into mechanotransduction mechanisms regulating final organ size. In particular, Yap/Taz react to mechanical cues provided by contact inhibition or matrix rigidity (Zhao et al., 2007)(Dupont et al., 2011). When cells are sparse or the matrix is stiff, Yap/Taz are activated and translocate to the nucleus, promoting the transcription of its target genes and consequently promoting proliferation (Figure 7A). In opposition, when cells are confluent or the matrix is soft, Yap/Taz are retained in the cytoplasm and thus inactive (Figure 7B). As introduced previously, these mechanical cues induce changes in cell geometry and cell cytoskeleton, in particular F-actin localization. In particular, when cells are round, small and Yap is inactive, F-actin is localized mostly to the cortical regions of the cell, associated with the cell membrane and junctions; in contrast, when cells become flat, spread and Yap is active, F-actin re-localizes to stress fibers, in the medial cytoplasm (Dupont et al., 2011)(Wada et al., 2011).

The link between Yap/Taz and F-actin is still not fully understood, but it has been shown that manipulating F-actin brings functional consequences for Yap/Taz. When F-actin polymerization is impaired, Yap/Taz are also inhibited, even when the environmental surroundings of the cells, such as stiff matrices, prone to Yap/Taz activation in the nucleus (Dupont et al., 2011). This has also been shown by specific genetic manipulations in genes that affect F-actin polymerization state, such as CapZ, Gelsolin or Cofilin. These are F-actin capping/severing proteins, which when downregulated, lead to Yap/Taz activation in situations that normally these would be inactive, such as dense cultured cells (Aragona et al., 2013). Similar

phenotypes in Yap/Taz intracellular localization are obtained when chemically inhibiting contractility associated proteins RhoGTPase, Myosin Light Chain 2 or ROCK, reflecting that Yap/Taz are indeed responding to changes in cytoskeletal tension (Dupont et al., 2011).

The fact that Yap/Taz react to changes in F-actin levels and not other actin types, reveals a specific growth function for this molecule depending on extracellular tension the cells are exposed to (Dupont et al., 2011)(Reddy et al., 2013). The ways by which F-actin and Yap/Taz can interact are still elusive, but several models have been proposed, namely: tethering mechanisms, in which F-actin filaments are able to grasp Yap when localized at the cortical level, releasing it when F-actin is re-localized into medial cytoplasmic stress fibers; or specific interactions of Yap/Taz with F-actin modulators and adaptors that bind to F-actin ends depending on its cytoskeletal conformation, influencing Yap's activation state (Matsui and Lai, 2013).

Closely related with the actin cytoskeleton and central to Yap/Taz regulation are cell-cell junctions, namely the adherens junction complex via Alpha-Catenin. As stated previously, these junctions present mechanosensory roles in contact inhibition of proliferation. In confluent conditions, Alpha-Catenin is stabilized at the membrane level and retains Yap in the cytoplasm via interaction with its PDZ domain, consequently leading to its degradation via 14-3-3 recruitment. Conversely, in sparse culture conditions, Alpha-Catenin is not at the cell membrane allowing a re-localization of Yap to the nucleus (Schlegelmilch et al., 2011)(Silvis et al., 2011) (Figure 7). Since Alpha-Catenin is a membrane structural linker and is able to bundle F-actin (Shapiro and Weis, 2009), alternative joint regulatory modes for Alpha-Catenin and the Hippo/Yap pathway remain to be explored, either directly or through adaptor proteins, like Ajuba, Zyxin or Angiomotin (Marie et al., 2003)(Rauskolb et al., 2014)(Mana-Capelli et al., 2014).

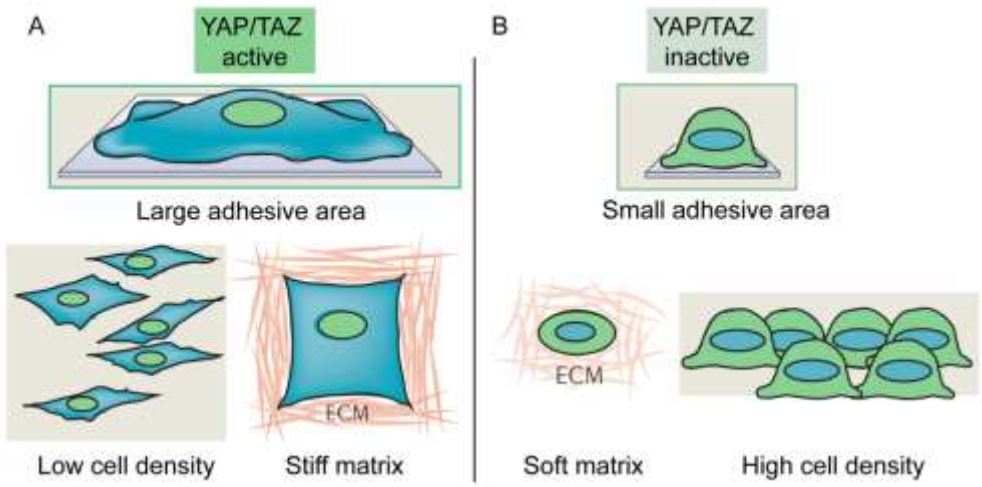

Figure 7. Multiple mechanical inputs regulate Yap/Taz activation. A Large adhesive areas lead to Yap/Taz activation (nuclear localization). This can be caused by low cell densities and/or stiff matrices. **B** Small adhesive areas lead to Yap/Taz inactivation (cytoplasmic localization). This can result of soft matrices and/or high cell densities. Adapted from Halder *et al*., 2012.

4.2 Roles in Repair and Regeneration

Due to its functions in regulating cell numbers during developmental processes, the Hippo pathway has become a key pathway to be addressed in repair situations. The initial clue that this pathway could play a major role in injury recovering tissues was found in the *Drosophila* intestine. It was shown that upon damage, Yki is activated in the intestinal stem cells and enterocytes, allowing proliferation to occur replacing the needed cells. In this system, the activation of the JNK and Jak/Stat signaling pathways that inhibit the Hippo core kinase cascade leads to Yki activation (Shaw et al., 2010)(Staley and Irvine, 2010). This phenomenon was found to be conserved in mouse models of intestinal repair, with Yap being required for

proper intestine regeneration but not for the normal homeostasis process (Cai et al., 2010)(Zhou et al., 2011).

More recently, in neonatal mice hearts, which retain the ability to restore cardiomyocyte numbers upon damage, has been shown that Yap/Taz promote this regenerative capacity by stimulating IGF and Wnt pathways. Conversely, in the adult mice heart that shows limited regenerative abilities, the core kinase Hippo cascade appears to be active even in injury situations, restricting Yap pro-proliferative abilities (Xin et al., 2013)(Heallen et al., 2013). Also in mouse models, Yap and Taz were shown to regulate cutaneous wound healing: downregulation of either of these genes leads to a delay in wound healing (Lee et al., 2013)

In animals with greater regenerative capabilities such as flatworms, Yki/Yap have pleiotropic functions related to size control, namely in maintaining organ homeostasis and regeneration, stem cell proliferation and axial patterning (Lin and Pearson, 2014)(Demircan and Berezikov, 2013). In epimorphic regeneration situations, the role of the Hippo/Yap pathway remains little investigated, nevertheless in *Xenopus* limb bud regeneration it has been shown that Yap was upregulated upon amputation and controlled cell proliferation levels, being required for regeneration to proceed (Hayashi et al., 2014). Moreover, through the use of a conditional dominant negative form of Yap, ectopic apoptosis was induced and regeneration was defective (Hayashi et al., 2014).

4.3 Regulatory Functions in Stemness and Differentiation

Since the initial reports on the role of Hippo pathway controlling developmental cell proliferation and consequently organ size, several studies have arisen drawing attention to its potential functions as a main regulator of cell differentiation and establishing cell fate. In particular,

studies in various tissue specific progenitors and stem cell types have shown that ectopic expression of Yap inhibits differentiation and maintains undifferentiated progenitor states, namely in the epidermis, intestine, muscle, neural tube as well as mesenchymal stem cell populations (Figure 8A). This effect was also observed in mouse embryonic stem cells and in induced pluripotent stem cells. On the contrary, Yap knockdown leads to loss of pluripotency states (Zhao et al., 2011)(Hiemer and Varelas, 2013).

Importantly, Yap/Taz are involved in the determination of the first cell fate decision in the mouse embryo: the choice between trophectoderm and inner cell mass. The intracellular distribution of Yap/Taz within the blastocyst is controlled by apical-basal polarity proteins. The more compacted, apolar cells with cytoplasmic Yap/Taz, will become inner cell mass cells; conversely, in sparser, polarized cells with nuclear Yap/Taz, trophectoderm forms (Nishioka et al., 2009)(Varelas, 2014) (Figure 8B).

In regeneration situations that depend on stem cell activation, such as the intestine, Yap/Taz not only stimulate proliferation, but also maintain and expand the progenitor pool, via cooperation with other signaling pathways, such as Wnt and TGFβ (Mauviel et al., 2011)(Azzolin et al., 2012)(Barry et al., 2012)(Fujii et al., 2012). Recently, it has been shown that Yap plays a key role in inducing dedifferentiation of hepatocytes upon partial liver removal, through activation of the Notch pathway (Yimlamai et al., 2014). In the context of epimorphic regeneration, in which several lineages must dedifferentiate and contribute to the blastema, Yap/Taz roles have never been addressed.

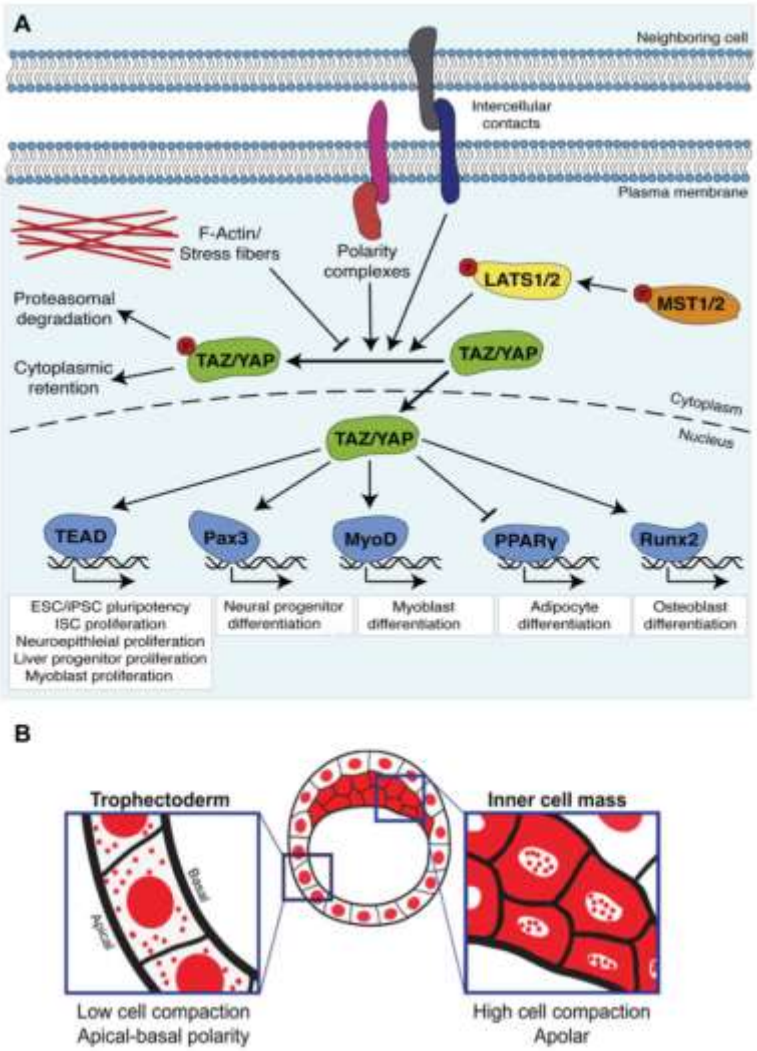

Figure 8. Yap/Taz intracellular localization influences cell differentiation decisions. A Active Yap/Taz can bind to a variety of transcription factors promoting self-renewal or differentiation of different cell types, directing cell fate. ESC, embryonic stem cells; iPSC, induced pluripotent stem cells; ISC, intestinal stem cells. Adapted from Hiemer and Varelas, 2013. **B** Depending on their intracellular localization, Yap/Taz lead to different cell fate outcomes in the early mouse embryo. In the outer cells, Yap/Taz are active (nuclear) leading to trophectoderm formation; in the inner cells, Yap/Taz are inactive (cytoplasmic) leading to inner cell mass formation. Adapted from Varelas, 2014.

4.4 The Hippo/Yap pathway in Zebrafish

In zebrafish, the conservation in components and function of the Hippo pathway has remained little explored, although the main core components are present and many similarities with the mammals' Hippo pathway do exist. Several studies have shown important roles for some members of the Hippo pathway, namely Yap and Taz, during zebrafish development. These include the developing zebrafish brain, eyes, neural crest and pronephros (Jiang et al., 2009)(Engel et al., 2009)(Yuan et al., 2009)(Hu et al., 2013). Importantly, some studies have identified a role in cell differentiation during zebrafish development similar to what has been described in mammals (Hong et al., 2005)(Gee et al., 2011)(Asaoka et al., 2014). Nonetheless issues addressing growth control for the establishment or recovery of final organ size have never been thoroughly addressed.

5. Aims and Scope

The ability to recapitulate a lost organ upon severe tissue damage is a prominent feature of vertebrate epimorphic regeneration. In this process, the accurate retrieval of native organ size and form constitute important characteristics. Classically, studies on regenerative growth control have focused on morphological properties. More recently, a molecular approach has been undertaken and led to the identification of regulatory factors, whose contribution to final organ size is still not entirely understood.

This PhD thesis aims at understanding the fundamental biology of size-control during regeneration, using the zebrafish caudal fin and fin fold as model systems. The central intent is to study, identify and extend the knowledge on the mechanisms by which final organ size is accomplished and how this process is regulated by positional information cues during injury situations.

In *Chapter II*, I demonstrate that the larval fin fold is a suitable model for *in vivo* regeneration studies, by using live imaging, and explore the relations between tissues and cells contributing for this regenerative system. This analysis was performed with the goal of further understanding the mechanisms and cell behaviors by which regenerating systems sustain positional memory.

In *Chapter III*, I describe the establishment of a chemical screen assay in zebrafish fin fold regeneration, designed to target and identify small molecules affecting organ size upon amputation. This strategy pursued the main objective of broadening our knowledge of signaling pathways that instruct or interfere with position information, affecting final size during epimorphic regeneration.

In *Chapter IV*, I investigate how regenerative growth is governed by extracellular mechanical inputs in the adult zebrafish caudal fin, influencing the recovery of fin size upon injury. In particular, the primary purpose of this

work was to explore new and alternative mechanisms of growth control within the epimorphic regeneration field.

The final chapter of this thesis, *Chapter V*, is a general discussion of the results obtained, integrating and correlating them with the most recent literature. Furthermore, I propose future directions for the study of positional memory and organ size in regeneration as well as consider parallels on growth control between regeneration and cancer biology.

6. References

Aragona, M., Panciera, T., Manfrin, A., Giulitti, S., Michielin, F., Elvassore, N., Dupont, S., and Piccolo, S. (2013). A Mechanical Checkpoint Controls Multicellular Growth through YAP/TAZ Regulation by Actin-Processing Factors. Cell 1–13.

Asaoka, Y., Hata, S., Namae, M., Furutani-Seiki, M., and Nishina, H. (2014). The Hippo Pathway Controls a Switch between Retinal Progenitor Cell Proliferation and Photoreceptor Cell Differentiation in Zebrafish. PLoS One *9*, e97365.

Azevedo, A.S., Grotek, B., Jacinto, A., Weidinger, G., and Saúde, L. (2011). The Regenerative Capacity of the Zebrafish Caudal Fin Is Not Affected by Repeated Amputations. PLoS One *6*, e22820.

Azzolin, L., Zanconato, F., Bresolin, S., Forcato, M., Basso, G., Bicciato, S., Cordenonsi, M., and Piccolo, S. (2012). Role of TAZ as Mediator of Wnt Signaling. Cell *151*, 1443–1456.

Barry, E.R., Morikawa, T., Butler, B.L., Shrestha, K., Rosa, R. De, Yan, K.S., Fuchs, C.S., Magness, S.T., Smits, R., Ogino, S., et al. (2012). Restriction of intestinal stem cell expansion and the regenerative response by YAP. Nature.

Blum, N., and Begemann, G. (2011). Retinoic acid signaling controls the formation, proliferation and survival of the blastema during adult zebrafish fin regeneration. Development *116*, 107–116.

Boominathan, V.P., and Ferreira, T.L. (2012). Factors promoting increased rate of tissue regeneration: the zebrafish fin as a tool for examining tissue engineering design concepts. Zebrafish *9*, 207–219.

Bossuyt, W., Chen, C., Chen, Q., Sudol, M., Mcneill, H., Pan, D., Kopp, a, and Halder, G. (2013). An evolutionary shift in the regulation of the Hippo pathway between mice and flies. Oncogene 1–11.

Brunet, T., Bouclet, A., Ahmadi, P., Mitrossilis, D., Driquez, B., Brunet, A.-C., Henry, L., Serman, F., Béalle, G., Ménager, C., et al. (2013). Evolutionary conservation of early mesoderm specification by mechanotransduction in Bilateria. Nat. Commun. *4*, 2821.

Cai, J., Zhang, N., Zheng, Y., de Wilde, R.F., Maitra, A., and Pan, D. (2010). The Hippo signaling pathway restricts the oncogenic potential of an intestinal regeneration program. Genes … *24*, 2383–2388.

Calve, S., and Simon, H.-G. (2012). Biochemical and mechanical environment cooperatively regulate skeletal muscle regeneration. FASEB J. 1–8.

Campbell, L.J., Suárez-Castillo, E.C., Ortiz-Zuazaga, H., Knapp, D., Tanaka, E.M., and Crews, C.M. (2011). Gene expression profile of the regeneration epithelium during axolotl limb regeneration. Dev. Dyn. *240*, 1826–1840.

Chera, S., Ghila, L., Dobretz, K., Wenger, Y., Bauer, C., Buzgariu, W., Martinou, J., and Galliot, B. (2009). Apoptotic cells provide an unexpected source of Wnt3 signaling to drive hydra head regeneration. Dev. Cell *17*, 279–289.

Cho, E., Feng, Y., Rauskolb, C., Maitra, S., Fehon, R., and Irvine, K.D. (2006). Delineation of a Fat tumor suppressor pathway. Nat. Genet. *38*, 1142–1150.

Christensen, R.N., and Tassava, R. a (2000). Apical epithelial cap morphology and fibronectin gene expression in regenerating axolotl limbs. Dev. Dyn. *217*, 216–224.

Conlon, I., and Raff, M. (1999). Size control in animal development. Cell *96*, 235–244.

Dane, P.J., and Tucker, J.B. (1985). Modulation of epidermal cell shaping and extracellular matrix during caudal fin morphogenesis in the zebra fish Brachydanio rerio. J. Embryol. Exp. Morphol. *87*, 145–161.

Demircan, T., and Berezikov, E. (2013). The Hippo pathway regulates stem cells during homeostasis and regeneration of the flatworm Macrostomum lignano. Stem Cells Dev. *22*, 2174–2185.

Desprat, N., Supatto, W., Pouille, P.-A., Beaurepaire, E., and Farge, E. (2008). Tissue deformation modulates twist expression to determine anterior midgut differentiation in Drosophila embryos. Dev. Cell *15*, 470–477.

DuFort, C.C., Paszek, M.J., and Weaver, V.M. (2011). Balancing forces: architectural control of mechanotransduction. Nat. Rev. Mol. Cell Biol. *12*, 308–319.

Dunis, D. a, and Namenwirth, M. (1977). The role of grafted skin in the regeneration of x-irradiated axolotl limbs. Dev. Biol. *56*, 97–109.

Dupont, S., Morsut, L., Aragona, M., Enzo, E., Giulitti, S., Cordenonsi, M., Zanconato, F., Le Digabel, J., Forcato, M., Bicciato, S., et al. (2011). Role of YAP/TAZ in mechanotransduction. Nature *474*, 179–183.

Durán, I., Marí-Beffa, M., Santamaría, J.A., Becerra, J., and Santos-Ruiz, L. (2011). Actinotrichia collagens and their role in fin formation. Dev. Biol. *354*, 160–172.

Eagle, H., and Levine, E. (1967). Growth regulatory effects of cellular interaction. Nature.

Echeverri, K., Clarke, J.D.W., and Tanaka, E.M. (2001). In vivo imaging indicates muscle fiber dedifferentiation is a major contributor to the regenerating tail blastema. Dev. Biol. *236*, 151–164.

Endo, T., Bryant, S. V, and Gardiner, D.M. (2004). A stepwise model system for limb regeneration. Dev. Biol. *270*, 135–145.

Engel, C., Moeller, M.J., Englert, C., Bollig, F., Scha, T., Mlodzik, M., Huber, T.B., Kuehn, E.W., Kim, E., Kramer-zucker, A., et al. (2009). Scribble participates in Hippo signaling and is

required for normal zebrafish pronephros development. Proc. Natl. Acad. Sci. U. S. A. *106*, 8579–8584.

Engler, A.J., Sen, S., Sweeney, H.L., and Discher, D.E. (2006). Matrix elasticity directs stem cell lineage specification. Cell *126*, 677–689.

Enyedi, B., Kala, S., Nikolich-Zugich, T., and Niethammer, P. (2013). Tissue damage detection by osmotic surveillance. Nat. Cell Biol. *15*, 1–10.

Feitosa, N.M., Zhang, J., Carney, T.J., Metzger, M., Korzh, V., Bloch, W., and Hammerschmidt, M. (2012). Hemicentin 2 and Fibulin 1 are required for epidermal-dermal junction formation and fin mesenchymal cell migration during zebrafish development. Dev. Biol. *369*, 235–248.

Ferretti, P., and Health, C. (2006). Regeneration of vertebrate appendages. eLS 1–7.

Fujii, M., Toyoda, T., Nakanishi, H., Yatabe, Y., Sato, A., Matsudaira, Y., Ito, H., Murakami, H., Kondo, Y., Kondo, E., et al. (2012). TGF-β synergizes with defects in the Hippo pathway to stimulate human malignant mesothelioma growth. J. Exp. Med. *209*, 479–494.

Gao, F.B., Durand, B., and Raff, M. (1997). Oligodendrocyte precursor cells count time but not cell divisions before differentiation. Curr. Biol. *7*, 152–155.

Gargioli, C., and Slack, J.M.W. (2004). Cell lineage tracing during Xenopus tail regeneration. Development *131*, 2669–2679.

Gee, S.T., Milgram, S.L., Kramer, K.L., Conlon, F.L., and Moody, S. a (2011). Yes-Associated Protein 65 (YAP) Expands Neural Progenitors and Regulates Pax3 Expression in the Neural Plate Border Zone. PLoS One *6*, e20309.

Genevet, A., and Tapon, N. (2011). The Hippo pathway and apico-basal cell polarity. Biochem. J. *436*, 213–224.

Geraudie, J., and Singer, M. (1985). Necessity of an adequate nerve supply for regeneration of the amputated pectoral fin in the teleost Fundulus. J. Exp. Zool. *234*, 367–374.

Goldsmith, M.I., Fisher, S., Waterman, R., and Johnson, S.L. (2003). Saltatory control of isometric growth in the zebrafish caudal fin is disrupted in long fin and rapunzel mutants. Dev. Biol. *259*, 303–317.

Goldsmith, M.I., Iovine, M.K., Reilly-pol, T.O., and Johnson, S.L. (2006). A developmental transition in growth control during zebrafish caudal fin development. Dev. Biol. *296*, 450 – 457.

Gomez, G. a, McLachlan, R.W., and Yap, A.S. (2011). Productive tension: force-sensing and homeostasis of cell-cell junctions. Trends Cell Biol. *21*, 499–505.

Gould, S. (1966). Allometry and size in ontogeny and phylogeny. Biol. Rev.

Goulev, Y., Fauny, J.D., Gonzalez-Marti, B., Flagiello, D., Silber, J., and Zider, A. (2008). SCALLOPED interacts with YORKIE, the nuclear effector of the hippo tumor-suppressor pathway in Drosophila. Curr. Biol. *18*, 435–441.

Grotek, B., Wehner, D., and Weidinger, G. (2013). Notch signaling coordinates cellular proliferation with differentiation during zebrafish fin regeneration. Development *1423*, 1412–1423.

Guellec, D.L.E., Morvan-Dubois, G., Sire, J.-Y., and Le Guellec, D. (2004). Skin development in bony fish with particular emphasis on collagen deposition in the dermis of the zebrafish (Danio rerio). Int. J. Dev. Biol. *48*, 217–231.

Gustafson, T., and Wolpert, L. (1967). Cellular movement and contact in sea urchin morphogenesis. Biol. Rev. Camb. Philos. Soc. *42*, 442–498.

Halder, G., Dupont, S., and Piccolo, S. (2012). Transduction of mechanical and cytoskeletal cues by YAP and TAZ. Nat. Rev. Mol. Cell Biol. *13*, 591–600.

Hayashi, S., Tamura, K., and Yokoyama, H. (2014). Yap1, transcription regulator in the Hippo signaling pathway, is required for Xenopus limb bud regeneration. Dev. Biol. *388*, 57–67.

Heallen, T., Morikawa, Y., Leach, J., Tao, G., Willerson, J.T., Johnson, R.L., and Martin, J.F. (2013). Hippo signaling impedes adult heart regeneration. Development *140*, 4683–4690.

Hiemer, S.E., and Varelas, X. (2013). Stem cell regulation by the Hippo pathway. Biochim. Biophys. Acta *1830*, 2323–2334.

Hong, J., Hwang, E.S., McManus, M.T., Amsterdam, A., Tian, Y., Kalmukova, R., Mueller, E., Benjamin, T., Spiegelman, B.M., Sharp, P. a, et al. (2005). TAZ, a transcriptional modulator of mesenchymal stem cell differentiation. Science *309*, 1074–1078.

Hu, J., Sun, S.S., Jiang, Q., Wang, W., Gui, Y., and Song, H. (2013). Yes-Associated Protein (Yap) Is Required for Early Embryonic Development in Zebrafish (Danio Rerio). Int. J. Biol. Sci. *9*, 267–278.

Huang, J., Wu, S., Barrera, J., Matthews, K., and Pan, D. (2005). The Hippo signaling pathway coordinately regulates cell proliferation and apoptosis by inactivating Yorkie, the Drosophila Homolog of YAP. Cell *122*, 421–434.

Huxley, J., and Beer, G. De (1934). The elements of experimental embryology. … Elem. Exp. Embryol.

Iovine, M.K., and Johnson, S.L. (2000). Genetic analysis of isometric growth control mechanisms in the zebrafish caudal fin. Genetics *155*, 1321–1329.

Ishida, T., Nakajima, T., Kudo, A., and Kawakami, A. (2010). Phosphorylation of Junb family proteins by the Jun N-terminal kinase supports tissue regeneration in zebrafish. Dev. Biol. *340*, 468–479.

Iten, L.E., and Bryant, S. V (1976). Regeneration from different levels along the tail of the newt, Notophthalmus viridescens. J. Exp. Zool. *196*, 293–306.

Itou, J., Kawakami, H., Burgoyne, T., and Kawakami, Y. (2012). Life-long preservation of the regenerative capacity in the fin and heart in zebrafish. Biol. Open *1*, 739–746.

Jiang, Q., Liu, D., Gong, Y., Wang, Y., Sun, S., Gui, Y., and Song, H. (2009). Yap Is Required for the Development of Brain, Eyes, and Neural Crest in Zebrafish. Biochem. Biophys. Res. Commun. *384*, 114–119.

Jopling, C., Sleep, E., Raya, M., Martí, M., Raya, A., and Izpisúa Belmonte, J.C. (2010). Zebrafish heart regeneration occurs by cardiomyocyte dedifferentiation and proliferation. Nature *464*, 606–609.

Jopling, C., Boue, S., and Izpisua Belmonte, J.C. (2011). Dedifferentiation, transdifferentiation and reprogramming: three routes to regeneration. Nat. Rev. Mol. Cell Biol. *12*, 79–89.

Justice, R.W., Zilian, O., Woods, D.F., Noll, M., and Bryant, P.J. (1995). The Drosophila tumor suppressor gene warts encodes a homolog of human myotonic dystrophy kinase and is required for the control of cell shape and proliferation. Genes Dev. *9*, 534–546.

Kango-Singh, M., Nolo, R., Tao, C., Verstreken, P., Hiesinger, P.R., Bellen, H.J., and Halder, G. (2002). Shar-pei mediates cell proliferation arrest during imaginal disc growth in Drosophila. Development *129*, 5719–5730.

Kawakami, A. (2010). Stem cell system in tissue regeneration in fish. Dev. Growth Differ. *52*, 77–87.

Kawakami, A., Fukazawa, T., and Takeda, H. (2004). Early fin primordia of zebrafish larvae regenerate by a similar growth control mechanism with adult regeneration. Dev. Dyn. *231*, 693–699.

Knopf, F., Hammond, C., Chekuru, A., Kurth, T., Hans, S., Weber, C.W., Mahatma, G., Fisher, S., Brand, M., Schulte-Merker, S., et al. (2011). Bone Regenerates via Dedifferentiation of Osteoblasts in the Zebrafish Fin. Dev. Cell *20*, 713–724.

Kragl, M., Knapp, D., Nacu, E., Khattak, S., Schnapp, E., Epperlein, H.-H., and Tanaka, E.M. (2008). Novel insights into the flexibility of cell and positional identity during urodele limb regeneration. Cold Spring Harb. Symp. Quant. Biol. *73*, 583–592.

Kragl, M., Knapp, D., Nacu, E., Khattak, S., Maden, M., Epperlein, H.H., and Tanaka, E.M. (2009). Cells keep a memory of their tissue origin during axolotl limb regeneration. Nature *460*, 60–65.

Kuan, C.Y., Roth, K. a, Flavell, R. a, and Rakic, P. (2000). Mechanisms of programmed cell death in the developing brain. Trends Neurosci. *23*, 291–297.

Kumar, A., Godwin, J.W., Gates, P.B., Garza-Garcia, A.A., and Brockes, J.P. (2007). Molecular basis for the nerve dependence of limb regeneration in an adult vertebrate. Science *318*, 772–777.

Lai, Z.-C., Wei, X., Shimizu, T., Ramos, E., Rohrbaugh, M., Nikolaidis, N., Ho, L.-L., and Li, Y. (2005). Control of cell proliferation and apoptosis by mob as tumor suppressor, mats. Cell *120*, 675–685.

Lee, M.-J., Ran Byun, M., Furutani-Seiki, M., Hong, J.-H., and Jung, H.-S. (2013). YAP and TAZ Regulate Skin Wound Healing. J. Invest. Dermatol. 1–8.

Lee, Y., Grill, S., Sanchez, A., Murphy-Ryan, M., and Poss, K.D. (2005). Fgf signaling instructs position-dependent growth rate during zebrafish fin regeneration. Development *132*, 5173–5183.

Lee, Y., Hami, D., De Val, S., Kagermeier-Schenk, B., Wills, A.A., Black, B.L., Weidinger, G., and Poss, K.D. (2009). Maintenance of blastemal proliferation by functionally diverse epidermis in regenerating zebrafish fins. Dev. Biol. *331*, 270–280.

Lei, Q.-Y., Zhang, H., Zhao, B., Zha, Z.-Y., Bai, F., Pei, X.-H., Zhao, S., Xiong, Y., and Guan, K.-L. (2008). TAZ promotes cell proliferation and epithelial-mesenchymal transition and is inhibited by the hippo pathway. Mol. Cell. Biol. *28*, 2426–2436.

Lin, A.Y.T., and Pearson, B.J. (2014). Planarian yorkie/YAP functions to integrate adult stem cell proliferation, organ homeostasis and maintenance of axial patterning. Development 1–12.

Liu, Z., Tan, J.L., Cohen, D.M., Yang, M.T., Sniadecki, N.J., Alom, S., Nelson, C.M., and Chen, C.S. (2010). Mechanical tugging force regulates the size of cell – cell junctions. PNAS.

Lund, T.C., Patrinostro, X., Kramer, A.C., Stadem, P., Higgins, L., Markowski, T.W., Wroblewski, M.S., Lidke, D.S., Tolar, J., and Blazar, B.R. (2014). Sdf1 Expression Reveals a Source of Perivascular-Derived Mesenchymal Stem Cells in Zebrafish. Stem Cells 1–17.

Maden, M. (1976). Blastemal kinetics and pattern formation during amphibian limb regeneration. J. Embryol. Exp. Morphol. *36*, 561–574.

Mana-Capelli, S., Paramasivam, M., Dutta, S., and McCollum, D. (2014). Angiomotins link F-actin architecture to Hippo pathway signaling. Mol. Biol. Cell 1–29.

Marie, H., Pratt, S.J., Betson, M., Epple, H., Kittler, J.T., Meek, L., Moss, S.J., Troyanovsky, S., Attwell, D., Longmore, G.D., et al. (2003). The LIM protein Ajuba is recruited to cadherin-dependent cell junctions through an association with alpha-catenin. J. Biol. Chem. *278*, 1220–1228.

Mathew, L.K., Sengupta, S., Franzosa, J.A., Perry, J., La Du, J., Andreasen, E.A., and Tanguay, R.L. (2009). Comparative expression profiling reveals an essential role for raldh2 in epimorphic regeneration. J. Biol. Chem. *284*, 33642–33653.

Matsui, Y., and Lai, Z.-C. (2013). Mutual regulation between Hippo signaling and actin cytoskeleton. Protein Cell *4*, 904–910.

Mauviel, a, Nallet-Staub, F., and Varelas, X. (2011). Integrating developmental signals: a Hippo in the (path)way. Oncogene 1–14.

Mcclatchey, A.I., and Yap, A.S. (2012). Contact inhibition (of proliferation) redux. Curr. Opin. Cell Biol. *24*, 685–694.

Mercer, S.E., Odelberg, S.J., and Simon, H.-G. (2013). A dynamic spatiotemporal extracellular matrix facilitates epicardial-mediated vertebrate heart regeneration. Dev. Biol.

Mescher, a L. (1976). Effects on adult newt limb regeneration of partial and complete skin flaps over the amputation surface. J. Exp. Zool. *195*, 117–128.

Morgan, T. (1900). Regeneration in teleosts. Dev. Genes Evol.

Morgan, T.H. (1901). Regeneration.

Morgan, T.H. (1902). Further experiments on the regeneration of the tail of fishes. Arch. Für Entwicklungsmechanik Der Org. *14*, 539–561.

Morgan, T.T.H. (1906). The Physiology of Regeneration. J. Exp. Zool. *4*, 118–127.

Münch, J., González-Rajal, A., and de la Pompa, J.L. (2013). Notch regulates blastema proliferation and prevents differentiation during adult zebrafish fin regeneration. Development *140*, 1402–1411.

Murawala, P., Tanaka, E.M., and Currie, J.D. (2012). Regeneration: the ultimate example of wound healing. Semin. Cell Dev. Biol. *23*, 954–962.

Nabrit, S.M. (1929). THE ROLE OF THE FIN RAYS IN THE REGENERATION IN THE TAIL-FINS OF FISHES: IN FUNDULUS AND GOLDFISH. Biol. Bull. *56*, 60–63.

Nachtrab, G., Kikuchi, K., Tornini, V. a, and Poss, K.D. (2013). Transcriptional components of anteroposterior positional information during zebrafish fin regeneration. Development *3764*, 3754–3764.

Nacu, E., and Tanaka, E.M. (2010). Limb Regeneration: A New Development? Annu. Rev. Cell Dev. Biol. *27*, 409–440.

Nechiporuk, A., and Keating, M.T. (2002). A proliferation gradient between proximal and msxb-expressing distal blastema directs zebrafish fin regeneration. Development *129*, 2607–2617.

Neufeld, T.P., de la Cruz, a F., Johnston, L. a, and Edgar, B. a (1998). Coordination of growth and cell division in the Drosophila wing. Cell *93*, 1183–1193.

Niethammer, P., Grabher, C., Look, A.T., and Mitchison, T.J. (2009). A tissue-scale gradient of hydrogen peroxide mediates rapid wound detection in zebrafish. Nature *459*, 996–999.

Nishioka, N., Inoue, K., Adachi, K., Kiyonari, H., Ota, M., Ralston, A., Yabuta, N., Hirahara, S., Stephenson, R.O., Ogonuki, N., et al. (2009). The Hippo signaling pathway components Lats and Yap pattern Tead4 activity to distinguish mouse trophectoderm from inner cell mass. Dev. Cell *16*, 398–410.

Pan, D. (2010). The hippo signaling pathway in development and cancer. Dev. Cell *19*, 491–505.

Peyton, S.R., Ghajar, C.M., Khatiwala, C.B., and Putnam, A.J. (2007). The emergence of ECM mechanics and cytoskeletal tension as important regulators of cell function. Cell Biochem. Biophys. *47*, 300–320.

Poleo, G., Brown, C.W., Laforest, L., and Akimenko, M. a (2001). Cell proliferation and movement during early fin regeneration in zebrafish. Dev. Dyn. *221*, 380–390.

Raff, M.C. (1992). Social controls on cell survival and cell death. Nature *356*, 397–400.

Raff, M.C. (1996). Size control: the regulation of cell numbers in animal development. Cell *86*, 173–175.

Rauskolb, C., Pan, G., Reddy, B.V.V.G., Oh, H., and Irvine, K.D. (2011). Zyxin links fat signaling to the hippo pathway. PLoS Biol. *9*, e1000624.

Rauskolb, C., Sun, S., Sun, G., Pan, Y., and Irvine, K.D. (2014). Cytoskeletal Tension Inhibits Hippo Signaling through an Ajuba-Warts Complex. Cell *158*, 143–156.

Reddy, P., Deguchi, M., Cheng, Y., and Hsueh, A.J.W. (2013). Actin cytoskeleton regulates hippo signaling. PLoS One *8*, e73763.

Regué, L., Mou, F., and Avruch, J. (2013). G protein-coupled receptors engage the mammalian Hippo pathway through F-actin: F-Actin, assembled in response to Galpha12/13 induced RhoA-GTP, promotes dephosphorylation and activation of the YAP oncogene. Bioessays *35*, 430–435.

Rieger, S., and Sagasti, A. (2011). Hydrogen peroxide promotes injury-induced peripheral sensory axon regeneration in the zebrafish skin. PLoS Biol. *9*, e1000621.

Robinson, B.S.S., and Moberg, K.H.H. (2011). Cell–Cell Junctions: α-Catenin and E-Cadherin Help Fence In Yap1. Curr. Biol. *21*, R890–R892.

Roensch, K., Tazaki, A., Chara, O., and Tanaka, E. (2013). Progressive Specification Rather than Intercalation of Segments During Limb Regeneration. Science (80-.). *342*, 1375–1379.

Santamaria, J.A., Becerra, J., and Santamaría, J. a (1991). Tail fin regeneration in teleosts: cell-extracellular matrix interaction in blastemal differentiation. J. Anat. *176*, 9–21.

Santos-Ruiz, L., Santamaría, J.A., Ruiz-Sánchez, J., and Becerra, J. (2002). Cell proliferation during blastema formation in the regenerating teleost fin. Dev. Dyn. *223*, 262–272.

Santos-Ruiz, L., Santamaría, J.A., and Becerra, J. (2005). Cytoskeletal dynamics of the teleostean fin ray during fin epimorphic regeneration. Differentiation. *73*, 175–187.

Satoh, A., Gardiner, D.M., Bryant, S. V, and Endo, T. (2007). Nerve-induced ectopic limb blastemas in the Axolotl are equivalent to amputation-induced blastemas. Dev. Biol. *312*, 231–244.

Schlegelmilch, K., Mohseni, M., Kirak, O., Pruszak, J., Rodriguez, J.R., Zhou, D., Kreger, B.T., Vasioukhin, V., Avruch, J., Brummelkamp, T.R., et al. (2011). Yap1 Acts Downstream of a-Catenin to Control Epidermal Proliferation. Cell *144*, 782–795.

Shao, J., Chen, D., Ye, Q., Cui, J., Li, Y., and Li, L. (2011). Tissue regeneration after injury in adult zebrafish: The regenerative potential of the caudal fin. Dev. Dyn. *240*, 1271–1277.

Shapiro, L., and Weis, W.I. (2009). Structure and biochemistry of cadherins and catenins. Cold Spring Harb. Perspect. Biol. *1*, a003053.

Shaw, R.L., Kohlmaier, A., Polesello, C., Veelken, C., Edgar, B. a, and Tapon, N. (2010). The Hippo pathway regulates intestinal stem cell proliferation during Drosophila adult midgut regeneration. Development *4158*, 4147–4158.

Silvis, M.R., Kreger, B.T., Lien, W.-H.W.-H., Klezovitch, O., Rudakova, G.M., Camargo, F.D., Lantz, D.M., Seykora, J.T., Vasioukhin, V., and Marianna, G. (2011). α-catenin is a tumor suppressor that controls cell accumulation by regulating the localization and activity of the transcriptional coactivator Yap1. Sci. Signal. *4*, ra33–ra33.

Singer, M. (1952). The influence of the nerve in regeneration of the amphibian extremity. Q. Rev. Biol. *27*, 169–200.

Singh, S.P.P., Holdway, J.E.E., and Poss, K.D.D. (2012). Regeneration of Amputated Zebrafish Fin Rays from De Novo Osteoblasts. Dev. Cell *22*, 879–886.

Slanchev, K., Carney, T.J., Stemmler, M.P., Koschorz, B., Amsterdam, A., Schwarz, H., and Hammerschmidt, M. (2009). The epithelial cell adhesion molecule EpCAM is required for epithelial morphogenesis and integrity during zebrafish epiboly and skin development. PLoS Genet. *5*, e1000563.

Sousa, S., Afonso, N., Bensimon-Brito, A., Fonseca, M., Simões, M., Leon, J., Roehl, H., Cancela, M.L., and Jacinto, A. (2011). Differentiated skeletal cells contribute to blastema formation during zebrafish fin regeneration. Development *138*, 3897–3905.

Spallanzani, L. (1769). An essay on animal reproductions.

Staley, B.K., and Irvine, K.D. (2010). Warts and yorkie mediate intestinal regeneration by influencing stem cell proliferation. Curr. Biol. *20*, 1580–1587.

Stepniak, E., Radice, G.L., and Vasioukhin, V. (2009). Adhesive and signaling functions of cadherins and catenins in vertebrate development. Cold Spring Harb. Perspect. Biol. *1*, a002949.

Stewart, S., and Stankunas, K. (2012). Limited dedifferentiation provides replacement tissue during zebrafish fin regeneration. Dev. Biol. *365*, 339–349.

Tamura, K., Ohgo, S., and Yokoyama, H. (2010). Limb blastema cell: a stem cell for morphological regeneration. Dev. Growth Differ. *52*, 89–99.

Tapon, N., Harvey, K.F., Bell, D.W., Wahrer, D.C.R., Schiripo, T. a, Haber, D. a, and Hariharan, I.K. (2002). salvador Promotes both cell cycle exit and apoptosis in Drosophila and is mutated in human cancer cell lines. Cell *110*, 467–478.

Tassava, R. a, and Garling, D.J. (1979). Regenerative responses in larval axolotl limbs with skin grafts over the amputation surface. J. Exp. Zool. *208*, 97–110.

Tu, S., and Johnson, S.L. (2011). Fate restriction in the growing and regenerating zebrafish fin. Dev. Cell *20*, 725–732.

Turing, A. (1952). The chemical basis of morphogenesis. Philos. Trans. R. … *237*, 37–72.

Udan, R.S., Kango-Singh, M., Nolo, R., Tao, C., and Halder, G. (2003). Hippo promotes proliferation arrest and apoptosis in the Salvador/Warts pathway. Nat. Cell Biol. *5*, 914–920.

Varelas, X. (2014). The Hippo pathway effectors TAZ and YAP in development, homeostasis and disease. Development *141*, 1614–1626.

Vogel, V., and Sheetz, M. (2006). Local force and geometry sensing regulate cell functions. Nat. Rev. Mol. Cell Biol. *7*, 265–275.

Vogel, a, Ross, R., and Raines, E. (1980). Role of serum components in density-dependent inhibition of growth of cells in culture. Platelet-derived growth factor is the major serum determinant of saturation density. J. Cell Biol. *85*, 377–385.

Wada, K., Itoga, K., Okano, T., Yonemura, S., and Sasaki, H. (2011). Hippo pathway regulation by cell morphology and stress fibers. Development *138*, 3907–3914.

Wartlick, O., Kicheva, A., and Gonzalez-Gaitan, M. (2009). Morphogen gradient formation. Cold Spring Harb. … 1–22.

Wartlick, O., Mumcu, P., Jülicher, F., and Gonzalez-Gaitan, M. (2011). Understanding morphogenetic growth control -- lessons from flies. Nat. Rev. Mol. Cell Biol. *12*, 594–604.

Wehner, D., Cizelsky, W., Vasudevaro, M.D., Ozhan, G., Haase, C., Kagermeier-Schenk, B., Röder, A., Dorsky, R.I., Moro, E., Argenton, F., et al. (2014). Wnt/β-Catenin Signaling Defines Organizing Centers that Orchestrate Growth and Differentiation of the Regenerating Zebrafish Caudal Fin. Cell Rep. 1–15.

Wolpert, L. (1969). Positional information and the spatial pattern of cellular differentiation. J. Theor. Biol. *25*, 1–47.

Wolpert, L. (2011). Positional information and patterning revisited. J. Theor. Biol. *269*, 359–365.

Wood, A., and Thorogood, P. (1984). An analysis of in vivo cell migration during teleost fin morphogenesis. J. Cell Sci. *222*, 205–222.

Xin, M., Kim, Y., Sutherland, L.B., Murakami, M., Qi, X., Mcanally, J., Porrello, E.R., Mahmoud, a. I., Tan, W., Shelton, J.M., et al. (2013). Hippo pathway effector Yap promotes cardiac regeneration. Proc. Natl. Acad. Sci. 1–6.

Xu, T., Wang, W., Zhang, S., Stewart, R. a, and Yu, W. (1995). Identifying tumor suppressors in genetic mosaics: the Drosophila lats gene encodes a putative protein kinase. Development *121*, 1053–1063.

Yelon, D., Ticho, B., Halpern, M.E., Ruvinsky, I., Ho, R.K., Silver, L.M., and Stainier, D.Y. (2000). The bHLH transcription factor hand2 plays parallel roles in zebrafish heart and pectoral fin development. Development *127*, 2573–2582.

Yimlamai, D., Christodoulou, C., Galli, G.G., Yanger, K., Pepe-Mooney, B., Gurung, B., Shrestha, K., Cahan, P., Stanger, B.Z., and Camargo, F.D. (2014). Hippo pathway activity influences liver cell fate. Cell *157*, 1324–1338.

Yoo, S.K., Freisinger, C.M., Lebert, D.C., and Huttenlocher, A. (2012). Early redox, Src family kinase, and calcium signaling integrate wound responses and tissue regeneration in zebrafish. J. Cell Biol. *199*, 225–234.

Yoshinari, N., Ishida, T., Kudo, A., and Kawakami, A. (2009). Gene expression and functional analysis of zebrafish larval fin fold regeneration. Dev. Biol. *325*, 71–81.

Yu, J., Zheng, Y., Dong, J., Klusza, S., Deng, W.-M., and Pan, D. (2010). Kibra functions as a tumor suppressor protein that regulates Hippo signaling in conjunction with Merlin and Expanded. Dev. Cell *18*, 288–299.

Yuan, Y., Lin, S., Zhu, Z., Zhang, W., and Lai, Z. (2009). The mob as tumor suppressor (mats1) gene is required for growth control in developing zebrafish embryos. Int. J. Dev. Biol. *53*, 525–533.

Yue, T., Tian, A., and Jiang, J. (2012). The cell adhesion molecule echinoid functions as a tumor suppressor and upstream regulator of the Hippo signaling pathway. Dev. Cell *22*, 255–267.

Zhang, J., Ji, J.-Y., Yu, M., Overholtzer, M., Smolen, G. a, Wang, R., Brugge, J.S., Dyson, N.J., and Haber, D. a (2009). YAP-dependent induction of amphiregulin identifies a non-cell-autonomous component of the Hippo pathway. Nat. Cell Biol. *11*, 1444–1450.

Zhang, J., Wagh, P., Guay, D., Sanchez-Pulido, L., Padhi, B.K., Korzh, V., Andrade-Navarro, M.A., and Akimenko, M.-A. (2010). Loss of fish actinotrichia proteins and the fin-to-limb transition. Nature 1–5.

Zhao, B., Wei, X., Li, W., Udan, R.S., Yang, Q., Kim, J., Xie, J., Ikenoue, T., Yu, J., Li, L., et al. (2007). Inactivation of YAP oncoprotein by the Hippo pathway is involved in cell contact inhibition and tissue growth control. Genes Dev. *21*, 2747–2761.

Zhao, B., Ye, X., Yu, J.J., Li, L., Li, W., Li, S., Lin, J.D., Wang, C.-Y., Chinnaiyan, A.M., Lai, Z.-C., et al. (2008). TEAD mediates YAP-dependent gene induction and growth control. Genes Dev. *22*, 1962–1971.

Zhao, B., Tumaneng, K., and Guan, K.-L. (2011). The Hippo pathway in organ size control, tissue regeneration and stem cell self-renewal. Nat. Cell Biol. *13*, 877–883.

Zhou, D., Zhang, Y., Wu, H., Barry, E., Yin, Y., Lawrence, E., Dawson, D., Willis, J.E., Markowitz, S.D., Camargo, F.D., et al. (2011). Mst1 and Mst2 protein kinases restrain intestinal stem cell proliferation and colonic tumorigenesis by inhibition of Yes-associated protein (Yap) overabundance. Proc. Natl. Acad. Sci. U. S. A.

CHAPTER II

DYNAMICS OF ZEBRAFISH FIN FOLD REGENERATION

A MODEL FOR IN VIVO REGENERATION STUDIES

This chapter is based in the following manuscript:

***In Vivo* Cell and Tissue Dynamics Underlying Zebrafish Fin Fold Regeneration**
Rita Mateus, Telmo Pereira, Sara Sousa, Joana Esteves de Lima, Susana Pascoal, Leonor Saúde and Antonio Jacinto (2012), PLoS ONE 7(12): e51766.
doi:10.1371/journal.pone.0051766

“It is possible that during the initiation of migration, the mesenchymal cells are under strongest 'directive' influence (…)”

In *An Analysis of In Vivo Cell Migration during Teleost Fin Morphogenesis*
A.Wood and P. Thorogood, 1984

CONTENTS

The author of this thesis performed all the experiments. All the authors contributed to the experimental conception and design. Sara Sousa and Joana Esteves de Lima helped executing some of the experiments. Data analysis was done by the author of this thesis together with Telmo Pereira, Leonor Saúde and António Jacinto. Sara Sousa established the *osteopontin*:eGFP transgenic line. Manuscript preparation was done by the thesis author and António Jacinto.

1. Summary

Zebrafish (*Danio rerio*) has a remarkable capacity to regenerate many organs and tissues. During larval stages the fin fold allows the possibility of performing long time-lapse imaging making this system very appealing to study the relationships between tissue movements, cell migration and proliferation necessary for the regeneration process. Through the combined use of transgenic fluorescently-labeled animals and confocal microscopy imaging, we characterized *in vivo* the complete fin fold regeneration process. We show, for the first time, that there is an increase in the global rate of epidermal growth as a response to tissue loss. Also enhanced significantly is cell proliferation, which upon amputation happens in a broad area concerning the amputation level and not in a blastema-restricted way. This reveals a striking difference with regard to the adult fin regeneration system. Finally, an accumulation of migratory, shape-changing fibroblasts occurs proximally to the wound area, resembling a blastemal-like structure, which may act as a signaling center for the regeneration process to proceed. These findings provide a novel *in vivo* description of fundamental mechanisms occurring during the fin fold regeneration process, thereby contributing to a better knowledge of this regenerative system and to reveal variations in the epimorphic regeneration field.

1.1 Keywords

Regeneration, zebrafish, fin fold, development, migration, *in vivo* characterization.

2. Introduction

Most vertebrates, including humans, are unable to regenerate the majority of lost or damaged tissues. In contrast, lower vertebrates such as zebrafish (*Danio rerio*) are able to regenerate many of their organs upon amputation. These animals have the amazing and extremely useful capacity of restoring a fully functional organ, through a process of epimorphic regeneration. This type of regeneration involves a specialized and transient tissue, the blastema, that plays a key role in the signaling and proliferation events that are necessary to recover the lost organ (Morgan, 1901). The blastema is composed of undifferentiated cells that are recruited to the amputation plane (Echeverri et al., 2001)(Kragl et al., 2009)(Knopf et al., 2011)(Sousa et al., 2011), and is enclosed by a wound epidermis that also plays a central role in terms of signaling (Lee et al., 2009)(Campbell et al., 2011)(Campbell et al., 2008).

The zebrafish has emerged as a powerful model system to perform regeneration studies due to its high regenerative potential coupled to availability of genetic tools. Kawakami *et al* (2004) proposed a new zebrafish-based regeneration system: the early fin primordium (or fin fold) of the 2 days post-fertilization (dpf) larva (Kawakami et al., 2004). This model was established on the basis of its similarities to the adult zebrafish caudal fin system. In particular, the existence of the three regeneration phases (wound healing, blastema formation and regenerative outgrowth), the formation of similar structures upon amputation (i.e. wound epidermis) and a large number of coincident upregulated expression markers (Yoshinari et al., 2009)(Ishida et al., 2010). In addition, the fin fold model presents some advantages in comparison to the adult model, namely the speed of regeneration, since in the fin fold the full process takes only 72 hours to complete restoration of the lost tissue, and the structural simplicity of this non-vascularized appendage (Mathew et al., 2009) since it is only composed of five layers of tissue. In the larva fin fold, a middle layer of

mesenchyme, composed of fibroblast-like cells (Wood and Thorogood, 1984)(Feitosa et al., 2012), nerves and actinotrichia (Durán et al., 2011)(Zhang et al., 2010), is surrounded by two layers of epidermis containing basal p63-positive keratinocytes, with underlying basement membranes (Slanchev et al., 2009)(Dane and Tucker, 1985) (Figure 1A).

Our goal was to characterize *in vivo* the complete fin fold regeneration process, by using advanced time-lapse confocal imaging of transgenic animals. In particular, we followed the three regeneration stages to unveil how the tissue behaves and recovers after an amputation, in terms of interactions between epidermal layers of tissue and individual migratory mesenchymal cells. Furthermore, we analyzed the orientation of cell division and rate of proliferation in a systematic manner. We show that there is an increase in the global rate of epidermal growth as a response to tissue loss that is not directly dependent on local proliferation. Interestingly, proliferation is enhanced upon amputation but happens in a broad area surrounding the amputation level and not in a blastema-restricted way. This reveals a striking difference with regard to the adult system. Additionally, we found that a population of polarized, migratory, shape-changing mesenchymal cells accumulates proximally to the wound area, resembling a blastemal-like structure, which may act as a signaling center for the regenerative process (Process Overview Figure 1B).

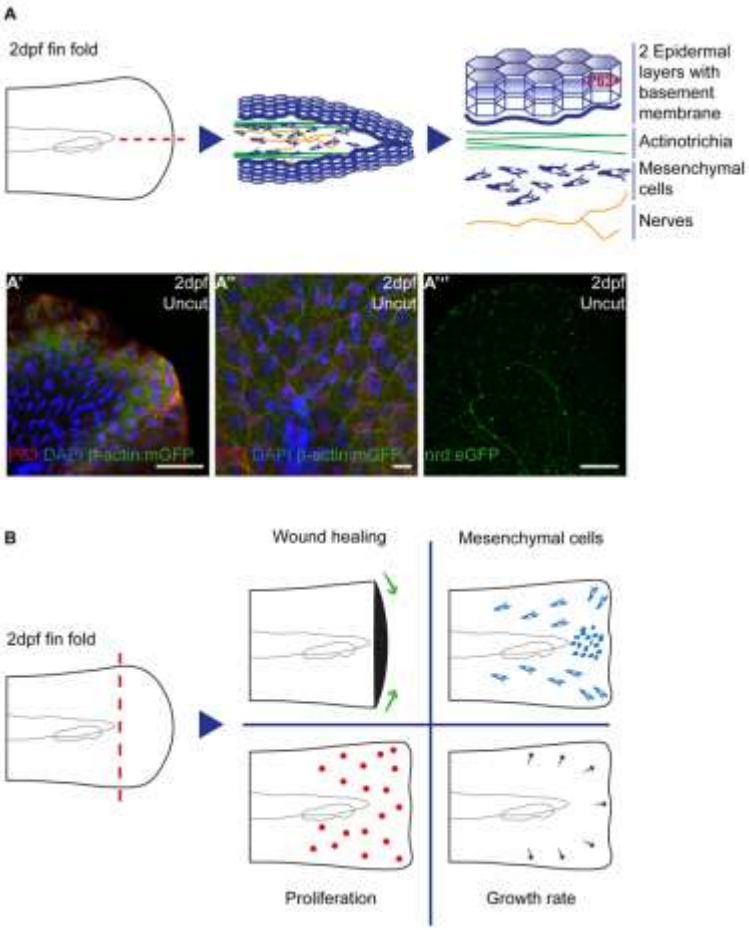

Figure 1. Fin fold organization and regeneration. A Representation of the composition of the 2 dpf fin fold cell types and structures, including their respective organization. **A', A'', A'''** Representative *in vivo* fin fold images to illustrate the previous described structures. **A'-A''** Immunostaining with anti-P63 and anti-GFP together with DAPI, in 2 dpf uncut *β–actin*:mGFP transgenic larvae. Note that P63 only labels a subset of the epithelial nuclei, which corresponds to the lower epithelial cell layer of the fin fold. Epithelial cell membranes are evidenced by the expression of the transgene. Scale bars correspond to 50µm and 10µm respectively. **A'''** Live imaging of 2 dpf uncut *nrd*:eGFP transgenics, that is expressed in the nerves throughout the fin fold. Scale bar corresponds to 50µm. **B** Schematic overview representing the main findings occurring after amputation of the 2 dpf larva fin fold, as a part of the regenerative process, addressed throughout this chapter.

3. Materials and Methods

3.1 Ethics Statement

All experiments involving animals were approved by the Animal User and Ethical Committees at Instituto de Medicina Molecular, according with directives from Direcção Geral Veterinária (PORT 1005/92).

3.2 Zebrafish lines, maintenance and surgery

All Zebrafish lines used were maintained in a re-circulating system with a 14 h/day and 10 h/night cycle at 28°C. Embryos were gathered as described in *The Zebrafish Book* and kept in E3 zebrafish embryo medium at 28°C until reaching the desired developmental stage. Both AB and Tuebingen wild-type lines were used. The transgenic lines used for live imaging were: Tg*(β-actin:mGFP*) (Cooper et al., 2005), Tg(*H2a.f/z-GFP*)^{kca66} (Geldmacher-voss et al., 2001), Tg(*actb1:myl12.1-eGFP*) (Behrndt et al., 2012), Tg(*EF1α:mKO2-zCdt1(1/190)*)^{rw0405b} (Sugiyama et al., 2009) and GT(*ctnna-Citrine*)^{ct3a} (Žigman et al., 2010). These lines were kindly provided by Mathias Koppen, Zirc, Carl-Philipp Heisenberg, Atsushi Miyawaki and Mihaela Zigman, respectively. The mutant line *ppt*^{ta98} (Hammerschmidt et al., 1996) was kindly given by Carl-Philipp Heisenberg. All fin fold amputations were performed in embryos anaesthetized in 0.1% MS-222 (Sigma) using a scalpel as previously described (Kawakami et al., 2004). Regeneration was then allowed to proceed until defined time points at 28°C.

3.3 *osteopontin:eGFP* transgenic line generation

A bacterial artificial chromosome (BAC) that included the zebrafish *osteopontin* (also known as *spp1*) locus (CH73-213K3, BACPAC Resources Center) was used as a template to amplify a 1295bp fragment, comprising the 1244bp sequence upstream of the translational start site and the first 51bp of the coding sequence. The following set of primers were used for amplification: Fwd 5'CATGATATCTCAGGGCACTACGG3' and Rev 5'TACACAGAAGACTGTGGCGACG3'. The promoter region was cloned in a modified version of pMinitol:MCS (Balciunas et al., 2006) that included *βglobin-5´HS4* insulator sequences flanking the transgene (Bessa et al., 2009). Microinjections to generate the transgenic embryos were performed at one cell-stage of wild-type AB strain, according to standard procedures. The final plasmid was named *pMinitol2.5-osteopontin:eGFP* and 52 ng/µL of DNA was co-injected with 112ng/µL of capped transposase mRNA and 1% of rhodamine B dextran (10,000 MW, Invitrogen), diluted in 1x Danieau's solution (58 mM NaCl, 0.7 mM KCl, 0.4 mM $MgSO_4$, 5 mM HEPES, 0.6 mM $Ca(NO_3)_2$).

3.4 Microinjection of zebrafish embryos

Wild-type AB strain one-cell stage embryos were injected using standard procedures with 100pg Utrophin-GFP mRNA, produced by linearization of pcs2-utrophin-GFP (Burkel et al., 2007) with NotI (Fermentas), and transcribed using the SP6 mMESSAGE mMACHINE High Yield Capped RNA Transcription Kit (Ambion). A PV-820 Pico-injector (World Precision Instruments) and a Narashige micromanipulator were used for microinjection.

3.5 Live imaging

Wound healing time-lapse imaging was performed in 2 dpf injected Utrophin-GFP, *actb1:myl12.1-eGFP* or *ctnna-Citrine* transgenic embryos. Animals were amputated 5 minutes prior to imaging. Sequential time-lapse imaging was performed in *β-actin:mGFP*, *H2a.f/z-GFP* and of 2 dpf, 3 dpf and 4 dpf embryos both in uncut and amputated fin folds at several regeneration stages. In both cases, a Zeiss5Live confocal microscope was used and images were acquired using a 20x dipping objective every minute for wound healing imaging, every 2 minutes for *β-actin:mGFP* experiments, and every 10 minutes for *H2a.f/z-GFP*. Long time-lapse imaging (up to 12h) and shape monitoring time-lapse imaging (up to 3h) was performed using 2dpf double positive embryos from an *osteopontin:eGFP* and *EF1α:mKO2-zCdt1* cross both in uncut and amputated fin folds. Images were acquired every 5 minutes for long time-lapse and every minute for shape monitoring time-lapse, using a ZeissLSM710 with a 40x oil objective. All *in vivo* imaging was performed in anaesthetized animals with 0.1% MS222 (Sigma) diluted in E3 zebrafish embryo medium.

3.6 Immunofluorescence

This protocol was adapted from Neugebauer et al., 2009 with the following modifications: embryos were fixed in 4% paraformaldehyde (PFA) (Sigma) at 4°C overnight (o/n), then transferred to 100% Methanol (MeOH) (Merck) and stored at -20ºC o/n. Then embryos were rehydrated gradually in series of MeOH/phosphate-buffered saline (PBS) and washed twice for 5 minutes with 1% PBS-TritonX-100, followed by a 7 minute permeabilization with 100% acetone at -20ºC. Then the embryos were washed in 0.1% Triton-X100, 1% DMSO (Sigma) and 1% Bovine Serum Albumin (BSA) (Sigma) in PBS (PBDX), followed by a 2 hour blocking in 0.1% Triton-X100, 1% DMSO,

1% BSA and 5% goat serum in PBS. The embryos were incubated in primary antibodies (listed in Appendix IV) diluted in blocking solution, o/n at 4ºC. The embryos were then washed several times in PBDX and incubated in secondary antibodies (listed in Appendix IV) and/or with phalloidin (1:200, conjugated with Alexa Fluor 568, Invitrogen) diluted in blocking solution, o/n at 4ºC. The next day, embryos were washed several times as previously and DAPI (Sigma) was applied in 0.001mg/mL of PBS. Embryos were mounted in 80% Glycerol, 2% DABCO (Sigma) diluted in PBS and then imaged using a ZeissLSM710 confocal microscope. In stainings where phalloidin was used, there was no MeOH transfer and there was a direct continuation of the protocol after o/n fixation with PFA.

3.7 3D Image processing

To create the 3D images, the original z-stack acquired data was treated using the Imaris software with the *easy 3D* option.

3.8 Image analysis and quantification

For all movie analysis, maximum intensity z-stack projections were made using the LSM Image Browser software.

For tissue movement analysis, raw images were registered using the ImageJ plugin StackReg (rigidbody transformation), to correct for non-specific movement. Vector velocity fields were obtained using mpiv toolbox for Matlab (64 pixel window, 0.5 window overlap, 40 pixel window displacement, mqd algorithm, with two recursive checks). Resultant vector fields were filtered (median filter, threshold 2, kriging interpolation) and smoothed (weighting method) to remove stray vectors and homogenize the result respectively. This analysis was performed using three images, equally separated in time (2.5 hours), for each time-lapse movie. To remove erratic

vectors which appear outside the fin fold area, images were segmented using the Matlab watershed algorithm (binary conversion threshold=0) and eroded (disk size=3 pixels). The obtained segmented mask was used to reveal the real vectors. The three resultant vector fields were averaged point by point to generate vector field images. The average tissue velocity for each movie was obtained by averaging the vector norms. Resultant data was plotted using GraphPad Prism software and two-tailed Mann-Whitney tests were performed between the several conditions ($p<0.05$). 5 samples were used for each condition.

Proliferation analysis was performed using an ImageJ plugin, ObjectJ. This plugin was used to manually identify: all cytokinesis events, taking into account their orientation, fin fold area and the notochord axis. Resultant data was processed, normalized (area normalization) and corrected (fin fold rotation and translation) in Matlab. Images showing all cell divisions were created using Matlab to project all cell divisions in the correct location relative to the keyframe chosen to represent the movie. Cell division angles were separated into regions according to their location (angle with notochord axis). For each region, angles were divided in 45 degrees intervals, and plotted accordingly. Normalized cell divisions (total numbers) were plotted using GraphPad Prism software, and two-tailed Mann-Whitney tests were performed between the several conditions ($p<0.05$). For each condition the sample number is $n=5$.

Mesenchymal cell movies were registered using the ImageJ plugin MultiStackReg (rigidbody transformation), to correct for non-specific movement.

4. Results

4.1 Wound healing is initiated by an abrupt tissue contraction and formation of an actomyosin cable.

Upon amputation, the regeneration process is initiated by a wound healing phase. To start the *in vivo* characterization of this process we looked at the dynamics of wound closure upon injury. For that we used live cytoskeleton markers and established a fast time-lapse imaging protocol. In the fin fold, the wound healing is achieved through a rapid contraction of the epidermal tissue through the formation of an actomyosin cable at the leading edge. The accumulation of both Actin and Myosin is observed as early as 5 minutes post-amputation (minpa), before the main tissue contraction events have happened (Figure 2A, E). By 8 minpa the cable is fully formed (Figure 2B, F arrow) and from this time point until one hour post-amputation (hpa), the tissue contraction exerted by the actomyosin cable appears to be the driving force for the wound to close and to allow the opposite leading edge cells to connect and seal the hole (Figure 2A-D and E-H, arrowheads). After the wound is closed (1 hpa), the cable is no longer detected and the tissue relaxes back to its original shape (1-3 hpa). Also present at the wound leading edge cells is the adherens junction component, Alpha-Catenin, which accumulates in a similar manner to Actin and Myosin (Figure 2 I-L). To confirm that this protein co-localizes with the actomyosin cable, we performed immunohistochemistry in 5 minpa Alpha-Catenin transgenics and observed that indeed Alpha-Catenin co-localizes with F-Actin in the cable (Figure 3). This indicates that the actomyosin cable at the leading edge is a complex structure readily assembled to enable contraction of the tissue and sealing of the open wound.

In order to address if the fin fold regeneration dynamics can be affected by the type of injury and/or size of it, we compared the regenerative ability of fin folds with different amputation planes. We could observe that the dynamics were similar in all cases analyzed, namely: in fin folds that were amputated just distal to the notochord (Regular cut); in fin folds that were amputated at a central position between the notochord and the fin tip (Half-size cut); and in fin folds that were diagonally amputated in the dorsal side (Diagonal cut). In all cases the fins recovered at the same time, even though the fins that suffered a Regular cut had to regenerate more tissue in the same time period (Figure 4). Also there were no differences between different zebrafish wild type strains. Since the regeneration dynamics were similar we opted to do a more thorough analysis of the whole process after using always a Regular cut.

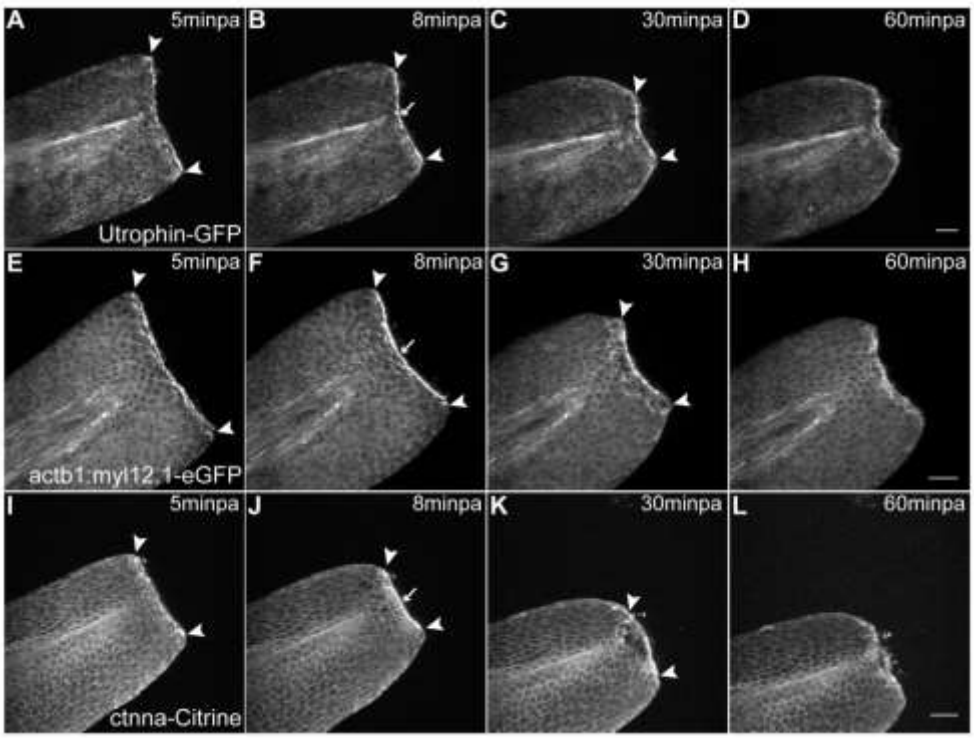

Figure 2. Abrupt tissue contraction and actomyosin cable formation initiate wound healing. A–D Sequential images of a representative *in vivo* 55 min time-lapse movie of an

Utrophin-GFP mRNA-injected 2 dpf larva at different time-points after amputation. **A** At 5minpa, there is accumulation of Actin at the leading edge cells. **B** By 8 minpa the Actin cable is assembled (arrow) and there is tissue contraction - note displacement of arrowheads in comparison with A. **C** At 30 minpa, the tissue has fully contracted. **D** At 60 minpa, the wound inflicted by the amputation is closed. **E–H** Sequential images of a representative in vivo 55 min time-lapse movie of a 2 dpf *actb1*:myl12.1-eGFP transgenic larva. **E** At 5minpa, there is accumulation of Myosin at the leading edge cells. **F** By 8 minpa the Myosin cable is assembled (arrow) and there is tissue contraction – note displacement of arrowheads in comparison with E. **G** At 30 minpa, the tissue has fully contracted. **H** At 60 minpa, the wound inflicted by the amputation is closed. **I–L** Sequential images of a representative *in vivo* 55 min time-lapse movie of a 2 dpf ctnna-Citrine transgenic larva at different time-points after amputation. **I** At 5minpa, there is accumulation of Alpha-Catenin at the leading edge cells. **J** By 8 minpa this accumulation appears to localize to the actomyosin cable (arrow) and there is tissue contraction - note displacement of arrowheads in comparison with I. **K** At 30 minpa, the tissue has fully contracted and Alpha-Catenin is still localized at the wound edge. **L** At 60 minpa, the wound inflicted by the amputation is closed. Anterior is on the left and scale bars correspond to 50μm in all images; n = 5 larvae per condition. See also Movies 1-3.

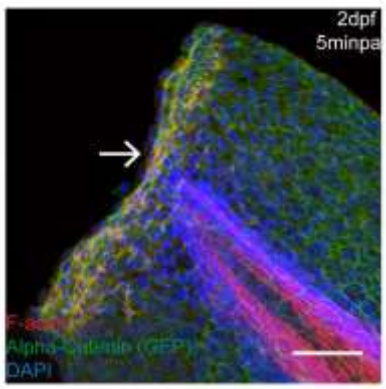

Figure 3. Alpha-Catenin is present in the actin cable during wound healing. Representative frame part of the 3D reconstruction of a representative immunostaining against anti-GFP to detect Alpha-Catenin (green) and phalloidin to detect F-actin (red) in 2 dpf 5 minpa Alpha-Catenin-Citrine (ctnna-Citrine) transgenic larva. Arrow indicates the presence of the actin cable. Scale bar corresponds to 50μm. n=5 larvae. See also Movie 4.

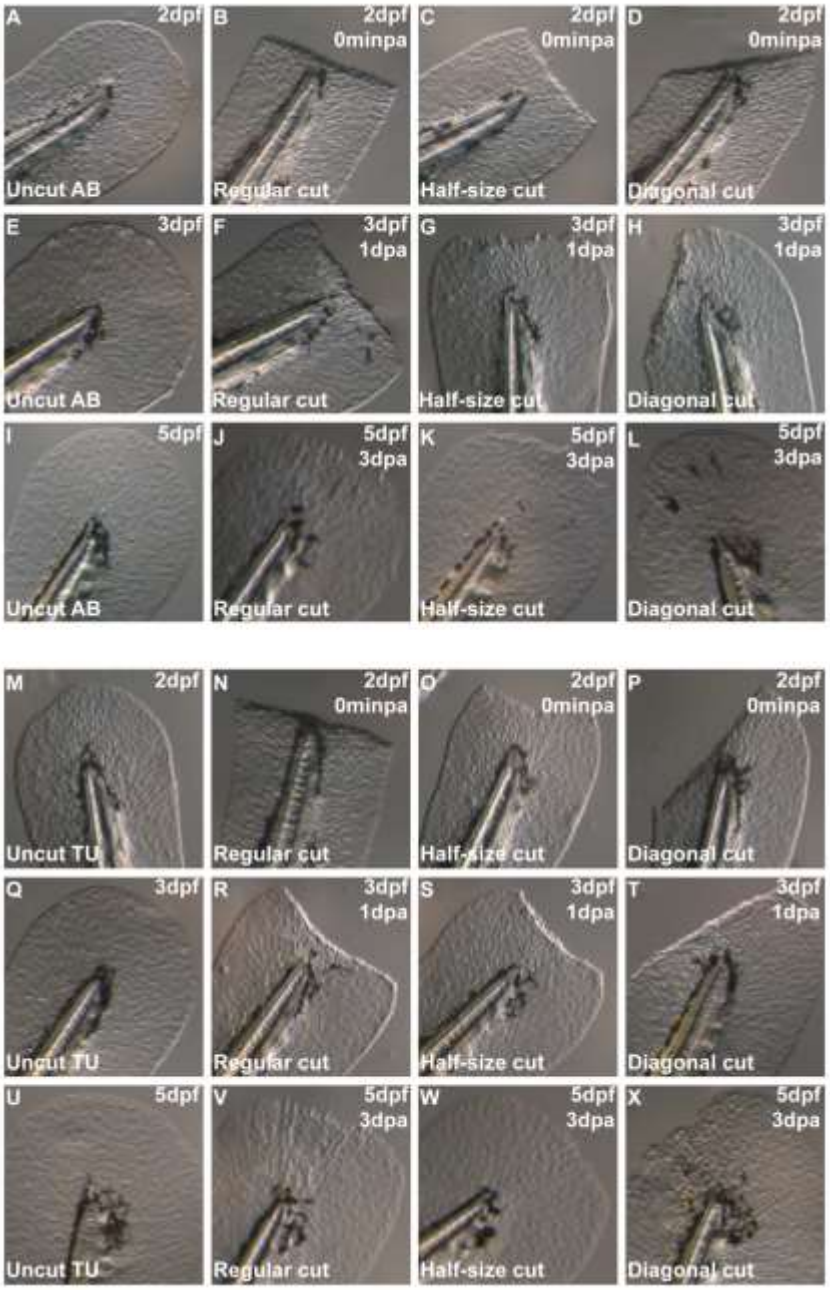

Figure 4. The fin fold regeneration dynamics are independent of the size of amputation. Representative brightfield live images of AB (**A–L**) and TU (**M–X**) wild-type larvae during several stages of the regenerative process and their respective age-matched uncut controls. Larvae were subjected to different amputation planes (Regular, Half-size and

Diagonal cuts) and followed throughout the next 3 regenerating days, time point in which the regenerative ability was accessed. 5 Larvae per condition.

4.2 Epidermal tissue growth is increased upon fin fold amputation but maintains its developmental pattern.

Following the termination of the wound healing phase, blastema formation takes place and then the fin outgrows. In the zebrafish fin fold, these two last stages are closely interconnected as the fin fold regenerates in a short period of time. Therefore, we opted to not distinguish between these two phases in very precise time points and instead we considered them as one continuous and progressive process. In order to follow the behavior of epidermal cells, which are the main tissue type that composes the fin fold, we did 5 hour long sequential time-lapse imaging starting at 1 hpa in the fin fold of 2 dpf larvae, using the transgenic *β-actin:mGFP* larvae (Cooper et al., 2005), that labels cell outlines (see Experimental Outline Figure 5A). We compared the behavior of this tissue upon amputation in 6 time points along the blastema and outgrowth phases with its behavior during normal development in age-matched uncut fins. To quantitatively analyze these data, we performed an image correlation analysis on our images to estimate the velocity fields throughout the fin fold along time. This allowed us not only to see the final position and direction of the displacement vectors in the fin fold epidermis, but also to calculate the rate at which the tissue is expanding. Taking this into account, the general pattern of epidermal growth during development of the fin fold in 2 dpf, 3 dpf and 4 dpf zebrafish larvae is characterized as being radial, expanding distally along the anterior-posterior axis and to the fin's sides (Figure 5B Uncut). During the blastema and outgrowth phases of regeneration, this pattern is maintained (Figure 5B), but its average velocity is significantly increased with regard to the age-matched uncut controls, mainly in the distal periphery of the epidermal

tissue (Figure 5C Red Areas). This increase in the average speed in a specific direction of epidermal growth is observed throughout most stages of regeneration when compared to the corresponding uncut developmental stages (Figure 5D). In summary, the fin fold epidermis has a defined pattern of growth that is not influenced by the occurrence of an amputation. Nevertheless, to recover from amputation, the epidermal tissue responds by significantly increasing its growth rate.

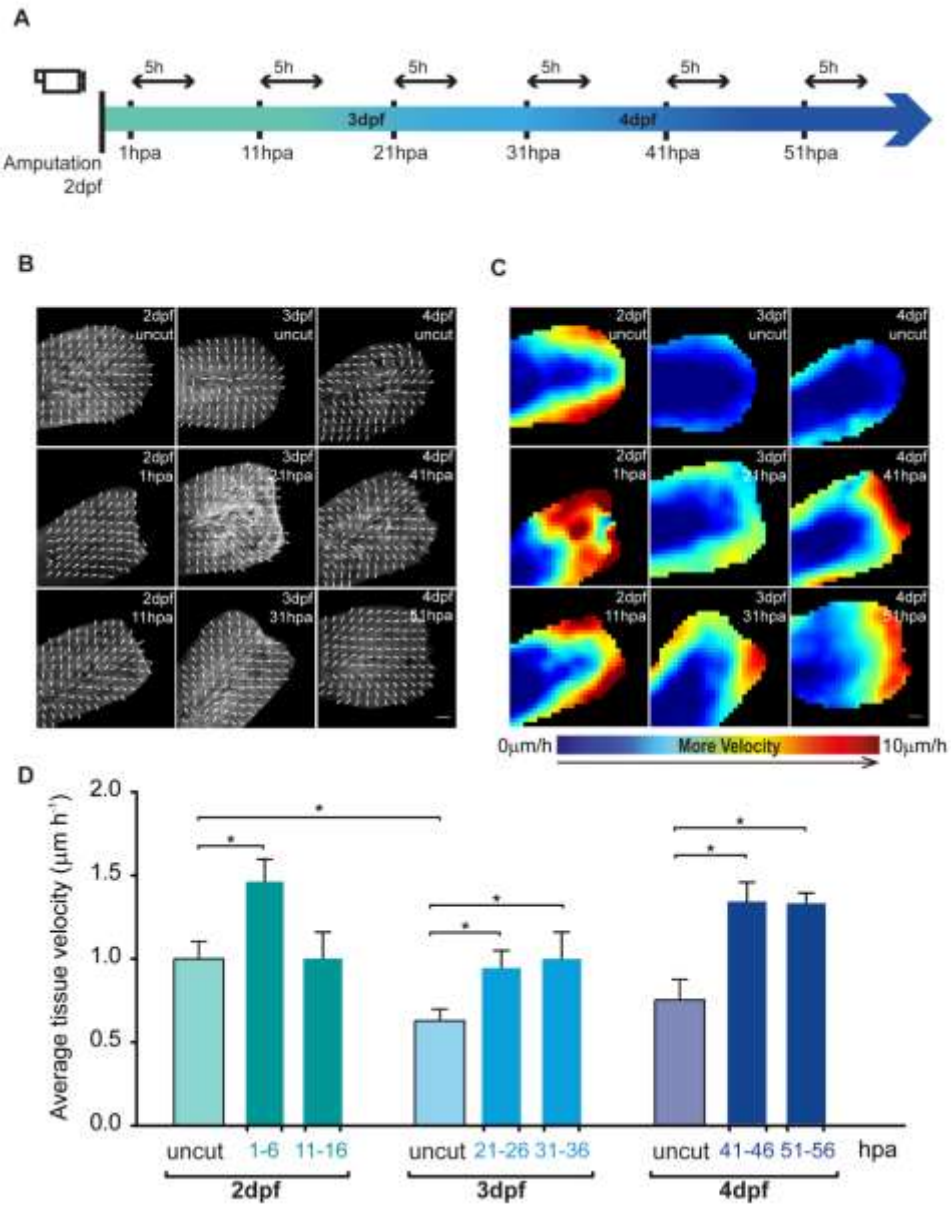

Figure 5. Epidermal tissue growth is enhanced upon fin fold amputation. A Experimental outline of the live imaging procedures taking into account not only the post amputation hours (hpa) but also the developmental days of the larvae (dpf). All the amputations were performed in 2 dpf larvae, and these were allowed to regenerate until the desired hour, the time point in which they were imaged for 5 hours. Taking into account that

the regeneration procedure takes several days, age-matched uncut controls were imaged in the same conditions and for the same amount of time for accurate comparison. **B** Representative maps of vector velocity fields (VVFs) depicting the tissue movement direction along 5h sequential time-lapse imaging of the fin fold regenerative process and respective age-matched uncut controls of *β-actin*:mGFP transgenics. **C** Representative heat maps of the VVFs shown in B depicting the tissue velocity in the fin fold area along the same 5h sequential blocks of the fin fold regenerative process and respective age-matched uncut controls. The red end of the spectrum correlates with higher velocity (0 to 10 μm.hour^{-1}) within a given experiment. **D** Average velocity (μm.hour^{-1}) of VVFs of 5 larvae per condition represented in B–C. Color code matches the Experimental Outline in A. *P value<0.05; Mann-Whitney test values: 2 dpf uncut<>3 dpf uncut = 0.03; 2 dpf uncut<>1–6 hpa = 0.03; 3 dpf uncut<>21–26 hpa = 0.03; 3 dpf uncut<>31–36 hpa = 0.03; 4 dpf uncut<>41–46 hpa = 0.03; 4 dpf uncut<>51–56 hpa = 0.02; 5 larvae per condition. Anterior is on the left and scale bars correspond to 50μm. See also Movies 5-6.

4.3 Proliferation significantly increases during regeneration in a non-circumscribed area.

One of the key characteristics of epimorphic regeneration is the occurrence of a boost of proliferation, precisely restricted in time and space mainly in the blastema (Nechiporuk and Keating, 2002). To determine whether the observed increase in the velocity of epidermal growth can be due to an increase in proliferation, we performed our *in vivo* time-lapse assay in uncut and amputated fins (Figure 5A). In order to detect the nuclei of all cells present in the fin fold, we used the transgenic *H2a.f/z-GFP* (Geldmacher-voss et al., 2001) and quantified all visible cytokinesis events. We found that during larval development, the proliferation rate was progressively reduced from younger (2 dpf) to older (4 dpf) larvae (Figure 6A-B Uncut). In amputated animals, we observed no differences in the number of cell divisions in the initial stages after wound healing (1-6 hpa), when compared

to the 2 dpf uncut control. On the other hand, by 11-16 hpa the cell proliferation had increased significantly when compared to the uncut control (Figure 6B). At 21-26 hpa, the proliferation continued to be significantly higher with regard to 3 dpf uncut controls, albeit at lower levels than those recorded at 11-16 hpa. From 21 hpa until the end of the regenerative process the proliferation levels kept decreasing, until reaching the same rate as uncut controls (Figure 6A-B 4 dpf). These results led us to conclude that during regeneration of the fin fold, proliferation is precisely controlled in time. Regarding spatial restriction, we surprisingly observed that the fin fold tissue responded to the amputation by increasing proliferation in a global manner, instead of being restricted to the most distal portion of the fin fold (Figure 6A), in clear contrast to what happens during zebrafish adult caudal fin regeneration where proliferation is mainly observed within the blastema region (Nechiporuk and Keating, 2002)(Santos-Ruiz et al., 2002). Since proliferation events are many times associated and dependent on apoptosis (Chera et al., 2009), we performed immunohistochemistry to detect active caspase 3 in uncut and amputated fins throughout the regenerative process and could never find significant levels of apoptosis in both experimental conditions (Figure 7). In conclusion, the zebrafish fin fold shows a timely control of proliferation upon amputation, but this is not delimited to a region of the fin fold, happening generally throughout the fin.

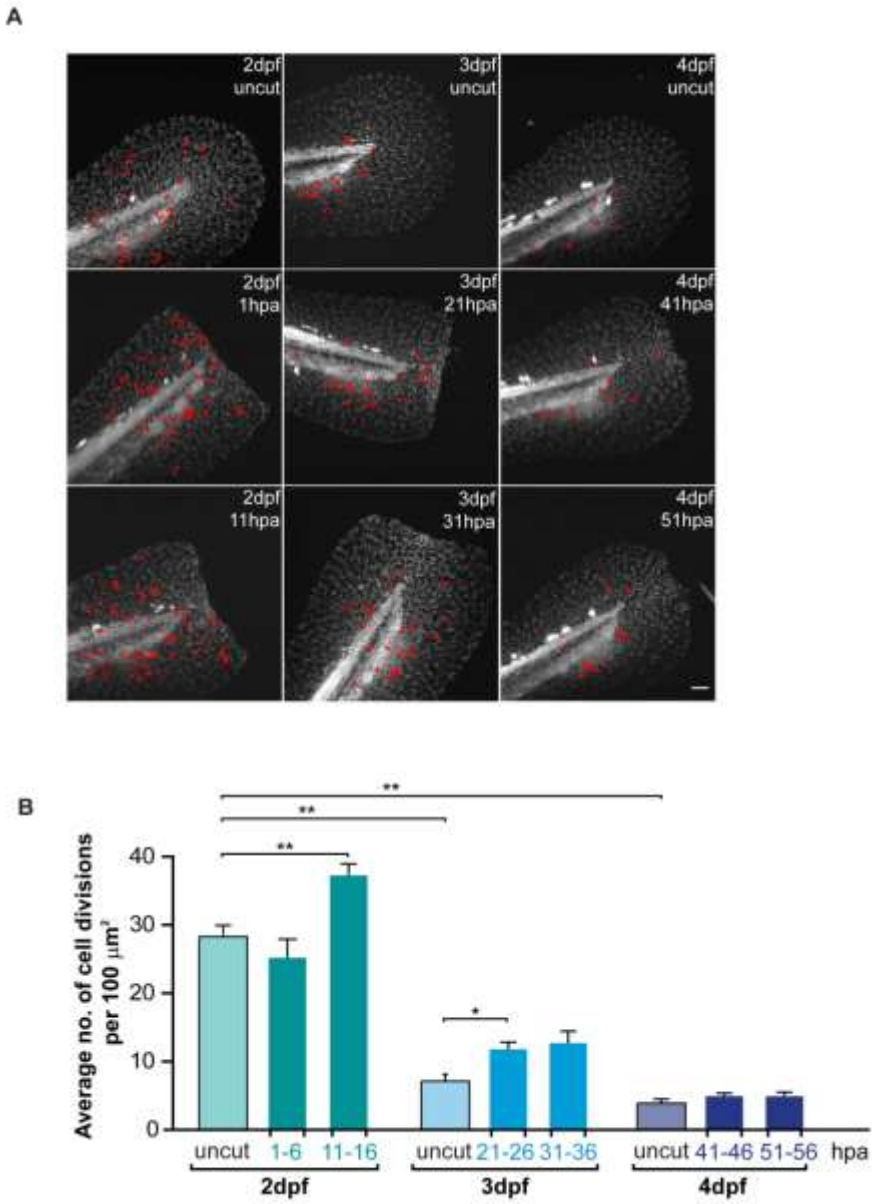

Figure 6. Global levels of proliferation significantly increase during regeneration in a non-spatially restricted manner. A Representative projections of H2a.f/z-GFP transgenics showing total cell divisions (marked in red) which occurred during 5 hour sequential time-lapse imaging movies of the fin fold regenerative process and respective age-matched uncut controls. **B** Average number of cell divisions occurring per 100μm^2 in the several conditions

represented in A. Color code matches the Experimental Outline in Fig. 3A. **P value<0.01, *P value<0.05; Mann-Whitney test values: 2 dpf uncut<>3 dpf uncut = 0.008; 2 dpf uncut<>4 dpf uncut = 0.008; 2 dpf uncut<>11–16 hpa = 0.008; 3 dpf uncut<>21–26 hpa = 0.02; 3 dpf uncut<>31–36 hpa = 0.06; 5 larvae per condition. Anterior is on the left and scale bars correspond to 50µm. See also Movies 7-8.

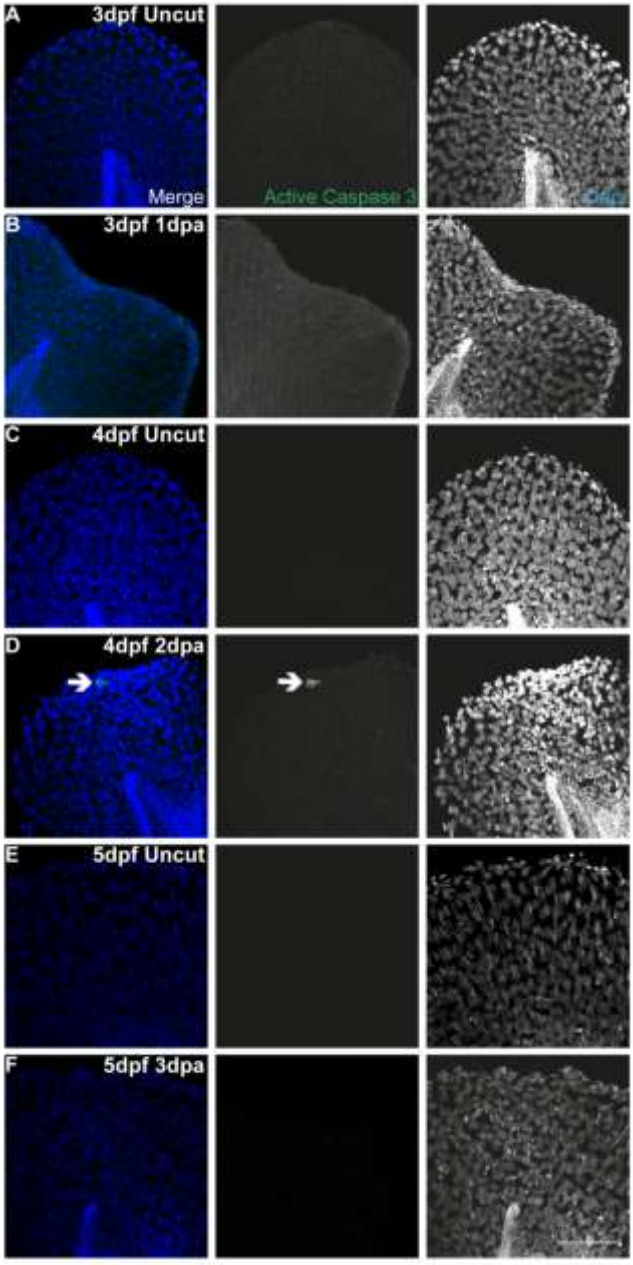

Figure 7. Apoptosis is not present during fin fold regeneration. Representative immunofluorescence with anti-Active Caspase3 in uncut and amputated larvae of 3 dpf (**A–B**), 4 dpf (**C–D**) and 5 dpf (**E–F**). Arrow indicates the presence of an apoptotic cell. n=5 larvae per condition. Scale bar corresponds to 50µm in all images.

4.4 Cell divisions in the fin fold are stereotypically oriented during normal development and follow a randomization tendency upon amputation.

It has been shown that the orientation of cell division is essential during embryonic development and contributes throughout growth and patterning events of several structures as well as during elongation of the embryo (Quesada-Hernández et al., 2010)(Žigman et al., 2010). Since we observed significant changes in the cell proliferation rate upon amputation, we asked whether the orientation of cell division could contribute to the regeneration of the fin fold. To analyze this, we divided the fin fold in 4 regions by establishing 2 main axes, one parallel along the notochord (anterior-posterior axis) and one just distal to the tip of the notochord, perpendicular to it (dorso-ventral axis) (Figure 8). This allowed us to have a reference point to measure the angles at which cytokinesis occurs, in a 360 degree scale. In 2 dpf uncut control larvae, in regions 1 and 4, which are laterally located to the notochord, 78% and 67% of all cell divisions observed occurred in the anterior-posterior (A-P) axis, respectively (Figure 8A). These had a predominant angle of cytokinesis occurring mainly in the intervals of 315-45 degrees and 135-225 degrees (Figure 8A and Figure 9). Hence the major direction of growth in these regions is parallel to the notochord, which likely contributes to the elongation of the body axis (Figure 8A'). Regarding regions 2 and 3, distally located to the notochord, 57% and 74% of the cell divisions occurred in the dorso-ventral (D-V) axis respectively, since they had a predominant angle of cytokinesis in the interval of 225-315 degrees and 45-135 degrees (Figure 8A). This pattern of growth likely allows the fin fold to expand to its sides (Figure 8A'). These results are in accordance with the pattern of growth obtained in our vector velocity field analysis (Figure 5B) and led us to conclude that the cell divisions in the zebrafish fin fold are

stereotypically oriented during its development. A more detailed analysis using 45 degree angle intervals led to the same conclusions (Figure 9).

Nevertheless, upon amputation, no statistically significant differences were observed in any of the analyzed regions when compared to uncut controls. Cell divisions happening in regions 1 and 4 kept the same behavior as in uncut controls, preserving the stereotypical orientations (Figure 8B-C; B'-C'; Regions 1 and 4); however, we verified a slight increase in the percentage of cell divisions in the A-P axis in regions 2 and 3 when compared to the same regions in uncut controls, both in the first regeneration time point (Figure 8B) as well as in the proliferation peak time point (Figure 8C). Thus, there seems to be a tendency for randomization of the angles of cell division during these regeneration stages (Figure 8B'-C'). During later stages of regeneration, we could not establish this analysis due to low cell division numbers.

Taking into account that we observed a tendency for randomization during the wild-type fin fold regenerative process, we decided to functionally determine if disruption of cell division orientation could influence fin fold regeneration. For that, we tested the regenerative capacity of the zebrafish mutant *pipetail (ppt),* a mutant for *wnt5b* (Hammerschmidt et al., 1996). It has been shown that this gene is part of the non-canonical WNT and planar cell polarity signaling pathways; *ppt -/-* animals have impaired cell movements during posterior tailbud formation, leading to defects in tail elongation and resulting in posterior body shortening (Marlow et al., 2004). Importantly, *wnt5b* together with other members of the PCP pathway have been implicated in establishing stereotypical cell divisions during morphogenesis (Kilian et al., 2003)(Gong et al., 2004). By amputating the fin fold of homozygous *ppt* mutants at 2 dpf, we found that they were capable of regenerate within 3 days, being morphologically similar to wild-type (Figure 10A-B). By quantifying the fin fold area of 5 dpf mutants at 3 dpa versus matching wildtype larvae, we did not find significant differences

(Figure 10C). Although noticeably notochord defects could be noticed in the *ppt* -/- larvae, this phenotype did not appear to influence the regenerative process (Figure 10A-B, arrow).

In summary, we conclude that changes in the pattern of cell division orientation do not seem to be a major determinant of fin growth during regeneration.

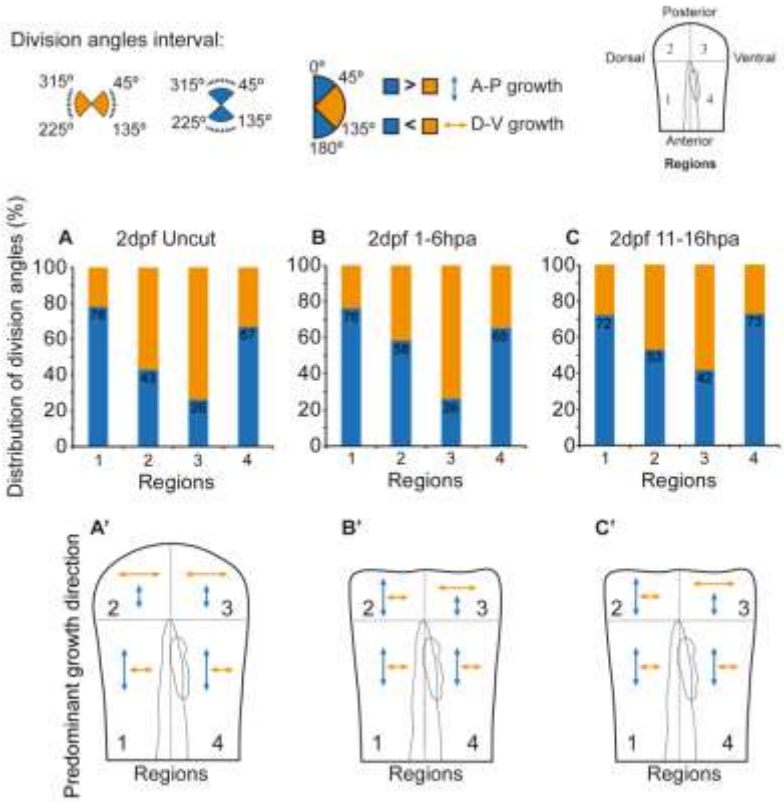

Figure 8. Cell division orientation in the fin fold shows a tendency for randomization predisposition upon amputation. Distribution of division angles according to the interval of 225–315º and 45–135º (orange) or 315–45º and 135–225º (blue) in the designated regions 1–4 of the fin fold in **A** 2 dpf uncut control **B** 2 dpf 1–6 hpa **C** 2 dpf 11–16 hpa. Predominant growth direction in the regions 1–4 taking into account the orientation of the majority of cell divisions happening in **A'** 2 dpf uncut control **B'** 2 dpf 1–6 hpa **C'** 2 dpf 11–16 hpa. n=193

divisions in 2 dpf uncut, n=175 divisions in 2 dpf 1–6 hpa, n=258 divisions in 2 dpf 11–16 hpa; 5 larvae per condition.

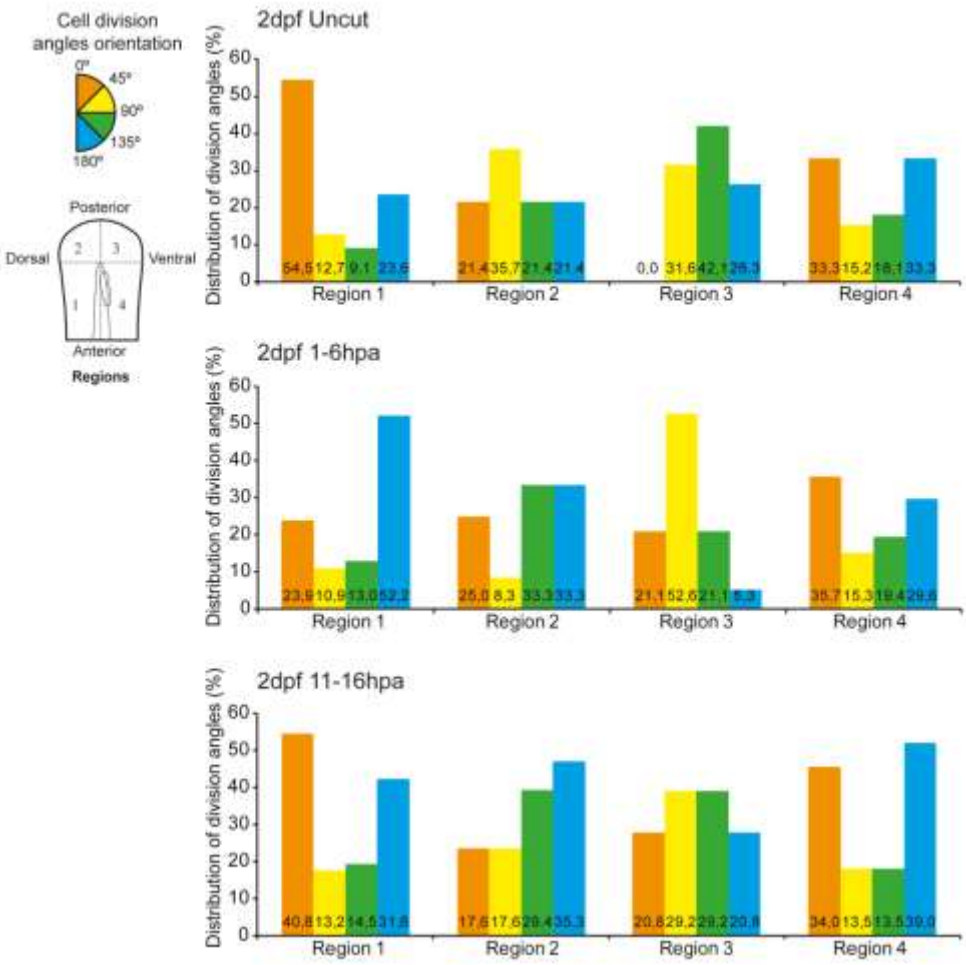

Figure 9. Detailed distribution of cell division angles in the 4 regions of the fin fold. Distribution of cell division angles according to the interval of 0-45º (orange), 45–90º (yellow), 90-135º (green) and 135–180º (blue) in the designated regions 1–4 of the fin fold.

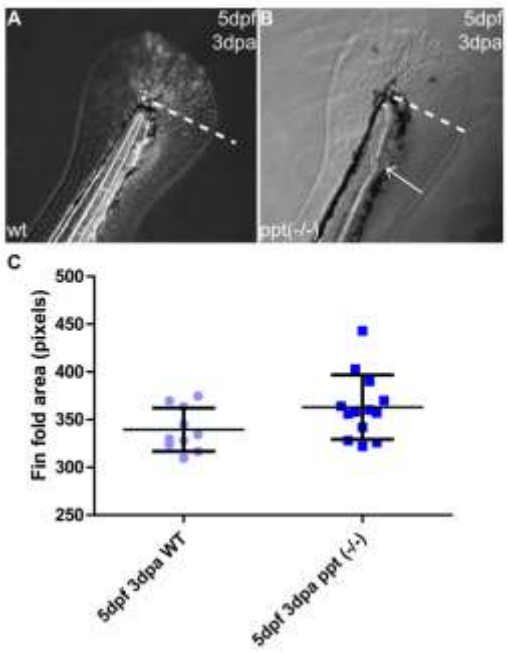

Figure 10. *Pipetail* mutants accomplish fin fold regeneration in a similar manner to wild-type. Representative brightfield live images of 5 dpf 3dpa wild-type, wt (**A**) and homozygous pipetail mutants, ppt (-/-) (**B**). Arrow indicates notochord defects in ppt (-/-) mutants. Dashed lines indicate amputation plane. **C** Quantification of average fin fold area (pixels) of 5 dpf 3 dpa wt and ppt (-/-) larvae. n=10 wt larvae; 13 ppt (-/-) larvae.

4.5 Mesenchymal cells alter their shape and migrate distally upon amputation.

Besides the epidermis, the fin fold is composed of mesenchymal cells. It has been suggested that these cells give rise to the blastema upon amputation like in the adult fin system (Kawakami, 2010), although to our knowledge there is no detailed *in vivo* characterization of these cells during regeneration of the fin fold. These mesenchymal cells are fibroblast-like with a very particular shape, being very elongated with extended protrusions and stretched nuclei (Wood and Thorogood, 1984)(Zhang et al., 2010). It is also known that they are migratory and play a role in providing stabilization and structure to the fin fold by secreting actinotrichia (Wood and Thorogood, 1984)(Zhang et al., 2010)(Feitosa et al., 2012). To understand the function of these cells during regeneration, we used a transgenic that expresses GFP driven by the *osteopontin* promoter. This transgenic labels numerous

structures in the zebrafish, including the mesenchymal cells in the fin fold (Figure 11). To follow and track the migration of these cells, we performed time-lapse imaging (up to 12 hour long) of double positive larvae for *osteopontin:eGFP* and for the cell cycle nuclear marker *EF1α:mKO2-zCdt1* (see Methods). We found that during development at 2 dpf, the *osteopontin*-positive mesenchymal cells do not appear to migrate (Figure 12A-C). However, upon amputation, as early as 30 minpa, a fraction of the mesenchymal cells actively migrated towards the injury (Figure 12D-F). The migrating cells were originally located radially around the notochord, in the center of the fin fold. In addition to migrating, these cells lost their original elongated shape and acquired a more rounded form (Figure 12D-F, Zoom panels, white dots), accumulating distally to the notochord in a blastemal-like zone. Of note, the *osteopontin-eGFP* positive mesenchymal cells always maintained the *mKO2-zCdt1* labeling during the *in vivo* imaging (Figure 12) and throughout the next regenerating days (Figure 13). The protein zCdt1 is a marker for the G0-G1 phase of the cell cycle (Sugiyama et al., 2009), therefore our results indicate that these cells are kept in this phase of the cell cycle, even upon amputation. These data allow us to conclude that the observed changes in cell shape are not directly linked to cell proliferation.

To characterize further the spatiotemporal dynamics leading to small morphology changes in the mesenchymal cells at a single cell level, we performed faster and shorter (up to 3h with acquisition every minute) time-lapse imaging of the same transgenic *EF1α:mKO2-zCdt1;osteopontin:eGFP*, starting at 5 minutes after amputation. In fact, by monitoring the mesenchymal cells in this manner we could detect the initial loss of elongation and rounding up of these cells as early as 35 minpa, and until 1h35 minpa there was a progressive change of morphology (Figure 12G-J Zoom panels, white dots). These changes happened at the same time as the wound healing process was still taking place, indicating a quick reaction of the mesenchymal cells upon amputation and coincided with the

onset of distal migration of these cells. To clarify further the correlation between the migration and the change of cell shape of the mesenchymal cells, we accessed their polarization state. In migrating mesenchymal cells, centrosomes typically assume a position between the leading edge and the nucleus (Gomes et al., 2005)(Sepich et al., 2011). To address this in our system, we compared the location of the centrosome/microtubule organizing center (MTOC) relative to the cell nucleus (Sepich et al., 2011), by performing gamma-tubulin (γTubulin) immunohistochemistry in *osteopontin:eGFP* transgenic animals. We found that in 2 dpf uncut fin folds, the *osteopontin* positive mesenchymal cells had their MTOCs positioned between the nucleus and the stretched protrusions, and in many of these cells, the distance between the MTOC and the nucleus was remarkable (Figure 14, A-A' Uncut). Upon amputation, during the cell shape change and active migration time-points (1 hpa), the MTOC position was maintained between the nucleus and leading edge of the cells, but in close proximity to the nucleus, indicating that these cells did not lose their polarization state during these events (Figure 14, B-B' 1 hpa). By 1 day post-amputation (dpa), when the distal migration and change of shape events are completely concluded, the MTOC position was variable (Figure 14, C-C' 1 dpa): in some cells the MTOC was positioned still between the nucleus and leading edge while in others the MTOC assumed a position in the rear of the cell. This indicates that the polarization of mesenchymal cells can be lost after the complete accumulation in the blastemal-like zone.

To address whether the cell shape changes in mesenchymal cells would continue throughout the rest of the regenerative process, we did immunohistochemistry in the *osteopontin:eGFP* transgenic fish. We confirmed that at 1 and 2 dpa, groups of mesenchymal cells had accumulated near the amputation plane and had become rounder both in terms of cytoplasm and nucleus, when compared with uncut controls (Figure 15A-D *osteopontin:eGFP* and Dapi). In addition, the cortical F-actin present in the regenerating fin fold had developed a complex meshwork in the round

cells (Figure 15B,D F-Actin). Both of these features were undetected at 3 dpa and cell shapes resembled the uncut control, indicating that these events were specific to the regeneration process (Figure 15E-F).

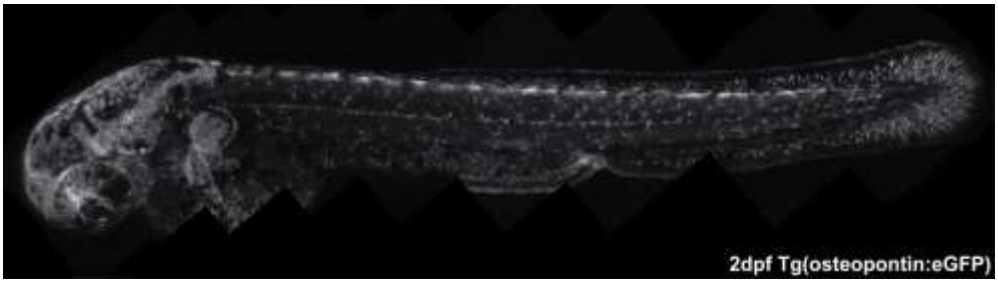

Figure 11. Expression pattern of the 2 dpf transgenic *osteopontin*:eGFP. At this stage of development, this transgenic has labeled the fin fold mesenchymal cells, but also other mesenchymal cells that are spread out along the midline and somites. Besides these, the pectoral fin, the eye and the brain are also GFP positive.

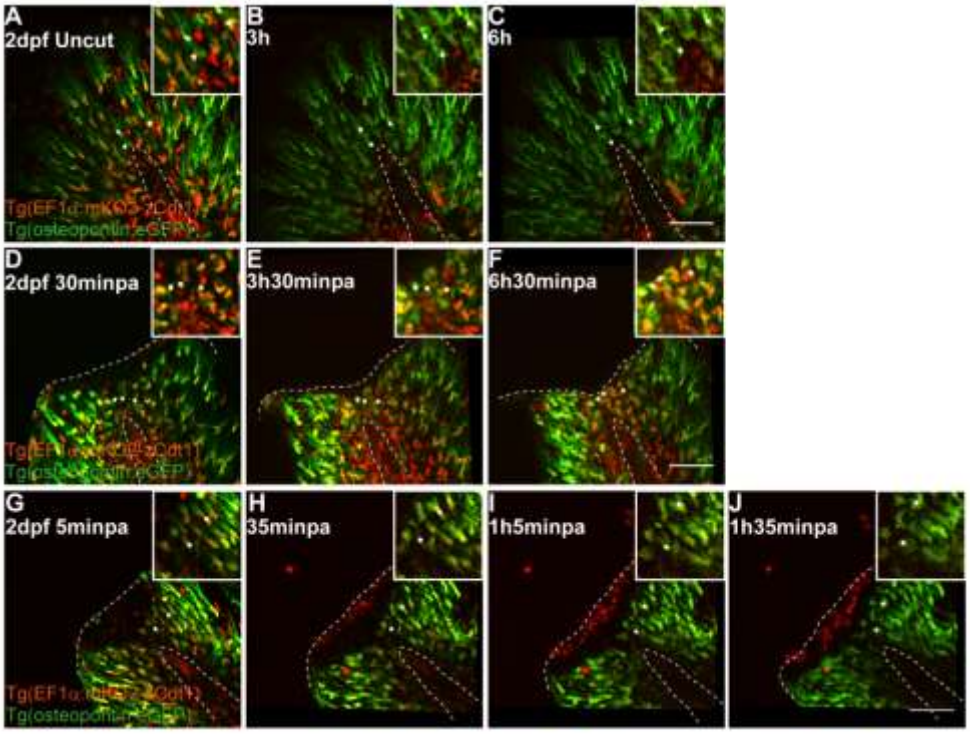

Figure 12. Mesenchymal cells in the fin fold change shape and migrate distally upon injury. A–C Sequential images of a representative *in vivo* 6h time-lapse movie of a 2 dpf uncut *EF1α*:mKO2-zCdt1;*osteopontin*:eGFP transgenic larva. **D–F** Sequential images of a representative *in vivo* 6h time-lapse movie of a 2 dpf 30 minpa *EF1α*:mKO2-zCdt1;*osteopontin*:eGFP transgenic larva. **G–J** Sequential images of a representative *in vivo* 1h30 time-lapse movie of a 2 dpf 5 minpa *EF1α*:mKO2-zCdt1;*osteopontin*:eGFP transgenic larva. Zoom panels highlight osteopontin positive mesenchymal cells in the central area of the fin fold in the respective time point. White dots mark the same cells along time to allow for better visualization and tracking of cell migration. Dashed lines indicate the outline of the notochord and the edge of the amputated fin fold. Scale bars correspond to 50μm in all images; 3–5 larvae per condition. See also Movies 9-10.

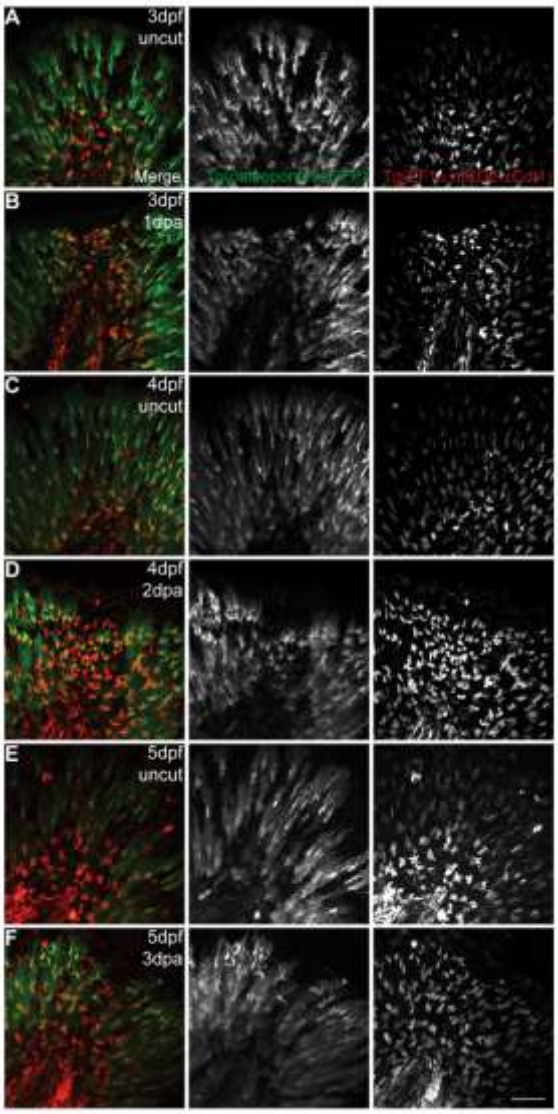

Figure 13. The mesenchymal cells are maintained in G0-G1 phases of the cell cycle regardless of an amputation. Live imaging representative images of double transgenic *EF1α*:mKO2-zCdt1;*osteopontin*:eGFP larvae during several stages of the regenerative process and their respective controls. **A, C, E** are uncut (3 dpf, 4 dpf and 5 dpf respectively) and age matched controls for **B, D, F** (3 dpf 1 dpa, 4 dpf 2 dpa, 5 dpf 3 dpa respectively). Merged and single color images corresponding to *osteopontin:eGFP* labeling the cytoplasm of the mesenchymal cells (green) and mKO2-zCdt1 labeling the nuclei of fin fold cells in G0–G1 phases of the cell cycle (red). 3 larvae per condition. Scale bar corresponds to 50μm.

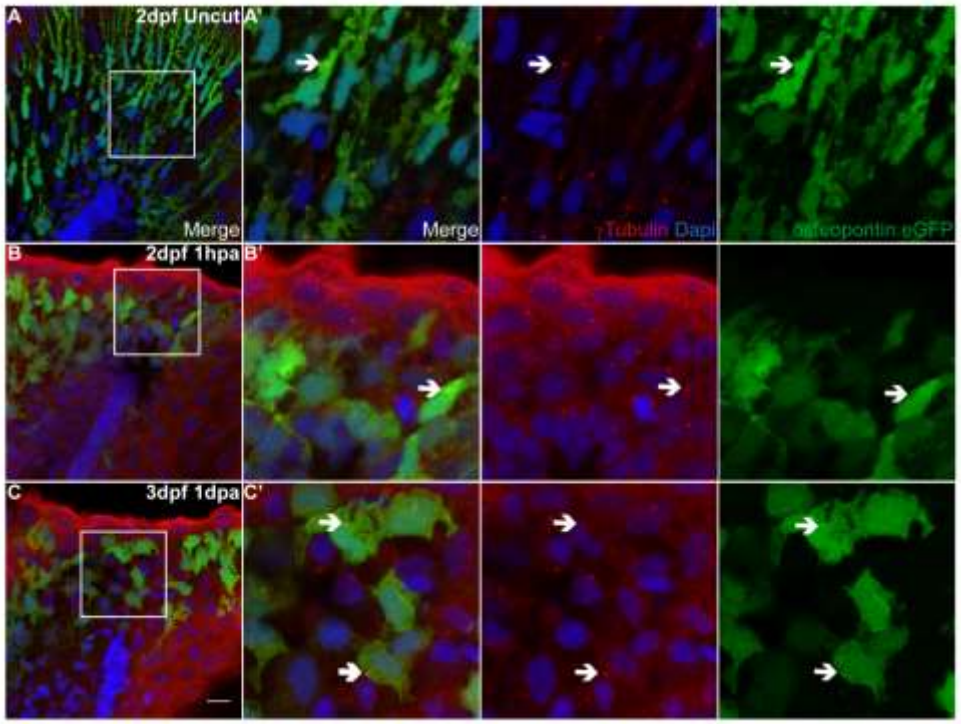

Figure 14. The mesenchymal cells are polarized. A Representative immunostaining with anti-GFP and anti-γTubulin in 2 dpf uncut transgenic *osteopontin*:eGFP larvae (single frame). **B-C** Representative immunostaining with anti-GFP anti-γTubulin in amputated transgenic *osteopontin*:eGFP larvae of 2 dpf 1 hpa and 3 dpf 1 dpa (single frames). **A'-C'** Representative single frames of the corresponding zoomed area represented by a square in A–C. Merged and single color images of the MTOC (γTubulin, red) together with the nuclei (DAPI, blue) and *osteopontin*:eGFP labeling the mesenchymal cells (anti-GFP, green), respectively. The arrows highlight the presence of a MTOC to allow better comparison of its position relative to the corresponding nucleus. 5 Larvae per condition. Scale bar corresponds to 50µm in all images.

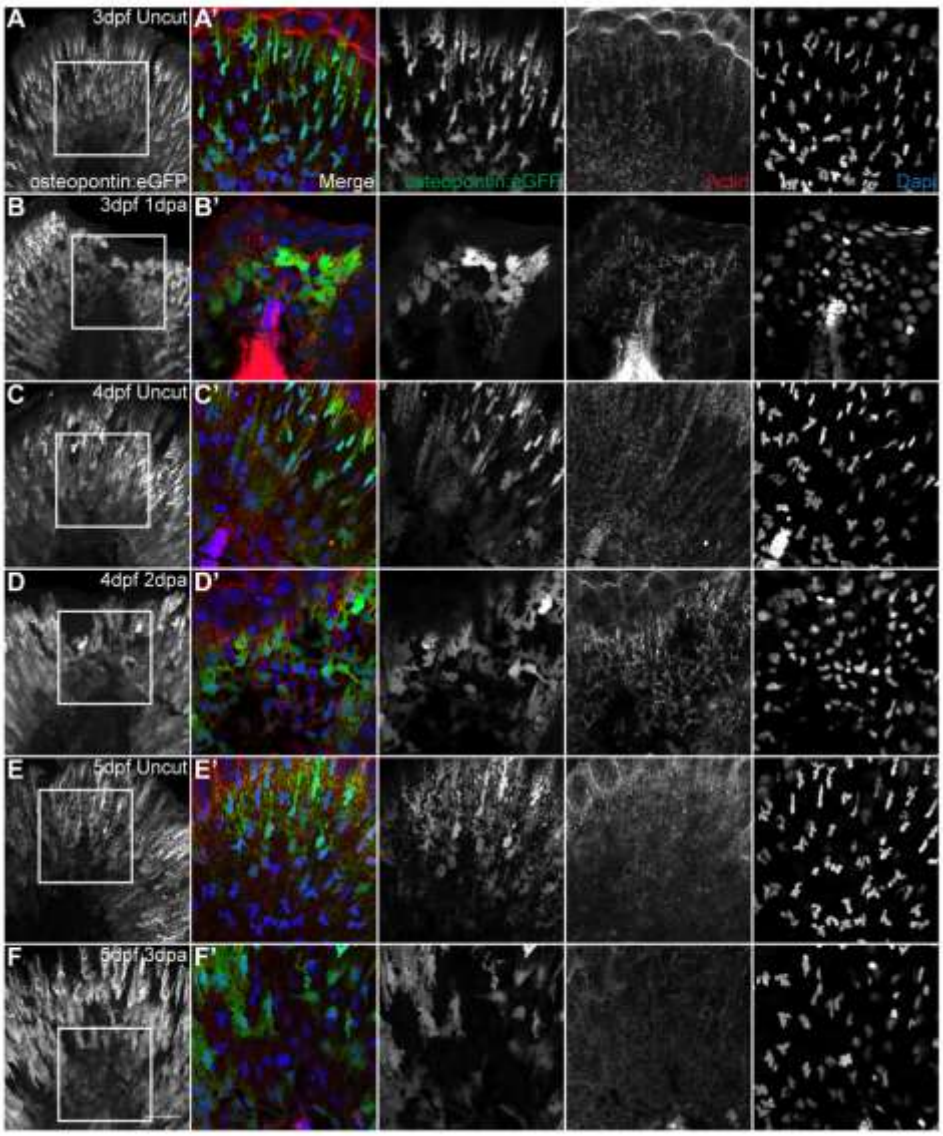

Figure 15. The shape modification of mesenchymal cells lasts throughout and is specific of regeneration. A, C, E Representative immunostaining with anti-GFP in uncut transgenic *osteopontin*:eGFP larvae of 3 dpf, 4 dpf and 5 dpf respectively. **B, D, F** Representative immunostaining with anti-GFP in amputated transgenic *osteopontin*:eGFP larvae of 3 dpf 1 dpa, 4 dpf 2 dpa and 5 dpf 3 dpa respectively. **A–F** Representative z-stack projections of the *osteopontin*:eGFP labeling. **A'–F'** Representative single frames of the

corresponding zoomed area represented by a square in A–F. Merged and single color images of *osteopontin*:eGFP labeling the mesenchymal cells (anti-GFP, green), F-actin (phalloidin, red) and nuclei (DAPI, blue), respectively. 5 Larvae per condition. Scale bar corresponds to 50μm in all images.

5. Discussion

In this work we have systematically characterized the fin fold regeneration process through *in vivo* studies. We analyzed the wound closure dynamics, the contributions of epidermal growth, proliferation levels and orientation of cell divisions necessary to achieve a functional and properly sized fin fold. Also, we have explored the role of mesenchymal cells in this process.

Our findings show that during zebrafish fin fold regeneration there is an actomyosin based mechanism used for wound closure, which seems to be conserved in many other organisms (Macmanus et al., 2005)(Wood et al., 2002)(Danjo and Gipson, 1998). This process is extremely rapid and involves major tissue contraction and relaxation. Importantly, the co-localization of the adherens junctions component Alpha-Catenin with the actomyosin cable raises interesting questions about the complexity and function of this essential structure. This is in accordance with the presence of another adherens junctions marker, Beta-Catenin, at the leading edge cells during wound healing of the zebrafish fin fold (Ishida et al., 2010).

During fin development, the epidermis has a precise pattern of movement and growth that is maintained in the blastema and outgrowth phases of regeneration. On the other hand, during regeneration, the growth rate is significantly increased in all time points apart from 11-16 hpa, to recover the fin's original shape and size in a timely manner. Interestingly, there is a significant increase in proliferation in response to the amputation, which happens precisely at 11-16 hpa. This indicates that, like in the adult caudal fin regeneration system, the proliferation is controlled in time (Nechiporuk and Keating, 2002). However, in contrast to the adult system, this increase in proliferation does not seem to be spatially restricted (Nechiporuk and Keating, 2002)(Santos-Ruiz et al., 2002). In fact, during the proliferation peak, we noticed cytokinesis events happening in a broad area of the fin fold, and not only in the most distal tissue. It appears that the fin fold

blastema does not have a specific function for proliferation and in that way it is not a classical blastema, as observed in the adult system.

Previous reports have shown that proliferation of blastema-like cells increases upon amputation of the larval fin fold, however, the authors suggested that such proliferation is spatially restricted (Kawakami et al., 2004)(Yoshinari et al., 2009)(Ishida et al., 2010). This work was based on BrdU pulse-chase experiments where cells were labeled at different time points after amputation and their position within the fin fold accessed at the end of the regeneration process. In contrast our data shows that in the first hours after amputation the number of cell divisions increases but not in a preferential region of the fin. We propose that this discrepancy might be due to the distinct methods used to determine proliferation in the two studies. We believe that our characterization of the full process *in vivo* clearly reveals a global proliferation response, a property that appears to be specific of fin fold regeneration.

When comparing the epidermal growth and proliferation events, we observed that the tissue growth rate seems to increase with time during the regeneration process at the same time as proliferation slows down (compare Figures 5D and 6B), implying that tissue growth is compensated by a mechanism that does not depend on proliferation. The only time point at which the velocity of epidermal growth is not significantly increased is when the proliferation is at its peak (between 11 and 16 hpa), suggesting that there are other outgrowth mechanisms that contribute crucially to this process.

We show, for the first time, that the mesenchymal cells present in the fin fold react to amputation by migrating and accumulating distally. This is accompanied by a change of cell shape and an increase in the complexity of the cortical network of actin that is assembled in these cells. In fact, previous reports addressing these cells during fin fold regeneration, show that there is an increase in the condensation of their nuclei (Kawakami et al., 2004). This is in accordance with our cell shape change results, where we

found a clear transformation of the mesenchymal cells typical shape into a more round form, including in their nuclear shape. This alteration in shape could be due to these cells entering an active cell cycle process, initiating cell division; however this does not seem to be the case, since the mesenchymal cells remain in the G0-G1 phase of the cell cycle throughout the full regeneration process. It is also possible that this change in morphology is part of a dedifferentiation process triggered by the amputation, as in the adult caudal fin model where these cells acquire a round form and migrate distally to constitute the blastema (Knopf et al., 2011)(Sousa et al., 2011); nevertheless the differentiation state of the fin fold mesenchymal cells is still uncharacterized. There are indications that during the fin fold development, these cells acquire progressively their protrusive morphology, suggesting that this is consistent with a more differentiated status (Wood and Thorogood, 1984)(Feitosa et al., 2012); if that is the case, then the mesenchymal cells may be undergoing dedifferentiation during the fin fold's regenerative process. The function of these cells in the regeneration process is still unclear, but it is possible that they are part of a signaling center (Yoshinari et al., 2009)(Mathew et al., 2009)(Pittlik and Begemann, 2012), and to that extent, constitute the so-called blastema in a comparable manner to the adult system.

6. References

Balciunas, D., Wangensteen, K.J., Wilber, A., Bell, J., Geurts, A., Sivasubbu, S., Wang, X., Hackett, P.B., Largaespada, D. a, McIvor, R.S., et al. (2006). Harnessing a high cargo-capacity transposon for genetic applications in vertebrates. PLoS Genet. *2*, e169.

Behrndt, M., Salbreux, G., Campinho, P., Hauschild, R., Oswald, F., Roensch, J., Grill, S.W., and Heisenberg, C.-P. (2012). Forces driving epithelial spreading in zebrafish gastrulation. Science *338*, 257–260.

Bessa, J., Tena, J.J., de la Calle-Mustienes, E., Fernández-Miñán, A., Naranjo, S., Fernández, A., Montoliu, L., Akalin, A., Lenhard, B., Casares, F., et al. (2009). Zebrafish enhancer detection (ZED) vector: a new tool to facilitate transgenesis and the functional analysis of cis-regulatory regions in zebrafish. Dev. Dyn. *238*, 2409–2417.

Burkel, B.M., von Dassow, G., Bement, W.M., and Dassow, G. Von (2007). Versatile fluorescent probes for actin filaments based on the actin-binding domain of utrophin. Cell Motil. Cytoskeleton *64*, 822–832.

Campbell, L.J., Crews, C.M., and Sciences, M.L. (2008). Wound epidermis formation and function in urodele amphibian limb regeneration. Cell. Mol. Life Sci. *65*, 73–79.

Campbell, L.J., Suárez-Castillo, E.C., Ortiz-Zuazaga, H., Knapp, D., Tanaka, E.M., and Crews, C.M. (2011). Gene expression profile of the regeneration epithelium during axolotl limb regeneration. Dev. Dyn. *240*, 1826–1840.

Chera, S., Ghila, L., Dobretz, K., Wenger, Y., Bauer, C., Buzgariu, W., Martinou, J., and Galliot, B. (2009). Apoptotic cells provide an unexpected source of Wnt3 signaling to drive hydra head regeneration. Dev. Cell *17*, 279–289.

Cooper, M.S., Szeto, D.P., Sommers-herivel, G., Topczewski, J., Solnica-Krezel, L., Kang, H., Johnson, I., Kimelman, D., and Al, C.E.T. (2005). Visualizing morphogenesis in

transgenic zebrafish embryos using BODIPY TR methyl ester dye as a vital counterstain for GFP. Dev. Dyn. *232*, 359–368.

Dane, P.J., and Tucker, J.B. (1985). Modulation of epidermal cell shaping and extracellular matrix during caudal fin morphogenesis in the zebra fish Brachydanio rerio. J. Embryol. Exp. Morphol. *87*, 145–161.

Danjo, Y., and Gipson, I.K. (1998). Actin "purse string" filaments are anchored by E-cadherin-mediated adherens junctions at the leading edge of the epithelial wound, providing coordinated cell movement. J. Cell Sci. *111 (Pt 2*, 3323–3332.

Durán, I., Marí-Beffa, M., Santamaría, J.A., Becerra, J., and Santos-Ruiz, L. (2011). Actinotrichia collagens and their role in fin formation. Dev. Biol. *354*, 160–172.

Echeverri, K., Clarke, J.D.W., and Tanaka, E.M. (2001). In vivo imaging indicates muscle fiber dedifferentiation is a major contributor to the regenerating tail blastema. Dev. Biol. *236*, 151–164.

Feitosa, M., Zhang, J., Thomas, J., Metzger, M., Korzh, V., Hammerschmidt, M., Feitosa, N.M., Carney, T.J., and Bloch, W. (2012). Hemicentin 2 and Fibulin 1 are required for epidermal-dermal junction formation and fin mesenchymal cell migration during zebrafish development. Dev. Biol. *369*, 235–248.

Geldmacher-voss, S.P.B., Pauls, S., Geldmacher-Voss, B., and Campos-Ortega, J. a (2001). A zebrafish histone variant H2A.F/Z and a transgenic H2A.F/Z:GFP fusion protein for in vivo studies of embryonic development. Dev. Genes Evol. *211*, 603–610.

Gomes, E.R., Jani, S., and Gundersen, G.G. (2005). Nuclear movement regulated by Cdc42, MRCK, myosin, and actin flow establishes MTOC polarization in migrating cells. Cell *121*, 451–463.

Gong, Y., Mo, C., and Fraser, S.E. (2004). Planar cell polarity signalling controls cell division orientation during zebrafish gastrulation. *430*, 689–693.

Hammerschmidt, M., Pelegri, F., Mullins, M.C., Kane, D. a, Brand, M., van Eeden, F.J., Furutani-Seiki, M., Granato, M., Haffter, P., Heisenberg, C.P., et al. (1996). Mutations affecting morphogenesis during gastrulation and tail formation in the zebrafish, Danio rerio. Development *123*, 143–151.

Ishida, T., Nakajima, T., Kudo, A., and Kawakami, A. (2010). Phosphorylation of Junb family proteins by the Jun N-terminal kinase supports tissue regeneration in zebrafish. Dev. Biol. *340*, 468–479.

Kawakami, A. (2010). Stem cell system in tissue regeneration in fish. Dev. Growth Differ. *52*, 77–87.

Kawakami, A., Fukazawa, T., and Takeda, H. (2004). Early fin primordia of zebrafish larvae regenerate by a similar growth control mechanism with adult regeneration. Dev. Dyn. *231*, 693–699.

Kilian, B., Mansukoski, H., Carreira, F., Ulrich, F., Tada, M., Heisenberg, C.-P., and Barbosa, F.C. (2003). The role of Ppt/Wnt5 in regulating cell shape and movement during zebrafish gastrulation. Mech. Dev. *120*, 467–476.

Knopf, F., Hammond, C., Chekuru, A., Kurth, T., Hans, S., Weber, C.W., Mahatma, G., Fisher, S., Brand, M., Schulte-Merker, S., et al. (2011). Bone Regenerates via Dedifferentiation of Osteoblasts in the Zebrafish Fin. Dev. Cell *20*, 713–724.

Kragl, M., Knapp, D., Nacu, E., Khattak, S., Maden, M., Epperlein, H.H., and Tanaka, E.M. (2009). Cells keep a memory of their tissue origin during axolotl limb regeneration. Nature *460*, 60–65.

Lee, Y., Hami, D., De Val, S., Kagermeier-Schenk, B., Wills, A.A., Black, B.L., Weidinger, G., and Poss, K.D. (2009). Maintenance of blastemal proliferation by functionally diverse epidermis in regenerating zebrafish fins. Dev. Biol. *331*, 270–280.

Macmanus, C.F., Tipping, N.E., and Wilson, D.J. (2005). A Rho-dependent actin purse-string is involved in wound repair in the early chick amnion following surgical puncture. Wound Repair Regen. *14*, 61–65.

Marlow, F., Gonzalez, E.M., Yin, C., Rojo, C., and Solnica-Krezel, L. (2004). No tail co-operates with non-canonical Wnt signaling to regulate posterior body morphogenesis in zebrafish. Development *131*, 203–216.

Mathew, L.K., Sengupta, S., Franzosa, J.A., Perry, J., La Du, J., Andreasen, E.A., and Tanguay, R.L. (2009). Comparative expression profiling reveals an essential role for raldh2 in epimorphic regeneration. J. Biol. Chem. *284*, 33642–33653.

Morgan, T.H. (1901). REGENERATION AND LIABILITY TO INJURY. Science *14*, 235–248.

Nechiporuk, A., and Keating, M.T. (2002). A proliferation gradient between proximal and msxb-expressing distal blastema directs zebrafish fin regeneration. Development *129*, 2607–2617.

Neugebauer, J.M., Amack, J.D., Peterson, A.G., Bisgrove, B.W., and Yost, H.J. (2009). FGF signalling during embryo development regulates cilia length in diverse epithelia. Nature *458*, 651–654.

Pittlik, S., and Begemann, G. (2012). New sources of retinoic acid synthesis revealed by live imaging of an Aldh1a2-GFP reporter fusion protein throughout zebrafish development. Dev. Dyn. *241*, 1205–1216.

Quesada-Hernández, E., Caneparo, L., Schneider, S., Winkler, S., Liebling, M., Fraser, S.E., and Heisenberg, C.-P. (2010). Stereotypical cell division orientation controls neural rod midline formation in zebrafish. Curr. Biol. *20*, 1966–1972.

Santos-Ruiz, L., Santamaría, J.A., Ruiz-Sánchez, J., and Becerra, J. (2002). Cell proliferation during blastema formation in the regenerating teleost fin. Dev. Dyn. *223*, 262–272.

Sepich, D.S., Usmani, M., Pawlicki, S., and Solnica-Krezel, L. (2011). Wnt/PCP signaling controls intracellular position of MTOCs during gastrulation convergence and extension movements. Development *138*, 543–552.

Slanchev, K., Carney, T.J., Stemmler, M.P., Koschorz, B., Amsterdam, A., Schwarz, H., and Hammerschmidt, M. (2009). The epithelial cell adhesion molecule EpCAM is required for epithelial morphogenesis and integrity during zebrafish epiboly and skin development. PLoS Genet. *5*, e1000563.

Sousa, S., Afonso, N., Bensimon-Brito, A., Fonseca, M., Simões, M., Leon, J., Roehl, H., Cancela, M.L., and Jacinto, A. (2011). Differentiated skeletal cells contribute to blastema formation during zebrafish fin regeneration. Development *138*, 3897–3905.

Sugiyama, M., Sakaue-Sawano, A., Iimura, T., Fukami, K., Kitaguchi, T., Kawakami, K., Okamoto, H., Higashijima, S., and Miyawaki, A. (2009). Illuminating cell-cycle progression in the developing zebrafish embryo. Proc. Natl. Acad. Sci. U. S. A. *106*, 20812–20817.

Wood, A., and Thorogood, P. (1984). An analysis of in vivo cell migration during teleost fin morphogenesis. J. Cell Sci. *222*, 205–222.

Wood, W., Jacinto, A., Grose, R., Woolner, S., Gale, J., Wilson, C., and Martin, P. (2002). Wound healing recapitulates morphogenesis in Drosophila embryos. Nat. Cell Biol. *4*, 907–912.

Yoshinari, N., Ishida, T., Kudo, A., and Kawakami, A. (2009). Gene expression and functional analysis of zebrafish larval fin fold regeneration. Dev. Biol. *325*, 71–81.

Zhang, J., Wagh, P., Guay, D., Sanchez-Pulido, L., Padhi, B.K., Korzh, V., Andrade-Navarro, M.A., and Akimenko, M.-A. (2010). Loss of fish actinotrichia proteins and the fin-to-limb transition. Nature 1–5.

Žigman, M., Trinh, L. a, Fraser, S.E., Moens, C.B., and Zigman, M. (2010). Zebrafish neural tube morphogenesis requires Scribble-dependent oriented cell divisions. Curr. Biol. *21*, 79–86.

7. Acknowledgements

The authors thank the Fish Facility technicians Lara M. Carvalho, Fábio Valério and Aida Barros for support with animal care. We thank Lara C. J. Carvalho, Duarte Mesquita, Anabela Bensimon-Brito and Ana Sofia Azevedo for reading the manuscript and for insightful discussions and Inês Cristo for help with Imaris Software. We also thank Susana Lopes for reagents.

CHAPTER III

CHEMICAL MODULATION OF ZEBRAFISH FIN FOLD REGENERATION

IDENTIFICATION OF NOVEL SMALL MOLECULE REGULATORS OF SIZE CONTROL IN REGENERATION

“Whether after a certain time the reproduction becomes equal to the old part, both in bulk and length?”

In *An essay in animal reproductions*
L. Spallanzani, 1769

CONTENTS

The author of this thesis performed all the experiments.

1. Summary

Upon amputation, the zebrafish has the extraordinary ability to regenerate the missing organ part, recovering precisely its original size and pattern. Which regulators take part in such a remarkable and exact process is yet to be determined. During larval stages, the fin fold allows the possibility of performing *in vivo* medium throughput chemical screens making this a straightforward system to search for new regulators of fin size during regeneration. In this work we functionally addressed this longstanding question by screening 1200 small molecules during the entire fin fold regenerative process, these being the first time that were tested in this context. From this chemical library, we found 14 compounds having an inhibitory effect on the regenerative process, leading to reduced growth of the fin fold. These results present a starting point to understand the mechanisms of size control during fin fold regeneration.

1.1 Keywords

Regeneration, zebrafish, fin fold, chemical screen, positional memory, size control.

2. Introduction

One of the hallmarks of epimorphic regeneration is that, upon amputation, there is an accurate recovery of the injured organ to its original size and pattern (Spallanzani, 1769). This property, designated as positional memory, states that the cells within a certain location of the stump can identify signals that instruct them in restoring the missing structure (Morgan, 1906)(Wolpert, 1969). Importantly, such signals have been considered morphogens, secreted signaling molecules, which can trigger the cells into events such as proliferation, apoptosis, differentiation and cell re-arrangements. These processes must proceed in a specified manner, within certain controlled and proportional levels, so that growth of the organ is achieved gradually and robustly.

The regenerative growth rate has been one of the readouts of the existence of positional memory within regenerating appendages (Iten and Bryant, 1976)(Maden, 1976), since it will vary according to the amount of tissue that is amputated: the growth rate will be faster when there is a need to regenerate a greater portion of the appendage. This position-dependent growth rate suggests that concentration gradients of morphogenetic information are present along the proximo-distal axis of the organs regulating the regenerative growth rate and directing the cells in how much tissue is absent (Wolpert, 1969)(Wolpert, 2011). If this is the case, in an injury situation, regardless of how the existing signaling gradients are established and maintained, their disruption by a sudden overexpression or downregulation of an interfering molecule would affect the growth rate of amputated appendages, depending on the gradient's orientation. Another possibility is that a morphogen would have a restricted location and pattern of expression within the regenerating tissue, providing local information to the cells at a specific time during the process.

In the fish caudal fins, the existence of positional memory during regeneration appears to occur in a similar way to the morphological events described in the limbs of salamanders and newts (Morgan, 1906)(Nabrit, 1929). However, the maintenance of the original size upon injury remains with little molecular evidence. To date, it has been shown that Fgf plays a role in the regulation of proliferation along the proximal-distal axis of the regenerating caudal fin (Lee et al., 2005). Moreover, other signaling pathways that are essential for the regenerative process can also influence the proliferation levels in the fin; for example, *wnt5b* mutants have to a certain extent longer fins upon amputation (Stoick-Cooper et al., 2007), and stimulation of *shh* with the use of *smoothened* agonists also leads to an enhanced proliferation in the blastema (Lee et al., 2009). Despite these examples, limited signaling pathways have been addressed during regeneration. This showcases the need for regeneration exploratory studies, in order to find possible signaling molecules that could act as morphogens instructing positional information via concentration gradients.

Here we address this issue by establishing a chemical screen to search for new molecules that can modulate growth during regeneration *in vivo*. We use the zebrafish larvae fin fold as a screenable model since upon amputation there is a robust recovery of their fin fold size (Kawakami et al., 2004)(our own work). This indicates that, like in the adult caudal fin system, there is also the presence of positional memory upon amputation, although the tissue has a simpler organization, containing less cell types (Wood and Thorogood, 1984)(Feitosa et al., 2012)(Durán et al., 2011)(Zhang et al., 2010)(Slanchev et al., 2009)(Dane and Tucker, 1985). The propensity to screen large numbers of animals, their small size and capacity to regenerate within three days made this an appealing model system.

We show that out of 1200 small molecules screened during fin fold regeneration 14 compounds were found to interfere with this process, leading to less growth phenotypes. This analysis led to the discovery of

inhibitory molecules never before associated with regeneration, possibly revealing new insights into this process.

3. Materials and Methods

3.1 Ethics Statement

All experiments involving animals were approved by the Animal User and Ethical Committees at Instituto de Medicina Molecular, according with directives from Direcção Geral Veterinária (PORT 1005/92).

3.2 Zebrafish lines, maintenance and surgery

Zebrafish AB wild-type strain lines were used and maintained in a re-circulating system with a 14 h/day and 10 h/night cycle at 28°C. Embryos were gathered as described in *The Zebrafish Book* and kept in E3 (5mM NaCl, 0,17mM KCl, 0,33mM $CaCl_2$, 0,33mM $MgSO_4$, 10^{-5}% Methylene Blue) zebrafish embryo medium at 28°C until reaching the desired developmental stage. All fin fold amputations were performed in 2 days post fertilization (dpf) larvae anaesthetized in 0.1% MS-222 (Sigma) using a scalpel as previously described (Kawakami et al., 2004). Regeneration was then allowed to proceed until defined time points at 28°C.

3.3 Chemical screen

The small molecule library Prestwick from Prestwick Chemical (1200 compounds, Illkirch, France) was used for the screen. Two fin fold amputated larvae at 2 dpf were arrayed per each well in black 96-well plates with a clear flat bottom (Nunc). Each well contained 300µL of buffered E3 without Methylene Blue (10mM Hepes, pH 7.0) with an individual chemical compound at a final concentration of 25µM. The amputated larvae were incubated in the compound for 3 days at 28ºC. Control larvae were treated with 1% DMSO (Sigma) in parallel wells of each plate. At 3 days post amputation and 5 dpf, the phenotypes were assessed by anaesthetizing the

larvae and acquiring images in a Zeiss Axiovert 200 with a phase contrast 1.5x objective for automated acquisition of all wells in the plate (for a global overview) and with a 20x phase contrast objective for detailed fin fold images.

3.4 Validation of specific small molecules

For all the compounds that presented a growth phenotype, a repetition of the assay in three separate wells was performed in order to confirm the results. After this, if the phenotype was consistent, validation with the commercial individual compounds was performed.

3.5 Database

For compilation of all the screen generated information, a custom database was created using Filemaker with the following entry fields: chemical name, screen ID, location of the compound in the original Prestwick plate, final concentration in the well, known mechanisms of action, phenotype assessment, chemical structure and larvae results images. This allowed not only finding and comparing information in a faster manner, but also allowed for general data consultation.

4. Results

4.1 Establishment of a screenable Zebrafish regeneration assay.

As a starting point to try to understand how size-control is regulated in the zebrafish fin fold, a chemical screening strategy was developed in 2 dpf larvae to find new molecules capable of altering fin fold size. By using larvae at this stage we could apply the previously established fin fold regeneration model system (Kawakami et al., 2004) and test many compounds in a time and cost effective manner. We decided to use a commercially available small molecule library, Prestwick, composed of 1200 FDA approved compounds. This choice was made not only because of the large chemical diversity of molecules present in the library but also due to the availability of information regarding possible mechanisms of action as a result of their employment in diverse therapies.

The screening assay consisted in exposing the zebrafish larvae to the compounds right after amputation and throughout the entire regeneration period (3 days) at a restrictive final concentration of 25µM (Mathew et al., 2007). This would allow us to identify as many molecules as possible that could have a specific mode of action in the different regenerative phases, possibly resulting in different phenotypic outcomes. After this, the animals were screened for a growth phenotype: positive, when the fin fold length was larger than controls; neutral, when the fin fold recovered to the same size as controls; or negative, when the fin fold length was smaller than controls (Figure 1). At this time, the analysis of the compound phenotypes included a morphological examination of possible toxic effects and preliminary analysis of the regeneration structures (i.e. presence of wound epidermis), which allowed an initial assessment of which regeneration phase the molecule could be acting. In order to have replicates and avoid false positives, each well contained two larvae to be exposed to the same

molecule; the compound was considered a candidate molecule for a positive hit only if both larvae exhibited the same growth phenotype. Following identification, validation of the candidate molecules was pursued by repeating the assay in three independent wells, each containing 2 larvae. If the growth phenotype was maintained following this initial validation, then the candidate molecule would be considered a positive hit in that growth phenotype category.

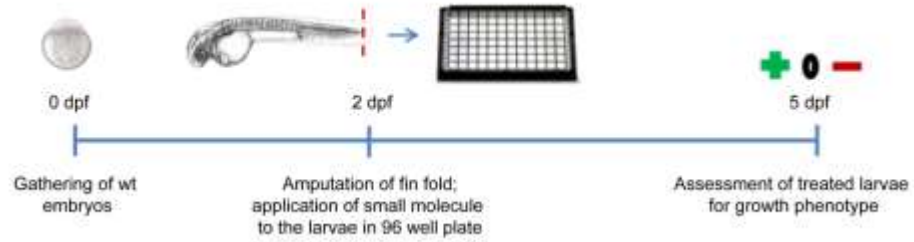

Figure 1. Experimental outline of the fin fold regeneration chemical screening assay. It is possible to retrieve the wild type (wt) zebrafish embryos (Day 0), amputate and expose them to the compound libraries (Day 2) and finally assess the possible drug effects in growth by morphological observation (Day 5).

As reported previously, the zebrafish fin fold can recover its size upon amputation to the same as uncut age-matched siblings, demonstrating that the tissue is not only competent of recovering to its original developmental size at the time of the amputation, but also capable of recovering to its current developmental stage size (Kawakami et al., 2004)(Mateus et al., 2012). This remarkable property indicates that the rate of regenerative growth must not only accompany the rate of developmental growth, but also be able to efficiently surpass it to allow for a successful regenerative process. As a further confirmation of this capacity, which was the premise of

our screening assay, we quantified the length of 5 dpf fin folds that were: subjected to no amputation (Figure 2 5dpf Uncut); amputated at 2 dpf (Figure 2 5dpf 3dpa Untreated); amputated at 2 dpf and treated with 1% DMSO (Figure 2 5dpf 3dpa DMSO). For all of these conditions, some of the larvae were incubated in normal E3 media and part were kept in buffered E3 media. The basis for the use of buffered E3 was that it should maintain the pH at a steadier level throughout the experimental time of the screening assay, an essential feature for maximum efficiency of the small molecules to be tested. We observed that the amputated fin folds' size was always recovered to uncut levels independently of the different conditions applied, reinforcing our screening readout robustness.

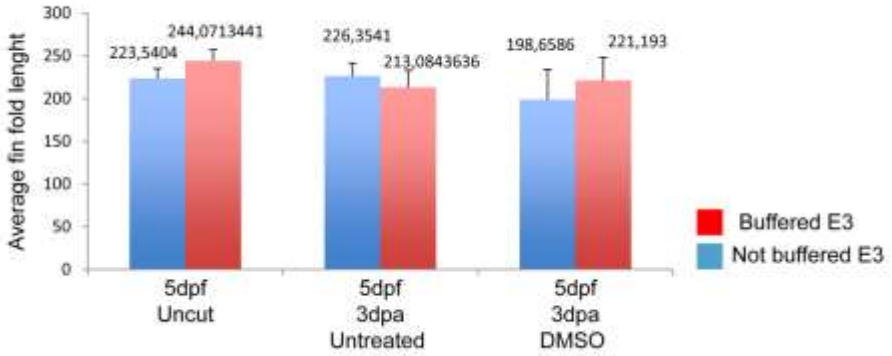

Figure 2. The fin fold size is recovered to its developmental stage counterpart upon amputation. Average fin fold length (pixels) of 5 dpf larvae in different conditions: uninjured fin fold (5dpf Uncut), amputated fin fold at 2 dpf (5 dpf 3 dpa Untreated) and amputated fin fold at 2 dpf and exposed to 1% DMSO (5 dpf 3 dpa DMSO). For all fin fold conditions, larvae were kept for 3 days in Buffered E3 (red) or Not Buffered, regular E3 (blue). n=30 larvae per condition.

4.2 Identification of positive controls within the glucocorticoid cluster.

The existence within the Prestwick library of a number of compounds belonging to the glucocorticoid cluster allowed having internal screening controls since this family of molecules has been shown to inhibit fin fold and adult caudal fin regeneration in zebrafish (Mathew et al., 2007). Thus, it provided us with a phenotype of less growth and the published compounds were considered positive controls in the screen, validating our experimental assay. These were the following: beclomethasone dipropionate, clobetasol propionate, triamcinolone, halcinonide and hydrocortisone (Figure 3A-E). In addition to the replicated phenotypes, we confirmed also the concentrations for proper action of some of these small molecules, since some showed levels of toxicity (Figure 3A-A'', B-B'', C-C''). Moreover, all the compounds belonging to the glucocorticoid and anti-inflammatory clusters present in the library (24 molecules) were grouped together with the previously published compounds and not pursued as possible candidate molecules due to their identified inhibitory role in regeneration (Figure 4 for representative examples).

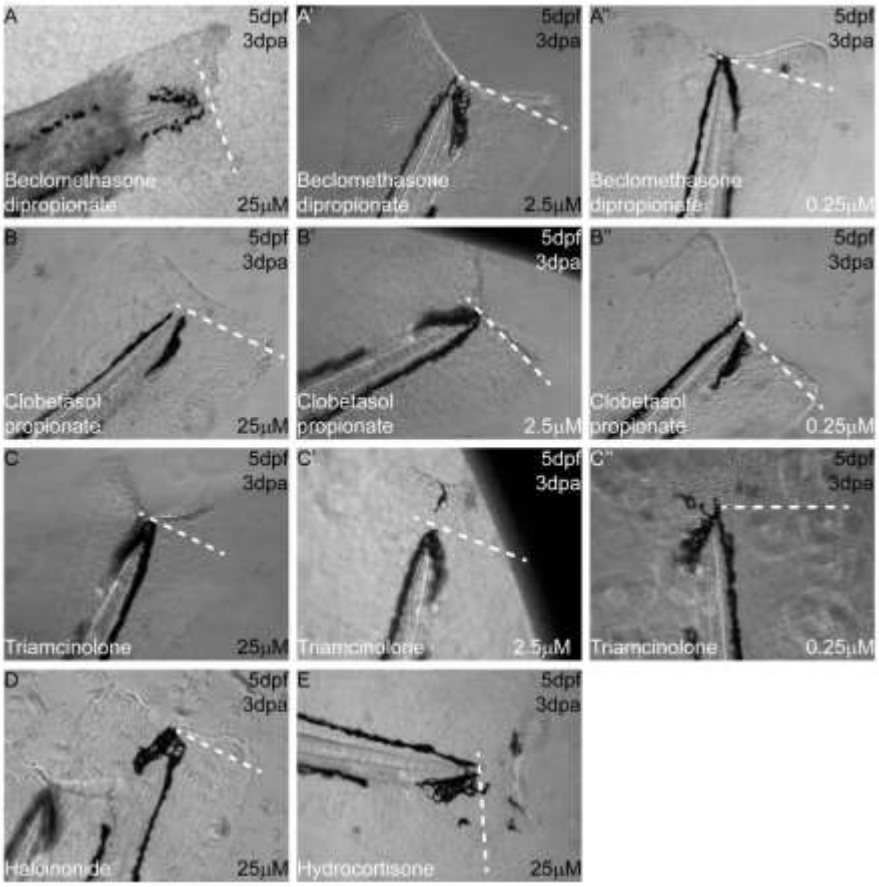

Figure 3. Known glucocorticoids found blindly as positive controls. A-A'' Representative images of 5 dpf 3 dpa larvae exposed to beclomethasone dipropionate in different concentrations: 25μM (**A**), 2.5μM (**A'**) and 0.25μM (**A''**). **B-B''** Representative images of 5 dpf 3 dpa larvae exposed to clobetasol propionate in different concentrations: 25μM (**B**), 2.5μM (**B'**) and 0.25μM (**B''**). Representative images of 5 dpf 3 dpa larvae exposed to triamcinolone in different concentrations: 25μM (**C**), 2.5μM (**C'**) and 0.25μM (**C''**). **D** Representative image of a 5 dpf 3 dpa larva exposed to halcinonide at 25μM. **E** Representative image of a 5 dpf 3 dpa larva exposed to hydrocortisone at 25μM. Dashed lines indicate amputation plane. n=2 larvae per condition.

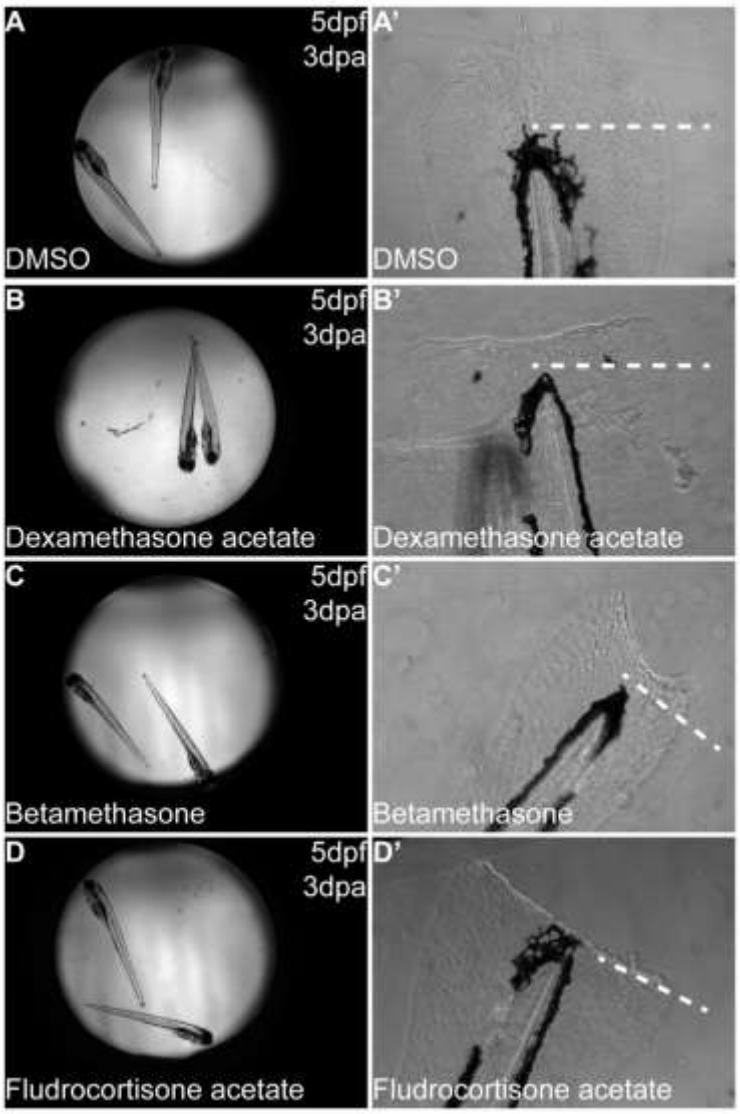

Figure 4. Glucocorticoids present in the chemical screen. A-D Overview of screen plate wells with treated larvae at 5 dpf 3 dpa, after exposure to the represented glucocorticoids. **A'-D'** Zoom of previous image highlighting the fin fold phenotype upon exposure to the compound during the regenerative process. **A** DMSO; **B** Dexamethasone acetate; **C** Betamethasone; **D** Fludrocortisone acetate. Dashed lines indicate amputation plane. Dashed lines indicate amputation plane. n=2 larvae per condition.

4.3 Toxicity screen assay

During the course of the chemical screen, some molecules were identified as toxic at the standard concentration used (25µM). These associated phenotypes appeared completely independent of the possible fin fold regeneration phenotypes and included the existence of lethal (animal death) and sublethal toxicological endpoints (heart edema, body curvature) (Figure 5B, C and D respectively) (Fraysse et al., 2006). To overcome possible masking effects caused by the general toxicity of some molecules, not allowing for a proper evaluation of fin fold growth phenotypes, we performed a toxicity screen. This assay consisted in re-evaluating all the compounds that had scored morphological toxicity phenotypes upon treatment of the larvae (234 molecules; 19,5% of the total screened molecules) in two lower concentrations: 1/10 (2.5µM) and 1/100 (0.25µM) of the original concentration (25µM). If at certain lower concentration the molecules did not present a toxicity phenotype, but showed a fin fold growth phenotype, then those molecules were considered as candidate hits. This analysis allowed the discovery of several candidate hits in both growth categories: 2 small molecules leading to positive growth phenotypes (Oxethazaine - Na+ channel blocker, Celecoxib - cyclooxygenase-2 inhibitor) and 6 small molecules leading to negative growth phenotypes (Troglitazone - peroxisome proliferator, Oxibendazol - anthelmintic, Dienestrol - nuclear receptor ligand, non-steroidal estrogen, Diloxanide furoate - antiamebic, Norgestimate - progestogen, Melengestrol acetate - progestogen (Figure 6 for representative examples of each phenotype class).

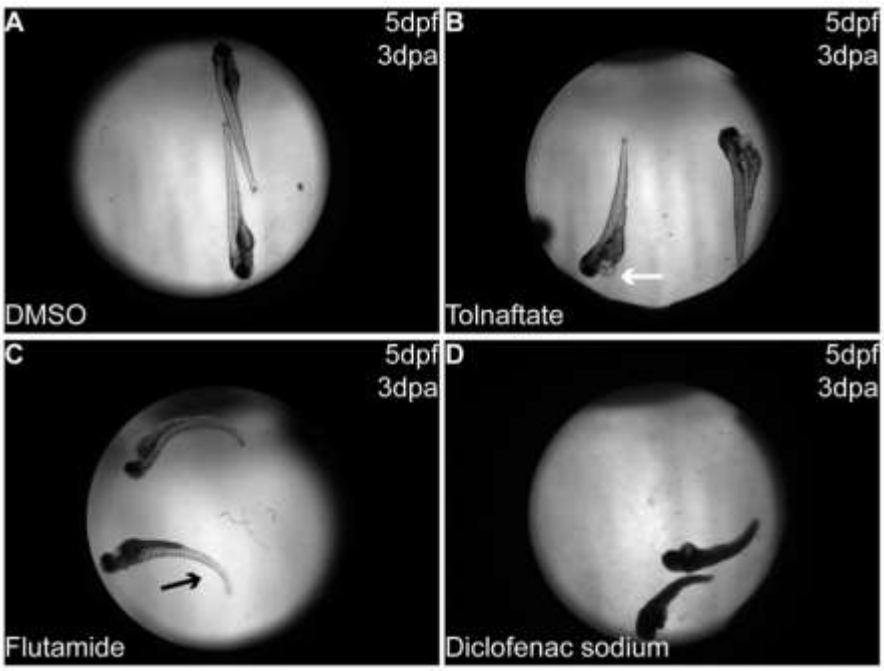

Figure 5. Screen phenotypes associated with toxicity. Representative phenotypes classified as toxic upon 3 days exposure to different small molecules at a concentration of 25µM. **A** DMSO control; **B** Tolnaftate (heart edema); **C** Flutamide (body curvature); **D** Diclofenac sodium (animal death). Arrows indicate the associated toxic phenotype. n=2 larvae per condition.

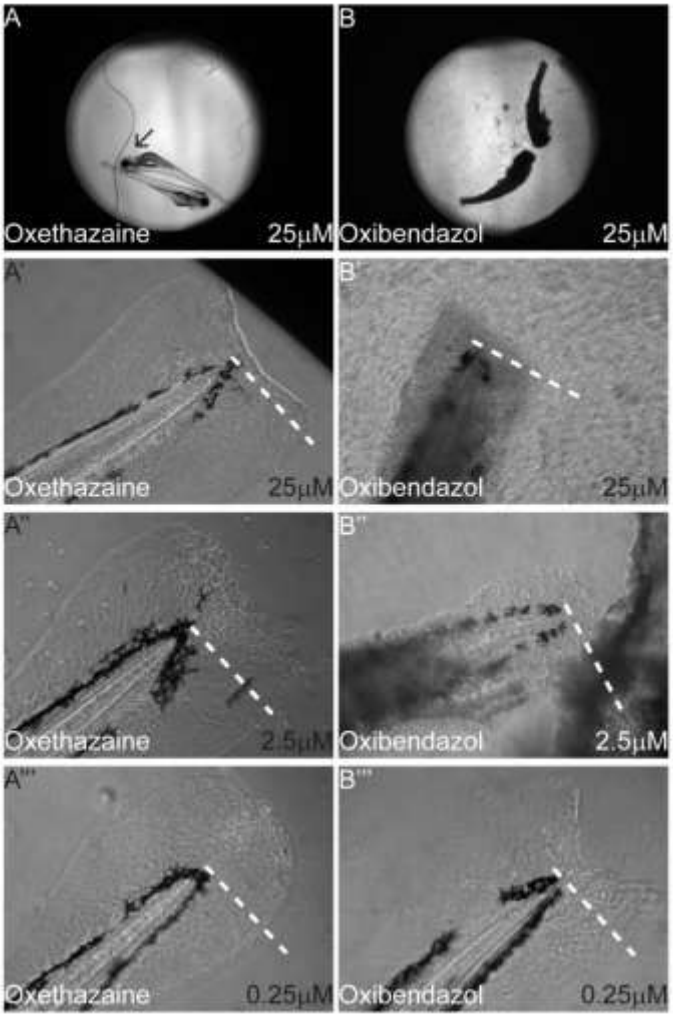

Figure 6. Candidate molecules identified in the toxic screen. Representative images of phenotypes of 5 dpf 3 dpa larvae associated with compound toxicity at 25µM and afterwards screened at lower concentrations of the same molecule. **A-A'''** Oxethazaine exposed larvae leading to a positive phenotype regarding fin fold growth; **B-B'''** Oxibendazol exposed larvae leading to a negative phenotype regarding fin fold growth. **A-B** Overview of screen plate wells with larvae after exposure to the represented compound at 25µM; **A'-B'** Corresponding zoom of previous images highlighting the fin fold phenotype; **A''-B''** Representative images of fin folds of larvae exposed to the represented compound at 2.5µM; **A'''-B''** Representative

images of larvae fin folds after exposition to the represented compound at 0.25µM. Dashed lines indicate amputation plane. Arrows indicate toxicity phenotype. n=2 larvae per condition.

4.4 Candidate molecules

After screening the entire Prestwick library and performed the toxicity screen assay, we found in total 88 candidate hit molecules, in which 17 of them showed a positive growth phenotype and 71 a negative growth phenotype. This corresponded to a 7.3% putative hit rate. To understand if there was a predominance of a certain type of molecules we searched for known characteristics and mechanisms of action and grouped them into clusters of shared properties (Figure 7). To confirm the initial phenotypes observed, we re-tested the candidate hit molecules. Upon this, none of the 17 possible candidate hits that had presented a positive growth phenotype maintained it and were therefore, considered false positives. However, from the negative growth phenotype group, 14 candidates were validated, hence they were kept as positive hits for this growth category (Figure 8), corresponding to a hit rate of 1.2%.

Among the validated hits, we observed that chemical diversity leading to impaired regeneration phenotypes was preserved. Interestingly from the 14 compounds, 8 were referenced as neuroactive substances having effects in several classes of neurotransmitters:

- Ropinirole hydrocloride – non-ergoline D2, D3 and D4 dopamine receptor agonist with highest affinity for D4
- Sertindole - Dopamine D2/Serotonin 5-HT2 receptor antagonist
- Loxapine succinate – Dopamine antagonist
- Galanthamine hydrobromide – cholinesterase inhibitor
- Ipsapirone – Serotonin receptor type1a agonist

- Norcyclobenzaprine – acts selectively on serotonin receptor type 2a and alpha-2 adrenergic receptors
- Tomoxetine hydrochloride – norepinephrine reuptake inhibitor

Moreover, two molecules were classified as phosphodiesterase inhibitors (Papaverine hydrochloride and Sulmazole), one as a nucleic acid synthesis inhibitor (Rimantadine), one as a vasodilator (Eburnamonine) and two as hormones (Nomegestrol/Megestrol acetate and Alprostadil). Lastly, we found that vitamin B (Folic acid) also led to less growth of the fin fold.

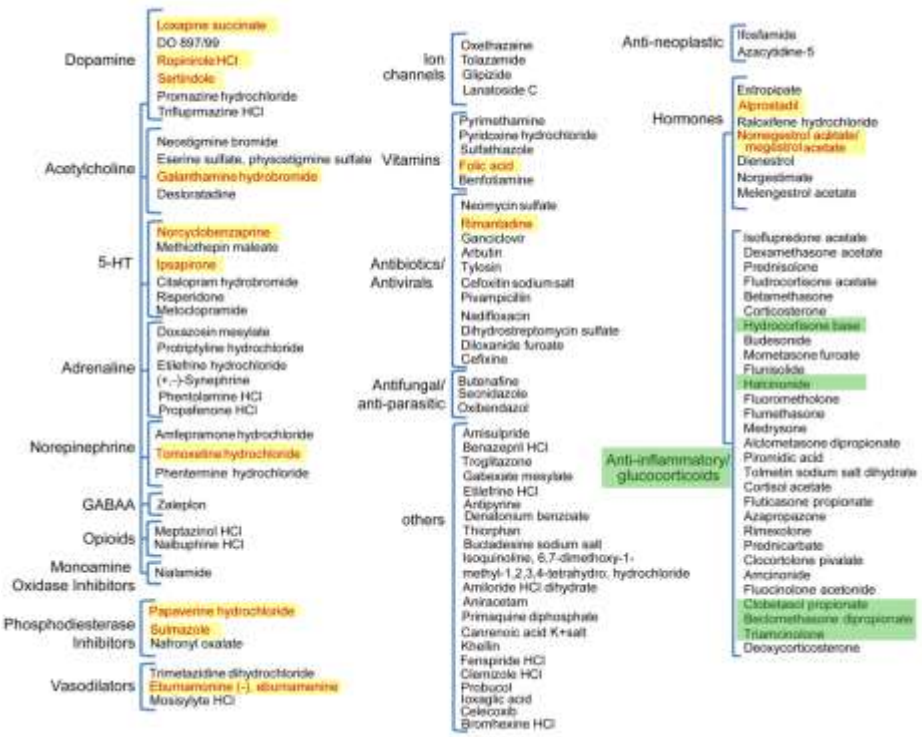

Figure 7. Global overview of all candidate molecules found in the chemical screen. Chart displaying all the initial putative positive hits found upon amputation of the fin fold, grouped into functional categories. Highlights in red and yellow show which compounds were confirmed as positive hits. Green highlights the compounds used as positive controls.

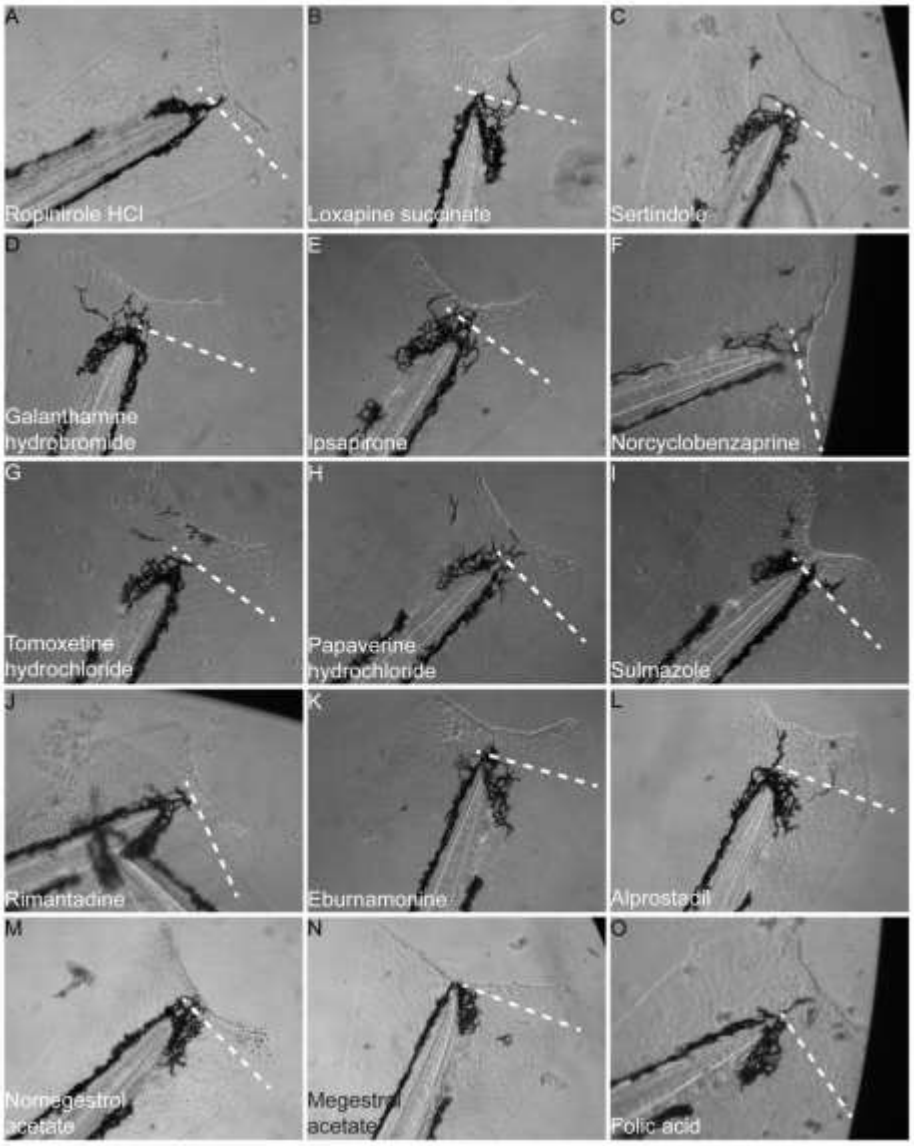

Figure 8. Positive hits leading to impaired regeneration phenotypes. Representative images of fin fold phenotypes of 5dpf 3dpa larvae associated with less growth after exposure to the small molecules classified as positive hits in the chemical screen. **A** Ropinirole hydrochloride; **B** Loxapine succinate; **C** Sertindole; **D** Galanthamine hydrobromide; **E** Ipsapirone; **F** Norcyclobenzaprine; **G** Tomoxetine hydrochloride; **H** Papaverine hydrochloride; **I** Sulmazole; **J** Rimantadine; **K** Eburnamonine; **L** Alprostadil **M** Nomegestrol

acetate; **N** Megestrol acetate; **O** Folic acid. Due to similarity in chemical structure and function, nomegestrol acetate and megestrol acetate were considered as only one positive hit. Dashed lines indicate amputation plane. n=8 larvae per condition.

5. Discussion

In this work we have searched for molecules that would functionally impact the fin fold regeneration process. We performed an *in vivo* chemical screen to identify compounds that would in some way lead to a regeneration specific growth phenotype.

Our findings reinforce previous reports that the 2 dpf larvae fin fold is an easy and fast system to conduct chemical screens (Mathew et al., 2007)(Molina et al., 2009). We were capable of screening 1200 small molecules in the amputated fin fold, replicate previous published results and identify 14 new small molecules that interfere with regenerative fin fold growth, indicating that this is indeed a robust model.

Our goal relied on the ability of the fin fold to regain not only its original size, but also recover to its age-matched developmental size; this remarkable feature proved to be easily accessible in this type of functional studies. Nevertheless our analysis has also shown that inhibitory growth effects are more commonly achieved than enhancing growth effects during regeneration. This difficulty in identifying growth stimulators may be due to the complexity of the mechanisms that regulate positional memory and information within the regenerating organs. In addition, our assay design exposed larvae during entire regenerative process, without compound renovation; this could also have resulted in a bias for compound identification, since possible compound degradation towards the end of exposure and, consequently, in later regeneration stages, may have prevented identification of growth triggering small molecules. In contrast, these results can also be a consequence of the existence of different mechanisms that regulate fin fold size, independently of signaling molecules.

The identified inhibitory growth phenotypes could indicate that the associated compounds are possibly inhibiting the action of an important

factor for regeneration; they could also indicate that they are activating some factor that generally needs to be inhibited for regeneration to proceed. Henceforth, further studies on understanding the mechanisms of action and possible molecular targets of each of the identified compounds remain to be explored. This could be achieved by testing the effects of the small molecules in established processes occurring during fin fold regeneration, namely: cell proliferation, actomyosin cable formation, mesenchymal cell migration or expression of specific regeneration genes, together with tests during adult caudal fin regeneration.

6. References

Dane, P.J., and Tucker, J.B. (1985). Modulation of epidermal cell shaping and extracellular matrix during caudal fin morphogenesis in the zebra fish Brachydanio rerio. J. Embryol. Exp. Morphol. *87*, 145–161.

Durán, I., Marí-Beffa, M., Santamaría, J.A., Becerra, J., and Santos-Ruiz, L. (2011). Actinotrichia collagens and their role in fin formation. Dev. Biol. *354*, 160–172.

Feitosa, N.M., Zhang, J., Carney, T.J., Metzger, M., Korzh, V., Bloch, W., and Hammerschmidt, M. (2012). Hemicentin 2 and Fibulin 1 are required for epidermal-dermal junction formation and fin mesenchymal cell migration during zebrafish development. Dev. Biol. *369*, 235–248.

Fraysse, B., Mons, R., and Garric, J. (2006). Development of a zebrafish 4-day embryo-larval bioassay to assess toxicity of chemicals. Ecotoxicol. Environ. Saf. *63*, 253–267.

Iten, L.E., and Bryant, S. V (1976). Regeneration from different levels along the tail of the newt, Notophthalmus viridescens. J. Exp. Zool. *196*, 293–306.

Kawakami, A., Fukazawa, T., and Takeda, H. (2004). Early fin primordia of zebrafish larvae regenerate by a similar growth control mechanism with adult regeneration. Dev. Dyn. *231*, 693–699.

Lee, Y., Grill, S., Sanchez, A., Murphy-Ryan, M., and Poss, K.D. (2005). Fgf signaling instructs position-dependent growth rate during zebrafish fin regeneration. Development *132*, 5173–5183.

Lee, Y., Hami, D., De Val, S., Kagermeier-Schenk, B., Wills, A.A., Black, B.L., Weidinger, G., and Poss, K.D. (2009). Maintenance of blastemal proliferation by functionally diverse epidermis in regenerating zebrafish fins. Dev. Biol. *331*, 270–280.

Maden, M. (1976). Blastemal kinetics and pattern formation during amphibian limb regeneration. J. Embryol. Exp. Morphol. *36*, 561–574.

Mateus, R., Pereira, T., Sousa, S., de Lima, J.E., Pascoal, S., Saúde, L., and Jacinto, A. (2012). In vivo cell and tissue dynamics underlying zebrafish fin fold regeneration. PLoS One *7*, e51766.

Mathew, L.K., Sengupta, S., Kawakami, A., Andreasen, E.A., Lohr, C. V, Loynes, C.A., Renshaw, S.A., Peterson, R.T., Tanguay, R.L., and Lo, C. V (2007). Unraveling tissue regeneration pathways using chemical genetics. *282*, 35202–35210.

Molina, G., Vogt, A., Bakan, A., Dai, W., Queiroz de Oliveira, P., Znosko, W., Smithgall, T.E., Bahar, I., Lazo, J.S., Day, B.W., et al. (2009). Zebrafish chemical screening reveals an inhibitor of Dusp6 that expands cardiac cell lineages. Nat. Chem. Biol. *5*, 680–687.

Morgan, T.T.H. (1906). The Physiology of Regeneration. J. Exp. Zool. *4*, 118–127.

Nabrit, S.M. (1929). THE ROLE OF THE FIN RAYS IN THE REGENERATION IN THE TAIL-FINS OF FISHES: IN FUNDULUS AND GOLDFISH. Biol. Bull. *56*, 60–63.

Slanchev, K., Carney, T.J., Stemmler, M.P., Koschorz, B., Amsterdam, A., Schwarz, H., and Hammerschmidt, M. (2009). The epithelial cell adhesion molecule EpCAM is required for epithelial morphogenesis and integrity during zebrafish epiboly and skin development. PLoS Genet. *5*, e1000563.

Spallanzani, L. (1769). An essay on animal reproductions.

Stoick-Cooper, C.L., Weidinger, G., Riehle, K.J., Hubbert, C., Major, M.B., Fausto, N., and Moon, R.T. (2007). Distinct Wnt signaling pathways have opposing roles in appendage regeneration. Development *134*, 479–489.

Wolpert, L. (1969). Positional information and the spatial pattern of cellular differentiation. J. Theor. Biol. *25*, 1–47.

Wolpert, L. (2011). Positional information and patterning revisited. J. Theor. Biol. *269*, 359–365.

Wood, A., and Thorogood, P. (1984). An analysis of in vivo cell migration during teleost fin morphogenesis. J. Cell Sci. *222*, 205–222.

Zhang, J., Wagh, P., Guay, D., Sanchez-Pulido, L., Padhi, B.K., Korzh, V., Andrade-Navarro, M.A., and Akimenko, M.-A. (2010). Loss of fish actinotrichia proteins and the fin-to-limb transition. Nature 1–5.

7. Acknowledgements

The author thanks the Fish Facility technicians Lara M. Carvalho, Fábio Valério and Aida Barros for support with animal care.

CHAPTER IV

MECHANISMS OF TISSUE GROWTH CONTROL DURING ADULT ZEBRAFISH CAUDAL FIN REGENERATION

GROWTH REGULATION DETERMINED BY CELL DENSITY, CYTOSKELETON AND THE HIPPO/YAP PATHWAY IN REGENERATION

This chapter is based in the following manuscript:

Yap control of tissue growth is dependent on cell density and F-actin cytoskeleton during zebrafish caudal fin regeneration

Rita Mateus, Gonçalo Brito, Ana Farinho, Fábio Valério and António Jacinto.

“The great powers of growth in a regenerating part may be local in their influence and not transferable to other parts.”

In *The Physiology of Regeneration*

T.H. Morgan, 1906

CONTENTS

The author of this thesis performed all the experiments. All the authors contributed to the experimental conception and design. Gonçalo Brito, Ana Farinho and Fábio Valério helped executing some of the experiments. Data analysis was done by the author of this thesis together with Gonçalo Brito and António Jacinto. Gonçalo Brito helped establishing the *ctgfa*:eGFP transgenic line. Manuscript preparation was done by the thesis author and António Jacinto.

1. Summary

Caudal fin regeneration is characterized by a proliferation boost occurring in a time and space defined manner in the mesenchymal blastema. This allows a gradual and robust restoration of original fin size. However, how this process is regulated and established is not well understood. Here we report that the fully formed blastema shows different cell densities along the proximal-distal axis, which correlate with alterations in cell morphology, cytoskeleton and cell-cell contacts in a proximal-distal manner within the mesenchymal cells. Importantly, these modifications are tightly associated with the dynamic intracellular location of Yap, the Hippo pathway co-effector. By functionally manipulating Yap *in vivo*, we observed that its activation state regulates cell proliferation levels and affects the expression of several key signaling pathways during regeneration. In particular, active Yap stimulates proliferation in the proximal lower cell density areas of the blastema. Conversely, Yap inactivation occurs in the distal high cell density, non-proliferative region. In addition, by interfering with F-actin polymerization dynamics *in vivo*, we show that Yap activation is dependent on F-actin distribution, which also correlates with cell density along the mesenchymal blastema. We propose that Yap is an important regulator of fin regeneration and its activity is controlled by mechanical tension conferred by cell density and transduced by the actin cytoskeleton.

1.1 Keywords

Zebrafish, regeneration, tissue growth, Hippo, Yap, organ size, mechanotransduction, contact inhibition, F-Actin.

2. Introduction

The ability of adult animals to regenerate lost or injured organs is restricted to few examples in nature. The zebrafish (*Danio rerio*) is one of these impressive cases, being able to regrow a fully efficient and anatomically similar organ through an epimorphic regeneration process (Morgan, 1901). The caudal fin is one of the most attractive organs to be employed in regeneration studies due to its accessibility, simple tissue structure and reproducible regeneration in a couple of weeks.

Caudal fin regeneration proceeds in three main phases: wound healing, blastema formation and outgrowth. Upon amputation, wound healing starts by immediate migration of the epidermis adjacent to the stump, which will give rise to a specialized wound epidermis. This initial phase is completed at approximately 18 hours post amputation (hpa) and the resulting tissue will provide important signals to the underlying mesenchyme (Poleo et al., 2001)(Lee et al., 2009).The blastema will then begin to form, entailing the migration of differentiated intrarray mesenchymal cells towards the stump that de-differentiate and proliferate in a lineage restricted fashion (Knopf et al., 2011)(Sousa et al., 2011)(Tu and Johnson, 2011)(Stewart and Stankunas, 2012). Once the blastema is fully formed at 48 hpa, it is divided into regions: a distal region associated with little proliferation and stem cell-like properties and a proximal region where most of the proliferation and differentiation events occur. By 72 hpa, in the outgrowth phase, these regions along the proximal-distal axis become more distinct, with a non-proliferative most distal blastema tip, a medial region where cell proliferation is mainly occurring and a proximal region where differentiation is taking place. At this time the cell cycle accelerates, enabling the fin to restore all its missing structures (Nechiporuk and Keating, 2002)(Wehner et al., 2014).

A remarkable feature of this process is that upon amputation, the caudal fin regenerates the precise amount of tissue that was lost, at the correct

location. This indicates that a positional memory instructs the blastema cells according to their proximo-distal location in the fin (Lee et al., 2005)(Azevedo et al., 2012). Coupled to this property, the regenerative process is maintained independently of the number of amputations applied and the fish age (Azevedo et al., 2011)(Itou et al., 2012). Such properties point toward a tight growth control program, involving good coordination between proliferation and positional information along the caudal fin, in order to direct cells where to go and what to become during epimorphic regeneration. Though it is yet unclear how these two central processes are molecularly controlled, it most likely comprises the integration of various signals to control final organ size (Wolpert, 2011). Regarding cell proliferation in the regenerating fin, many signaling pathways have been linked to its regulation (Stoick-cooper et al., 2007)(Blum and Begemann, 2011)(Münch et al., 2013)(Chablais et al., 2010). To date, FGF has been the only morphogen to demonstrate capability of promoting an increase in the fin's proliferation rate in a proximal-distal gradient-like manner (Lee et al., 2005). More recently, the inhibition of the phosphatase Calcineurin and the presence of bioelectric signals through potassium channels were shown to be necessary for the fin to acquire proportionate growth both during development and regenerative processes (Perathoner et al., 2014)(Kujawski et al., 2014). Clearly it becomes crucial to elucidate the cellular mechanisms used to stop proliferation, as well as understand what regulates the final size of the renewed organ.

One signaling pathway that has arisen as a potential regulator of growth during regeneration is the conserved Hippo pathway, which is essential for proper regulation of developmental organ growth in *Drosophila* and vertebrates (Pan, 2010). This protein kinase cascade can be activated by multiple inputs and ultimately converges in the phosphorylation and inactivation of its effectors, the transcriptional activator Yap and its paralogue Taz, by excluding one or both from the nucleus (Huang et al., 2005)(Dong et al., 2007). When free to enter the nucleus, Yap/Taz bind to

different partners, namely the TEAD family of transcription factors, and together stimulate the transcription of diverse target genes (Mahoney et al., 2005)(Zhao et al., 2008).

Different studies have recently implicated the involvement of the Hippo pathway in regulation of repair mechanisms. Indeed several reports have established a role for this pathway as a mediator of intestinal repair, both in *Drosophila* and mice (Cai et al., 2010)(Staley and Irvine, 2010)(Shaw et al., 2010). It has also been shown that Yap and upstream Hippo pathway members enhance and are required for the regenerative capabilities of injured mice hearts (Xin et al., 2013)(Heallen et al., 2013). In animals with higher regenerative aptitudes, this signaling pathway has been studied to a smaller extent, nevertheless showing that it can play key roles during this process (Demircan and Berezikov, 2013)(Lin and Pearson, 2014)(Hayashi et al., 2014). Moreover, the link between extracellular matrix stiffness, cell morphology and the actin cytoskeleton has been proven as a mode for Yap/Taz activation *in vitro* (Dupont et al., 2011)(Wada et al., 2011). Activation of Yap/Taz can also be cell density dependent (Zhao et al., 2007), possibly through the action of adherens junctions (Schlegelmilch et al., 2011)(Silvis et al., 2011). These findings imply that cells in an organ are able to interpret the physical signals from their surroundings and transduce those mechanical cues into actual signaling by activation of Yap/Taz.

In Zebrafish, the Hippo pathway has been identified for its functions during development of several organs (Engel et al., 2009)(Jiang et al., 2009)(Hu et al., 2013), but little is known about its role in organ growth. In zebrafish regeneration situations, where accurate growth must be controlled, this pathway has never been addressed, including during caudal fin regeneration. Furthermore, the contribution of mechanotransduction, cytoskeleton and adhesion has remained limited in this *in vivo* context (Santos-Ruiz et al., 2005)(Stewart et al., 2014).

Here we explore the hypothesis that changes in tissue tension and cell density inherent to wounding and regeneration of the caudal fin, trigger a

series of events that control regeneration through the Hippo pathway. Our results indicate that Yap is dynamically regulated intracellularly, required for controlling proliferation within the blastema and necessary for regeneration to proceed. Interestingly, we found that Yap inactivation correlates with high cell density areas and Alpha-catenin and F-actin localization, suggesting that tension, conferred through a contact inhibition of proliferation mechanism and sensed through the junctions and the cytoskeleton, could be one of the mechanisms of balancing proliferation levels within the blastema (Figure 1. Graphical abstract). Finally, we show that F-actin controls Yap intracellular dynamics *in vivo*. We propose that the blastema is constrained by different levels of mechanical forces that are mechanotransduced by Yap, this being one of the means of achieving the final organ size during epimorphic regeneration.

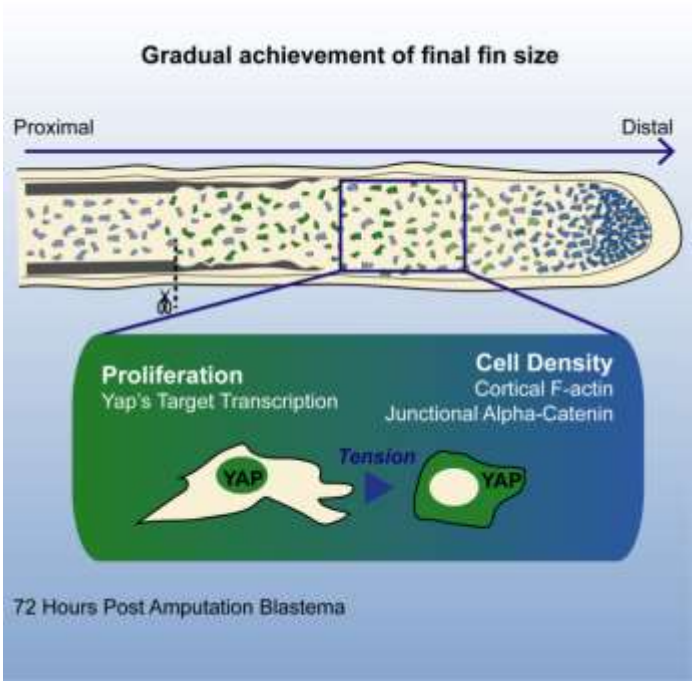

Figure 1. Graphical abstract

3. Materials and Methods

3.1 Ethics Statement

All experiments involving animals were approved by the Animal User and Ethical Committees at Instituto Medicina Molecular and Instituto Gulbenkian Ciência, according to European Union directives and Portuguese law (Directive 2010/63/EU and Decreto-Lei 113/2013).

3.2 Zebrafish lines, maintenance and fin amputation

All Zebrafish (*Danio rerio)* lines used were maintained in a re-circulating system with a 14 h/day and 10 h/night cycle at 28°C. Experiments were performed in 3-9 months old wild-type AB strain adult zebrafish. All caudal fin amputations were performed in fish anaesthetized in 160mg/mL MS-222 (Sigma) using a scalpel as previously described (Poss et al., 2000). Regeneration was allowed to proceed until defined time points at 33°C, except for heat-shock experiments. For all heat-shock experiments, transgenic fish and siblings were maintained at 28ºC and heat-shocked once daily at 38ºC for 1 hour, by incubating them in a water bath. Subsequently fish were transferred to 28ºC until desired time points. All live imaging was done in anaesthetized fish and images were acquired using a Zeiss V12 Lumar equipped with a Zeiss digital camera. The transgenic lines used were: GT(*ctnna-Citrine*)^{ct3a} (Žigman et al., 2010), Tg(EF1α:mAG-zGem(1/100))^{rw0410h} (Sugiyama et al., 2009), hsp70:RFP-CAyap and hsp70:RFP-DNyap (Fang and Poss, *manuscript in preparation*). These lines were kindly provided by Mihaela Zigman, Atsushi Miyawaki and Kenneth Poss.

3.3 *ctgfa*:eGFP transgenic line generation

To create the *ctgfa*:eGFP reporter line, a pBSII-SK+ vector containing a 3.0Kbp upstream promoter fragment of *ctgfa*, flanked with *I-SceI* sites, was coinjected with *I-SceI* meganuclease (Roche), as published (Soroldoni et al., 2009). This construct was kindly provided by Dr. Jyh-Yih Chen and the original promoter sequence has been published by his laboratory (Chiou et al., 2006). Transgenic animals were selected starting at 24 hours post fertilization by eGFP fluorescence along the body. Microinjections to generate transgenic embryos were performed at one cell-stage in wild-type AB strain zebrafish embryos.

3.4 Chemical treatments

For Jasplakinolide (Jasp) (Sta Cruz Biotechnology) treatments, 72 hpa ctnna-Citrine fish were injected intraperitoneally with 7,1µg Jasp/fish gram in dimethyl sulfoxide (DMSO, Sigma) (injection with 10µL/fish gram of 1mM Jasp working solution). Fish were injected 30 minutes prior to fixation with a 30G U-100 insulin syringe (BD Micro-Fine). Control fish were injected in parallel with an equivalent volume of DMSO. Fins of treated fish were fixed in 4% paraformaldehyde (Sigma) in PBS o/n and then processed for cryosections (see Immunofluorescence section) or were pooled for RNA extraction directly in Trizol reagent (see Total RNA isolation and quantitative realtime PCR section).

3.5 *In situ* hybridization

Whole-mount *in situ* hybridizations were performed as described (Sousa et al., 2011). The *yap1*, *stk3*, *sav1*, *frdm6*, *nf2b* genes were PCR-cloned by TA overhangs in PGEM-T-easy (Promega) by using primers listed in Appendix

II and using 5 dpf zebrafish total cDNA. The *ctgfa* plasmid for probe synthesis was kindly given by Dr. Uwe Strahle (Dickmeis et al., 2004). DIG-labeled antisense RNA probes for all studied genes were synthesized as previously described (Henrique et al., 1995). Details for RNA probes are listed in Appendix III. Images of *in situ* hybridizations were obtained with a Leica Z6APO stereomicroscope equipped with a Leica DFC490 digital camera or a Zeiss V12 Lumar equipped with a Zeiss digital camera.

3.6 Immunofluorescence

This protocol was adapted from Mateus et al., 2012 with the following modifications: after o/n fixation with 4% paraformaldehyde, fins were saturated in 30% sucrose (Sigma) in PBS o/n, then embedded in 7,5% gelatin (Sigma)/ 15% sucrose in PBS and subsequently frozen in liquid nitrogen. Longitudinal sections were cut at 12µm using a Microm cryostat and maintained at -20°C afterwards. Sections in slides were thawed 15 min at room temperature, washed twice in PBS at 37°C for 10 min, washed once in 0.1M glycine (Sigma) in PBS for 10 min, followed by acetone permeabilization and onwards as described. Cryosections were counterstained with DAPI (0.001 mg/mL in PBS, Sigma). Sections were mounted with DAKO Fluorescent Mounting Media and imaged using a Zeiss LSM710 confocal microscope. In stainings where phalloidin was used (1:200, conjugated with Alexa Fluor 568, Invitrogen), upon fixation there was no methanol transfer and fins proceeded directly to PBS-30% sucrose. The antibodies used are listed in Appendix IV.

3.7 Image analysis and quantification

For all image analysis, maximum intensity z-stack projections were made using the ImageJ software, except when noted. For concatenation of several

images along the proximal-distal axis of the same longitudinal section, the ImageJ plugin 3D Stitching, was used. XZ projections were performed by using the Dynamic Reslice tool in ImageJ, using synchronized channels.

For quantification of Yap intracellular localization, longitudinal sections of individual regenerating blastemas in defined time points stained with anti-Yap and DAPI, were imaged with a Zeiss LSM710 confocal microscope using identical settings (magnification, contrast, gain and exposure time) and XZ projections were made. For each XZ projection, we applied a threshold (8-25 index) in the DAPI channel (visualizing nuclei) to create a binary mask. The DAPI binary mask was superimposed to the anti-Yap channel using the Image Calculator (Multiply option), resulting in the nuclear Yap images. The same approach was followed to obtain cytoplasmic Yap images using the inverse mask. The average intensities of nuclear and cytoplasmic Yap images were determined and normalized to the area. The resultant individual data was processed using Excel, where a ratio of nuclear Yap intensity over cytoplasmic Yap values was calculated for each sample. Total ratios for each condition were plotted using GraphPad Prism software and non-parametric, two-tailed Mann-Whitney tests were performed between the several conditions.

Proliferation quantifications were performed using an ImageJ plugin, ObjectJ. This plugin was used to manually identify all Geminin and pH3 positive cells and quantify the respective blastema area including the 1st segment proximal to the amputation level. Resultant data was processed and normalized (area normalization) using Excel. Normalized cell divisions (total numbers) were plotted using GraphPad Prism software, and two-tailed Mann-Whitney tests were performed between the several conditions. For each condition n=15 sections, 3 fish.

For cell density measurements in the blastema, longitudinal sections of individual regenerating blastemas in defined time points counterstained with DAPI to reveal their total nuclei, were imaged with a Zeiss LSM710 confocal microscope using identical settings (magnification, contrast, gain and

exposure time). Intensity measurements along blastemas including the 1st segment proximal to the amputation plane were done with the Plot profile tool in ImageJ along rectangular regions of interest (Knopf et al., 2011). For each condition n=7 sections, 3 fish.

For intercellular mesenchymal space quantifications in the blastema, longitudinal sections of *ctgfa*:eGFP individual regenerating blastemas in defined time points were analyzed after immunofluorescence with anti-GFP, to reveal the mesenchymal cells morphology and space occupied within the blastema. Imaging was performed in a similar way as above. A threshold (index 35) was applied to the images in order to label all the intercellular mesenchymal space, the LUT was inverted and intensity measurements were performed in a similar way as above. For each condition n=9 sections, 3 fish.

For cell aspect ratio determination, individual mesenchymal cells were manually outlined using ImageJ and measurements to determine values for *x* (major) and *y* (minor) axes of the cells were performed using the Fit Ellipse plugin. Resultant individual data was processed using Excel, where *y* divided by *x* values for each cell were plotted in order to have individual cell aspect ratios - in which a perfect circular shape corresponds to a ratio between *y* and *x* equal to 1. Total ratios for each condition were plotted using GraphPad Prism software, and two-tailed Mann-Whitney tests were performed between the several conditions. n=45 total cells per condition; 5 cells randomly selected per image; 9 sections; 3 fish per condition.

3.8 Total RNA isolation and quantitative realtime PCR (qPCR)

For gene expression analysis, regenerated tissue from 5 caudal fins, including one ray segment of the stump, were harvested per experiment and pooled for each sample. Regenerated tissue from heat-shock transgenics and siblings was retrieved at 2 hours after completion of the heat-shock.

Regenerated tissue from JASP and DMSO injected animals was retrieved at 30 minutes post injection or at 2 hours post injection. All samples were analyzed in biological and technical triplicate for each gene. RNA was extracted using Trizol reagent (Invitrogen) and treated with DnaseI (Roche) according to the manufacturer's protocol. cDNA was synthesized from 1µg total RNA using the Transcriptor High Fidelity cDNA Synthesis Kit (Roche), following the oligo dT protocol. qPCR was performed using a Roche LightCycler 480 and FastStart Essential DNA Green Master Mix. Cyclic conditions were: 15min at 95°C followed by 55 amplification cycles, each cycle for 30s at 95°C, 15s at 68°C. Gene expression values were normalized using the *elongation factor 1α* (*ef1α,* NM_131263) housekeeping gene and fold change was calculated using the ΔΔCt method. Results were plotted using GraphPad Prism software and two-tailed, non-parametric paired Wilcoxon tests were performed between the several conditions. Primer sequences are listed in Appendix II.

4. Results

4.1 Yap has a dynamic intracellular localization according to the stage and region of the blastema

A hallmark of Yap and Taz activation, co-effectors of the Hippo pathway, is their translocation from the cytoplasm to the nucleus (Yagi et al., 1999)(Zhao et al., 2007)(Oh and Irvine, 2008). In order to understand if Yap could become activated during the caudal fin regenerative process, we assessed its protein expression by performing immunofluorescence in longitudinal sections of the fin rays. This characterization showed striking intracellular dynamics in several stages of the regenerative blastema. Upon amputation, as early as 6 hours post amputation (hpa), the mesenchymal cells in the segment next to the amputation plane displayed Yap translocation to the nucleus, in contrast to uncut and 3 hpa fins, where Yap was uniformly present in the cytoplasm (Figure 2A-C, G). This suggests that Yap becomes activated early in the regenerative process, in the wound healing phase. The nuclear localization of Yap was maintained at 24 hpa as mesenchymal cells migrated to the forming blastema (Figure 2D). By 48 hpa, when the blastema was fully formed, we detected different regions of intracellular Yap: in proximal regions Yap was mostly nuclear, whereas in distal regions it was mainly cytoplasmic (Figure 2E, G). This expression pattern correlates with the known proliferative regions in the fully formed blastema (Nechiporuk and Keating, 2002)(Santos-Ruiz et al., 2002), where the proximal region contains most of the proliferative events in contrast with the distal region which has little proliferation. Finally, during blastema outgrowth at 72 hpa, these regions were more defined, with Yap more cytoplasmic in the distal-most region and progressively becoming nuclear towards the proximal region (Figure 2F, G). This led us to believe that Yap could be playing an active role in controlling the proliferation levels during

caudal fin regeneration. Of note, the assessment of Yap intracellular localization by quantifying the average intensity ratios between nuclear and cytoplasmic Yap in the 48 hpa distal and 72 hpa distal-most regions showed that these were comparable to uncut ratio values, suggesting that Yap is inactive in these blastema areas.

To determine if other Hippo pathway members were present during zebrafish caudal fin regeneration, we analyzed their expression in different regenerative stages through *in situ* hybridization and quantitative PCR (qPCR) (Figure 3A-B). We observed that core components of the Hippo pathway (*stk3*, *sav1*, *lats2, yap1*, *wwtr1*, *nf2b*, *frmd6*) and possible DNA binding partners for Yap (*tead1a and tead4)* were expressed in the blastema, but the Hippo pathway core components were not upregulated upon amputation, indicating that the pathway main regulatory events are not occurring at the transcriptional level. Subsequently we addressed the expression of phosphorylated active forms of Mst 1/2 and Lats 1/2 as well as total NF2 in 72 hpa blastemas by immunohistochemistry. We noticed an increase of phosphorylated Mst 1/2 and Lats 1/2 in the distal areas where Yap is more cytoplasmic (Figure 4A-B), and the presence of NF2 throughout the blastema (Figure 4C). This suggests that upstream members of the Hippo pathway capable of inactivating Yap are present in the blastema and appear to be active specifically in the distal region where Yap is mainly cytoplasmic, indicating a possible regulatory mode. Together these results show that this pathway is conserved in zebrafish and activated in the blastema during caudal fin regeneration.

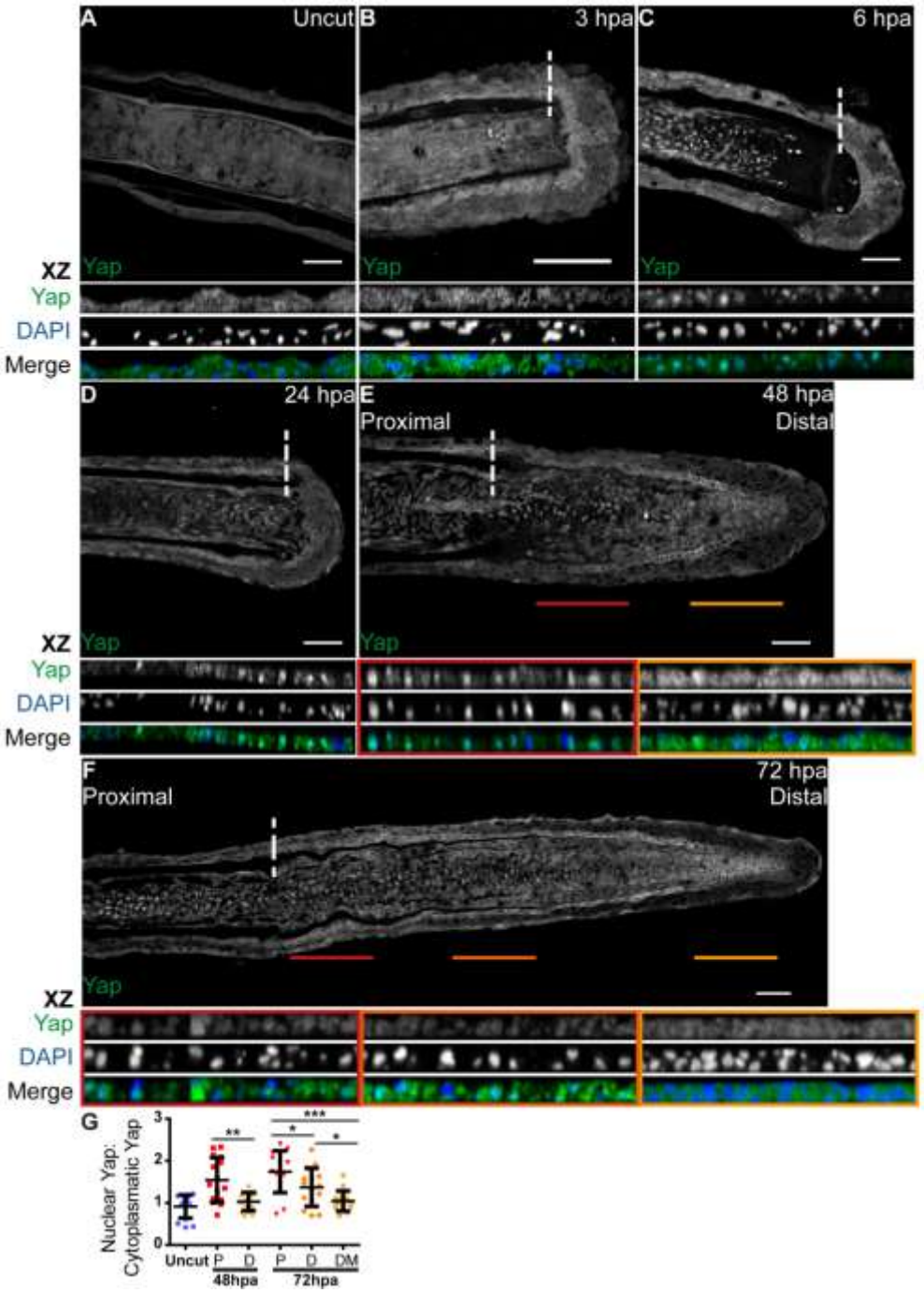

Figure 2. Yap is present and highly dynamic during the regenerative process. A-F Representative immunostainings with anti-Yap in longitudinal sections of the caudal fin throughout several regenerative stages. **A** Uncut control; **B** 3 hpa; **C** 6 hpa; **D** 24 hpa; **E** 48

hpa; **F** 72 hpa. Single color and merged XZ projections panels of mesenchymal region are shown to highlight Yap's intracellular localization. Distal (yellow) and proximal (red) colored lines in 48 hpa (E), and distal-most (yellow), distal (orange) and proximal (red) colored lines in 72 hpa (F) panels correspond to the mesenchymal area in the medial blastema where the XZ projection was made in the above section. Dashed lines indicate amputation plane. n=10-15 sections; 5 fish per condition. Scale bars correspond to 50μm. **G** Quantification of average Yap intracellular localization by expressing a ratio between average intensities of Nuclear Yap:Cytoplasmic Yap of XZ projections from blastemas at different time points. Higher ratio values correspond to higher intensities of nuclear Yap. P corresponds to XZ of proximal regions (red); D corresponds to XZ of distal regions (orange); DM corresponds to XZ of distal-most regions (yellow). *P value<0.05, **P value<0.01, ***P value<0.001; two tailed, non-parametric Mann-Whitney test. n=15 sections, 5 fish per condition.

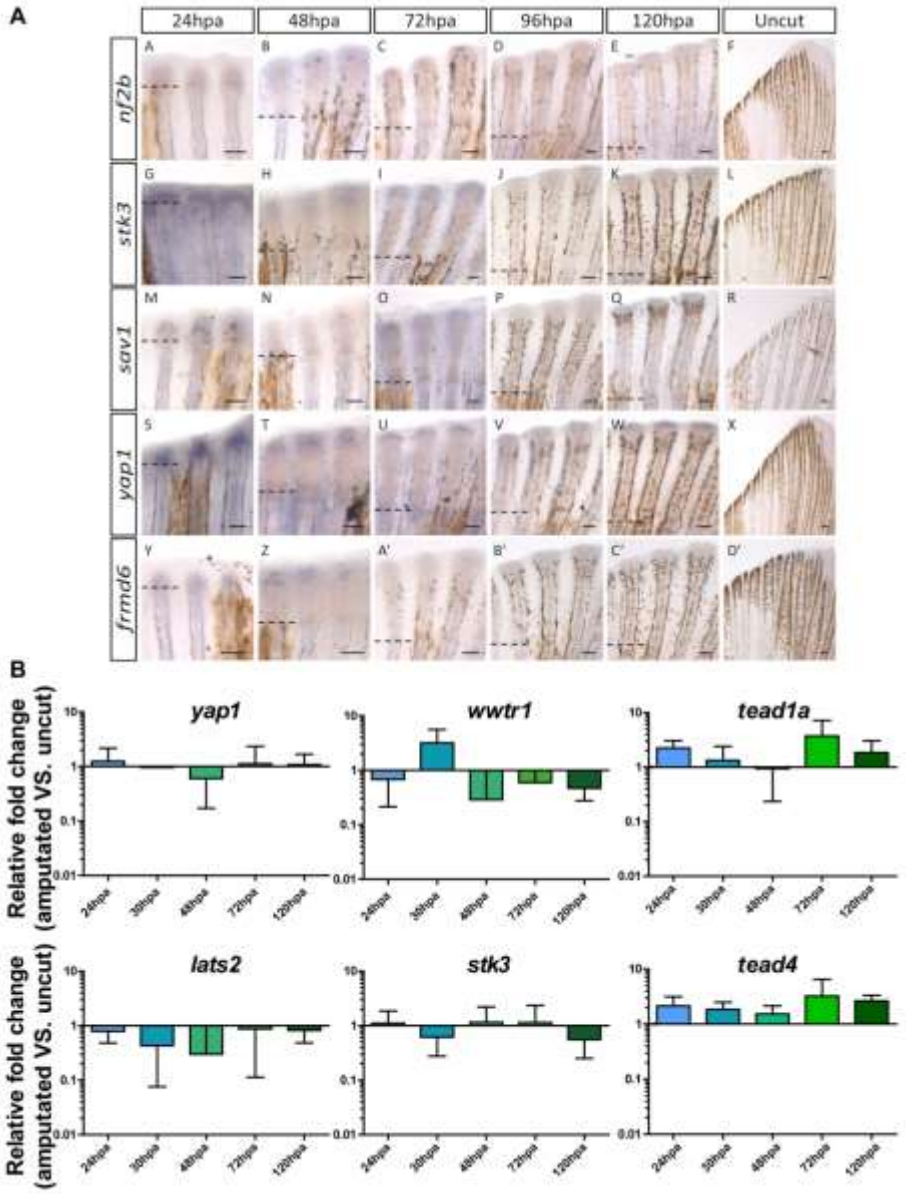

Figure 3. Hippo pathway components are present during zebrafish caudal fin regeneration. A Representative *in situ* hybridizations for *nf2b*, *stk3*, *sav1*, *yap1* and *frmd6* at 24 hpa, 48hpa, 72 hpa, 96 hpa, 120 hpa and uncut fins. n=3 fins per condition. Scale bars correspond to 100µm. Dashed lines indicate amputation plane. **B** qPCR determination of *yap1*, *wwtr1, lats2, stk3, tead1a* and *tead4* relative expression levels during several regenerative stages (24 hpa, 30 hpa, 48 hpa, 72 hpa and 120 hpa) versus uncut controls. Logarithmic scale, base 10.

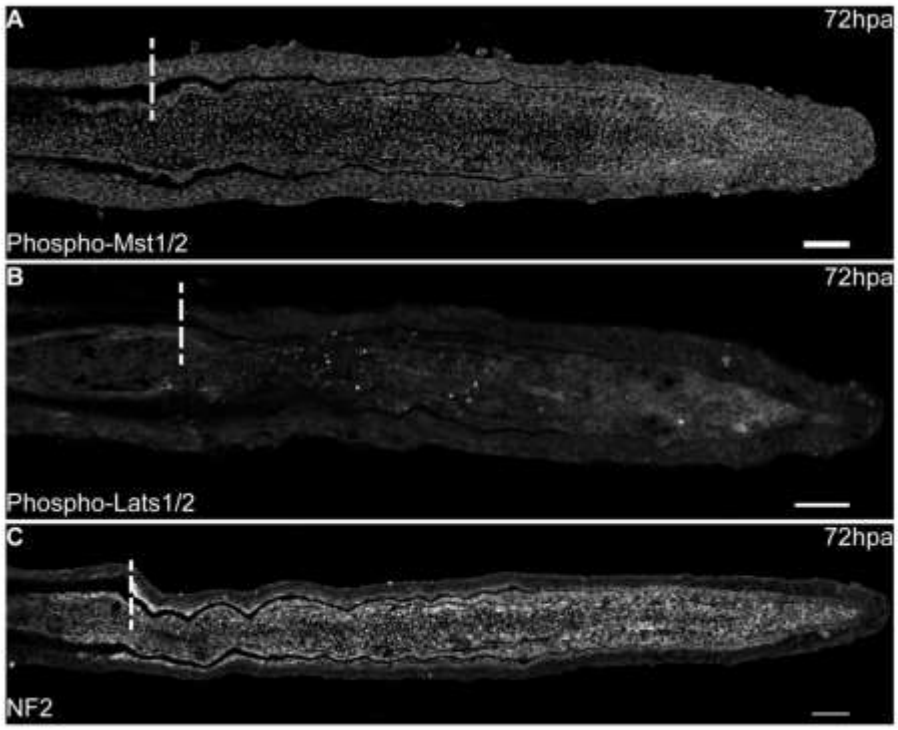

Figure 4. Upstream members of the Hippo pathway are present in the outgrowth blastema. Representative immunofluorescence images against phosphorylated Mst 1/2 **(A)**, phosphorylated Lats 1/2 **(B)** and total NF2 **(C)**, in 72 hpa blastemas. n=9 sections, 3 fish per condition. Dashed lines indicate amputation plane. Scale bars correspond to 50µm.

4.2 Yap controls proliferation levels during regeneration

To demonstrate that Yap could indeed be controlling proliferation in the regenerating blastema, we used conditional heat-shock transgenics to functionally manipulate Yap (Fang and Poss, *manuscript in preparation*). These allowed us to constitutively activate Yap (hsp70:RFP-CAyap, referred as CA-yap, Figure 5A) and to dominantly inactivate Yap (hsp70:RFP-DNyap, referred as DN-yap, Figure 5A) in an effective manner. Upon a single heat shock, *yap1* expression was induced 6-fold in CA-yap and 115-

fold in DN-yap transgenics (Figure 6B). We observed that in both cases, by applying a daily heat-shock during the blastema forming phases (24 hpa and 48 hpa, Figure 6A), regeneration was impaired at 72 hpa (Figure 6C-F). To understand if the phenotypes could be due to proliferation defects, we applied the same heat-shock protocol in the functional Yap transgenics coupled to S/G2/M cell cycle marker transgenic fish, Ef1α:mag-zGeminin (Sugiyama et al., 2009). Immunohistochemistry analysis of Geminin expression together with the mitosis marker phospho-Histone 3 (pH3), revealed more proliferation in CA-yap double transgenics resulting in a mispatterned and smaller blastema by 60 hpa when compared to sibling controls (Figure 6G-H, K). Conversely, in DN-yap transgenics the proliferation was reduced causing an undersized blastema. This likely happens due to a cell cycle delay at G2/M phases (Xia et al., 2002), since cells were able to enter the cell cycle and express Geminin, but not to proceed to mitosis, shown by the reduction of pH3 (Figure 6I-J, L). By detecting in these conditions the expression of RFP, which is fused to the respective Yap manipulated form in each transgenic, we observed differences in Yap intracellular dynamics: in CA-yap transgenics, Yap is nuclear (Figure 6H') and in DN-yap transgenics, Yap is cytoplasmic (Figure 6J'). This confirms the intracellular localization of CA-Yap and DN-Yap proteins, since they functionally localize to the expected intracellular compartment. The differences in proliferation phenotypes, suggest that a tight equilibrium of proliferation is required for regeneration to occur.

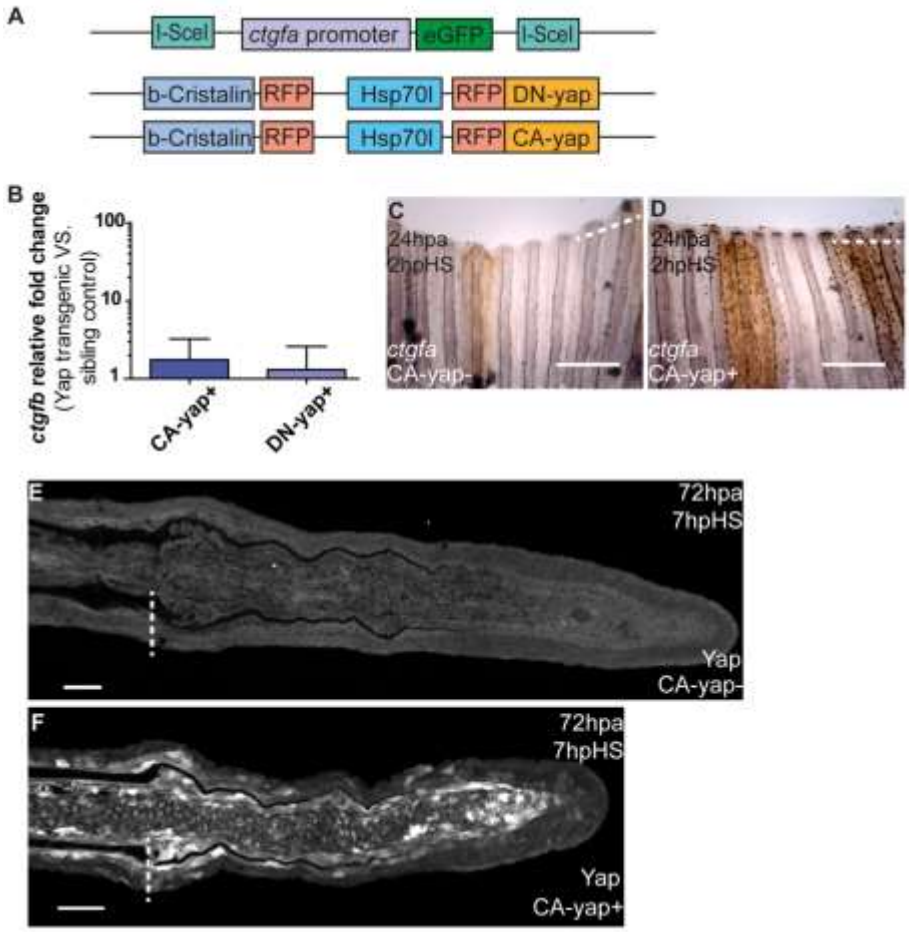

Figure 5. *ctgfa* is conserved as a direct transcriptional target of Yap in Zebrafish. A Schematics of the constructs of the transgenics used in this study. **B** qPCR determination of *ctgfb* relative expression levels in CA-yap and DN-yap positive transgenics versus respective sibling controls, upon single heat-shock induction at 72 hpa. RNA extraction was performed 2 hours after heat-shock. Logarithmic scale, base 10. **C-D** Representative *in situ* hybridization for *ctgfa* in 24 hpa fins of sibling control of CA-yap **(C)** and CA-yap positive fish **(D)**. Fins were collected 2h post single heat-shock (2 hpHS) induction of transgenics. n=3 fins per condition. Scale bars correspond to 500µm. **E-F** Representative immunostaining with anti-Yap in 72 hpa longitudinal sections of *ctgfa*:eGFP; CA-yap double transgenics, fins were fixed 7 hours post single heat-shock (7 hpHS). **E** Yap staining in sibling control of CA-yap; **F** Yap staining in CA-yap positive. Note that due to high Yap levels in F, normal settings in

acquisition of images in E-F had to be decreased to avoid image saturation. n=9 sections, 3 fish per condition. Scale bars correspond to 50µm. Dashed lines indicate amputation plane.

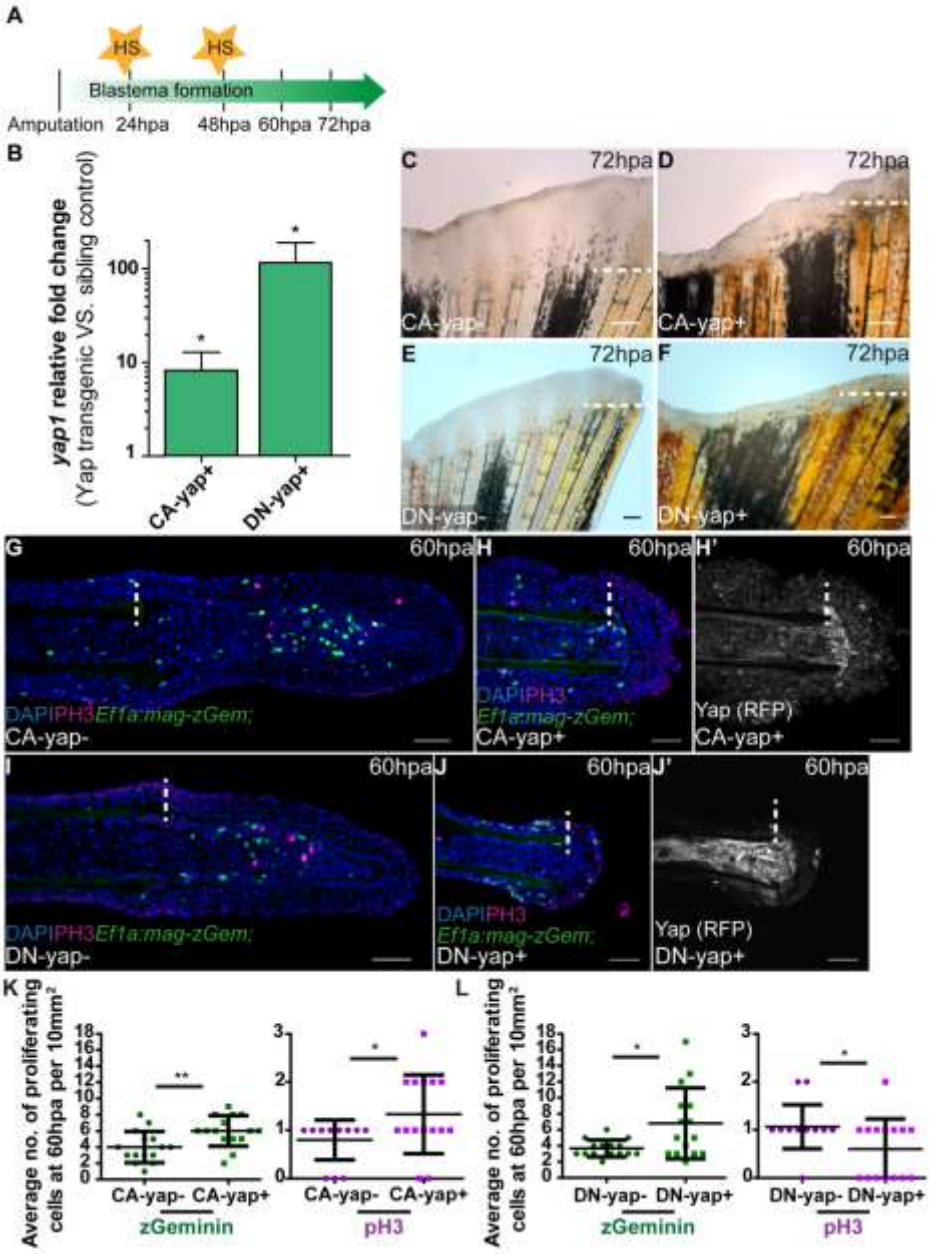

Figure 6. Yap influences the proliferation in the blastema. A Experimental outline of the daily heat-shock protocol applied to access functionality of Yap during regeneration. After

amputations were executed, fish were allowed to regenerate 24h, time in which the first heat-shock was performed. A second heat-shock at 48 hpa was applied and phenotypes were accessed at 60 hpa or 72 hpa. The same protocol was applied to sibling controls. **B** qPCR determination of *yap1* expression levels in Yap transgenics versus respective sibling controls upon single heat-shock at 72 hpa. RNA extraction was performed 2h after heat-shock. *P value<0.01; two tailed, non-parametric paired Wilcoxon test, logarithmic scale, base 10. **C-F** Representative brightfield images of Yap transgenics and sibling controls at 72 hpa after protocol applied in A. **C** CA-yap control; **D** CA-yap positive; **E** DN-yap control; **F** DN-yap positive. n=5 fish per condition. Scale bars correspond to 200µm. **G-J** Representative immunofluorescence with anti-pH3 in 60 hpa longitudinal sections of double transgenics Ef1α:mag-zGeminin; CA-yap/DN-yap and sibling controls after protocol defined in A. **G** CA-yap control; **H** CA-yap positive; **I** DN-yap control; **J** DN-yap positive. **H', J'** Corresponding CA-Yap/DN-Yap RFP expression in functional transgenics after protocol described in A, at 60 hpa. Siblings do not show RFP expression. **K, L** Quantification of average proliferation labeled with Geminin and pH3 occurring per $10mm^2$ in Ef1α:mag-zGeminin; CA-yap/DN-yap transgenics and respective siblings, at 60 hpa. **K** CA-yap proliferation quantification; **M** DN-yap proliferation quantification. *P value<0.05, **P value<0.01; two tailed, non-parametric Mann-Whitney test. n=15 sections, 3 fish per condition. Scale bars correspond to 50µm.

4.3 Yap regulates the expression of known targets and regeneration factors

To ascertain that by manipulating Yap we were affecting its activation state through the induction of transcription of downstream genes, we searched for bona fide Yap transcriptional targets in the regenerating blastema by performing quantitative PCR (qPCR) upon heat-shock induction in Yap functional transgenics. We found that *connective tissue growth factor A* (*ctgfa*) and *amphiregulin*, two of Yap's well characterized targets (Zhao et

al., 2008)(Zhang et al., 2009), were upregulated in CA-yap transgenics but not in DN-yap cases when compared to siblings (Figure 7A-B). Since in zebrafish the *ctgf* gene is duplicated (Fernando et al., 2010), we confirmed that the observed effect is *ctgfa* specific (Figure 5B). The upregulation of *ctgfa* in response to Yap activation was also confirmed through *in situ* hybridization performed in CA-yap transgenics versus siblings, upon single heat-shock induction (Figure 5C-D). In addition, we monitored *ctgfa* activation dynamics *in vivo* with a reporter line (*ctgfa*:eGFP, Figure 5A) coupled with the functional Yap transgenics. We observed that by 7 hours post a single heat-shock (hpHS) given at 72 hpa, the expression of *ctgfa* was upregulated in regenerating blastemas of double transgenics *ctgfa*:eGFP; CA-yap when compared to siblings (Figure 7C-D). Conversely, in *ctgfa*:eGFP; DN-yap transgenics, *ctgfa* expression remained equal to siblings in the same time frame post heat-shock, in agreement with qPCR results (Figure 7E-F). Furthermore, evidence of Yap activation in double transgenics *ctgfa*:eGFP; CA-yap was obtained by performing immunofluorescence against Yap in the same fins monitored *in vivo* (Figure 5E-F). We observed that by 7 hpHS, Yap was more nuclear in those fins, confirming the efficiency of the heat-shock. These results allowed us to conclude that the regeneration phenotypes observed in the functional transgenics are specific to Yap manipulation and that *ctgfa* is likely to be a direct target of Yap in zebrafish, as it is in higher vertebrates. Of note, *ctgf* can also be a downstream transcriptional target of other signaling pathways, namely WNT and TGFβ, as shown in other systems (Luo et al., 2004)(Fujii et al., 2012). This possibly explains why in the *ctgfa*:eGFP reporter line, there is GFP expression in mesenchymal cells, even in regions where Yap is not active, indicating the existence of other means of *ctgfa* regulation not exclusive of Yap.

To further explore mechanistically these observations, we analyzed the expression of several genes known to be involved in regeneration by performing qPCR upon heat-shock induction in Yap transgenics. We found

that in CA-yap transgenics, a number of these factors were significantly downregulated, namely *fgf20a*, *wnt10a*, *lef1* and *shh*, while *dkk1b* was highly upregulated (Figure 7G). In contrast, in DN-yap transgenics, there was the opposite tendency of expression, with *fgf20a* upregulated (Figure 7H). Of interest *msxB*, *bmp2a* and *bmp2b* did not appear to be affected by Yap manipulations (Figure 7G-H). These results indicate that Yap has the ability to regulate a number of key regeneration molecules. The impairment of regeneration that occurs in CA-Yap and DN-Yap transgenics is likely to be a combination of changes in expression of those factors with effects in cell proliferation.

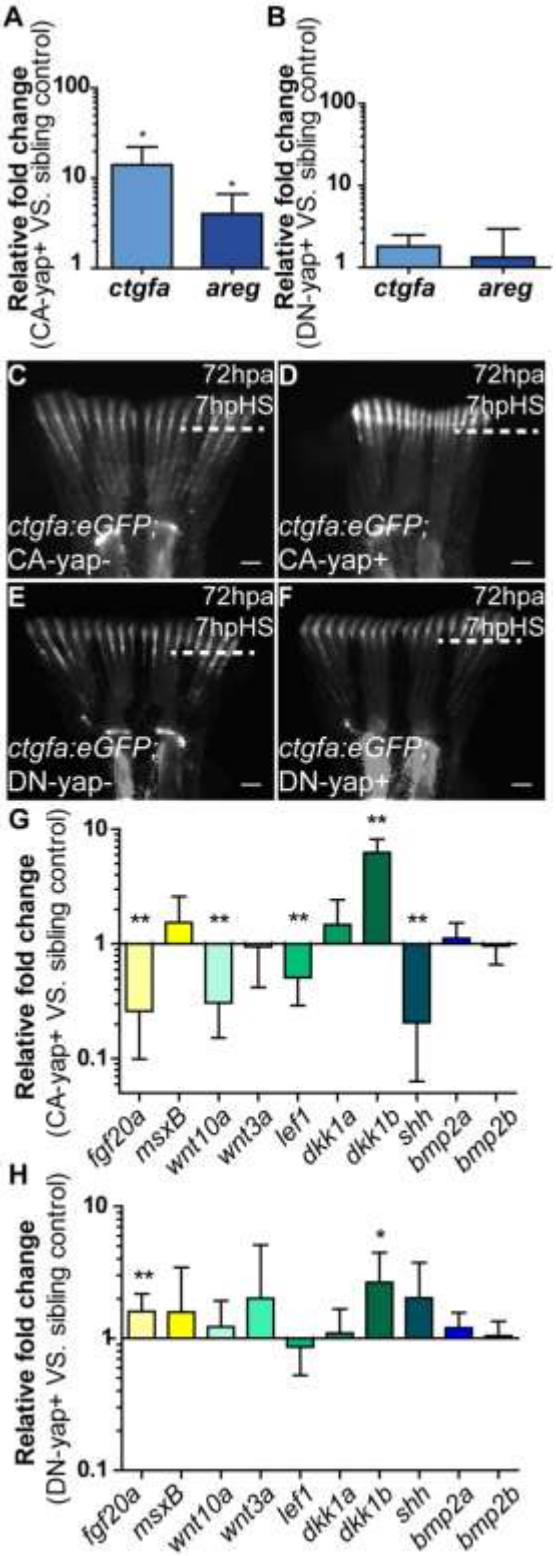

Figure 7. Transcriptional gene regulation induced by Yap. A-B qPCR determination of *ctgfa* and *amphiregulin* (*areg*) expression levels in Yap transgenics versus respective sibling controls upon single heat-shock at 72 hpa. **A** Relative expression levels in fins of CA-yap positive transgenics; **B** Relative expression levels in fins of DN-yap positive transgenics. RNA extraction was performed 2h after heat-shock. *P value<0.01; two tailed, non-parametric paired Wilcoxon test, logarithmic scale, base 10. **C-F** Representative *ctgfa* expression levels in double transgenics *ctgfa*:eGFP; CA-yap/DN-yap and sibling controls upon heat-shock at 72hpa. Images were acquired at 7 hours post heat-shock (hpHS). **C** CA-yap control; **D** CA-yap positive; **E** DN-yap control; **F** DN-yap positive. n=5 fish per condition. Scale bars correspond to 500µm. Dashed lines indicate amputation plane. **G-H** qPCR determination of *fgf20a, msxB, wnt10a, wnt3a, lef1, dkk1a, dkk1b, shh, bmp2a, bmp2b* expression levels in Yap transgenics versus respective sibling controls upon single heat-

shock at 72hpa. **G** Relative expression levels in fins of CA-yap positive transgenics; **H** Relative expression levels in fins of DN-yap positive transgenics. RNA extraction was performed 2h after heat-shock. *P value<0.05, **P value<0.01; two tailed, non-parametric paired Wilcoxon test, logarithmic scale, base 10.

4.4 Yap is not activated in uninjured caudal fins

It is known that fins grow throughout the life of adult fish, depending on a homeostasis process involving some of the genes necessary for epimorphic regeneration (Wills et al., 2008). To test if in an uninjured situation Yap could lead to proliferation phenotypes related to the ones observed during epimorphic regeneration, we applied the same daily heat-shock protocol as before (Figure 6A) to both Yap functional transgenics and respective siblings in uncut situations. Remarkably, we observed that in uncut fins CA-yap induction lead to no morphological changes (Figure 8A-B). Also *in vivo* upregulation of *ctgfa* upon single heat-shock by 7 hpHS in uncut double transgenics *ctgfa*:eGFP; CA-yap was not detected (Figure 8C-D), indicating that even though the constitutively active form of Yap was being driven, that was not enough to stimulate the transcription of its target gene. This points to the existence of a robust inhibitory mechanism for homeostatic proliferation in adult fins. The same results were observed with DN-yap uncut transgenics (Figure 8E-H). By amputating just half of the caudal fin in *ctgfa*:eGFP; CA-yap double transgenics and applying the same single heat-shock protocol at 72 hpa, we observed no changes in *ctgfa* expression in the uncut half of the fin when compared to sibling controls. However, in the amputated fin half of *ctgfa*:eGFP; CA-yap positive transgenics, we observed the expected induction of *ctgfa* at 7 hpHS (Figure 8I-J). The uninjured adult caudal fin tissue is known for its liability for silencing transgenes (Thummel et al., 2006). To confirm that the previous results were not consequences from such an effect, we applied single heat-shocks in the functional

transgenics with 72 hpa half fin amputations and performed *yap1 in situ* hybridizations. In both CA-yap and DN-yap there was a clear *yap1* upregulation upon transgene activation when compared to siblings expression (Figure 8K-N), both in the amputated and uncut fins (Figure 8K'-N', K''-N''). This indicates that Yap transgenes can be transcribed in uninjured, homeostatic situations, but fin cells appear to be in a non-responsive state. During epimorphic regeneration, however, cells appear to be prone to respond to Yap activity, causing specific phenotypes.

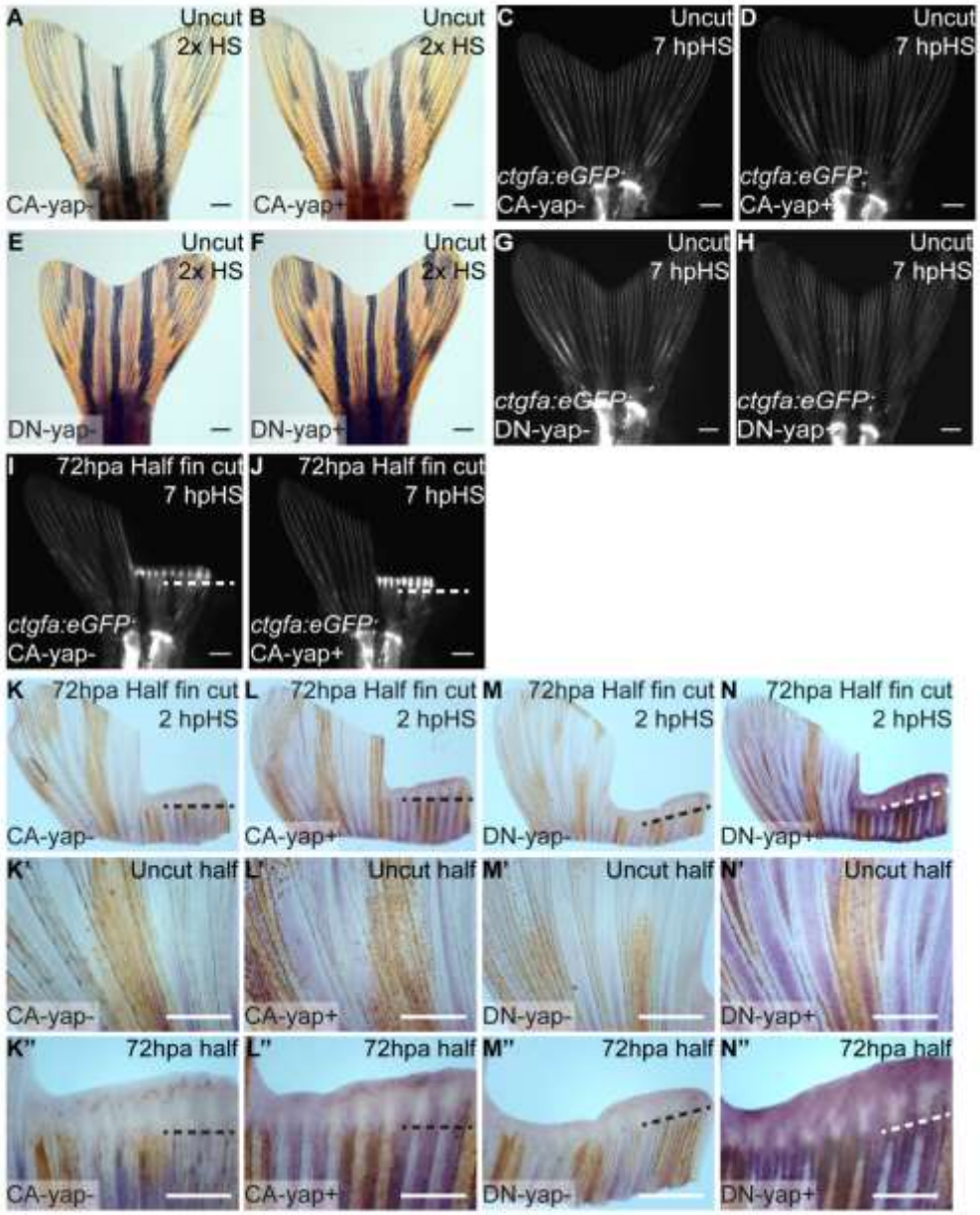

Figure 8. Yap is not activated in a homeostatic context. A-B, E-F Representative brightfield images of uninjured CA-yap/DN-yap transgenics upon heat-shock in 2 consecutive days, phenotypes were accessed on the next day. **A** CA-yap control; **B** CA-yap positive; **E** DN-yap control; **F** DN-yap positive. **C-D, G-H** Representative *ctgfa* expression levels in double transgenics *ctgfa*:eGFP; CA-yap/DN-yap and sibling controls upon single heat-shock

in uninjured animals, images were acquired at 7 hours post heat-shock (hpHS). **C** CA-yap control; **D** CA-yap positive; **G** DN-yap control; **H** DN-yap positive. **I-J** Representative *ctgfa* expression levels in double transgenics *ctgfa*:eGFP; CA-yap upon single heat-shock in 72 hpa half fin amputated animals, images were acquired at 7 hpHS; **I** CA-yap sibling control; **J** CA-yap positive. n=5 fish per condition. **K-N** Representative *in situ* hybridizations for *yap1* in 72 hpa half amputated fins of sibling control of CA-yap **(K)**, CA-yap positive fish **(L)**, sibling control of DN-yap **(M)**, DN-yap positive fish **(N)**. Corresponding zoomed images of the uncut half **(K'-N')** and 72 hpa blastema half **(K''-N'')** of the *in situs* shown in K-N, highlighting the differences in *yap1* expression in both CA-yap and DN-yap transgenics versus siblings. Fins were collected 2h post single heat-shock (2 hpHS) induction of transgenics. n=3 fins per condition. Scale bars correspond to 500µm. Dashed lines indicate amputation plane.

4.5 Cell density along the blastema associates with the localization of active Yap

One possible explanation for the regulation of Yap intracellular dynamics in the regenerating blastema is that changes in the cell matrix rigidity and/or in cell density triggered by the amputation can modify tissue tension, thus affecting cell morphology as well as cell area (Zhao et al., 2007)(Dupont et al., 2011)(Wada et al., 2011)(Aragona et al., 2013). These changes could be sensed at the cell membrane, through its junctions and cytoskeleton and control Yap's activation and proliferation levels (Schlegelmilch et al., 2011)(Kim et al., 2011)(Fernández et al., 2011). To test this hypothesis, we established a cell density map along the proximal-distal (PD) axis of the regenerating blastema by measuring the average intensity of mesenchymal nuclei labeled with DAPI in different regeneration stages. We found that at 24 hpa, while the blastema is being formed, cell density appears to be homogeneous along the PD axis (Figure 9A-B). Strikingly, at 48 and 72 hpa, when the blastema is fully formed, we observed that cell density was differential within the blastema: cell density was higher in distal regions

when compared to proximal regions of the same samples (Figure 9C-F). The high cell density regions correlated with the distal regions where Yap is mainly cytoplasmic, thus mostly inactive, suggesting that cell density could control Yap inactivation through a contact inhibition mechanism *in vivo* (compare Figure 9C-F with Figure 2E-F). To understand if these cell density changes translated into an effect in cell morphology, we performed immunofluorescence against GFP in *ctgfa*:eGFP transgenics, as this marker allowed us to label all mesenchymal cells, in the same regeneration stages as the cell density measurements. We observed that at 24 hpa, the mesenchymal cells were variable in shape, presenting many protrusions, in agreement with their migratory phenotype for blastema formation. When quantifying their cell aspect ratio, which provides a measurement of how round the cells are, by representing the relation between the *x* and *y* axes of the cell, the 24 hpa mesenchymal cells had an average aspect ratio of 0.42 (Figure 10B, G-H). At this stage, the quantification of the space between mesenchymal cells along the PD axis revealed that cells were uniformly spread throughout the blastema (Figure 10A). Consistent with the cell density data, by 48 and 72 hpa, the mesenchymal cells towards the distal region became more compact (Figure 10C-D, E-F), reflecting the increase in cell density and not a major change in cell size along the PD axis. Regarding morphology, these distal cells showed significantly less variability in shape, being rounder and lacking protrusions (average aspect ratio of 0.71 and 0.67, for 48hpa and 72hpa respectively), when compared with the cells of the corresponding proximal region (0.50 and 0.48 for 48 hpa and 72 hpa respectively) or 24 hpa blastemas (Figure 10G, I-L). This suggests that blastema cells adapt their morphology to tension changes, conferred by the density of their surroundings, and that these mechanical cues have effects on Yap intracellular localization.

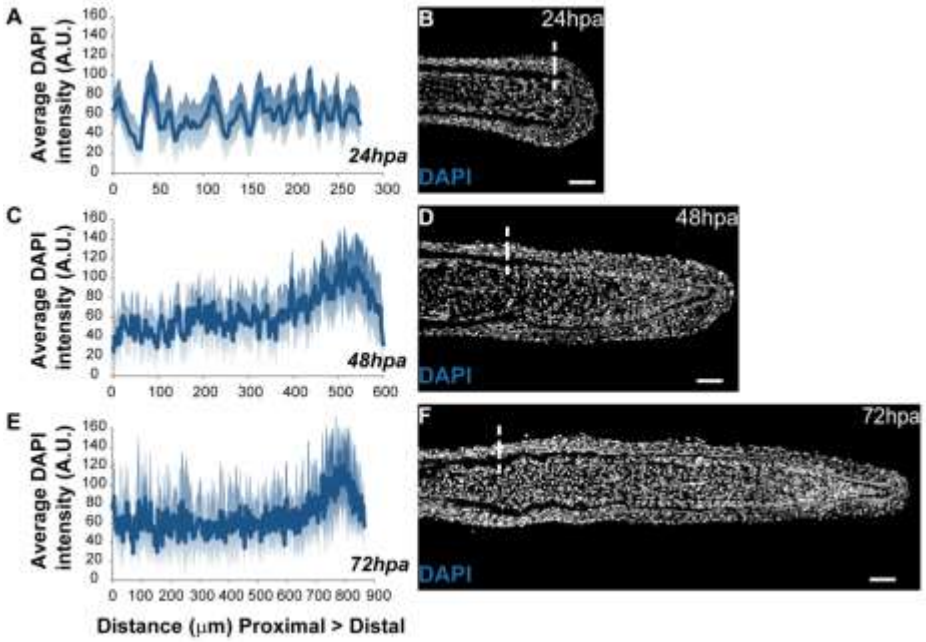

Figure 9. Mesenchymal cell density changes according to the regenerative stage. A, C, E Quantification of average DAPI intensity (in arbitrary units, A.U.) in the mesenchymal cells along the proximal-distal axis (μm) of the regenerating blastema at 24 hpa **(A)**, 48 hpa **(C)** and 72 hpa **(E)**. For all measurements, areas from the medial blastema were considered. n=7 sections, 3 fish per condition; shadows indicate the standard deviation of the mean for each curve. **B, D, F** Representative images of DAPI stained longitudinal sections of the blastema. **B** 24 hpa; **D** 48 hpa; **F** 72 hpa. Dashed lines indicate amputation plane. Scale bars correspond to 50μm.

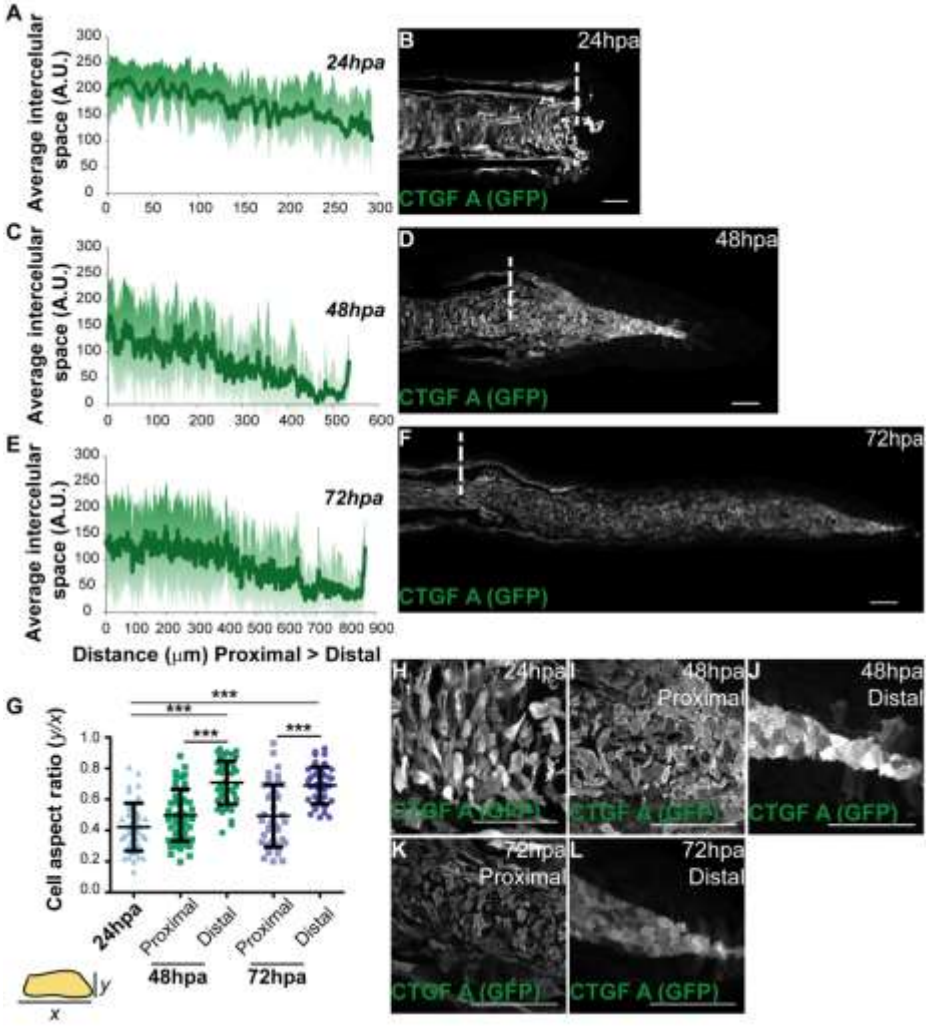

Figure 10. Mesenchymal cell morphology is altered in accordance with changes in cell density. A, C, E Quantification of average space (in arbitrary units, A.U.) between mesenchymal cells along the proximal-distal axis (μm) at 24 hpa **(A)**, 48 hpa **(C)** and 72 hpa blastemas **(E)**. For all measurements, areas from the medial blastema were considered. n=9 sections; 3 fish per condition; shadows indicate the standard deviation of the mean for each curve. **B, D, F** Representative images of anti-GFP stained longitudinal sections of *ctgfa*:eGFP transgenics. **B** 24 hpa; **D** 48 hpa; **F** 72 hpa. **G** Quantification of average cell aspect ratio of mesenchymal cells of 24 hpa, 48 hpa and 72 hpa, in which *y* is the minor axis

of the cell and *x* the major axis of the cell. A perfect circular shape corresponds to a ratio between *y* and *x* of 1. ***P value<0.0001; two tailed, non-parametric Mann-Whitney test. n=45 total cells per condition; 5 cells were randomly selected per image; 9 sections; 3 fish per condition. **H-L** Corresponding zoom panels of B, D, F highlight cell morphology of blastema mesenchymal cells at 24 hpa **(H)**, 48 hpa proximally **(I)**, 48 hpa distally **(J)**, 72 hpa proximally **(K)** and 72hpa distally **(L)**. Dashed lines indicate amputation plane. Scale bars correspond to 50μm.

4.6 Alpha-Catenin correlates with Yap intracellular localization

To find possible adhesion and cytoskeleton associated proteins acting as cell density sensors in the blastema, through which Yap dynamics could be mediated, we performed an immunohistochemistry screen in fully formed blastemas (48 and 72 hpa) searching for differences in expression along the PD axis (Table 1). This led to the identification of several adhesion proteins present in specific cell types during regeneration (Figure 11). Interestingly, Alpha-Catenin was the only junctional protein localized in the mesenchymal cells in a PD dependent manner. By performing immunostainings against Yap and GFP in Alpha-Catenin protein trap transgenics (Žigman et al., 2010) at 72 hpa, we observed that the expression of endogenous Alpha-Catenin correlated with Yap intracellular dynamics (Figure 12A-B). In particular, the junctional localization of Alpha-Catenin in the distal, more dense and round, mesenchymal cells fit with the areas where Yap is more cytoplasmic (Figure 12D, F); conversely, in the proximal areas where Yap is more nuclear and cells are more sparse and protrusive, Alpha-Catenin was not present at the junctions (Figure 12C, E). This suggests that Alpha-Catenin could be working as a mechanosensor of cell density during the regenerative process and, like in other systems (Schlegelmilch et al., 2011), might inhibit Yap activation when cell-cell contacts are reinforced in response to a contact inhibition mechanism.

Table 1. Proteins screened through immunohistochemistry in the regenerating blastema. *(a)* Published in Stewart (2014), *(b)* Published in Jaźwińska (2007).

Protein	Present in blastema	Stages tested	Cell type labeled	Type of adhesion associated
Alpha-Catenin	Yes	Uncut, 24hpa, 48hpa, 72hpa	Most distal mesenchymal cells; osteoblasts; present in all layers of epidermis *(a)*	Adherens junction
Beta-Catenin	Yes	Uncut, 3hpa, 6hpa, 24hpa, 48hpa, 72hpa	In early stages in the mesenchyme, present in some layers of epidermis, osteoblasts *(a)*	Adherens junction
P120-Catenin	No	72hpa	--	Adherens junction
E-Cadherin	Yes	48hpa, 72hpa	All layers of epidermis	Adherens junction
N-Cadherin	Yes	72hpa	New osteoblasts *(a)*	Adherens junction
M-Cadherin	No	72hpa	--	Adherens junction
P-Cadherin	No	72hpa	--	Adherens junction
R-Cadherin	No	72hpa	--	Adherens junction
Cadherin 5	No	72hpa	--	Adherens junction
Cadherin 11	No	72hpa	--	Adherens junction
Zyxin	No	72hpa	--	Integrin associated protein
ZO-1	Yes	48hpa, 72hpa	Most apical layer of epidermis, blood vessels	Tight junction
Claudin 1	Yes	72hpa	Most epidermal layers	Tight junction
Fibronectin	Yes	48hpa, 72hpa	Extracellular matrix of all fibroblast-like cells	Extracellular matrix
Laminin	Yes	24hpa, 48hpa, 72hpa	Extracellular space between basal epidermal layer and mesenchyme, blood vessels	Extracellular matrix

Tenascin C	Yes	24hpa, 48hpa, 72hpa	Extracellular space of all mesenchyme *(b)*	Extracellular matrix
F-Actin (Phalloidin)	Yes	Uncut, 6hpa, 24hpa, 48hpa, 72hpa	Initially in epidermis, later restricted to most apical layer of epidermis and all mesenchyme, blood vessels	Cytoskeleton
Phospho-Myosin Light Chain 2	Yes	Uncut, 6hpa, 24hpa, 48hpa, 72hpa	Initially in epidermis, later both in epidermis and all mesenchyme, blood vessels	Cytoskeleton
Phospho-Ezrin/ Radixin/ Moesin (ERM)	Yes	48hpa, 72hpa	Similar to F-actin	Cytoskeleton, Actin associated protein
Scribble	No	72hpa	--	Tight junction
Vinculin	No	72hpa	--	Integrin associated protein

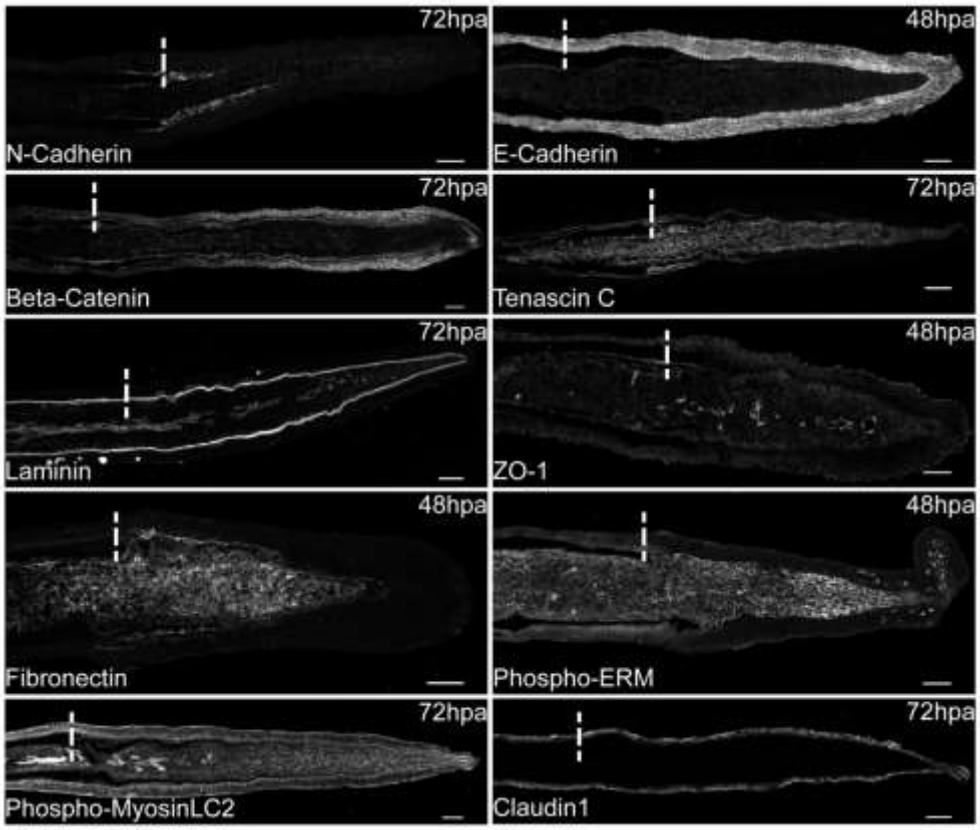

Figure 11. Novel adhesion and cytoskeleton proteins expressed in the regenerating blastema. Representative immunostainings of positive hits found in the adhesion and cytoskeleton related screen performed in fully formed blastemas (72 hpa and 48hpa longitudinal sections). n=3 sections per condition. Dashed lines indicate amputation plane. Scale bars correspond to 50μm.

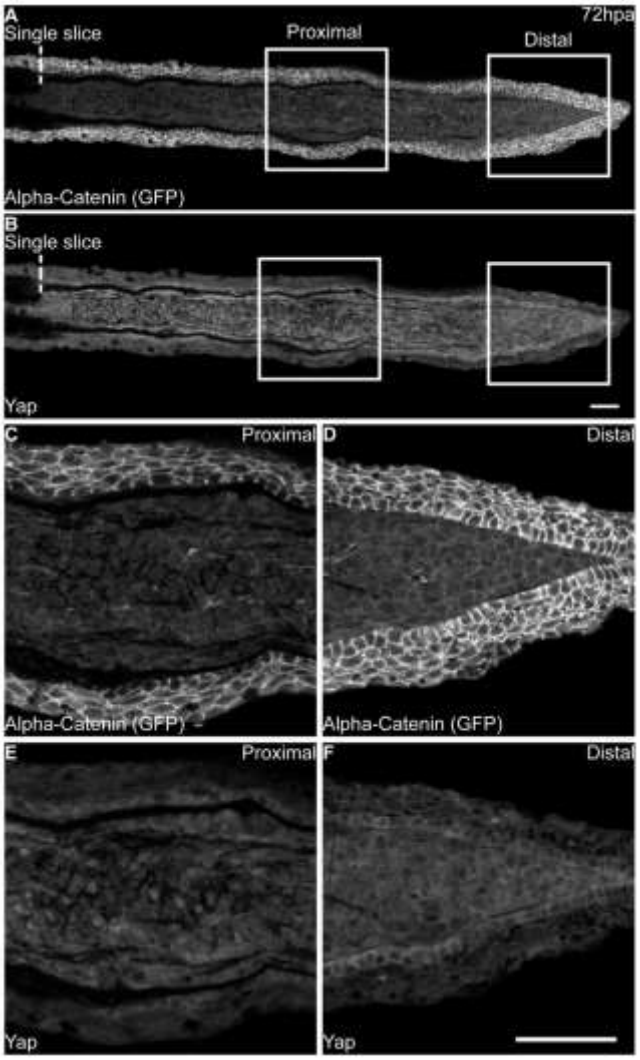

Figure 12. Alpha-Catenin accumulates in the most-distal region of the outgrowth blastema where Yap is mainly cytoplasmic. Representative immunofluorescence with anti-Yap and anti-GFP in 72hpa longitudinal sections of Alpha-Catenin transgenics. **A** Alpha-catenin expression; **B** Corresponding Yap expression. **C-F** Zoomed areas represented by squares in A-B. Proximal **(C)** and distal **(D)** images from A showing Alpha-Catenin expression. Corresponding proximal **(E)** and distal **(F)** images from B showing Yap expression. Dashed lines indicate amputation plane. n=9 sections, 3 fish. Scale bars correspond to 50µm.

4.7 F-Actin controls Yap dynamics

Taking into account that the cytoskeleton also plays an active role in mediating the mechanical forces to which cells are exposed to, we investigated F-actin localization along the PD axis of the regenerating blastema. By performing phalloidin stainings, we observed that F-actin also underwent changes along the PD axis in 72 hpa blastemas (Figure 13A-B): it localizes to the cortex in distal mesenchymal cells, where cell density is higher and Yap more cytoplasmic (Figure 13D, F, XZ Distal); in proximal regions, where cell density is lower and Yap nuclear, F-actin is present throughout the cell in the cytoplasm (Figure 13C, E, XZ Proximal). F-actin also co-localized partially with the accumulation of Alpha-Catenin at the junctions in the distal blastema (Figure 14).

To determine whether F-actin is involved in regulating Yap's activity (Dupont et al., 2011)(Wada et al., 2011)(Sansores-Garcia et al., 2011)(Fernández et al., 2011)(Reddy et al., 2013), we performed *in vivo* intraperitoneal injections of Jasplakinolide (Jasp), an inducer of F-actin polymerization and stabilizing compound (Bubb et al., 1994), in 72 hpa Alpha-Catenin transgenic zebrafish. We accessed Yap protein expression through immunostainings and observed that its intracellular localization was affected, as early as 30 minutes after Jasp injection. In particular, nuclear translocation of Yap was induced throughout the blastema in contrast to DMSO controls (Figure 15A-B) and was particularly evident in distal regions of Jasp treated animals (Figure 15C-E, compare DMSO XZ Distal with JASP XZ Distal). To confirm that Jasp was not only triggering Yap nuclear translocation but also its activation state, we performed qPCR for its target gene *ctgfa,* in Jasp versus DMSO injected animals. This analysis showed that upon 30 minutes of Jasp injection, the *ctgfa* transcription levels were not readily affected in the blastema; however, by 2 hours post Jasp injection there was a significant *ctgfa* upregulation when compared to DMSO animals (Figure 15F). This

suggests that by disrupting F-actin dynamics we are able to override the mechanical cues possibly provided by the high cell density in the distal tip of the blastema and with that control Yap and its downstream targets. When looking at the localization of Alpha-Catenin in these conditions, we found that this protein does not display modifications in its accumulation in the distal tip upon Jasp treatment (Figure 15G-J), indicating that Alpha-Catenin is not directly affected upon F-actin manipulation in the regenerating blastema. Altogether, these observations show that F-actin acts as an upstream regulator of Yap *in vivo*, controlling its activation during the regenerative process.

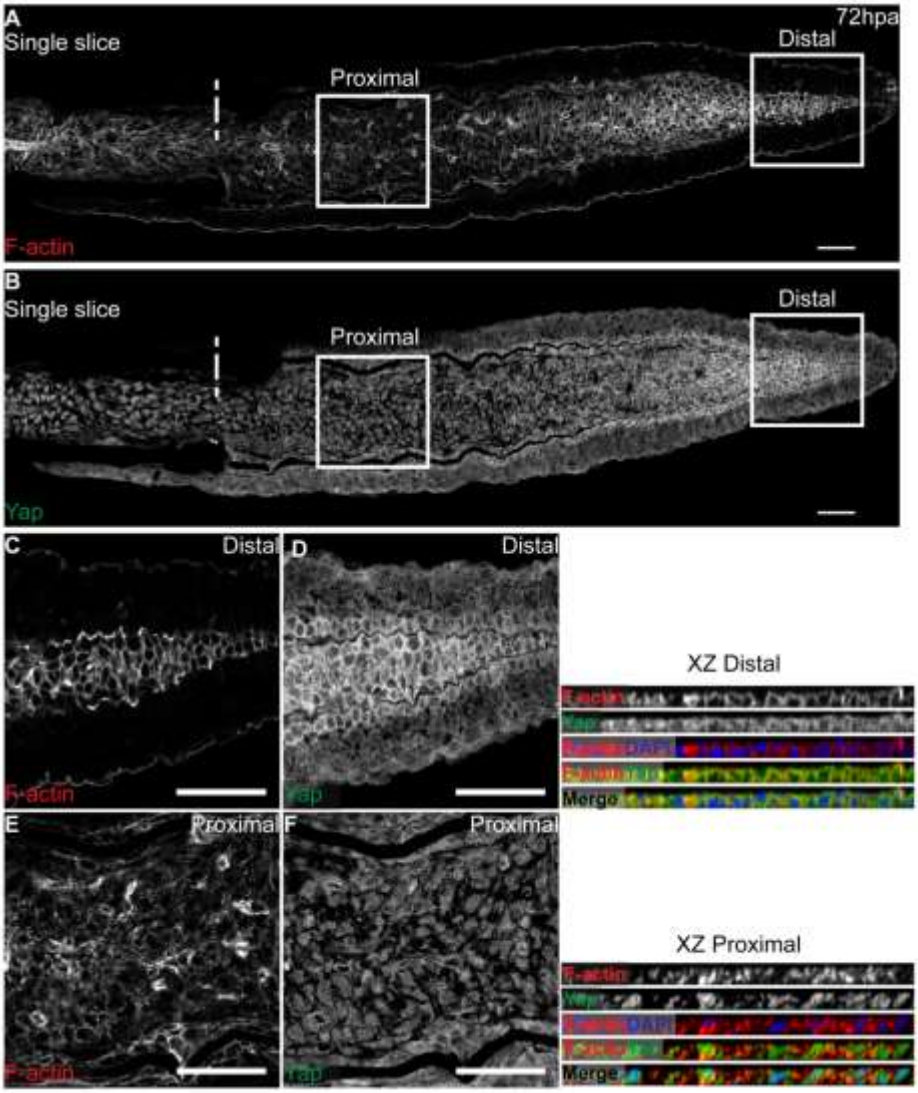

Figure 13. Differential proximo-distal expression of F-actin associates with Yap intracellular location. Representative immunofluorescence with anti-Yap and phalloidin (F-actin) in 72hpa longitudinal sections. **A** F-actin expression; **B** Corresponding Yap expression. **C-F** Zoomed areas represented by squares in A-B. Proximal **(C)** and distal **(D)** images from A showing F-actin expression. Corresponding proximal **(E)** and distal **(F)** images from B showing Yap expression. Single color and merged XZ projections of distal blastema images D-F and proximal blastema images C-E are shown to highlight intracellular localization.

Dashed lines indicate amputation plane. n=9 sections, 3 fish. Scale bars correspond to 50µm.

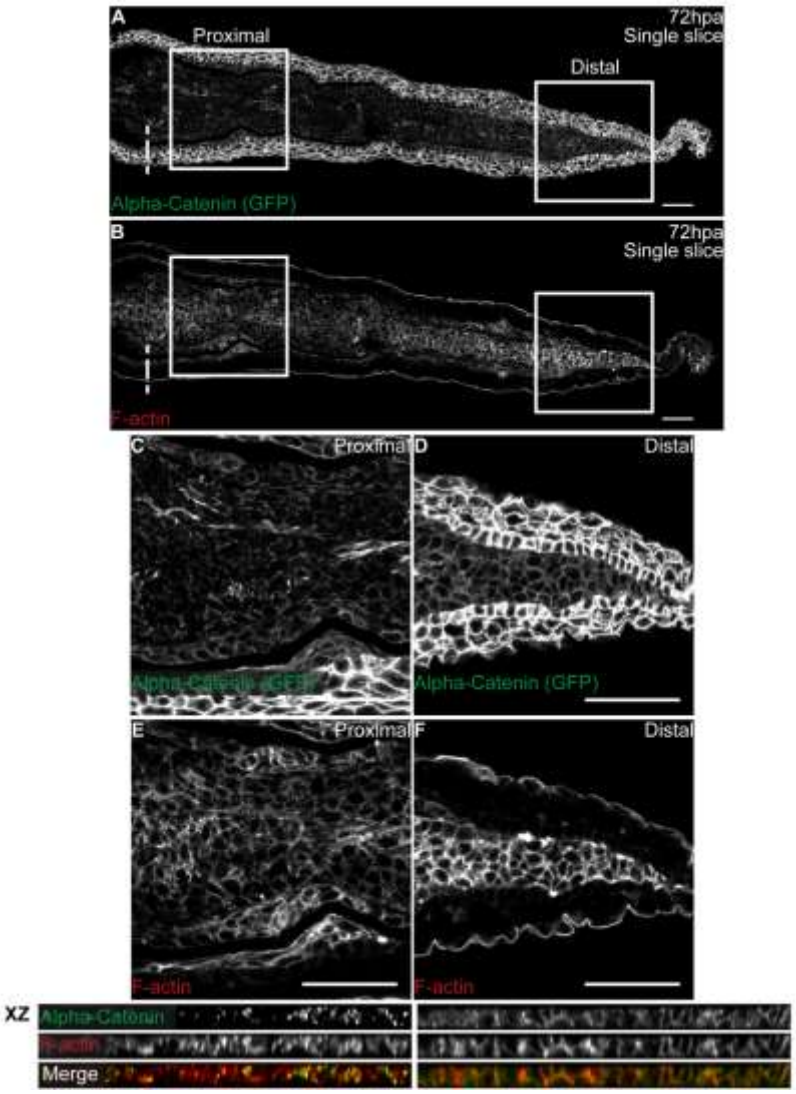

Figure 14. Alpha-catenin and F-actin partially co-localize in the regenerating blastema. **A** Representative immunofluorescence with anti-GFP and phalloidin (F-actin) in 72 hpa longitudinal sections of Alpha-catenin transgenics. **A** Representative single frame of Alpha-catenin; **B** Corresponding single frame of F-actin. **C-F** Corresponding zoomed areas represented by squares in A-B. Proximal **(C)** and distal **(D)** zoomed images from A showing

the differential Alpha-catenin expression along the PD axis. Corresponding proximal **(E)** and distal **(F)** zoomed images from B showing the differential F-actin expression along the PD axis. Single color and merged XZ projections of proximal blastema images D-F and distal blastema images C-E are shown below the corresponding panel to highlight intracellular localization. Dashed lines indicate amputation plane. n=9 sections, 3 fish. Scale bar corresponds to 50μm.

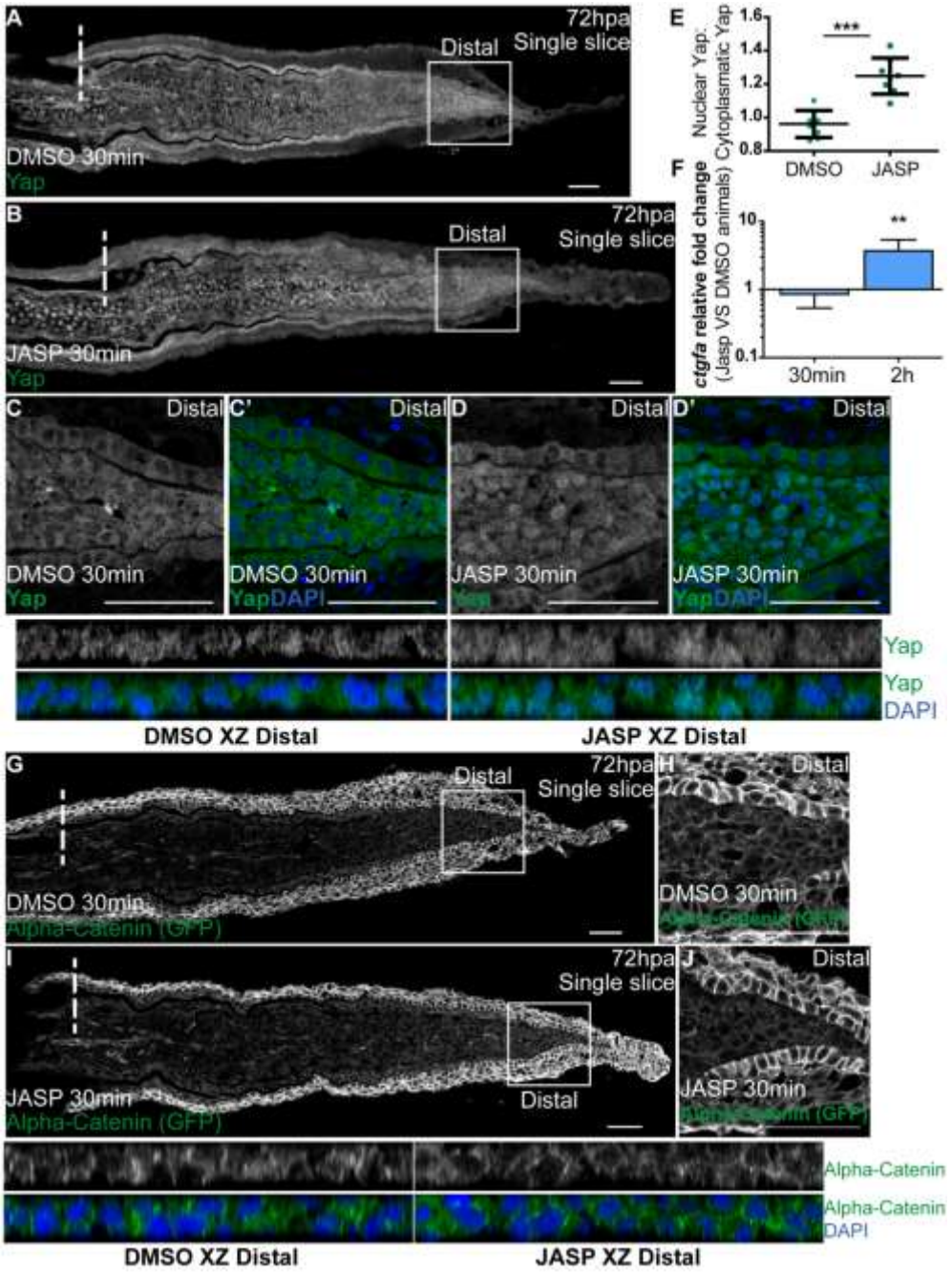

Figure 15. F-actin controls Yap intracellular dynamics. Representative immunofluorescence with anti-Yap and anti-GFP in 72hpa longitudinal sections of Alpha-Catenin transgenic animals injected with Jasplakinolide (JASP) and respective DMSO

controls. Yap expression in DMSO controls **(A)** and JASP animals **(B)**. **C-D** Zoomed areas represented by squares in A-B; single color images showing Yap expression and merged with DAPI in DMSO **(C-C')** and JASP **(D-D')** conditions. Corresponding XZ projections of distal blastema images C-D are shown to highlight intracellular localization in both situations (DMSO XZ Distal, JASP XZ Distal). **E** Quantification of average Yap intracellular localization by expressing a ratio between average intensities of Nuclear Yap:Cytoplasmic Yap of XZ projections from distal blastemas exposed to DMSO or JASP conditions, at 30 minutes post injection. Higher ratio values correspond to higher intensities of nuclear Yap. ***P value<0.001, two tailed, non-parametric Mann-Whitney test. n=8 sections, 4 fish per condition. **F** qPCR determination of *ctgfa* expression levels in JASP versus respective DMSO injected animals. Relative expression levels in fins of JASP injected animals at 30 minutes post injection and 2 hours post injection, time points in which RNA was readily extracted. **P value<0.01; two tailed, non-parametric paired Wilcoxon test, logarithmic scale, base 10. **G-I** Alpha-Catenin expression in DMSO controls **(G)** and JASP animals **(I)**. **H-J** Zoomed areas represented by squares in F-H, showing Alpha-Catenin expression in the distal blastema of DMSO controls **(H)** and JASP animals **(J)**. Corresponding XZ projections of distal blastema images G-I are shown to highlight intracellular localization in both situations; single color images showing Alpha-Catenin expression and merged with DAPI. Intraperitoneal injections were performed in 72 hpa animals, 30 minutes pre-fixation of the caudal fins. n=12 sections, 4 fish per condition. Dashed lines indicate amputation plane. Scale bars correspond to 50µm.

5. Discussion

Our study identifies a mechanism for the regulation of Yap activity within the zebrafish caudal fin regenerating blastema based on the differences in cell density along the mesenchymal tissue. The mesenchymal cells seem to respond to a mechanotransduction process that involves changes in cell morphology, junction assembly and cytoskeleton remodeling, which together lead to a graded control of tissue growth via Yap, a Hippo pathway effector.

In wild type settings, the regenerating blastema presents a compartmentalized organization once fully formed. The proximal mesenchymal region exhibits high proliferation and differentiation rates that progressively decrease towards the distal tip (Nechiporuk and Keating, 2002). We show that intracellular expression of Yap correlates with these spatially restricted regions and could account for the different levels of proliferation described. Remarkably, the same intracellular Yap dynamics also correlates with the degree of cell density within the proximal-distal axis of the blastema. In the distal high cell density domain, Yap is mainly cytoplasmic while in the proximal lower cell density domain, Yap is largely nuclear. The functional relevance of Yap intracellular localization was confirmed by genetic manipulation: overexpression of a constitutively active form of Yap leads to an increase in proliferation, while overexpression of a dominant negative form of Yap results in the opposing phenotype characterized by a cell cycle delay, halting proliferation between G2 and M phases (Xia et al., 2002). The effects of Yap are not only restricted to proliferation as it also affects the expression of several signaling factors involved in fin regeneration. Interestingly, regeneration specific genes such as *fgf20a* are upregulated when Yap activity is compromised in DN-yap transgenics and downregulated when Yap activity is enhanced in CA-yap transgenics. The size of the blastema is reduced in both cases, indicating

that Yap is on top of a complex network of tissue growth regulation during regeneration, not restricted to the control of proliferation.

Our observations suggest a mechanism of contact inhibition of proliferation that has been described to regulate Yap in various cell culture systems (Zhao et al., 2007)(Wada et al., 2011)(Mcclatchey and Yap, 2012). Recently it has been proposed that Yap dynamics can be controlled by different upstream cues that govern each other hierarchically when different levels of confluency are achieved (Aragona et al., 2013). In these epithelial systems, Yap is mostly nuclear in sparse cultures, fairly cytoplasmic in confluent cultures and completely cytoplasmic in dense cultures. In confluent situations, there is a relevant role for junction proteins and upstream Hippo pathway components in inactivating Yap. In contrast, in dense cultures, there is a dominant role of the extracellular matrix (ECM) stiffness and cytoskeleton mechanics over the other Yap inactivating mechanisms. Interestingly, in our *in vivo* system, the distal mesenchymal cells that exhibit high density and mostly cytoplasmic Yap appear to have features of both of these inactivating situations. Those blastemal cells present rounder cell morphology, have mature cell-cell contacts shown by the presence of Alpha-Catenin, seem to have an increase in activated Mst 1/2 and Lats 1/2, and display changes in F-actin intracellular localization. Physiologically, this suggests that a combination of several mechanical stress mechanisms exist to robustly inactivate Yap in the distal blastema; nevertheless the inactivation hierarchy of such mechanisms remains to be established.

The recruitment of Alpha-Catenin to the membrane as a consequence of high cell density may lead to accumulation of cortical F-actin that in turn drives the inactivation of Yap, resembling the process described in the mouse epidermis (Schlegelmilch et al., 2011). Interestingly, if we consider that less substrate contacts with the ECM are a consequence of high cell density, in which rounder blastema cells are packed, this should also lead to repositioning of F-actin to the cell cortex and exclusion of Yap from the nucleus. We can only speculate about the possible mechanical contribution

of ECM stiffness towards Yap inactivation, but it is tempting to associate the high cell density zone of the blastema with a possible soft substrate in which there is low mechanical tension conferred by the ECM. This would enable the system to have multiple ways of directing F-actin to the cell cortex and consequently inactivating Yap distally (Gumbiner and Kim, 2014). The initial step in the cascade of events leading to Yap inactivation in the distal tip needs further investigation, but it is conceivable that it depends primarily on the increase of density and cell contacts. The cause for cells accumulating distally remains unclear, possibly being a structural consequence of the surrounding epithelial layers that lead to physical constraints in the underlying mesenchyme.

We show that F-actin plays a major role in mediating the information from the surrounding environment and Yap dynamics *in vivo*. F-actin may be directly involved in sensing the mesenchymal cell density state and translate that into Yap activation, thus proliferation. The idea that F-actin can act as a mechanotransducer is not new (Romet-Lemonne and Jégou, 2013)(Heisenberg and Bellaïche, 2013), but here we reveal that it can contribute to control organ size during epimorphic regeneration. Additionally, by manipulating F-actin, the accumulation of Alpha-Catenin in the distal blastema was maintained; this could mean that Alpha-catenin is upstream of F-actin, reinforcing its possible role as a mechanotransducer in response to cell density changes in the blastema.

High cell density in the blastema seems to play an instructive role in the distal inactivation of Yap; it is unlikely however that low cell density is the initial Yap activation trigger, but may rather be a required permissive step. The first signs of Yap activation were observed at 6 hpa when cell migration towards the stump had not yet taken place; hence density in the blastema is unlikely to be considerably lower than the uncut mesenchymal tissue where Yap is inactive (Figure 2A-C). Yap activation could be linked to the appearance of F-actin in the mesenchyme or with the presence of soluble growth factors, such as WNT, which is known for its interplay with the Hippo

pathway and is also early activated upon amputation (Imajo et al., 2012)(Rosenbluh et al., 2012)(Stoick-cooper et al., 2007).

Our finding that Yap appears to be inhibited in uninjured, fully differentiated caudal fins supports the idea that Yap has a specific function during the regenerative process, when there is a need for a timely and precise control of tissue growth. This apparent prerequisite of a less differentiated environment is consistent with observations of phenotypes in other model systems, in which experimental manipulation of Yap leads to phenotypes only in tissues that are not fully differentiated. This is the case in embryonic development settings, adult contexts involving stem cell niches and in cancer models where cell plasticity is affected (Barry and Camargo, 2013)(Hiemer and Varelas, 2013). This is suggestive of multiple levels of Yap regulation in fully differentiated tissues.

The coordination between a number of signaling pathways and morphogens during fin regeneration is essential to guarantee robustness and to restore the correct final fin size. Our work shows for the first time that mechanical input within the blastema is also crucial for regeneration to occur. By a process of mechanotransduction, mediated via Alpha-Catenin and F-actin, Yap regulation is balanced, thus influencing cell proliferation and conferring an important *in vivo* physiological role to this member of the Hippo pathway.

6. References

Aragona, M., Panciera, T., Manfrin, A., Giulitti, S., Michielin, F., Elvassore, N., Dupont, S., and Piccolo, S. (2013). A Mechanical Checkpoint Controls Multicellular Growth through YAP/TAZ Regulation by Actin-Processing Factors. Cell 1–13.

Azevedo, A.S., Grotek, B., Jacinto, A., Weidinger, G., and Saúde, L. (2011). The Regenerative Capacity of the Zebrafish Caudal Fin Is Not Affected by Repeated Amputations. PLoS One *6*, e22820.

Azevedo, A.S., Sousa, S., Jacinto, A., and Saúde, L. (2012). An amputation resets positional information to a proximal identity in the regenerating zebrafish caudal fin. BMC Dev. Biol. *12*, 24.

Barry, E.R., and Camargo, F.D. (2013). The Hippo superhighway: signaling crossroads converging on the Hippo/Yap pathway in stem cells and development. Curr. Opin. Cell Biol. 1–7.

Blum, N., and Begemann, G. (2011). Retinoic acid signaling controls the formation, proliferation and survival of the blastema during adult zebrafish fin regeneration. Development *116*, 107–116.

Bubb, M.R., Senderowicz, A.M., Sausville, E.A., Duncan, K.L., and Korn, E.D. (1994). Jasplakinolide, a cytotoxic natural product, induces actin polymerization and competitively inhibits the binding of phalloidin to F-actin. J. Biol. Chem. *269*, 14869–14871.

Cai, J., Zhang, N., Zheng, Y., de Wilde, R.F., Maitra, A., and Pan, D. (2010). The Hippo signaling pathway restricts the oncogenic potential of an intestinal regeneration program. Genes Dev. *24*, 2383–2388.

Chablais, F., Jaz, A., and Jazwinska, A. (2010). IGF signaling between blastema and wound epidermis is required for fin regeneration. Development *137*, 871–879.

Chiou, M., Chao, T.-T., Wu, J., Kuo, C., and Chen, J. (2006). The physiological role of CTGF/CCN2 in zebrafish notochond development and biological analysis of the proximal promoter region. Biochem. Biophys. Res. Commun. *349*, 750–758.

Demircan, T., and Berezikov, E. (2013). The Hippo pathway regulates stem cells during homeostasis and regeneration of the flatworm Macrostomum lignano. Stem Cells Dev. *22*, 2174–2185.

Dickmeis, T., Plessy, C., Rastegar, S., Aanstad, P., Herwig, R., Chalmel, F., Fischer, N., and Strähle, U. (2004). Expression profiling and comparative genomics identify a conserved regulatory region controlling midline expression in the zebrafish embryo. Genome Res. *14*, 228–238.

Dong, J., Feldmann, G., Huang, J., Wu, S., Zhang, N., Comerford, S.A., Gayyed, M.F., Anders, R.A., Maitra, A., and Pan, D. (2007). Elucidation of a universal size-control mechanism in Drosophila and mammals. Cell *130*, 1120–1133.

Dupont, S., Morsut, L., Aragona, M., Enzo, E., Giulitti, S., Cordenonsi, M., Zanconato, F., Le Digabel, J., Forcato, M., Bicciato, S., et al. (2011). Role of YAP/TAZ in mechanotransduction. Nature *474*, 179–183.

Engel, C., Moeller, M.J., Englert, C., Bollig, F., Scha, T., Mlodzik, M., Huber, T.B., Kuehn, E.W., Kim, E., Kramer-zucker, A., et al. (2009). Scribble participates in Hippo signaling and is required for normal zebrafish pronephros development. Proc. Natl. Acad. Sci. U. S. A. *106*, 8579–8584.

Fernández, B.G., Gaspar, P., Brás-pereira, C., Jezowska, B., Rebelo, S.R., and Janody, F. (2011). Actin-Capping Protein and the Hippo pathway regulate F-actin and tissue growth in Drosophila. Development *138*, 2337–2346.

Fernando, C.A., Conrad, P.A., Bartels, C.F., Marques, T., To, M., Balow, S.A., Nakamura, Y., and Warman, M.L. (2010). Temporal and spatial expression of CCN genes in zebrafish. Dev. Dyn. *239*, 1755–1767.

Fior, R., Maxwell, A. a, Ma, T.P., Vezzaro, A., Moens, C.B., Amacher, S.L., Lewis, J., and Saúde, L. (2012). The differentiation and movement of presomitic mesoderm progenitor cells are controlled by Mesogenin 1. Development *139*, 4656–4665.

Fujii, M., Toyoda, T., Nakanishi, H., Yatabe, Y., Sato, A., Matsudaira, Y., Ito, H., Murakami, H., Kondo, Y., Kondo, E., et al. (2012). TGF-β synergizes with defects in the Hippo pathway to stimulate human malignant mesothelioma growth. J. Exp. Med. *209*, 479–494.

Gumbiner, B.M., and Kim, N.-G. (2014). The Hippo-YAP signaling pathway and contact inhibition of growth. J. Cell Sci. *127*, 709–717.

Hayashi, S., Tamura, K., and Yokoyama, H. (2014). Yap1, transcription regulator in the Hippo signaling pathway, is required for Xenopus limb bud regeneration. Dev. Biol. *388*, 57–67.

Heallen, T., Morikawa, Y., Leach, J., Tao, G., Willerson, J.T., Johnson, R.L., and Martin, J.F. (2013). Hippo signaling impedes adult heart regeneration. Development *140*, 4683–4690.

Heisenberg, C., and Bellaïche, Y. (2013). Forces in tissue morphogenesis and patterning. Cell *153*, 948–962.

Henrique, D., Adam, J., Myat, A., Chitnis, A., Lewis, J., and Ish-Horowicz, D. (1995). Expression of a Delta homologue in prospective neurons in the chick. Nature *375*, 787–790.

Hiemer, S.E., and Varelas, X. (2013). Stem cell regulation by the Hippo pathway. Biochim. Biophys. Acta *1830*, 2323–2334.

Hu, J., Sun, S.S., Jiang, Q., Wang, W., Gui, Y., and Song, H. (2013). Yes-Associated Protein (Yap) Is Required for Early Embryonic Development in Zebrafish (Danio Rerio). Int. J. Biol. Sci. *9*, 267–278.

Huang, J., Wu, S., Barrera, J., Matthews, K., and Pan, D. (2005). The Hippo signaling pathway coordinately regulates cell proliferation and apoptosis by inactivating Yorkie, the Drosophila Homolog of YAP. Cell *122*, 421–434.

Imajo, M., Miyatake, K., Iimura, A., Miyamoto, A., and Nishida, E. (2012). A molecular mechanism that links Hippo signalling to the inhibition of Wnt/β-catenin signalling. EMBO J. *31*, 1–14.

Itou, J., Kawakami, H., Burgoyne, T., and Kawakami, Y. (2012). Life-long preservation of the regenerative capacity in the fin and heart in zebrafish. Biol. Open *1*, 739–746.

Jaźwińska A, Badakov R, Keating MT (2007). Activin-betaA signaling is required for zebrafish fin regeneration. Curr Biol 17: 1390–1395.

Jiang, Q., Liu, D., Gong, Y., Wang, Y., Sun, S., Gui, Y., and Song, H. (2009). Yap Is Required for the Development of Brain, Eyes, and Neural Crest in Zebrafish. Biochem. Biophys. Res. Commun. *384*, 114–119.

Kawakami, K., Takeda, H., Kawakami, N., Kobayashi, M., Matsuda, N., and Mishina, M. (2004). A transposon-mediated gene trap approach identifies developmentally regulated genes in zebrafish. Dev. Cell *7*, 133–144.

Kim, N., Koh, E., Chen, X., and Gumbiner, B.M. (2011). E-cadherin mediates contact inhibition of proliferation through Hippo signaling-pathway components. Proc. Natl. Acad. Sci. U. S. A. *108*, 11930–11935.

Knopf, F., Hammond, C., Chekuru, A., Kurth, T., Hans, S., Weber, C.W., Mahatma, G., Fisher, S., Brand, M., Schulte-Merker, S., et al. (2011). Bone Regenerates via Dedifferentiation of Osteoblasts in the Zebrafish Fin. Dev. Cell *20*, 713–724.

Kujawski, S., Lin, W., Kitte, F., Börmel, M., Fuchs, S., Arulmozhivarman, G., Vogt, S., Theil, D., Zhang, Y., and Antos, C.L. (2014). Calcineurin Regulates Coordinated Outgrowth of Zebrafish Regenerating Fins. Dev. Cell 1–15.

Lee, Y., Grill, S., Sanchez, A., Murphy-Ryan, M., and Poss, K.D. (2005). Fgf signaling instructs position-dependent growth rate during zebrafish fin regeneration. Development *132*, 5173–5183.

Lee, Y., Hami, D., De Val, S., Kagermeier-Schenk, B., Wills, A.A., Black, B.L., Weidinger, G., and Poss, K.D. (2009). Maintenance of blastemal proliferation by functionally diverse epidermis in regenerating zebrafish fins. Dev. Biol. *331*, 270–280.

Lin, A.Y.T., and Pearson, B.J. (2014). Planarian yorkie/YAP functions to integrate adult stem cell proliferation, organ homeostasis and maintenance of axial patterning. Development 1–12.

Luo, Q., Kang, Q., Si, W., Jiang, W., Park, J.K., Peng, Y., Li, X., Luu, H.H., Luo, J., Montag, A.G., et al. (2004). Connective tissue growth factor (CTGF) is regulated by Wnt and bone morphogenetic proteins signaling in osteoblast differentiation of mesenchymal stem cells. J. Biol. Chem. *279*, 55958–55968.

Mahoney, W.M., Hong, J., Yaffe, M.B., and Farrance, I.K.G. (2005). The transcriptional co-activator TAZ interacts differentially with transcriptional enhancer factor-1 (TEF-1) family members. Biochem. J. *388*, 217–225.

Mateus, R., Pereira, T., Sousa, S., de Lima, J.E., Pascoal, S., Saúde, L., and Jacinto, A. (2012). In vivo cell and tissue dynamics underlying zebrafish fin fold regeneration. PLoS One *7*, e51766.

Mcclatchey, A.I., and Yap, A.S. (2012). Contact inhibition (of proliferation) redux. Curr. Opin. Cell Biol. *24*, 685–694.

Morgan, T.H. (1901). REGENERATION AND LIABILITY TO INJURY. Science *14*, 235–248.

Münch, J., González-Rajal, A., and de la Pompa, J.L. (2013). Notch regulates blastema proliferation and prevents differentiation during adult zebrafish fin regeneration. Development *140*, 1402–1411.

Nechiporuk, A., and Keating, M.T. (2002). A proliferation gradient between proximal and msxb-expressing distal blastema directs zebrafish fin regeneration. Development *129*, 2607–2617.

Oh, H., and Irvine, K.D. (2008). In vivo regulation of Yorkie phosphorylation and localization. Development *135*, 1081–1088.

Pan, D. (2010). The hippo signaling pathway in development and cancer. Dev. Cell *19*, 491–505.

Perathoner, S., Daane, J.M., Henrion, U., Seebohm, G., Higdon, C.W., Johnson, S.L., Nüsslein-Volhard, C., and Harris, M.P. (2014). Bioelectric Signaling Regulates Size in Zebrafish Fins. PLoS Genet. *10*, e1004080.

Poleo, G., Brown, C.W., Laforest, L., and Akimenko, M. a (2001). Cell proliferation and movement during early fin regeneration in zebrafish. Dev. Dyn. *221*, 380–390.

Poss, K.D.D., Shen, J., and Keating, M.T.T. (2000). Induction of lef 1 during zebrafish fin regeneration. Dev. Dyn. *219*, 282–286.

Reddy, P., Deguchi, M., Cheng, Y., and Hsueh, A.J.W. (2013). Actin cytoskeleton regulates hippo signaling. PLoS One *8*, e73763.

Romet-Lemonne, G., and Jégou, A. (2013). Mechanotransduction down to individual actin filaments. Eur. J. Cell Biol. *92*, 333–338.

Rosenbluh, J., Nijhawan, D., Cox, A.G.G., Li, X., Neal, J.T.T., Schafer, E.J.J., Zack, T.I.I., Wang, X., Tsherniak, A., Schinzel, A.C.C., et al. (2012). β-Catenin-Driven Cancers Require a YAP1 Transcriptional Complex for Survival and Tumorigenesis. Cell *151*, 1457–1473.

Sansores-Garcia, L., Bossuyt, W., Wada, K., Yonemura, S., Tao, C., Sasaki, H., and Halder, G. (2011). Modulating F-actin organization induces organ growth by affecting the Hippo pathway. EMBO J. *30*, 2325–2335.

Santos-Ruiz, L., Santamaría, J.A., Ruiz-Sánchez, J., and Becerra, J. (2002). Cell proliferation during blastema formation in the regenerating teleost fin. Dev. Dyn. *223*, 262–272.

Santos-Ruiz, L., Santamaría, J.A., and Becerra, J. (2005). Cytoskeletal dynamics of the teleostean fin ray during fin epimorphic regeneration. Differentiation. *73*, 175–187.

Schlegelmilch, K., Mohseni, M., Kirak, O., Pruszak, J., Rodriguez, J.R., Zhou, D., Kreger, B.T., Vasioukhin, V., Avruch, J., Brummelkamp, T.R., et al. (2011). Yap1 Acts Downstream of a-Catenin to Control Epidermal Proliferation. Cell *144*, 782–795.

Shaw, R.L., Kohlmaier, A., Polesello, C., Veelken, C., Edgar, B. a, and Tapon, N. (2010). The Hippo pathway regulates intestinal stem cell proliferation during Drosophila adult midgut regeneration. Development *4158*, 4147–4158.

Silvis, M.R., Kreger, B.T., Lien, W.-H.W.-H., Klezovitch, O., Rudakova, G.M., Camargo, F.D., Lantz, D.M., Seykora, J.T., Vasioukhin, V., and Marianna, G. (2011). α-catenin is a tumor suppressor that controls cell accumulation by regulating the localization and activity of the transcriptional coactivator Yap1. Sci. Signal. *4*, ra33–ra33.

Soroldoni, D., Hogan, B.M., and Oates, A.C. (2009). Simple and Efficient Transgenesis with Meganuclease Constructs in Zebrafish (Totowa, NJ: Humana Press).

Sousa, S., Afonso, N., Bensimon-Brito, A., Fonseca, M., Simões, M., Leon, J., Roehl, H., Cancela, M.L., and Jacinto, A. (2011). Differentiated skeletal cells contribute to blastema formation during zebrafish fin regeneration. Development *138*, 3897–3905.

Staley, B.K., and Irvine, K.D. (2010). Warts and yorkie mediate intestinal regeneration by influencing stem cell proliferation. Curr. Biol. *20*, 1580–1587.

Stewart, S., and Stankunas, K. (2012). Limited dedifferentiation provides replacement tissue during zebrafish fin regeneration. Dev. Biol. *365*, 339–349.

Stewart, S., Gomez, A.W., Armstrong, B.E., Henner, A., and Stankunas, K. (2014). Sequential and Opposing Activities of Wnt and BMP Coordinate Zebrafish Bone Regeneration. Cell Rep. *7*, 1–17.

Stoick-cooper, C.L.C.L., Weidinger, G., Riehle, K.J.K.J., Hubbert, C., Major, M.B.M.B., Fausto, N., and Moon, R.T.R.T. (2007). Distinct Wnt signaling pathways have opposing roles in appendage regeneration. Development *134*, 479–489.

Sugiyama, M., Sakaue-Sawano, A., Iimura, T., Fukami, K., Kitaguchi, T., Kawakami, K., Okamoto, H., Higashijima, S., and Miyawaki, A. (2009). Illuminating cell-cycle progression in the developing zebrafish embryo. Proc. Natl. Acad. Sci. U. S. A. *106*, 20812–20817.

Thummel, R., Burket, C.T., and Hyde, D.R. (2006). Two different transgenes to study gene silencing and re-expression during zebrafish caudal fin and retinal regeneration. ScientificWorldJournal. *6 Suppl 1*, 65–81.

Tu, S., and Johnson, S.L. (2011). Fate restriction in the growing and regenerating zebrafish fin. Dev. Cell *20*, 725–732.

Wada, K., Itoga, K., Okano, T., Yonemura, S., and Sasaki, H. (2011). Hippo pathway regulation by cell morphology and stress fibers. Development *138*, 3907–3914.

Wehner, D., Cizelsky, W., Vasudevaro, M.D., Ozhan, G., Haase, C., Kagermeier-Schenk, B., Röder, A., Dorsky, R.I., Moro, E., Argenton, F., et al. (2014). Wnt/β-Catenin Signaling Defines Organizing Centers that Orchestrate Growth and Differentiation of the Regenerating Zebrafish Caudal Fin. Cell Rep. 1–15.

Wills, A.A., Kidd, A.R., Lepilina, A., and Poss, K.D. (2008). Fgfs control homeostatic regeneration in adult zebrafish fins. Development *135*, 3063–3070.

Wolpert, L. (2011). Positional information and patterning revisited. J. Theor. Biol. *269*, 359–365.

Xia, H., Qi, H., Li, Y., Pei, J., Barton, J., Blackstad, M., Xu, T., and Tao, W. (2002). LATS1 tumor suppressor regulates G2/M transition and apoptosis. Oncogene *21*, 1233–1241.

Xin, M., Kim, Y., Sutherland, L.B., Murakami, M., Qi, X., Mcanally, J., Porrello, E.R., Mahmoud, a. I., Tan, W., Shelton, J.M., et al. (2013). Hippo pathway effector Yap promotes cardiac regeneration. Proc. Natl. Acad. Sci. 1–6.

Yagi, R., Chen, L.F., Shigesada, K., Murakami, Y., and Ito, Y. (1999). A WW domain-containing yes-associated protein (YAP) is a novel transcriptional co-activator. EMBO J. *18*, 2551–2562.

Zhang, J., Ji, J.-Y., Yu, M., Overholtzer, M., Smolen, G. a, Wang, R., Brugge, J.S., Dyson, N.J., and Haber, D. a (2009). YAP-dependent induction of amphiregulin identifies a non-cell-autonomous component of the Hippo pathway. Nat. Cell Biol. *11*, 1444–1450.

Zhao, B., Wei, X., Li, W., Udan, R.S., Yang, Q., Kim, J., Xie, J., Ikenoue, T., Yu, J., Li, L., et al. (2007). Inactivation of YAP oncoprotein by the Hippo pathway is involved in cell contact inhibition and tissue growth control. Genes Dev. *21*, 2747–2761.

Zhao, B., Ye, X., Yu, J.J., Li, L., Li, W., Li, S., Lin, J.D., Wang, C.-Y., Chinnaiyan, A.M., Lai, Z.-C., et al. (2008). TEAD mediates YAP-dependent gene induction and growth control. Genes Dev. *22*, 1962–1971.

Žigman, M., Trinh, L. a, Fraser, S.E., Moens, C.B., and Zigman, M. (2010). Zebrafish neural tube morphogenesis requires Scribble-dependent oriented cell divisions. Curr. Biol. *21*, 79–86.

7. Acknowledgements

We are grateful to Yi Fang and Kenneth Poss for sharing unpublished Yap functional transgenics. The authors thank Lara M. Carvalho and Aida Barros for support with fish care. We thank Lara C. Carvalho, Sara Sousa, Raquel Lourenço and Maria Gagliardi for reading the manuscript and insightful discussions, and Telmo Pereira for help with data analysis.

CHAPTER V

DISCUSSION

CONTENTS

Owing to the limited capacity of Humans in recovering from severe organ damage, the ultimate goal in regenerative medicine is to provide strategies to improve the proper replacement of injured tissues, leading to functional organs. By studying non-mammalian regenerative models, such as the Zebrafish, in which accurate organ substitution occurs naturally, new options may become available to exploit the potential of intrinsic tissue regeneration in humans. In particular, with this work I have investigated the innate ability of zebrafish to recover its fin size after injury and contributed to expand our understanding of how final growth is achieved and controlled during this process. Growth control is essential not only during organ regeneration but also in other processes like development and cancer, hence some of the results described in this thesis may provide useful knowledge across the biology of size field.

Insights into fin fold regeneration

By definition, *bona fide* epimorphic regeneration implies the formation of a blastema that leads to the recovery of lost tissues upon injury in developed animals (Morgan, 1901). By exploring the regeneration process of the established zebrafish 2 dpf fin fold, we found not only conserved, but also unique features of this model when compared to adult caudal fin regeneration.

We have demonstrated that during fin fold regeneration a wound epithelium rapidly forms, mesenchymal cells accumulate distally, and proliferation occurs in a time-restricted manner. These are all common features to fin fold and adult caudal fin regeneration, which complement previous studies and support the view that fin fold regeneration occurs in a similar manner to the adult system (Kawakami et al., 2004)(Yoshinari et al., 2009)(Mathew et al., 2007, 2009)(Ishida et al., 2010). We could demonstrate that there is a distal

accumulation of migratory, shape-changing fibroblasts, which appear to constitute a signaling center (Yoshinari et al., 2009)(Pittlik and Begemann, 2012), which resembles a blastema in its structure and formation. Despite this, we have not observed proliferation arising within those cells, rather noticing that it occurs in a wide area. This suggests that the fin fold blastema does not behave exactly as in the adult regenerating fin.

Remarkably, the fin fold growth rate upon amputation outperforms the adult's counterpart since this tissue recovers to its 5 dpf developmental size and pattern. This observation leads to considerations about positional identity and memory in this system. It is possible is that albeit this tissue is still being developmentally specified at 2 dpf, it has already acquired its proximal-distal positional values, which fin fold cells can recall in an injury situation. Another possibility is that positional identity cues are still being established from to 2-5 dpf, the developmental time points in which fin fold regeneration is inflicted. Therefore the tissue may independently attain its supposed size without resorting to positional memory, adopting a compensatory growth mechanism. By taking into account the example of the pectoral fin fold system, its anterior-posterior (AP) signature transcription factors are already present at 4 dpf, possibly indicating that establishment of positional values is an earlier event (Nachtrab et al., 2013). Nevertheless, the timing, nature and mode of action of the proximal-distal and dorso-ventral fin fold axial cues are still unknown.

We found that fin fold growth is not achieved solely by increasing cell numbers, given that the epithelial tissue is able to increase its growth rate after proliferation rates have decreased. This could be due to an increase in cell size, a remodeling of the epithelial cell layers or a contribution of other cell types present in the fin fold, reflecting another specific feature of this system that can provide knowledge on novel growth control mechanisms relevant for the field.

Growth and positional identity in epimorphic regeneration

An important consideration to undertake is whether the mechanisms that establish final size of an organ during development are the same as the ones that lead to its recovery in a regenerative process. Taking into account positional memory mechanisms, the recapitulation of ontogenetic positional information during epimorphic regeneration should occur. In agreement with this, recently it has been shown that basal expression levels of transcription factors are maintained and restricted to their signature AP domains, throughout the zebrafish life and regeneration (Nachtrab et al., 2013).

Interestingly, the adult fin cells that harbor the instructive information for recovering final size and form appear to be the same cells that contribute to blastema formation, these being the connective tissue cells, namely the intrarray osteoblasts and dermal fibroblasts (Nachtrab et al., 2013)(Perathoner et al., 2014)(Kujawski et al., 2014). This feature appears to be conserved also during axolotl limb regeneration, since it is the connective tissue (but not the muscle cells) that harbors the positional information that guides regenerative patterning (Nacu et al., 2013). In comparison, the 2 dpf fin fold tissue does not contain osteoblasts but has dermal fibroblasts. Taking into account that fin fold fibroblasts give rise to the adult dermal fibroblasts (Lee et al., 2013), it is possible that positional identity specification is already conferred within these cells at that developmental stage.

Despite our initial ideas, the mechanisms of ontogenetic size-control in fin fold and adult caudal fin can indeed be different. For instance, in the original zebrafish genetic screens, several mutants have been identified that develop enlarged fin folds (*dreumes*, *leprechaun* and *ukkie*), but presented regular sized adult fins. An interesting case is the mutant *dreumes,* which presented larger fin folds, however in adulthood showed smaller, but proportional, body and fin size (van Eeden et al., 1996). Conversely,

mutants having long (*long fin*, *another long fin* and *rapunzel*) or short/absent adult fins (*finless* and *shortfin*), have normal sized fin folds (van Eeden et al., 1996)(Iovine and Johnson, 2000)(Green et al., 2009). In line with this research, a recent study has pinpointed the genetic basis for the presented positive allometry in *another long fin* mutants (Perathoner et al., 2014). Perathoner and colleges show that missense mutations in the *kcnk5b* gene lead to increased conductance and hyperpolarization of two-pore domain potassium channels (K_{2P}), resulting in local action of these channels to control ontogenetic fin (and barbel) size. This increase in appendage growth was shown to be autonomous to the fin and barbel structures, not affecting body proportions, and relied on cell proliferation increase rather than cell size.

In addition, another recent study has shown that the positional identities of the adult caudal fin were altered by inhibiting Calcineurin with two small molecules, tacrolimus and cyclosporin A, leading also to positive allometric growth resulting in longer fins during development, homeostasis and regeneration (Kujawski et al., 2014). Though the full mechanistic basis for these phenotypes is yet unclear, this study elucidated that during wild type regenerative outgrowth, there is indeed a shift from isometric to allometric growth rates through the action of Calcineurin. This phosphatase appears to be active during homeostasis and until the blastema is fully formed, thereby inhibiting fast growth rates; when entering the regenerative outgrowth phase, Calcineurin is endogenously inhibited, leading to a growth rate increase; and finally when the fin has recovered its original size, it is re-activated. Cyclosporin A was screened as part of the Prestwick library, in our screening assay for compounds that would affect final fin fold size. However, this small molecule did not produce any increasing or inhibitory growth phenotypes, upon specific application during fin fold regeneration, reinforcing the differences between adult and fin fold systems in their regenerative size-control mechanisms.

The studies by Perathoner and Kujawski have contributed to the idea of multiple regulatory modes influencing ontogenetic and regenerative fin size and pattern (Perathoner et al., 2014)(Kujawski et al., 2014). In both cases, the manipulations performed led to proportionate overgrowths of the fin tissue, indicative that growth was achieved in a controlled manner. A more detailed analysis of these differences will be crucial to understand the mechanisms of establishment and control of ontogenetic and regenerative size control.

Biomechanical factors as regulators of regenerative size

The importance of biomechanical inputs in developmental processes has emerged recently as several groups started to identify mechanotransduction signaling pathways (Desprat et al., 2008)(Varelas et al., 2010)(Dupont et al., 2011)(Brunet et al., 2013). This has been particularly relevant in regulation of organ size and cell differentiation by the action of the Hippo/Yap pathway. Our work complements this view, as we show that during caudal fin regeneration this signaling pathway is regulated via changes in cell density and the cytoskeleton.

Our observation that the mesenchymal blastema has different levels of confluence provides evidence for a natural occurring process of contact inhibition of proliferation, in an *in vivo* context. Cell density within the blastema works as a mechanical stimulus that allows blastema cells to distinguish subtle temporal and spatial tension differences within their surroundings. As a result, these cells acquire different morphologies and strengthen their adhesion structures. Supporting this view, we found differences in the expression of Alpha-Catenin and F-actin according to the blastema cell density levels. Importantly, these changes are translated into differences in Yap activation, which controls a multitude of regeneration

factors and regulates proliferation, contributing for final size achievement. The existence of different cell densities along the PD axis of the blastema leads us to propose the blastema as dynamic structure that comprises different mechanical forces, which contribute as cues for restoration of the biomechanical equilibrium and tissue integrity. We believe that the nature of these mechanical forces can not only be derived from cell-cell applied tension, but also from tension conferred by the extracellular matrix into the cells, given that the blastema is a three-dimensional structure that responds to multiple inputs.

Already at the first step of regeneration, during wound healing, there are mechanical forces release that induce tissue displacement, migration and contractility of the epithelial cells (Poleo et al., 2001)(Mateus et al., 2012). This leads to cell rearrangements and cell shape changes that may trigger intracellular mechanotransduction pathways in the succeeding regenerative phases. Regarding the ECM, its mechanosensitive components may sense the disruption in tissue integrity and react by changing its conformation, exposing growth factor binding sites, as well as aggregate in clusters altering its rigidity (Vogel and Sheetz, 2006). The ECM can potentiate the transfer of information from the injury environment to the cell, leading to activation of mechanotransduction processes via the cytoskeleton. In spite of the unavailability of quantitative data in regenerative processes, it has been shown that during cutaneous wound healing, the ECM becomes stiffer (Schultz and Wysocki, 2009)(Wong et al., 2011). Recently the concept of a transitional ECM with specific roles in epimorphic regeneration situations has emerged, possibly leading to further understanding on how this complex protein scaffold can provide instructional cues directing cell behavior (Mercer et al., 2012).

Upon sealing of the wound, local differences in tension may provide spatial cues that conduct cells into performing specific actions in subsequent regenerative stages (blastema formation and regenerative outgrowth). These cell responses can be consequences of the blastema anatomy and

change dynamically as the ECM is remodeled, due to cell migration and establishment of cell-cell contacts between blastema cells. Tension differences may result from the regionalization of the blastema, which then leads to differential cell behaviors resulting in a properly sized and patterned organ.

How are mechanical forces established robustly in the blastema independently of the number of amputations? Can this be regarded as a compatible mechanism that provides positional memory instructions? Is it restricted to the regulation of certain cell functions, like proliferation? This information is most likely conferred in multiple ways and in close coordination with release and interpretation of morphogens, but their molecular nature and possible interactions is still unknown. Importantly, with this work we put forward the existence of different mechanical forces, mechanosensitive molecules and mechanotransduction signaling pathways as novel factors for attaining resilient epimorphic regeneration.

Main conclusions and Relevance

- The zebrafish fin fold model regenerates independently of spatial restricted proliferation.
- The larval fin fold and adult caudal fin appear to be governed by different size-control mechanisms.
- The adult fully formed blastema presents heterogeneous cell densities that are reflected in cell morphology and cytoskeleton changes.
- The adult blastema is the first described *in vivo* regenerative system that relies in contact inhibition of proliferation.
- The mesenchymal blastema expresses a multitude of adhesion molecules which may be relevant for cell-cell communication.
- The Hippo/Yap pathway is active in the mesenchymal blastema, where Yap acts as a mechanotransducer by responding to changes in the actin cytoskeleton.

Future Perspectives

Bioelectric signals

The existence of endogenous electric currents established within the tissues that undergo wound healing and regeneration has been long established (Borgens et al., 1977), but only recently the relevance of ion channels and their transporters has started to be unraveled. Interestingly, bioelectric fields in which differential accumulation of ions are detected across cell membranes can coordinate important cell functions during epimorphic regeneration, such as proliferation and dedifferentiation (Adams et al., 2007)(Monteiro et al., 2014). As discussed previously, gain of function mutations in potassium channels leads to caudal fin overgrowth (Perathoner et al., 2014). In addition, the calcium dependent phosphatase Calcineurin

needs to be transiently inhibited in the blastema to allow for proper size regulation of the fin (Kujawski et al., 2014). In this case, for Calcineurin to be active there is a need for an intracellular influx of calcium (Rusnak and Mertz, 2000). However, the mechanisms by which these ions regulate regeneration are yet unclear. It would thus be interesting to understand whether a common regulatory growth mechanism supported by ionic currents exists during caudal fin regeneration. Moreover, the possible regulation of intracellular calcium influxes during regeneration raises interesting questions of whether calcium could be involved in regulating the cytoskeleton and consequently the Hippo/Yap pathway. In wound healing, calcium fluxes have been shown to play a key role in modulating F-actin polymerization via actin binding proteins like Gelsolin (Antunes et al., 2013)(Yoo et al., 2012)(Razzell et al., 2013). Therefore, it is possible that calcium and F-actin regulate downstream mechanotransduction mechanisms in which the Hippo pathway, in particular Yap, could be involved.

Mechanical tension

The discovery of highly conserved mechanotransduction pathways like the Hippo/Yap pathway or Beta-Catenin, which can influence organ growth and differentiation, has revealed a new level of regulation in developmental processes with regard to mechanical tension (Desprat et al., 2008)(Varelas et al., 2010)(Dupont et al., 2011)(Brunet et al., 2013). In the epimorphic regeneration field, the understanding of how this process occurs is still incipient. Recent advances in technology that allow accurate measurement and manipulation of mechanical tension in living tissues will undoubtedly provide means of probing function of these physical properties of cells and organs. By being able to functionally manipulate cell density, measure tension in the different blastema regions and probe how stable are cell-cell

or cell-matrix contacts in blastema cells, we may start to clarify the importance of mechanical forces in the regenerative process.

Hippo pathway and cancer

Classically, the blastema is a structure associated with being transiently highly proliferative, yet possessing tumor restraining mechanisms (Brockes, 1998)(Pomerantz and Blau, 2013). Our finding that Yap is early activated and required during regeneration of the zebrafish caudal fin, captivated our interest in establishing parallels between epimorphic regeneration and cancer biology. In cancer model systems, inactivation of the upstream Hippo pathway members or activation of Yap promotes tumor overgrowth but also epithelial to mesenchymal transition, associated with invasive malignant migratory cancer phenotypes (Cordenonsi et al., 2011)(Hao et al., 2008)(Lei et al., 2008)(Overholtzer et al., 2006)(Zhang et al., 2008). The zebrafish does not possess special resistance to tumor formation mechanisms, actually being used as a disease model for many cancer types (Brockes, 1998)(White et al., 2013). Taking this into consideration, how can Yap be repeatedly activated upon amputation in the blastema and the fin achieves only proportionate growth, without tumor formation? One possible reason is the blastema environment itself. As considered before, the blastema has a variety of factors, genetic, biochemical and biophysical, that may regulate robustly Yap activity in time and space. Most likely, there is redundancy in regulatory mechanisms to prevent situations in which one may fail. These multiple levels of Yap regulation perhaps do not occur in a cancer situation, where most somatic tissues – when challenged with unusual high proliferative rates – fail to activate multiple growth control mechanisms. Another reason for the balanced growth of the blastema is that the Hippo/Yap pathway can also have other developmentally associated functions during regeneration aside from regulating organ size, such as

regulation of differentiation (Pomerantz and Blau, 2013). By promoting differentiation, upstream members of the Hippo pathway can restrict unnecessary proliferation, since mature cells often do not divide. Conversely, Yap activation may promote the undifferentiated nature of progenitor cells, so important to replenish all the necessary cell types for reconstitution of the missing organ (Hiemer and Varelas, 2013)(Mo et al., 2014)(Yimlamai et al., 2014). This beneficial property in injury situations may also constitute a hazard in cancer settings, leading to expansion and spreading of undifferentiated malignant cells. Therefore, by exploring further the regulatory mechanisms of the Hippo/Yap pathway in an *in vivo* system, such as the regenerating caudal fin, there is a possibility of better understanding of what is the basis for cancer development. Moreover, this knowledge may also contribute significantly to design and improve efficient regenerative therapies in tissues and organs that do not possess natural recovering mechanisms.

References

Adams, D.S., Masi, A., and Levin, M. (2007). H+ pump-dependent changes in membrane voltage are an early mechanism necessary and sufficient to induce Xenopus tail regeneration. Development *134*, 1323–1335.

Antunes, M., Pereira, T., Cordeiro, J. V., Almeida, L., and Jacinto, A. (2013). Coordinated waves of actomyosin flow and apical cell constriction immediately after wounding. J. Cell Biol. *202*, 365–379.

Borgens, R.B., Vanable, J.W., and Jaffe, L.F. (1977). Bioelectricity and regeneration: large currents leave the stumps of regenerating newt limbs. Proc. Natl. Acad. Sci. U. S. A. *74*, 4528–4532.

Brockes, J.P. (1998). Regeneration and cancer. Biochim. Biophys. Acta *1377*, M1–11.

Brunet, T., Bouclet, A., Ahmadi, P., Mitrossilis, D., Driquez, B., Brunet, A.-C., Henry, L., Serman, F., Béalle, G., Ménager, C., et al. (2013). Evolutionary conservation of early mesoderm specification by mechanotransduction in Bilateria. Nat. Commun. *4*, 2821.

Cordenonsi, M., Zanconato, F., Azzolin, L., Forcato, M., Rosato, A., Frasson, C., Inui, M., Montagner, M., Parenti, A.R.R., Poletti, A., et al. (2011). The Hippo Transducer TAZ Confers Cancer Stem Cell-Related Traits on Breast Cancer Cells. Cell *147*, 759–772.

Desprat, N., Supatto, W., Pouille, P.-A., Beaurepaire, E., and Farge, E. (2008). Tissue deformation modulates twist expression to determine anterior midgut differentiation in Drosophila embryos. Dev. Cell *15*, 470–477.

Dupont, S., Morsut, L., Aragona, M., Enzo, E., Giulitti, S., Cordenonsi, M., Zanconato, F., Le Digabel, J., Forcato, M., Bicciato, S., et al. (2011). Role of YAP/TAZ in mechanotransduction. Nature *474*, 179–183.

Van Eeden, F.J., Granato, M., Schach, U., Brand, M., Furutani-Seiki, M., Haffter, P., Hammerschmidt, M., Heisenberg, C.P., Jiang, Y.J., Kane, D. a, et al. (1996). Genetic analysis of fin formation in the zebrafish, Danio rerio. Development *123*, 255–262.

Green, J., Taylor, J.J., Hindes, A., Johnson, S.L., and Goldsmith, M.I. (2009). A gain of function mutation causing skeletal overgrowth in the rapunzel mutant. Dev. Biol. *334*, 224–234.

Hao, Y., Chun, A., Cheung, K., Rashidi, B., and Yang, X. (2008). Tumor suppressor LATS1 is a negative regulator of oncogene YAP. J. Biol. Chem. *283*, 5496–5509.

Hiemer, S.E., and Varelas, X. (2013). Stem cell regulation by the Hippo pathway. Biochim. Biophys. Acta *1830*, 2323–2334.

Iovine, M.K., and Johnson, S.L. (2000). Genetic analysis of isometric growth control mechanisms in the zebrafish caudal fin. Genetics *155*, 1321–1329.

Ishida, T., Nakajima, T., Kudo, A., and Kawakami, A. (2010). Phosphorylation of Junb family proteins by the Jun N-terminal kinase supports tissue regeneration in zebrafish. Dev. Biol. *340*, 468–479.

Kawakami, A., Fukazawa, T., and Takeda, H. (2004). Early fin primordia of zebrafish larvae regenerate by a similar growth control mechanism with adult regeneration. Dev. Dyn. *231*, 693–699.

Kujawski, S., Lin, W., Kitte, F., Börmel, M., Fuchs, S., Arulmozhivarman, G., Vogt, S., Theil, D., Zhang, Y., and Antos, C.L. (2014). Calcineurin Regulates Coordinated Outgrowth of Zebrafish Regenerating Fins. Dev. Cell 1–15.

Lee, R.T.H., Knapik, E.W., Thiery, J.P., and Carney, T.J. (2013). An exclusively mesodermal origin of fin mesenchyme demonstrates that zebrafish trunk neural crest does not generate ectomesenchyme. Development *140*, 2923–2932.

Lei, Q.-Y., Zhang, H., Zhao, B., Zha, Z.-Y., Bai, F., Pei, X.-H., Zhao, S., Xiong, Y., and Guan, K.-L. (2008). TAZ promotes cell proliferation and epithelial-mesenchymal transition and is inhibited by the hippo pathway. Mol. Cell. Biol. *28*, 2426–2436.

Mateus, R., Pereira, T., Sousa, S., de Lima, J.E., Pascoal, S., Saúde, L., and Jacinto, A. (2012). In vivo cell and tissue dynamics underlying zebrafish fin fold regeneration. PLoS One *7*, e51766.

Mathew, L.K., Sengupta, S., Kawakami, A., Andreasen, E.A., Lohr, C. V, Loynes, C.A., Renshaw, S.A., Peterson, R.T., Tanguay, R.L., and Lo, C. V (2007). Unraveling tissue regeneration pathways using chemical genetics. *282*, 35202–35210.

Mathew, L.K., Sengupta, S., Franzosa, J.A., Perry, J., La Du, J., Andreasen, E.A., and Tanguay, R.L. (2009). Comparative expression profiling reveals an essential role for raldh2 in epimorphic regeneration. J. Biol. Chem. *284*, 33642–33653.

Mercer, S.E., Cheng, C.-H., Atkinson, D.L., Krcmery, J., Guzman, C.E., Kent, D.T., Zukor, K., Marx, K. a, Odelberg, S.J., and Simon, H.-G. (2012). Multi-tissue microarray analysis identifies a molecular signature of regeneration. PLoS One *7*, e52375.

Mo, J.-S., Park, H.W., and Guan, K.-L. (2014). The Hippo signaling pathway in stem cell biology and cancer. EMBO Rep. *15*, 642–656.

Monteiro, J., Aires, R., Becker, J.D., Jacinto, A., Certal, A.C., and Rodríguez-León, J. (2014). V-ATPase Proton Pumping Activity Is Required for Adult Zebrafish Appendage Regeneration. PLoS One *9*, e92594.

Morgan, T.H. (1901). Regeneration.

Nachtrab, G., Kikuchi, K., Tornini, V. a, and Poss, K.D. (2013). Transcriptional components of anteroposterior positional information during zebrafish fin regeneration. Development *3764*, 3754–3764.

Nacu, E., Glausch, M., Le, H.Q., Damanik, F.F.R., Schuez, M., Knapp, D., Khattak, S., Richter, T., and Tanaka, E.M. (2013). Connective tissue cells, but not muscle cells, are involved in establishing the proximo-distal outcome of limb regeneration in the axolotl. Development *140*, 513–518.

Overholtzer, M., Zhang, J., Smolen, G. a, Muir, B., Li, W., Sgroi, D.C., Deng, C.-X., Brugge, J.S., and Haber, D. a (2006). Transforming properties of YAP, a candidate oncogene on the chromosome 11q22 amplicon. Proc. Natl. Acad. Sci. U. S. A. *103*, 12405–12410.

Perathoner, S., Daane, J.M., Henrion, U., Seebohm, G., Higdon, C.W., Johnson, S.L., Nüsslein-Volhard, C., and Harris, M.P. (2014). Bioelectric Signaling Regulates Size in Zebrafish Fins. PLoS Genet. *10*, e1004080.

Pittlik, S., and Begemann, G. (2012). New sources of retinoic acid synthesis revealed by live imaging of an Aldh1a2-GFP reporter fusion protein throughout zebrafish development. Dev. Dyn. *241*, 1205–1216.

Poleo, G., Brown, C.W., Laforest, L., and Akimenko, M. a (2001). Cell proliferation and movement during early fin regeneration in zebrafish. Dev. Dyn. *221*, 380–390.

Pomerantz, J.H., and Blau, H.M. (2013). Tumor suppressors: enhancers or suppressors of regeneration? Development *140*, 2502–2512.

Razzell, W., Evans, I.R., Martin, P., and Wood, W. (2013). Calcium flashes orchestrate the wound inflammatory response through DUOX activation and hydrogen peroxide release. Curr. Biol. *23*, 424–429.

Rusnak, F., and Mertz, P. (2000). Calcineurin: form and function. Physiol. Rev. *80*, 1483–1521.

Schultz, G.S., and Wysocki, A. (2009). Interactions between extracellular matrix and growth factors in wound healing. Wound Repair Regen. *17*, 153–162.

Varelas, X., Samavarchi-tehrani, P., Narimatsu, M., Weiss, A., Cockburn, K., Larsen, B.G., Rossant, J., and Wrana, J.L. (2010). The Crumbs Complex Couples Cell Density Sensing to Hippo-Dependent Control of the TGF-β-SMAD Pathway. Dev. Cell *19*, 831–844.

Vogel, V., and Sheetz, M. (2006). Local force and geometry sensing regulate cell functions. Nat. Rev. Mol. Cell Biol. *7*, 265–275.

White, R., Rose, K., and Zon, L. (2013). Zebrafish cancer: the state of the art and the path forward. Nat. Rev. Cancer *13*, 624–636.

Wong, V.W., Akaishi, S., Longaker, M.T., and Gurtner, G.C. (2011). Pushing back: wound mechanotransduction in repair and regeneration. J. Invest. Dermatol. *131*, 2186–2196.

Yimlamai, D., Christodoulou, C., Galli, G.G., Yanger, K., Pepe-Mooney, B., Gurung, B., Shrestha, K., Cahan, P., Stanger, B.Z., and Camargo, F.D. (2014). Hippo Pathway Activity Influences Liver Cell Fate. Cell *157*, 1324–1338.

Yoo, S.K., Freisinger, C.M., Lebert, D.C., and Huttenlocher, A. (2012). Early redox, Src family kinase, and calcium signaling integrate wound responses and tissue regeneration in zebrafish. J. Cell Biol. *199*, 225–234.

Yoshinari, N., Ishida, T., Kudo, A., and Kawakami, A. (2009). Gene expression and functional analysis of zebrafish larval fin fold regeneration. Dev. Biol. *325*, 71–81.

Zhang, J., Smolen, G. a, and Haber, D. a (2008). Negative regulation of YAP by LATS1 underscores evolutionary conservation of the Drosophila Hippo pathway. Cancer Res. *68*, 2789–2794.

APPENDIXES

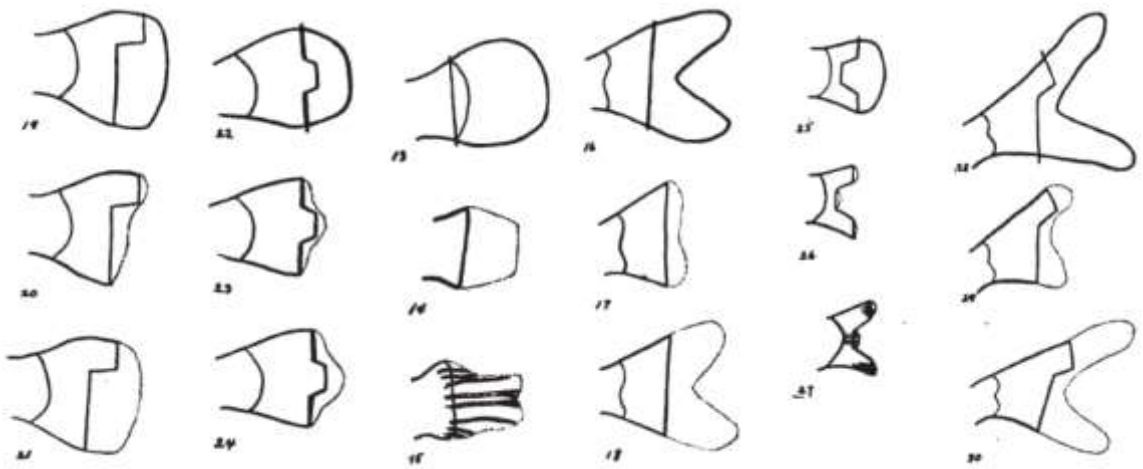

In *THE ROLE OF THE FIN RAYS IN THE REGENERATION IN THE TAIL-FINS OF FISHES*
S.L. Nabrit, 1929

APPENDIX i

Mateus, R *et al.* 2012

OPEN ACCESS Freely available online

PLOS ONE

In Vivo Cell and Tissue Dynamics Underlying Zebrafish Fin Fold Regeneration

Rita Mateus[1,3,4], Telmo Pereira[1,3,4], Sara Sousa[1,2], Joana Esteves de Lima[1], Susana Pascoal[1], Leonor Saúde[1,3], Antonio Jacinto[1,3,4]*

1 Instituto de Medicina Molecular, Faculdade de Medicina de Lisboa, Lisboa, Portugal, **2** PhD Programme in Experimental Biology and Biomedicine (5th PDBEB), Center for Neuroscience and Cell Biology, University of Coimbra, Coimbra, Portugal, **3** Instituto Gulbenkian Ciência, Oeiras, Portugal, **4** Centro de Estudos de Doenças Crónicas, Faculdade de Ciências Médicas, Campo Mártires da Pátria, Lisboa, Portugal

Abstract

Background: Zebrafish (*Danio rerio*) has a remarkable capacity to regenerate many organs and tissues. During larval stages the fin fold allows the possibility of performing long time-lapse imaging making this system very appealing to study the relationships between tissue movements, cell migration and proliferation necessary for the regeneration process.

Results: Through the combined use of transgenic fluorescently-labeled animals and confocal microscopy imaging, we characterized *in vivo* the complete fin fold regeneration process. We show, for the first time, that there is an increase in the global rate of epidermal growth as a response to tissue loss. Also enhanced significantly is cell proliferation, which upon amputation happens in a broad area concerning the amputation level and not in a blastema-restricted way. This reveals a striking difference with regard to the adult fin regeneration system. Finally, an accumulation of migratory, shape-changing fibroblasts occurs proximally to the wound area, resembling a blastemal-like structure, which may act as a signaling center for the regeneration process to proceed.

Conclusions: These findings provide a novel *in vivo* description of fundamental mechanisms occurring during the fin fold regeneration process, thereby contributing to a better knowledge of this regenerative system and to reveal variations in the epimorphic regeneration field.

Citation: Mateus R, Pereira T, Sousa S, de Lima JE, Pascoal S, et al. (2012) *In Vivo* Cell and Tissue Dynamics Underlying Zebrafish Fin Fold Regeneration. PLoS ONE 7(12): e51766. doi:10.1371/journal.pone.0051766

Editor: Carl-Philipp Heisenberg, Institute of Science and Technology Austria, Austria

Received July 31, 2012; **Accepted** November 7, 2012; **Published** December 20, 2012

Funding: RM, TP and SS receive PhD grants from Fundação para a Ciência e Tecnologia (FCT), Portugal. SP receives a post-doctoral grant from FCT. The research presented in this manuscript was partially funded by an European Research Council Starting Grant (2007-StG-208631). The funders had no role in study design; data collection, analysis, and interpretation; decision to publish, or preparation of the manuscript.

Competing Interests: The authors have declared that no competing interests exist.

* E-mail: antonio.jacinto@fcm.unl.pt

Introduction

Most vertebrates, including humans, are unable to regenerate the majority of lost or damaged tissues. In contrast, lower vertebrates such as zebrafish (*Danio rerio*) are able to regenerate many of their organs upon amputation. These animals have the amazing and extremely useful capacity of restoring a fully functional organ, through a process of epimorphic regeneration. This type of regeneration involves a specialized and transient tissue, the blastema, that plays a key role in the signaling and proliferation events that are necessary to recover the lost organ [1]. The blastema is composed of undifferentiated cells that are recruited to the amputation plane [2][3][4][5], and is enclosed by a wound epidermis that also plays a central role in terms of signaling [6][7][8].

The zebrafish has emerged as a powerful model system to perform regeneration studies due to its high regenerative potential coupled to availability of genetic tools. Kawakami *et al* (2004) proposed a new zebrafish-based regeneration system: the early fin primordium (or fin fold) of the 2 days post-fertilization (dpf) larva [9]. This model was established on the basis of its similarities to the adult zebrafish caudal fin system. In particular, the existence of the three regeneration phases (wound healing, blastema formation and regenerative outgrowth), the formation of similar structures upon amputation (i.e. wound epidermis), and a large number of coincident upregulated expression markers [10][11]. In addition, the fin fold model presents some advantages in comparison to the adult model, namely the speed of regeneration, since in the fin fold the full process takes only 72 hours to complete restoration of the lost tissue, and the structural simplicity of this non-vascularized appendage [12] since it is only composed of five layers of tissue. In the larva fin fold, a middle layer of mesenchyme, composed of fibroblast-like cells [13][14], nerves and actinotrichia [15][16], is surrounded by two layers of epidermis containing basal p63-positive keratinocytes, with underlying basement membranes [17][18] (Fig. 1A).

Our goal was to characterize *in vivo* the complete fin fold regeneration process, by using advanced time-lapse confocal imaging of transgenic animals. In particular, we followed the three regeneration stages to unveil how the tissue behaves and recovers after an amputation, in terms of interactions between epidermal layers of tissue and individual migratory mesenchymal cells. Furthermore, we analyzed the orientation of cell division and

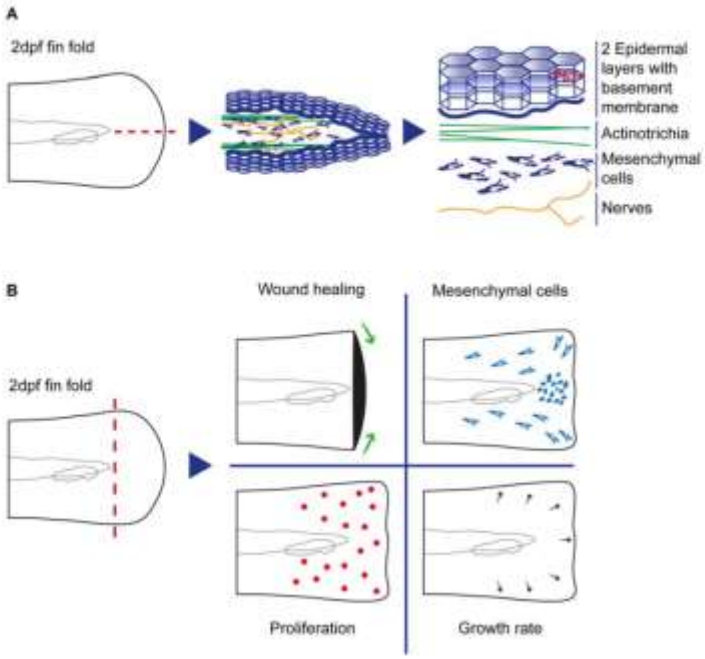

Figure 1. Fin fold organization and regeneration. A Representation of the composition of the 2 dpf fin fold cell types and structures, including their respective organization. **B** Schematic overview representing the main findings occurring after amputation of the 2 dpf larva fin fold, as a part of the regenerative process, addressed throughout the manuscript.
doi:10.1371/journal.pone.0051766.g001

rate of proliferation in a systematic manner. We show that there is an increase in the global rate of epidermal growth as a response to tissue loss that is not directly dependent on local proliferation. Interestingly, proliferation is enhanced upon amputation but happens in a broad area surrounding the amputation level and not in a blastema-restricted way. This reveals a striking difference with regard to the adult system. Additionally, we found that a population of polarized, migratory, shape-changing mesenchymal cells accumulates proximally to the wound area, resembling a blastemal-like structure, which may act as a signaling center for the regenerative process (Process Overview Fig. 1B).

Materials and Methods

Ethics Statement

All experiments involving animals were approved by the Animal User and Ethical Committees at Instituto de Medicina Molecular, according with directives from Direcção Geral Veterinária (PORT 1005/92).

Zebrafish lines, maintenance and surgery

All Zebrafish lines used were maintained in a re-circulating system with a 14 h/day and 10 h/night cycle at 28°C. Embryos were gathered as described in *The Zebrafish Book* and kept in E3 zebrafish embryo medium at 28°C until reaching the desired developmental stage. Both AB and Tuebingen wild-type lines were used. The transgenic lines used for live imaging were: Tg(*β-actin:mGFP*) [19], Tg(*H2a.f/z-GFP*)^{pw48} [20], Tg(*actb1:myl12.1-eGFP*) [21], Tg(*EF1α:mKO2-zCdt1(1/190)*)^{cw0140Tg} [22] and GT(*ctnne-Citrine*)^{ct3a} [23]. These lines were kindly provided by Mathias Koppen, Zirc, Carl-Philipp Heisenberg, Atsushi Miyawaki and Mihaela Zigman, respectively. All fin fold amputations were performed in embryos anaesthetized in 0.1% MS-222 (Sigma) using a scalpel as previously described [9]. Regeneration was then allowed to proceed until defined time points at 28°C.

osteopontin:eGFP transgenic line generation

A bacterial artificial chromosome (BAC) that included the zebrafish *osteopontin* (also known as *spp1*) locus (CH73-213K3, BACPAC Resources Center) was used as a template to amplify a 1295 bp fragment, comprising the 1244 bp sequence upstream of the translational start site and the first 51 bp of the coding sequence. The following set of primers were used for amplification: Fwd 5'CATGATATCTCAGGGCACTACGG3' and Rev 5'TACACAGAAGACTGTGGCGACG3'. The promoter region was cloned in a modified version of pMinitol:MCS [24] that included *βglobin-5'HS4* insulator sequences flanking the transgene [25]. The details on the cloning protocol can be provided upon request. Microinjections to generate the transgenic embryos were performed at one cell-stage of wild-type AB strain, according to standard procedures. The final plasmid was named *pMinitol2.5-osteopontin:eGFP* and 52 ng/μL of DNA was co-injected with

112 ng/µL of capped transposase mRNA and 1% of rhodamine B dextran (10,000 MW, Invitrogen), diluted in 1× Danieau's solution (58 mM NaCl, 0.7 mM KCl, 0.4 mM $MgSO_4$, 5 mM HEPES, 0.6 mM $Ca(NO_3)_2$).

Microinjection of zebrafish embryos

Wild-type AB strain one-cell stage embryos were injected using standard procedures with 100 pg Utrophin-GFP mRNA, produced by linearization of pcs2-utrophin-GFP [26] with NotI (Fermentas), and transcribed using the SP6 mMESSAGE mMACHINE High Yield Capped RNA Transcription Kit (Ambion). A PV-820 Pico-injector (World Precision Instruments) and a Narashige micromanipulator were used for microinjection.

Live imaging

Wound healing time-lapse imaging was performed in 2 dpf injected Utrophin-GFP, *actb1:myl12.1-eGFP* or *cinna-Citrine* transgenic embryos. Animals were amputated 5 minutes prior to imaging. Sequential time-lapse imaging was performed in *β-actin:mGFP* and *H2a.f/z-GFP* 2 dpf, 3 dpf and 4 dpf embryos both in uncut and amputated fin folds at several regeneration stages. In both cases, a Zeiss5Live confocal microscope was used and images were acquired using a 20× dipping objective every minute for wound healing imaging, every 2 minutes for *β-actin:mGFP* experiments, and every 10 minutes for *H2a.f/z-GFP* experiments. Long time-lapse imaging (up to 12 h) and shape monitoring time-lapse imaging (up to 3 h) was performed using 2 dpf double positive embryos from an *osterix:nGFP* and *EF1α:mKO2-zCdt1* cross both in uncut and amputated fin folds. Images were acquired every 5 minutes for long time-lapse and every minute for shape monitoring time-lapse, using a ZeissLSM710 with a 40× oil objective. All *in vivo* imaging was performed in anaesthetized animals with 0.1% MS222 (Sigma) diluted in E3 zebrafish embryo medium.

Immunofluorescence

This protocol was adapted from [27] with the following modifications: embryos were fixed in 4% paraformaldehyde (PFA) (Sigma) at 4°C overnight (o/n), then transferred to 100% Methanol (MeOH) (Merck) and stored at −20°C o/n. Then embryos were rehydrated gradually in series of MeOH/phosphate-buffered saline (PBS) and washed twice for 5 minutes with 1% PBS-TritonX-100, followed by a 7 minute permeabilization with 100% acetone at −20°C. Then the embryos were washed in 0.1% Triton-X100, 1% DMSO (Sigma) and 1% Bovine Serum Albumin (BSA) (Sigma) in PBS (PBDX), followed by a 2 hour blocking in 0.1% Triton-X100, 1% DMSO, 1% BSA and 5% goat serum in PBS. The embryos were incubated in primary antibodies (Anti-GFP rabbit, 1:100, Invitrogen; anti-γ Tubulin mouse, 1:200, Sigma; anti-active Caspase 3 rabbit, 1:400, AbCam) diluted in blocking solution, o/n at 4°C. The embryos were then washed several times in PBDX and incubated in secondary antibodies (1:500, Alexa Fluor 488 anti-rabbit, Alexa Fluor 568 anti-mouse, Invitrogen) and/or with phalloidin (1:200, conjugated with Alexa Fluor 568, Invitrogen) diluted in blocking solution, o/n at 4°C. The next day, embryos were washed several times as previously and DAPI (Sigma) was applied in 0.001 mg/mL of PBS. Embryos were mounted in 80% Glycerol, 2% DABCO (Sigma) diluted in PBS and then imaged using a ZeissLSM710 confocal microscope. In stainings where phalloidin was used, there was no MeOH transfer and there was a direct continuation of the protocol after o/n fixation with PFA.

3D Image processing

To create the 3D images, the original z-stack acquired data was treated using the Imaris software with the *easy 3D* option.

Image analysis and quantification

For all movie analysis, maximum intensity z-stack projections were made using the LSM Image Browser software.

For tissue movement analysis, raw images were registered using the ImageJ plugin StackReg (rigidbody transformation), to correct for non-specific movement. Vector velocity fields were obtained using mpiv toolbox for Matlab (64 pixel window, 0.5 window overlap, 40 pixel window displacement, mqd algorithm, with two recursive checks). Resultant vector fields were filtered (median filter, threshold 2, kriging interpolation) and smoothed (weighting method) to remove stray vectors and homogenize the result respectively. This analysis was performed using three images, equally separated in time (2.5 hours), for each time-lapse movie. To remove erratic vectors which appear outside the fin fold area, images were segmented using the Matlab watershed algorithm (binary conversion threshold = 0) and eroded (disk size = 3 pixels). The obtained segmented mask was used to reveal the real vectors. The three resultant vector fields were averaged point by point to generate vector field images. The average tissue velocity for each movie was obtained by averaging the vector norms. Resultant data was plotted using GraphPad Prism software, and two-tailed Mann-Whitney tests were performed between the several conditions ($p<0.05$). 5 samples were used for each condition.

Proliferation analysis was performed using an ImageJ plugin, ObjectJ. This plugin was used to manually identify: all cytokinesis events, taking into account their orientation, fin fold area and the notochord axis. Resultant data was processed, normalized (area normalization) and corrected (fin fold rotation and translation) in Matlab. Images showing all cell divisions were created using Matlab to project all cell divisions in the correct location relative to the keyframe chosen to represent the movie. Cell division angles were separated into regions according to their location (angle with notochord axis). For each region, angles were divided in 45 degrees intervals, and plotted accordingly. Normalized cell divisions (total numbers) were plotted using GraphPad Prism software, and two-tailed Mann-Whitney tests were performed between the several conditions ($p<0.05$). For each condition the sample number is n = 5.

Mesenchymal cell movies were registered using the ImageJ plugin MultiStackReg (rigidbody transformation), to correct for non-specific movement.

Results

Wound healing is initiated by an abrupt tissue contraction and formation of an actomyosin cable

Upon amputation, the regeneration process is initiated by a wound healing phase. To start the *in vivo* characterization of this process we looked at the dynamics of wound closure upon injury. For that we used live cytoskeleton markers and established a fast time-lapse imaging protocol. In the fin fold, the wound healing is achieved through a rapid contraction of the epidermal tissue through the formation of an actomyosin cable at the leading edge. The accumulation of both actin and myosin is observed as early as 5 minutes post-amputation (minpa), before the main tissue contraction events have happened (Fig. 2A, E, files S1, S2). By 8 minpa the cable is fully formed (Fig. 2B, F arrow) and from this time point until one hour post-amputation (hpa), the tissue contraction exerted by the actomyosin cable appears to be the driving force for the wound to close and to allow the opposite

leading edge cells to connect and seal the hole (Fig. 2A–D and E–H, arrowheads, files S1, S2). After the wound is closed (1 hpa), the cable is no longer detected and the tissue relaxes back to its original shape (1–3 hpa) (file S2). Also present at the wound leading edge cells is the adherens junction component, alpha-catenin, which accumulates in a similar manner to actin and myosin (Fig. 2 I–L, file S3). To confirm that this protein co-localizes with the actomyosin cable, we performed immunohistochemistry in 5 minpa alpha-catenin transgenics and observed that indeed alpha-catenin co-localizes with actin in the cable (file S4). This indicates that the actomyosin cable at the leading edge is a complex structure readily assembled to enable contraction of the tissue and sealing of the open wound.

In order to address if the fin fold regeneration dynamics can be affected by the type of injury and/or size of it, we compared the regenerative ability of fin folds with different amputation planes. We could observe that the dynamics were similar in all cases analyzed, namely: in fin folds that were amputated just distal to the notochord (Regular cut); in fin folds that were amputated at a central position between the notochord and the fin tip (Half-size cut); and in fin folds that were diagonally amputated in the dorsal side (Diagonal cut). In all cases the fins recovered at the same time, even though the fins that suffered a Regular cut had to regenerate more tissue in the same period (file S5). Also there were no differences between different zebrafish wild type strains. Since the regeneration dynamics were similar we opted to do a more thorough analysis of the whole process after using always a Regular cut.

Epidermal tissue growth is increased upon fin fold amputation but maintains its developmental pattern

Following the termination of the wound healing phase, blastema formation takes place and then the fin outgrows. In the zebrafish fin fold, these two last stages are closely interconnected as the fin regenerates in a short period of time. Therefore, we opted to not distinguish between these two phases in very precise time points and instead we considered them as one continuous and progressive process. In order to follow the behavior of epidermal cells, which are the main tissue type that composes the fin fold, we did 5 hour long sequential time-lapse imaging starting at 1 hpa in the fin fold of 2 dpf larvae, using the transgenic *β-actin:mGFP* larvae [19], that labels cell outlines (see Experimental Outline Fig. 3A). We compared the behavior of this tissue upon amputation in 6 time points along the blastema and outgrowth phases with its behavior during normal development in age-matched uncut fins. To quantitatively analyze these data, we performed an image correlation analysis on our images to estimate the velocity fields throughout the fin fold along time. This allowed us not only to see

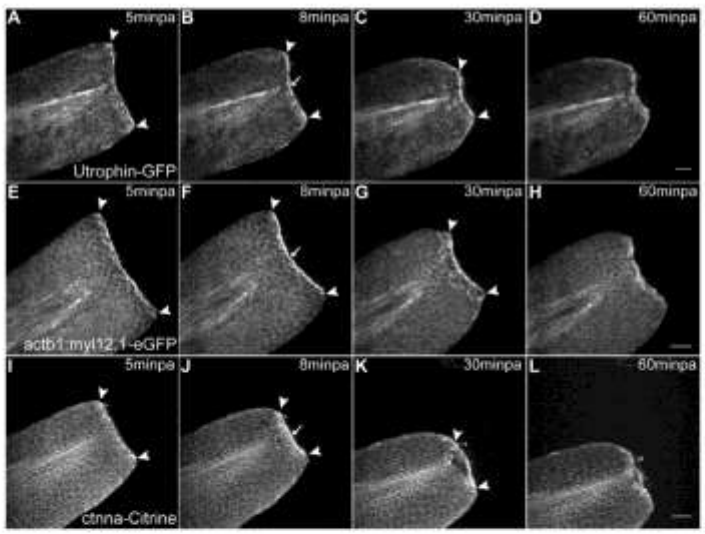

Figure 2. Abrupt tissue contraction and actomyosin cable formation initiate wound healing. A–D Sequential images of a representative *in vivo* 55 min time-lapse movie of an Utrophin-GFP mRNA-injected 2 dpf larva at different time-points after amputation. **A** At 5minpa, there is accumulation of actin at the leading edge cells. **B** By 8 minpa the actin cable is assembled (arrow) and there is tissue contraction - note displacement of arrowheads in comparison with A. **C** At 30 minpa, the tissue has fully contracted. **D** At 60 minpa, the wound inflicted by the amputation is closed. **E–H** Sequential images of a representative *in vivo* 55 min time-lapse movie of a 2 dpf *actb1:myl12.1-eGFP* transgenic larva. **E** At 5minpa, there is accumulation of myosin at the leading edge cells. **F** By 8 minpa the myosin cable is assembled (arrow) and there is tissue contraction - note displacement of arrowheads in comparison with E. **G** At 30 minpa, the tissue has fully contracted. **H** At 60 minpa, the wound inflicted by the amputation is closed. **I–L** Sequential images of a representative *in vivo* 55 min time-lapse movie of a 2 dpf *ctnna-Citrine* transgenic larva at different time-points after amputation. **I** At 5minpa, there is accumulation of alpha-catenin at the leading edge cells. **J** By 8 minpa this accumulation appears to localize to the actomyosin cable (arrow) and there is tissue contraction - note displacement of arrowheads in comparison with I. **K** At 30 minpa, the tissue has fully contracted and alpha-catenin is still localized at the wound edge. **L** At 60 minpa, the wound inflicted by the amputation is closed. Anterior is on the left and scale bars correspond to 50 μm in all images; n = 5 larvae per condition.
doi:10.1371/journal.pone.0051766.g002

the final position and direction of the displacement vectors in the fin fold epidermis, but also to calculate the rate at which the tissue is expanding. Taking this into account, the general pattern of epidermal growth during development of the fin fold in 2 dpf, 3 dpf and 4 dpf zebrafish larvae is characterized as being radial, expanding distally along the anterior-posterior axis and to the fin's sides (Fig. 3B Uncut). During the blastema and outgrowth phases of regeneration, this pattern is maintained (Fig. 3B), but its average velocity is significantly increased with regard to the age-matched uncut controls, mainly in the distal periphery of the epidermal tissue (Fig. 3C Red Areas). This increase in the average speed in a specific direction of epidermal growth is observed throughout most stages of regeneration when compared to the corresponding uncut developmental stages (Fig. 3D). In summary, the fin fold epidermis has a defined pattern of growth that is not influenced by the occurrence of an amputation. Nevertheless, to recover from amputation, the epidermal tissue responds by significantly increasing its growth rate.

Proliferation significantly increases during regeneration in a non-circumscribed area

One of the key characteristics of epimorphic regeneration is the occurrence of a boost of proliferation, precisely restricted in time and space mainly in the blastema [28]. To determine whether the observed increase in the velocity of epidermal growth can be due to an increase in proliferation, we performed our *in vivo* time-lapse assay in uncut and amputated fins (Fig. 3A). In order to detect the nuclei of all cells present in the fin fold, we used the transgenic *H2a.f/z-GFP* [20] and quantified all visible cytokinesis events. We found that during larval development, the proliferation rate was progressively reduced from younger (2 dpf) to older (4 dpf) larvae (Fig. 4A–B Uncut). In amputated animals, we observed no differences in the number of cell divisions in the initial stages after wound healing (1–6 hpa), when compared to the 2 dpf uncut control. On the other hand, by 11–16 hpa the cell proliferation had increased significantly when compared to the uncut control (Fig. 4B). At 21–26 hpa, the proliferation continued to be significantly higher with regard to 3 dpf uncut controls, albeit at lower levels than those recorded at 11–16 hpa. From 21 hpa until the end of the regenerative process the proliferation levels kept decreasing, until reaching the same rate as uncut controls (Fig. 4A–B 4 dpf). These results led us to conclude that during regeneration of the fin fold, proliferation is precisely controlled in time. Regarding spatial restriction, we surprisingly observed that the fin fold tissue responded to the amputation by increasing proliferation in a global manner, instead of being restricted to the most distal portion of the fin fold (Fig. 4A), in clear contrast to what happens during zebrafish adult caudal fin regeneration where proliferation is mainly observed within the blastema region [28][29]. Since proliferation events are many times associated and dependent on apoptosis [30], we performed immunohistochemistry to detect active caspase 3 in uncut and amputated fins throughout the regenerative process and could never find significant levels of apoptosis in both experimental conditions (File S6). In conclusion, the zebrafish fin fold shows a timely control of proliferation upon amputation, but this is not delimited to a region of the fin fold, happening generally throughout the fin.

Cell divisions in the fin fold are stereotypically oriented during normal development and follow a randomization tendency upon amputation

It has been shown that the orientation of cell division is essential during embryonic development and contributes throughout growth and patterning events of several structures as well as during elongation of the embryo [31][23]. Since we observed significant changes in the cell proliferation rate upon amputation, we asked whether the orientation of cell division could contribute to the regeneration of the fin fold. To analyze this, we divided the fin fold in 4 regions by establishing 2 main axes, one parallel along the notochord (anterior-posterior axis) and one just distal to the tip of the notochord, perpendicular to it (dorso-ventral axis) (Fig. 5). This allowed us to have a reference point to measure the angles at which cytokinesis occurs, in a 360 degree scale. In 2 dpf uncut control larvae, in regions 1 and 4, which are laterally located to the notochord, 78% and 67% of all cell divisions observed occurred in the anterior-posterior (A-P) axis, respectively (Fig. 5A). These had a predominant angle of cytokinesis occurring mainly in the intervals of 315–45 degrees and 135–225 degrees (Fig. 5A and file S6). Hence the major direction of growth in these regions is parallel to the notochord, which likely contributes to the elongation of the body axis (Fig. 5A'). Regarding regions 2 and 3, distally located to the notochord, 57% and 74% of the cell divisions occurred in the dorso-ventral (D-V) axis respectively, since they had a predominant angle of cytokinesis in the interval of 225–315 degrees and 45–135 degrees (Fig. 5A). This pattern of growth likely allows the fin fold to expand to its sides (Fig. 5A'). These results are in accordance with the pattern of growth obtained in our vector velocity field analysis (Fig. 3B) and led us to conclude that the cell divisions in the zebrafish fin fold are stereotypically oriented during its development. A more detailed analysis using 45 degree angle intervals led to the same conclusions (file S7).

Upon amputation, no statistically significant differences were observed in any of the analyzed regions when compared to uncut controls. Cell divisions happening in regions 1 and 4 kept the same behavior as in uncut controls, preserving the stereotypical orientations (Fig. 5B–C; B'–C'; Regions 1 and 4); nevertheless, we verified a slight increase in the percentage of cell divisions in the A-P axis in regions 2 and 3 when compared to the same regions in uncut controls, both in the first regeneration time point (Fig. 5B) as well as in the proliferation peak time point (Fig. 5C). Thus, there seems to be a tendency for randomization of the angles of cell division during these regeneration stages (Fig. 5B'–C'). During later stages of regeneration, we could not establish this analysis due to low cell division numbers. In summary, we conclude that changes in the pattern of cell division orientation do not seem to be a major determinant of fin growth during regeneration.

Mesenchymal cells alter their shape and migrate distally upon amputation

Besides the epidermis, the fin fold is composed of mesenchymal cells. It has been suggested that these cells give rise to the blastema upon amputation, like in the adult fin system [32], although to our knowledge there is no detailed *in vivo* characterization of these cells during regeneration of the fin fold. These mesenchymal cells are fibroblast-like with a very particular shape, being very elongated with extended protrusions and stretched nuclei [13][16]. It is also known that they are migratory, and play a role in providing stabilization and structure to the fin fold by secreting actinotrichia [13][16][14]. To understand the function of these cells during regeneration, we used a transgenic that expresses GFP driven by the *osteopontin* promoter. This transgenic labels numerous structures in the zebrafish, including the mesenchymal cells in the fin fold (file S8). To follow and track the migration of these cells, we performed time-lapse imaging (up to 12 hour long) of double positive larvae for *osteopontin:GFP* and for the cell cycle nuclear

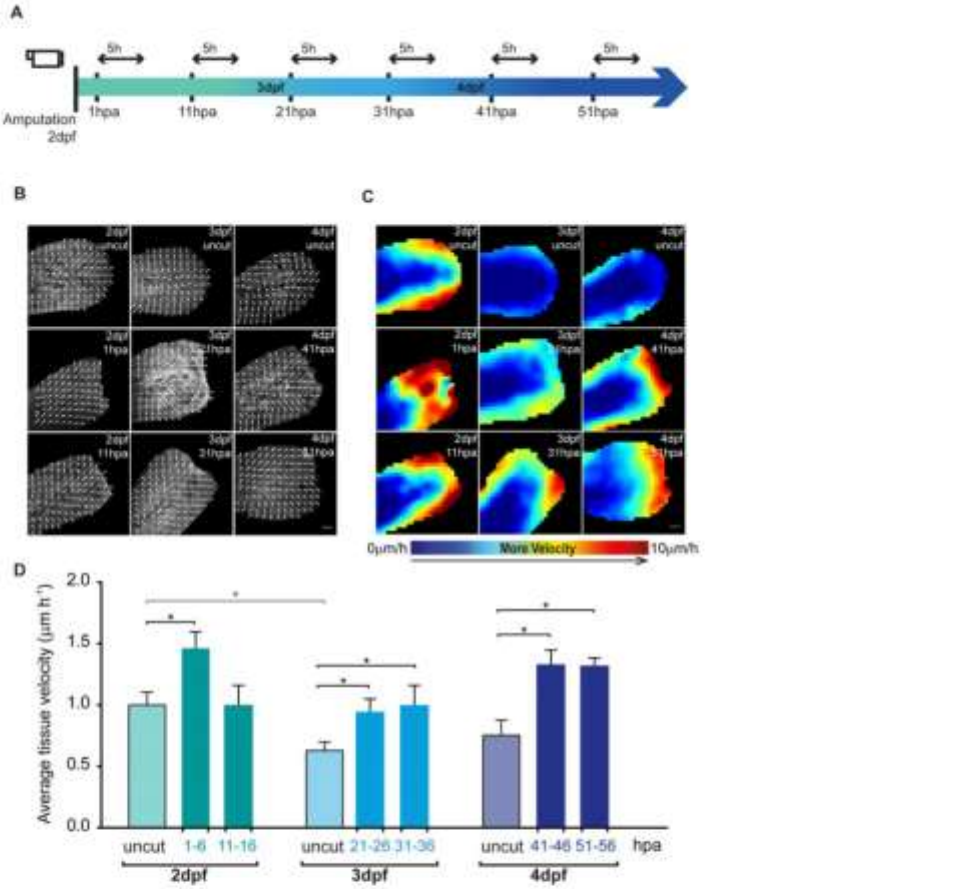

Figure 3. Epidermal tissue growth is enhanced upon fin fold amputation. A Experimental outline of the live imaging procedures taking into account not only the post amputation hours (hpa) but also the developmental days of the larvae (dpf). All the amputations were performed in 2 dpf larvae, and these were allowed to regenerate until the desired hour, the time point at which they were imaged for 5 hours. Taking into account that the regeneration procedure takes several days, age-matched uncut controls were imaged in the same conditions and for the same amount of time for accurate comparison. **B** Representative maps of vector velocity fields (VVFs) depicting the tissue movement direction along 5 h sequential time-lapse imaging of the fin fold regenerative process and respective age-matched uncut controls of *β-actin:mGFP* transgenics. **C** Representative heat maps of the VVFs shown in B depicting the tissue velocity in the fin fold area along the same 5 h sequential blocks of the fin fold regenerative process and respective age-matched uncut controls. Red end of the spectrum correlates with higher velocity (0 to 10 μm.hour^{-1}) within a given experiment. **D** Average velocity (μm.hour^{-1}) of VVFs of 5 larvae per condition represented in B–C. Color code matches the Experimental Outline in A. *P value<0.05; Mann-Whitney test values: 2 dpf uncut<>3 dpf uncut = 0.03; 2 dpf uncut<>1–6 hpa = 0.03; 3 dpf uncut<>21–26 hpa = 0.03; 3 dpf uncut<>31–36 hpa = 0.03; 4 dpf uncut<>41–46 hpa = 0.03; 4 dpf uncut<>51–56 hpa = 0.02; 5 larvae per condition. Anterior is on the left and scale bars correspond to 50 μm.

doi:10.1371/journal.pone.0051766.g003

marker *EF1a:mKO2-zCdt1* (see Methods). We found that during development at 2 dpf, the *osteopontin*-positive mesenchymal cells do not appear to migrate (Fig. 6A–C, file S9). However, upon amputation, as early as 30 minpa, a fraction of the mesenchymal cells actively migrated towards the injury (Fig. 6D–F, file S10). The migrating cells were originally located radially around the notochord, in the center of the fin fold. In addition to migrating, these cells lost their original elongated shape and acquired a more rounded form (Fig. 6D–F, Zoom panels, white dots), accumulating distally to the notochord in a blastemal-like zone. Of note, the *osteopontin-eGFP* positive mesenchymal cells always maintained the *mKO2-zCdt1* labeling during the *in vivo* imaging (Fig. 6) and throughout the next regenerating days (file S11). The protein zCdt1 is a marker for the G0-G1 phase of the cell cycle [22],

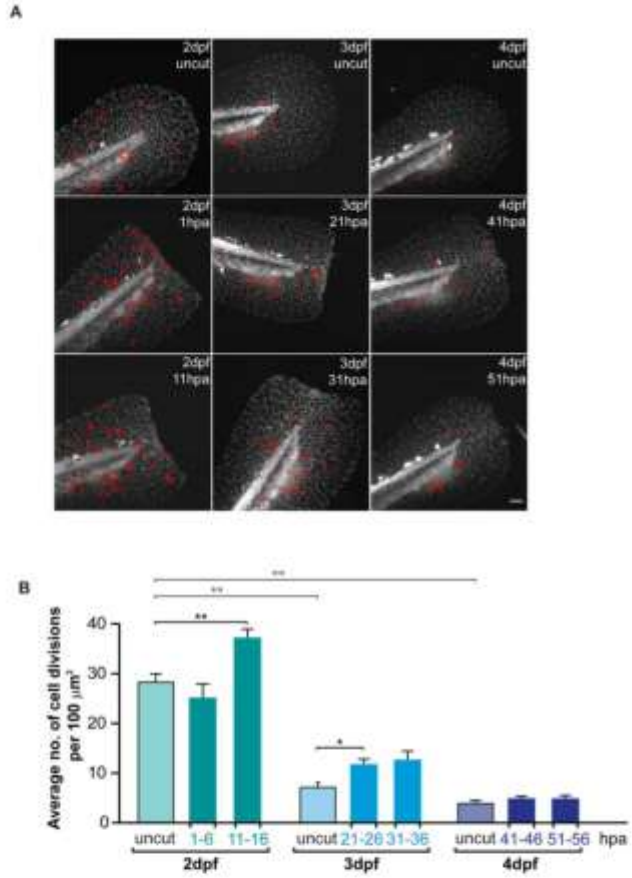

Figure 4. Global levels of proliferation significantly increase during regeneration in a non-spatially restricted manner. A Representative projections of *H2a.f/z-GFP* transgenics showing total cell divisions (marked in red) which occurred during 5 hour sequential time-lapse imaging movies of the fin fold regenerative process and respective age-matched uncut controls. **B** Average number of cell divisions occurring per 100 μm^2 in the several conditions represented in A. Color code matches the Experimental Outline in Fig. 3A. **P value<0.01, *P value<0.05; Mann-Whitney test values: 2 dpf uncut<>3 dpf uncut = 0.008; 2 dpf uncut<>4 dpf uncut = 0.008; 2 dpf uncut<>11–16 hpa = 0.008; 3 dpf uncut<>21–26 hpa = 0.02; 3 dpf uncut<>31–36 hpa = 0.06; 5 larvae per condition. Anterior is on the left and scale bars correspond to 50 μm.
doi:10.1371/journal.pone.0051766.g004

therefore our results indicate that these cells are kept in this phase of the cell cycle, even upon amputation. These data allow us to conclude that the observed changes in cell shape are not directly linked to cell proliferation.

To characterize further the spatiotemporal dynamics leading to small morphology changes in the mesenchymal cells at a single cell level, we performed faster and shorter (up to 3 h with acquisition every minute) time-lapse imaging of the same transgenic *EF1a:mKO2-zCdt1(cell cycle substrate):GFP*, starting at 5 minutes after amputation. In fact, by monitoring the mesenchymal cells in this manner we could detect the initial loss of elongation and rounding up of these cells as early as 35 minpa, and until 1h35 minpa this was a progressive change of morphology (Fig. 6G–J Zoom panels, white dots). These changes happened at the same time as the wound healing process was still taking place, indicating a quick reaction of the mesenchymal cells upon amputation and coincided with the onset of distal migration of these cells. To clarify further the correlation between the migration and the change of cell shape of the mesenchymal cells, we accessed their polarization state. In migrating mesenchymal cells, centrosomes typically assume a position between the leading edge and the nucleus [33][34]. To address this in our system, we compared the location of the centrosome/microtubule organizing center (MTOC) relative to the cell nucleus [34], by performing gamma-tubulin (γTubulin)

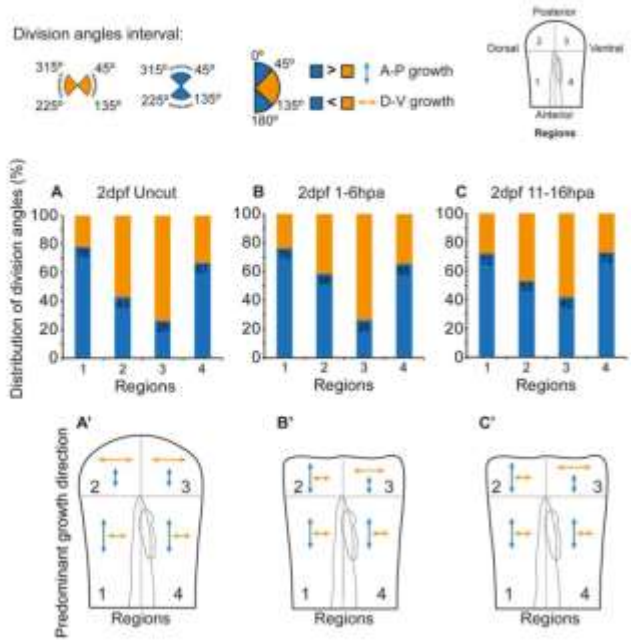

Figure 5. Cell division orientation in the fin fold shows a tendency for randomization predisposition upon amputation. Distribution of division angles according to the interval of 225–315° and 45–135° (orange) or 315–45° and 135–225° (blue) in the designated regions 1–4 of the fin fold in **A** 2 dpf uncut control **B** 2 dpf 1–6 hpa **C** 2 dpf 11–16 hpa. Predominant growth direction in the regions 1–4 taking into account the orientation of the majority of cell divisions happening in **A'** 2 dpf uncut control **B'** 2 dpf 1–6 hpa **C'** 2 dpf 11–16 hpa. n = 193 divisions in 2 dpf uncut, n = 175 divisions in 2 dpf 1–6 hpa, n = 258 divisions in 2 dpf 11–16 hpa; 5 larvae per condition.
doi:10.1371/journal.pone.0051766.g005

immunohistochemistry in *osteopontin:GFP* transgenic animals. We found that in 2 dpf uncut fin folds, the *osteopontin* positive mesenchymal cells had their MTOCs positioned between the nucleus and the stretched protrusions, and in many of these cells, the distance between the MTOC and the nucleus was remarkable (File S12, A–A' Uncut). Upon amputation, during the cell shape change and active migration time-points (1 hpa), the MTOC position was maintained between the nucleus and leading edge of the cells, but in close proximity to the nucleus, indicating that these cells did not lose their polarization state during these events (File S12, B–B' 1 hpa). By 1 day post-amputation (dpa), when the distal migration and change of shape events are completely concluded, the MTOC position was variable (File S12, C–C' 1 dpa); in some cells the MTOC was positioned still between the nucleus and leading edge while in others the MTOC assumed a position in the rear of the cell. This indicates that the polarization of mesenchymal cells can be lost after the complete accumulation in the blastemal-like zone.

To address whether the cell shape changes in mesenchymal cells would continue throughout the rest of the regenerative process, we did immunohistochemistry in the *osteopontin:GFP* transgenic fish. We confirmed that at 1 and 2 dpa, groups of mesenchymal cells had accumulated near the amputation plane and had become rounder both in terms of cytoplasm and nucleus, when compared with uncut controls (Fig. 7A–D *osteopontin:GFP* and Dapi). In addition, the cortical actin present in the regenerating fin fold had developed a complex meshwork in the round cells (Fig. 7B,D Actin). Both of these features were undetected at 3 dpa and cell shapes resembled the uncut control, indicating that these events were specific to the regeneration process (Fig. 7E–F).

Discussion

In this work we have systematically characterized the fin fold regeneration process through *in vivo* studies. We analyzed the wound closure dynamics, the contributions of epidermal growth, proliferation levels and orientation of cell divisions necessary to achieve a functional and proper sized fin fold. Also, we have explored the role of mesenchymal cells in this process.

Our findings show that during zebrafish fin fold regeneration there is an actomyosin based mechanism used for wound closure, which seems to be conserved in many other organisms [35][36][37]. This process is extremely rapid and involves major tissue contraction and relaxation. Importantly, the co-localization of the adherens junctions component alpha-catenin with the actomyosin cable raises interesting questions about the complexity and function of this essential structure. This is in accordance with the presence of another adherens junctions marker, beta-catenin, at the leading edge cells during wound healing of the zebrafish fin fold [11].

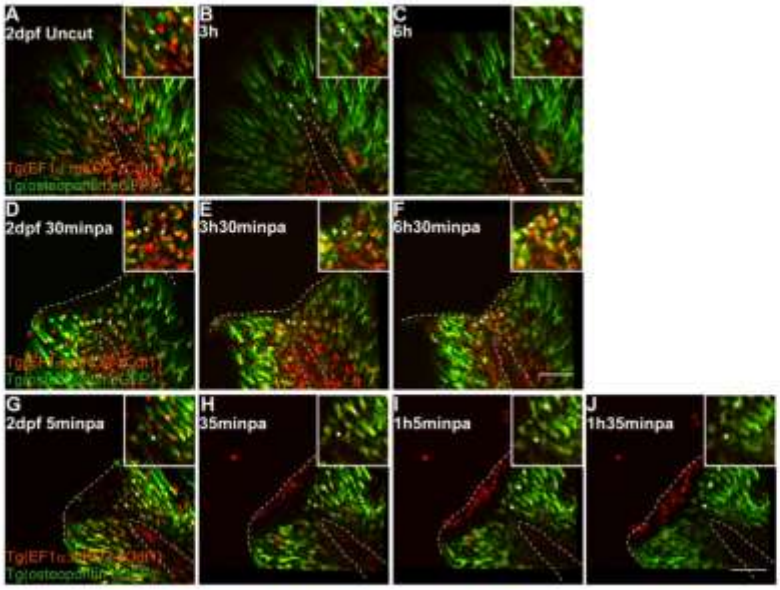

Figure 6. Mesenchymal cells in the fin fold change shape and migrate distally upon injury. A–C Sequential images of a representative *in vivo* 6 h time-lapse movie of a 2 dpf uncut *EF1α:mKO2-zCdt1;osteopontin:eGFP* transgenic larva. **D–F** Sequential images of a representative *in vivo* 6 h time-lapse movie of a 2 dpf 30 minpa *EF1α:mKO2-zCdt1;osteopontin:eGFP* transgenic larva. **G–J** Sequential images of a representative *in vivo* 1h30 time-lapse movie of a 2 dpf 5 minpa *EF1α:mKO2-zCdt1;osteopontin:eGFP* transgenic larva. Zoom panels highlight *osteopontin* positive mesenchymal cells in the central area of the fin fold in the respective time point. White dots mark the same cells along time to allow for better visualization and tracking of cell migration. Dashed lines indicate the outline of the notochord and the edge of the amputated fin fold. Scale bars correspond to 50 μm in all images; 3–5 larvae per condition.
doi:10.1371/journal.pone.0051766.g006

During fin development, the epidermis has a precise pattern of movement and growth that is maintained in the blastema and outgrowth phases of regeneration. On the other hand, during regeneration, the growth rate is significantly increased in all time points apart from 11–16 hpa, to recover the fin's original shape and size in a timely manner. Interestingly, there is a significant increase in proliferation in response to the amputation, which happens precisely at 11–16 hpa. This indicates that, like in the adult caudal fin regeneration system, the proliferation is controlled in time [28]. However, in contrast to the adult system, this increase in proliferation does not seem to be spatially restricted [28][29]. In fact, during the proliferation peak, we noticed cytokinesis events happening in a broad area of the fin fold, and not only in the most distal tissue. It appears that the fin fold blastema does not have a specific function for proliferation and in that way it is not a classical blastema, as observed in the adult system.

Previous reports have shown that proliferation of blastema-like cells increases upon amputation of the larval fin fold, however, the authors suggested that such proliferation is spatially restricted [9][10][11]. This work was based on BrdU pulse-chase experiments where cells were labeled at different time points after amputation and their position within the fin fold accessed at the end of the regeneration process. In contrast our data shows that in the first hours after amputation the number of cell divisions increases but not in a preferential region of the fin. We propose that this discrepancy might be due to the distinct methods used to determine proliferation in the two studies. We believe that our characterization of the full process *in vivo* clearly reveals a global proliferation response, a property that appears to be specific of fin fold regeneration.

When comparing the epidermal growth and proliferation events, we observed that the tissue growth rate seems to increase with time during the regeneration process at the same time as proliferation slows down (compare Fig. 3D and 4B), implying that tissue growth is compensated by a mechanism that does not depend on proliferation. The only time point at which the velocity of epidermal growth is not significantly increased is when the proliferation is at its peak (between 11 and 16 hpa), suggesting that there are other outgrowth mechanisms that contribute crucially to this process.

We show, for the first time, that the mesenchymal cells present in the fin fold react to amputation by migrating and accumulating distally. This is accompanied by a change of cell shape and an increase in the complexity of the cortical network of actin that is assembled in these cells. In fact, previous reports addressing these cells during fin fold regeneration, show that there is an increase in the condensation of their nuclei [9]. This is in accordance with our cell shape change results, where we found a clear transformation of the mesenchymal cells typical shape into a more round form, including in their nuclear shape. This alteration in shape could be due to these cells entering an active cell cycle process, initiating cell division; however this does not seem to be the case, since the

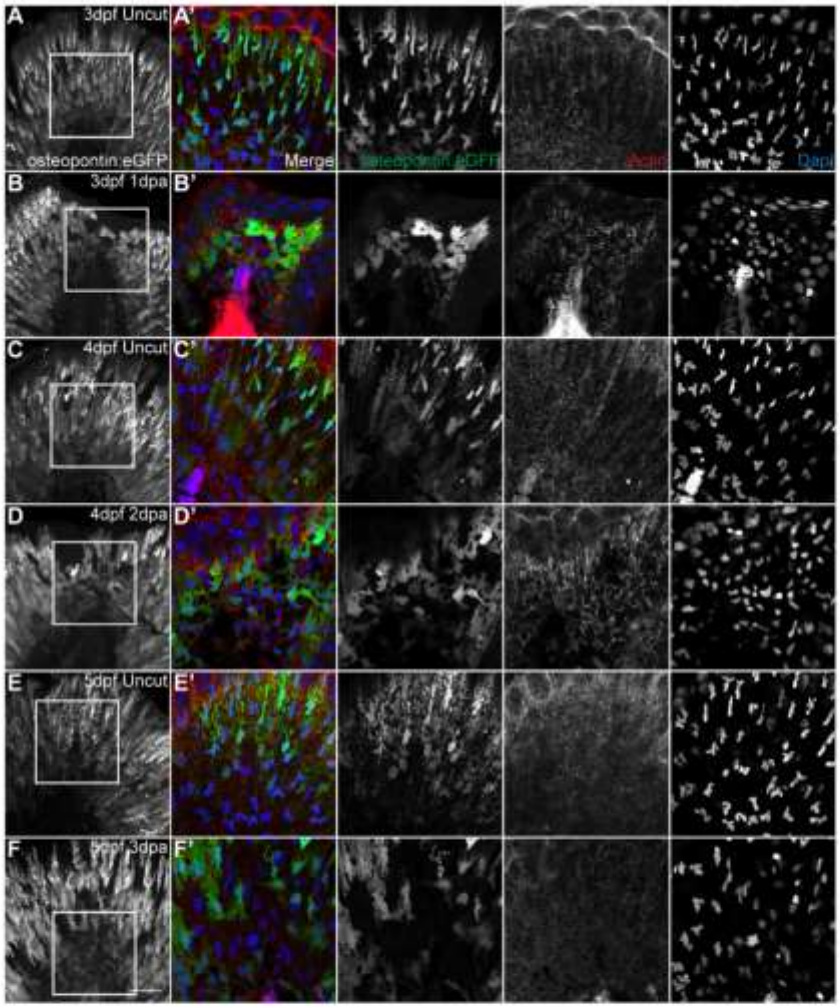

Figure 7. The shape modification of mesenchymal cells lasts throughout and is specific of regeneration. A,C,E Representative immunostaining with anti-GFP antibody in uncut transgenic *osteopontin:eGFP* larvae of 3 dpf, 4 dpf and 5 dpf respectively. **B,D,F** Representative immunostaining with anti-GFP antibody in amputated transgenic *osteopontin:eGFP* larvae of 3 dpf 1 dpa, 4 dpf 2 dpa and 5 dpf 3 dpa respectively. **A–F** Representative z-stack projections of the *osteopontin:eGFP* labeling. **A'–F'** Representative single frames of the corresponding zoomed area represented by a square in A–F. Merged and single color images of *osteopontin:eGFP* labeling the mesenchymal cells (anti-GFP, green), actin (phalloidin, red) and nuclei (DAPI, blue), respectively. 5 Larvae per condition. Scale bar corresponds to 50 µm in all images.
doi:10.1371/journal.pone.0051766.g007

mesenchymal cells remain in the G0–G1 phase of the cell cycle throughout the full regeneration process. It is also possible that this change in morphology is part of a dedifferentiation process triggered by the amputation, as in the adult caudal fin model where these cells acquire a round form and migrate distally to constitute the blastema [4][5]; nevertheless the differentiation state of the fin fold mesenchymal cells is still uncharacterized. There are indications that during the fin fold development, these cells acquire progressively their protrusive morphology, suggesting that this is consistent with a more differentiated status [13][14]; if that is the case, then the mesenchymal cells may be undergoing dedifferentiation during the fin fold's regenerative process. The function of

these cells in the regeneration process is still unclear, but it is possible that they are part of a signaling center [10][12][38], and to that extent, constitute the so-called blastema in a comparable manner to the adult system.

Conclusions

Altogether this study presents a global view and a better understanding of how the regenerative process is accomplished in the larvae fin fold. We performed a systematic analysis of the regenerative response of the main cell types present in this structure and characterized in detail several mechanisms by which the fin regenerates. With this work we show for the first time the *in vivo* dynamics of wound closure during the initial phases of the regeneration process; we illustrate the existence of a developmental pattern of growth of the fin fold, which is maintained upon amputation, albeit with a significantly increased rate of growth; we demonstrate that the cell proliferation response to damage in epidermal cells occurs in a broad region away from the wound, and lastly, we show that the mesenchymal cells are highly polarized and undergo dramatic cell shape changes during the regeneration process. These findings provide novel insight into the *in vivo* mechanisms occurring during the fin fold regeneration process, contributing to a better knowledge of this regenerative system and making it a valuable model to investigate further questions in the regeneration field.

Supporting Information

File S1 Wound healing process of 2 dpf Utrophin-GFP injected fish. 1 hour movie of a 2 dpf 5 minpa larva. Anterior is to the left. Scale bar corresponds to 50 µm.
(MOV)

File S2 Wound healing process of 2 dpf *actb1:myl12.1-eGFP* transgenic fish. 3 hours movie of a 2 dpf 5 minpa larva. Anterior is to the left. Scale bar corresponds to 50 µm.
(MOV)

File S3 Wound healing process of 2 dpf *Alpha-Catenin-Citrine* transgenic fish. 1 hour movie of a 2 dpf 5 minpa larva. Anterior is to the left. Scale bar corresponds to 50 µm.
(MOV)

File S4 Alpha-Catenin is present in the actin cable during wound healing. 3D reconstruction of a representative immunostaining against anti-GFP antibody to detect alpha-catenin (green) and phalloidin to detect actin (red) in 2 dpf 5 minpa *alpha-catenin-Citrine* (*ctnna-Citrine*) transgenic larva. n = 5 larvae.
(MOV)

File S5 The fin fold regeneration dynamics are independent of the size of amputation. Representative brightfield live images of AB (**A–L**) and TU (**M–X**) larvae during several stages of the regenerative process and their respective age-matched uncut controls. Larvae were subjected to different amputation planes (Regular, Half-size and Diagonal cuts) and followed throughout the next 3 regenerating days, time point in which the regenerative ability was accessed. 5 Larvae per condition.
(TIF)

File S6 Apoptosis is not present during fin fold regeneration. Representative immunofluorescence with anti-active Caspase3 antibody in uncut and amputated larvae of 3 dpf (**A–B**), 4 dpf (**C–D**) and 5 dpf (**E–F**). Arrow indicates the presence of an apoptotic cell. n = 5 larvae per condition. Scale bar corresponds to 50 µm in all images.
(TIF)

File S7 Detailed distribution of cell division angles in the 4 regions of the fin fold.
(TIF)

File S8 Expression pattern of the 2 dpf transgenic *osteopontin:eGFP*. At this stage of development, this transgenic has labeled the fin fold mesenchymal cells, but also other mesenchymal cells that are spread out along the midline and somites. Besides these, the pectoral fin, the eye and the brain are also GFP positive.
(TIF)

File S9 2 dpf Uncut control double transgenic *EF1α:mKO2-zCdt1;osteopontin:eGFP*. 6 hours movie of an uncut 2 dpf larva. Scale bar corresponds to 50 µm.
(MOV)

File S10 2 dpf 30 minpa double transgenic *EF1α:mKO2-zCdt1;osteopontin:eGFP*. 6 hours movie of a 2 dpf larva 30 minpa. Scale bar corresponds to 50 µm.
(MOV)

File S11 The mesenchymal cells are maintained in G0-G1 phases of the cell cycle regardless of an amputation. Live imaging representative images of double transgenic *EF1α:mKO2-zCdt1;osteopontin:GFP* larvae during several stages of the regenerative process and their respective controls. **A,C,E** are uncut (3 dpf, 4 dpf and 5 dpf respectively) and age matched controls for **B,D,F** (3 dpf 1 dpa, 4 dpf 2 dpa, 5 dpf 3 dpa respectively). Merged and single color images corresponding to *osteopontin:GFP* labeling the cytoplasm of the mesenchymal cells (green) and *mKO2-zCdt1* labeling the nuclei of fin fold cells in G0–G1 phases of the cell cycle (red). 3 larvae per condition. Scale bar corresponds to 50 µm.
(TIF)

File S12 The mesenchymal cells are polarized. A Representative immunostaining with anti-GFP and anti-γTubulin antibodies in 2 dpf uncut transgenic *osteopontin:eGFP* larvae (single frame). **B–C** Representative immunostaining with anti-GFP anti-γTubulin antibodies in amputated transgenic *osteopontin:eGFP* larvae of 2 dpf 1 hpa and 3 dpf 1 dpa (single frames). **A'–C'** Representative single frames of the corresponding zoomed area represented by a square in A–C. Merged and single color images of the MTOC (γTubulin, red) together with the nuclei (DAPI, blue) and *osteopontin:eGFP* labeling the mesenchymal cells (anti-GFP, green), respectively. The arrows highlight the presence of a MTOC to allow better comparison of its position relative to the corresponding nucleus. 5 Larvae per condition. Scale bar corresponds to 50 µm in all images.
(TIF)

Acknowledgments

The authors thank the Fish Facility technicians Lara M. Carvalho, Fábio Valério and Aida Barros for support with animal care. We thank Lara C. J. Carvalho, Duarte Mesquita, Anabela Bensimon-Brito and Ana Sofia Azevedo for reading the manuscript and for insightful discussions and Inês Crisóstomo for help with Imaris Software. We also thank Susana Lopes for reagents.

Author Contributions

Conceived and designed the experiments: RM JEL SP LS AJ. Performed the experiments: RM SS JEL. Analyzed the data: RM TP LS AJ. Contributed reagents/materials/analysis tools: RM TP SS. Wrote the paper: RM AJ.

References

1. Morgan TH (1901) REGENERATION AND LIABILITY TO INJURY. Science (New York, NY) 14: 235–248.
2. Echeverri K, Clarke JD, Tanaka EM (2001) In vivo imaging indicates muscle fiber dedifferentiation is a major contributor to the regenerating tail blastema. Developmental Biology 236: 151–164.
3. Kragl M, Knapp D, Nacu E, Khattak S, Maden M, et al. (2009) Cells keep a memory of their tissue origin during axolotl limb regeneration. Nature 460: 60–65.
4. Knopf F, Hammond C, Chekuru A, Kurth T, Hans S, et al. (2011) Bone Regenerates via Dedifferentiation of Osteoblasts in the Zebrafish Fin. Developmental Cell 20: 713–724.
5. Sousa S, Afonso N, Bensimon-Brito A, Fonseca M, Simões M, et al. (2011) Differentiated skeletal cells contribute to blastema formation during zebrafish fin regeneration. Development (Cambridge, England) 138: 3897–3905.
6. Lee Y, Hami D, De Val S, Kagermeier-Schenk B, Wills AA, et al. (2009) Maintenance of blastemal proliferation by functionally diverse epidermis in regenerating zebrafish fins. Developmental Biology 331: 270–280.
7. Campbell LJ, Suárez-Castillo EC, Ortiz-Zuazaga H, Knapp D, Tanaka EM, et al. (2011) Gene expression profile of the regeneration epithelium during axolotl limb regeneration. Developmental Dynamics 240: 1826–1840.
8. Campbell LJ, Crews CM (2008) Wound epidermis formation and function in urodele amphibian limb regeneration. Cellular and Molecular Life Sciences 65: 73–79.
9. Kawakami A, Fukazawa T, Takeda H (2004) Early fin primordia of zebrafish larvae regenerate by a similar growth control mechanism with adult regeneration. Developmental Dynamics 231: 693–699.
10. Yoshinari N, Ishida T, Kudo A, Kawakami A (2009) Gene expression and functional analysis of zebrafish larval fin fold regeneration. Developmental Biology 325: 71–81.
11. Ishida T, Nakajima T, Kudo A, Kawakami A (2010) Phosphorylation of Junb family proteins by the Jun N-terminal kinase supports tissue regeneration in zebrafish. Developmental Biology 340: 1–12.
12. Mathew LK, Sengupta S, Franzosa JA, Perry J, La Du J, et al. (2009) Comparative expression profiling reveals an essential role for raldh2 in epimorphic regeneration. The Journal of Biological Chemistry 284: 33642–33653.
13. Wood A (1984) An analysis of in vivo cell migration during teleost fin morphogenesis. Journal of Cell Science 222: 205–222.
14. Feitosa NM, Zhang J, Carney TJ, Metzger M, Korzh V, et al. (2012) Hemicentin 2 and Fibulin 1 are required for epidermal-dermal junction formation and fin mesenchymal cell migration during zebrafish development. Developmental Biology 369: 235–248.
15. Durán I, Marí-Beffa M, Santamaría J a, Becerra J, Santos-Ruiz L (2011) Actinotrichia collagens and their role in fin formation. Developmental Biology 354: 160–172.
16. Zhang J, Wagh P, Guay D, Sanchez-Pulido L, Padhi BK, et al. (2010) Loss of fish actinotrichia proteins and the fin-to-limb transition. Nature: 1–5.
17. Slanchev K, Carney TJ, Stemmler MP, Koschorz B, Amsterdam A, et al. (2009) The epithelial cell adhesion molecule EpCAM is required for epithelial morphogenesis and integrity during zebrafish epiboly and skin development. PLoS Genetics 5: e1000563.
18. Dane PJ, Tucker JB (1985) Modulation of epidermal cell shaping and extracellular matrix during caudal fin morphogenesis in the zebra fish Brachydanio rerio. Journal of Embryology and Experimental Morphology 87: 145–161.
19. Cooper MS, Szeto DP, Sommers-Herivel G, Topczewski J, Solnica-Krezel L, et al. (2005) Visualizing morphogenesis in transgenic zebrafish embryos using BODIPY TR methyl ester dye as a vital counterstain for GFP. Developmental Dynamics 232: 359–368.
20. Pauls S, Geldmacher-Voss B, Campos-Ortega J a (2001) A zebrafish histone variant H2A.F/Z and a transgenic H2A.F/Z:GFP fusion protein for in vivo studies of embryonic development. Development Genes and Evolution 211: 603–610.
21. Behrndt M, Salbreux G, Campinho P, Hauschild R, Oswald F, et al. (2012) Forces driving epithelial spreading in zebrafish gastrulation. Science (New York, NY) 338: 257–260.
22. Sugiyama M, Sakaue-Sawano A, Iimura T, Fukami K, Kitaguchi T, et al. (2009) Illuminating cell-cycle progression in the developing zebrafish embryo. Proceedings of the National Academy of Sciences of the United States of America 106: 20812–20817.
23. Žigman M, Trinh L a, Fraser SE, Moens CB, Zigman M (2010) Zebrafish neural tube morphogenesis requires Scribble-dependent oriented cell divisions. Current Biology 21: 79–86.
24. Balciunas D, Wangensteen KJ, Wilber A, Bell J, Geurts A, et al. (2006) Harnessing a high cargo-capacity transposon for genetic applications in vertebrates. PLoS Genetics 2: e169.
25. Bessa J, Tena JJ, de la Calle-Mustienes E, Fernández-Miñán A, Naranjo S, et al. (2009) Zebrafish enhancer detection (ZED) vector: a new tool to facilitate transgenesis and the functional analysis of cis-regulatory regions in zebrafish. Developmental Dynamics 238: 2409–2417.
26. Burkel BM, von Dassow G, Bement WM (2007) Versatile fluorescent probes for actin filaments based on the actin-binding domain of utrophin. Cell Motility and the Cytoskeleton 64: 822–832.
27. Neugebauer JM, Amack JD, Peterson AG, Bisgrove BW, Yost HJ (2009) FGF signalling during embryo development regulates cilia length in diverse epithelia. Nature 458: 651–654.
28. Nechiporuk A, Keating MT (2002) A proliferation gradient between proximal and msxb-expressing distal blastema directs zebrafish fin regeneration. Development 129: 2607–2617.
29. Santos-Ruiz L, Santamaría JA, Ruiz-Sánchez J, Becerra J (2002) Cell proliferation during blastema formation in the regenerating teleost fin. Developmental Dynamics 223: 262–272.
30. Chera S, Ghila L, Dobretz K, Wenger Y, Bauer C, et al. (2009) Apoptotic cells provide an unexpected source of Wnt3 signaling to drive hydra head regeneration. Developmental Cell 17: 279–289.
31. Quesada-Hernández E, Caneparo L, Schneider S, Winkler S, Liebling M, et al. (2010) Stereotypical cell division orientation controls neural rod midline formation in zebrafish. Current Biology 20: 1966–1972.
32. Kawakami A (2010) Stem cell system in tissue regeneration in fish. Development, Growth & Differentiation 52: 77–87.
33. Gomes ER, Jani S, Gundersen GG (2005) Nuclear movement regulated by Cdc42, MRCK, myosin, and actin flow establishes MTOC polarization in migrating cells. Cell 121: 451–463.
34. Sepich DS, Usmani M, Pawlicki S, Solnica-Krezel L (2011) Wnt/PCP signaling controls intracellular position of MTOCs during gastrulation convergence and extension movements. Development 138: 543–552.
35. Marmaras CF, Tipping NE, Wilson DJ (2005) A Rho-dependent actin purse-string is involved in wound repair in the early chick amnion following surgical puncture. Wound Repair and Regeneration 14: 61–65.
36. Wood W, Jacinto A, Grose R, Woolner S, Gale J, et al. (2002) Wound healing recapitulates morphogenesis in Drosophila embryos. Nature Cell Biology 4: 907–912.
37. Danjo Y, Gipson IK (1998) Actin "purse string" filaments are anchored by E-cadherin-mediated adherens junctions at the leading edge of the epithelial wound, providing coordinated cell movement. Journal of Cell Science 111: 3323–3332.
38. Pittlik S, Begemann G (2012) New sources of retinoic acid synthesis revealed by live imaging of an Aldh1a2-GFP reporter fusion protein throughout zebrafish development. Developmental Dynamics 241: 1205–1216.

APPENDIX ii

Primers used in this study

Gene/ Accession no.	Primer sequence		Human/ *Drosophila* orthologue
	Forward Primer (5')	Reverse Primer (3')	
frmd6 / NM_001020816	CCATCGATATGAGCAAACTGACTTTCCACA	CGGGCCCTTACACCACAAACTCTGGTTCTG	*frmd6 (willin) /expanded*
nf2b / NM_212951	CGGGCCTGGTTTAACACATA	CAACAGAGCTCGGATTGTTCT	*nf2/merlin*
sav1 / NM_001004560	GTGTCAGTGCCAACCTGGAT	AGTAAGCTGTCTGAGTGTGTCA	*salvador*
stk3 / NM_199672	GCAGTGCTTCCTTAAACTCCAAAC **qPCR:** CCCAGAACAGAGAGCGACGGCAACTCAACT	GCAGGAATCTAGAGTAAGATGCAG **qPCR:** GCCAGCACTCTCGGAACCAGACTTCACCAT	*mst2/hippo*
lats2 / ENSDART00000139620	**qPCR:** GCGTGCCCTGAAACAGACTGGTAGCCGTAA	**qPCR:** GCGTGCCCTGAAACAGACTGGTAGCCGTAA	*lats2/warts*
wwtr1/ NM_001037696	**qPCR:** TGTTACAGCATCCCGACCACTCCTGAAGAC	**qPCR:** CCAGGTGAGGAAGGGCTCGCTCTTGTT	*wwtr1(taz) /n.a.*
yap1 / NM_001139480	CGACTTTCCTTGAAAACGGT **qPCR:** AGCCAAAGTCCCACTCCAGACAAGCCAGTA	AAGGTGTAGTGCTGGGTTCG **qPCR:** GGCAGCGGCATGTCATCAGGTATCTCGTAA	*yap/yki*
tead1a / NM_212847.2	**qPCR:** GCGAACGGGCAAGACACGGACAAGAAAGC	**qPCR:** ACTGTGGATGGCTGTGGCGGAGACAATCTG	*tead1/ scalloped*
tead4 / XM_002666763.3	**qPCR:** AAGGAGGACTGAAGGAGCTGTTCGAGAAGG	**qPCR:** GCCGAATGAGCAGACTTTAGTGGAGGAGGT	*tead4 / scalloped*
ctgfa / NM_001015041	**qPCR:** TCCTCACAGAACCGCCACCTTGCCCAT	**qPCR:** TCACGCCATGTCGCCAACCATCTTCTTGT	*ctgf/n.a.*
ctgfb / NM_001102573	**qPCR:** GAGACAGGCATCTGCATGGCTCAAGAAGGT	**qPCR:** GTCGCACACCCACTCCTCACAGCACTT	*ctgf/n.a.*
amphiregulin / ENSDART00000114293	**qPCR:** ACACTTCCGTGCTGGATCATGTGACTGTGA	**qPCR:** TGGTTCTGCTCGTCTCCTTTACTGGCTTGG	*amphiregulin/n.a*

fgf20a / NM_001037103	**qPCR:** GGTTCGGTCCAAGGCACGAGG	**qPCR:** CGCTCGCCATGCCGATACAGG	*fgf20/n.a.*
msxB / NM_131260	**qPCR:** CCAGCAGGTCGCGTGTTCTCC	**qPCR:** GCTTGCGTAAGGTGCACGGC	*n.a./drop*
wnt10a / NM_130980	**qPCR:** GCTCTCACGACATCAGTTGGCACTCTCC	**qPCR:** AAGTAATCCATGCTGCTGCTGCTCTTCTGC	*wnt10a/wnt10*
wnt3a / NM_001007185	**qPCR:** GCCCTGATGCCCGCTCTGCTATGAATC	**qPCR:** CCGATGTTTCTCAACCACCATTTCCGATGC	*wnt3a/n.a.*
lef1 / NM_131426	**qPCR:** AAGGCCACCCGTACCCGAGT	**qPCR:** GGGTGAACGGCATGGGACGG	*lef1/pangolin*
dkk1a / NM_001281800	**qPCR:** ACATCCCAGGAGAACCACAG *(a)*	**qPCR:** AAACTTGTCCCTCTGTCAGCA *(a)*	*dkk1/n.a.*
dkk1b / NM_131003	**qPCR:** CTCCGCTCACCCAGGGAATACATCCTACAA	**qPCR:** ACCCGCCGCACCTGAACCGACTTTA	*dkk1/n.a.*
shha / NM_131063	**qPCR:** GGCCAGGGGTTAAGCTGCGT	**qPCR:** CGGCCTTCTGTCCTCCGTCC	*shh/hh*
bmp2a / NM_131359	**qPCR:** CACTCCGTGAACGCAGAGCAGGTTAGCA	**qPCR:** TCGTCTGGGATGGAGGTCAGGTTGAAGAGG	*bmp2/dpp*
bmp2b / NM_131360	**qPCR:** AACCTACAGCCATGACGGTCAAGGCACAG	**qPCR:** CGTTCCAGCCGACATCACTGAAGTCCACAT	*bmp2/dpp*

[(a)]Published in Stewart (2014).

APPENDIX iii

RNA probes used in this study

Gene	Vector	Sense Probe		Antisense Probe		Hybridization Temperature
		Restriction Enzyme	Polymerase	Restriction Enzyme	Polymerase	
frmd6	pCS2	EcoRV	SP6	BamHI	T3	68ºC
nf2b	pGEM-T-Easy	NcoI	SP6	SpeI	T7	67ºC
sav1	pGEM-T-Easy	NcoI	SP6	SalI	T7	66ºC
stk3	pGEM-T-Easy	ApaI	SP6	SalI	T7	67ºC
yap1	pGEM-T-Easy	SalI	T7	NcoI	SP6	68ºC
ctgfa [(a)]	pSport	BamHI	T7	EcoRI	SP6	67ºC

[(a)]Published in Dickmeis et al. (2004)

APPENDIX iv

Antibodies used in this study

Antibody	Host	Dilution	Company
Anti-Yap FL (63.07)	Mouse	1:100	Sta Cruz Biotechnology
Anti-Phospho Mst1(Thr18)/Mst2(Thr180)	Rabbit	1:100	Cell Signalling
Anti-Phospho Lats1 (Thr1079)	Rabbit	1:100	Cell Signalling
Anti-NF2	Rabbit	1:200	Sta Cruz Biotechnology
Anti-GFP	Rabbit	1:200	Invitrogen
Anti-Beta-Catenin	Mouse	1:200	BD Transduction labs
Anti-E-Cadherin	Mouse	1:200	BD Transduction labs
Anti-N-Cadherin	Mouse	1:100	BD Transduction labs
Anti-R-Cadherin	Mouse	1:100	BD Transduction labs
Anti-P-cadherin	Mouse	1:100	BD Transduction labs
Anti-M-cadherin	Mouse	1:100	BD Transduction labs
Anti-ZO1	Mouse	1:100	Invitrogen
Anti-Claudin1	Rabbit	1:100	Invitrogen
Anti-Fibronectin	Rabbit	1:100	Sigma
Anti-Laminin	Rabbit	1:100	Thermo Scientific
Anti-TenascinC	Rabbit	1:100	US Biological
Anti-Zyxin	Mouse	1:100	Sigma
Anti-Cadherin5	Mouse	1:100	BD Transduction labs
Anti-p120-Catenin	Mouse	1:100	BD Transduction labs
Anti-Alpha-Catenin	Mouse	1:100	BD Transduction labs
Anti-Cadherin11	Mouse	1:100	Invitrogen
Anti-Phospho Ezrin (Thr567)/ Radixin (Thr564)/ Moesin (Thr558)	Rabbit	1:100	Cell Signalling
Anti-Phospho Myosin Light Chain 2 (Ser19)	Rabbit	1:100	Cell Signalling
Anti-Scribble	Goat	1:100	Sta Cruz Biotechnology
Anti-Vinculin	Mouse	1:100	Sigma
Anti-Phospho Histone 3	Rabbit	1:400	Millipore
Anti-γ Tubulin	Mouse	1:200	Sigma
Anti-active Caspase 3	Rabbit	1:400	AbCam
Alexa 488 anti-rabbit	Goat	1:500	Invitrogen
Alexa 488 anti-mouse			
Alexa 568 anti-mouse			
Alexa 633 anti-rabbit			
Alexa 488 anti-goat	Donkey	1:500	Invitrogen